N-Heterocyclic Silylenes as ambiphilic Reagents in Main Group Chemistry and as Ligands in Transition Metal Chemistry

Dissertation zur Erlangung des naturwissenschaftlichen Doktorgrades

der Julius-Maximilians-Universität Würzburg

vorgelegt von

Mirjam Julia Krahfuß

aus Rosenheim

Würzburg, 2020

„Gegen Zielsetzungen ist nichts einzuwenden, sofern man sich dadurch nicht von interessanten Umwegen abhalten lässt.“

- Mark Twain

Eingereicht an der Fakultät für Chemie und Pharmazie der Julius-Maximilians-Universität Würzburg am:

Gutachter der schriftlichen Arbeit:

1. Gutachter: Prof. Dr. Udo Radius
2. Gutachter: Prof. Dr. Holger Braunschweig

Prüfer des öffentlichen Promotionskolloquiums:

1. Prüfer: Prof. Dr. Udo Radius
2. Prüfer: Prof. Dr. Holger Braunschweig
3. Prüfer: ……..

Datum des öffentlichen Promotionskolloquiums:

…….....

Doktorurkunde ausgehändigt am:

…….....

Die Experimente zur vorliegenden Arbeit wurden in der Zeit von August 2016 bis September 2020 am Institut für Anorganische Chemie der Julius-Maximilians-Universität unter Anleitung von Prof. Dr. Udo Radius durchgeführt.

Content

1 Motivation

The isolation of the first *N*-heterocyclic carbene (NHC), 1,3-diadamantyl-imidazolin-2-ylidene, by Arduengo in 1991[1] led to the opening of a wide field of research utilizing the new class of ligands which was further substantially expanded by Bertrand *et al*. in 2005 with the synthesis of cyclic (alkyl)(amino)carbenes (cAACs).[2] The efficiency of NHCs[3] and cAACs[4] as excellent ancillary ligands for transition metal complexes and for stabilization of low-coordinate transition metal centres is the result of their strong *σ*-donor properties and their sterically demanding structures.[5] The silicon analogues of NHCs, *N*-heterocyclic silylenes (NHSi)[6] and related compounds[7], however, have attracted less interest over the last few decades compared to their carbon counterparts. Due to the divalent silicon atom of NHSis, these silylenes are Lewis acids and bases simultaneously, which opens up a multitude of different reaction pathways. Although NHCs and NHSis are in principle isostructural, the replacement of the carbene carbon atom with a silicon atom has a significant impact on the electronic features and thus on the reactivity of NHSis compared to NHCs. Herein, the resulting differences in the reactivity of *N*-heterocyclic silylenes are examined using various examples from main group element and transition metal chemistry and are compared to the ubiquitous *N*-heterocyclic carbenes. First, the reactivity of $Dipp_2$NHSi (**1**) towards group 13 compounds, tin chlorides, elemental halides, aryl and alkyl halides as well as azides is examined. In the second part of this work, several transition metal complexes bearing carbonyl, cyclopentadienyl and halide ligands are reacted with silylene **1** and the influence of the halide ligand used is investigated.

Chapter I

N-Heterocyclic Silylenes as ambiphilic Reagents in Main Group Chemistry

2 *N*-Heterocyclic Silylenes as ambiphilic Reagents in Main Group Chemistry

2.1 Introduction

"Had I been so fortunate as to have obtained more certain evidences on this subject, and to have procured the metallic substances I was in search of, I should have proposed for them the names of silicium, alumium, zirconium, and glucium."

- Sir Humphry Davy, 1808[8]

Although Sir Humphry Davy remained unsuccessful in the isolation of the element silicon from silica by electrochemical treatment and in the presence of potassium, he proposed a name for the substance he was looking for in 1808. In 1824, Berzelius isolated elemental silicon from a silicon tetrafluoride atmosphere in which he heated potassium to reduce the silicon atom.[9] Since then, the chemistry of the second most abundant element in the earth´s crust[10] has experienced a continuous rise and has been examined in numerous studies.[11]

2.1.1 Silylenes: from short-lived intermediates to isolable reagents

The first example of a divalent silicon atom in the oxidation state +II was reported in 1937 by Schwarz and Pietsch who reduced $SiCl_4$ through glow discharge and obtained small amounts of dichloro silylene $SiCl_2$ as a colourless, air and moisture sensitive solid.[12] In the following decades, silylenes like dimethylsilylene Me_2Si[13] were studied at low temperatures in matrices, keeping silylenes from being used as reactants in the lab, or have been observed as reactive intermediates in chemical reactions.[14] This circumstance began to change when in 1986 Jutzi *et al.* reported the synthesis of the π-complex decamethyl silicocene $(\eta^5\text{-}C_5Me_5)_2Si$ which was the first at room temperature stable compound of divalent silicon.[15] In 1990, Müller *et al.* described the tetra-coordinate divalent Si(II) chelate compound $Si(CH(PMe_2)_2)_2$, which was obtained by reducing the disilane Si_2Cl_6 with $Li[C(PMe_2)_2(SiMe_3)]$.[16] In 1994, three years after

the isolation of the first free, stable *N*-heterocyclic carbene Ad_2Im (1,3-diadamantyl-imidazolin-2-ylidene)[1], Denk and co-workers isolated the bulky *tert*-butyl substituted *N*-heterocyclic silylene tBu_2NHSi[17] (1,3-di-*tert*-butyl-1,3-diaza-2-silacyclopent-4-en-2-ylidene, **II**-*t*Bu), whose structure is analogous to that of *N*-heterocyclic carbenes. From there, the chemistry of the divalent silicon compounds experienced a rapid rise and a variety of cyclic silylenes with different substitution patterns as well as varying ring sizes of the *N*-heterocycle have been reported (Figure 1). In the following, the two-coordinate representatives of this class of compounds are discussed in more detail, although it should be noted that a variety of three-coordinated cyclic silicon(II) compounds have been reported.[7c, 18] The earliest examples for *N*-heterocyclic silylenes are NHC analogue five-membered ring silylenes R_2NHSi which are stabilized by donating nitrogen groups (Figure 1, **I** – **II**).[17, 19] The substitution pattern is, compared to NHCs, rather limited with only a few alkyl and aryl substituted NHSis known. For alkyl substituents at the nitrogen atom, only the *tert*-butyl NHSi has been synthesized, for which both the backbone unsaturated[17] as well as a small number of saturated silylenes[19-20] are known.

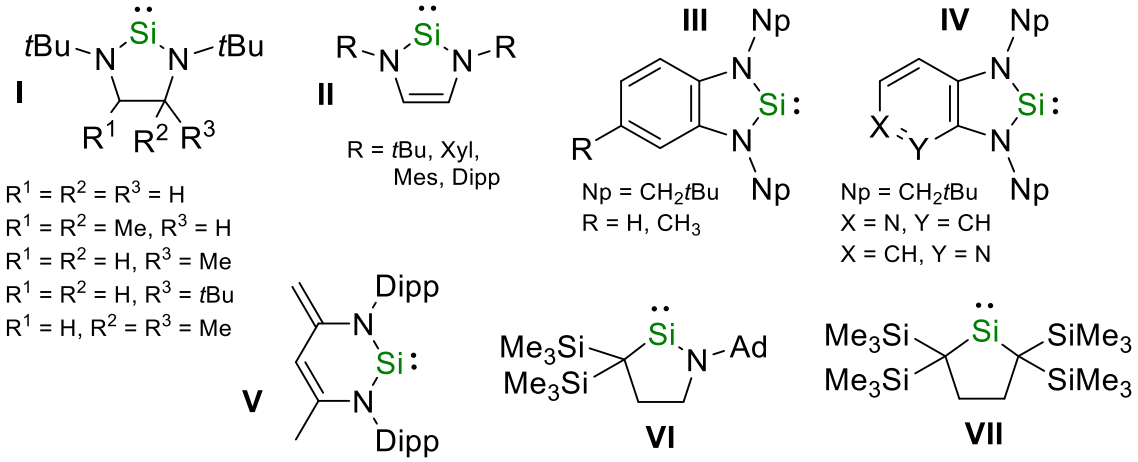

Figure 1. Examples for two-coordinate divalent cyclic silylenes.

For the aryl substituents, the range of groups used to form stable and isolable NHSis is limited to the phenyl derivatives xylyl (Xyl, 1,3-dimethylphenyl, **II-Xyl**)[6f], mesityl (Mes, 1,3,5-trimethylphenyl, **II-Mes**) and di*iso*propylphenyl (Dipp, **1**)[6e] (Figure 1, top middle). The benzannulated *N*-heterocyclic silylene Np_2NHSi^{benz} (Np = neopentyl; **III**)[6b] and the pyrido silylenes Np_2NHSi^{pyr} (pyr = pyrido; **IV**)[21] which have been

reported by Gehrhus and Heinicke can be considered as part of the backbone unsaturated NHSis (Figure 1, top right). Besides the five-membered silylenes, a six-membered two-coordinate NHSi (**V**) has been synthesized by Driess and co-workers[22] who used a monoanionic bidentate *β*-diketiminiate ligand to access the *N*-aryl heterofulvene-like silylene shown in Figure 1 (bottom left). Another interesting silicon(II) compound is the cAAC (cyclic (alkyl)(amino)carbene)[2] analogue, a cyclic (alkyl)(amino) silylene cAASi (**VI**), which has a adamantyl substituent at the nitrogen atom and bulky Me_3Si groups in *α*-position to the silylene silicon atom for additional steric stabilization (Figure 1, bottom middle).[6i] The dialkylsilylene **VII**[23] reported by Kira *et al.* is completely kinetically stabilized by bulky trimethylsilyl groups at both *α*-positions to the silylene silicon atom and, due to the missing donor group, no classic NHSi but shows a similar reactivity compared to the compounds described above.[24]

2.1.2 Synthetic routes for *N*-heterocyclic silylenes

Although several different substitution patterns are known, the synthesis of the alkyl and aryl, as well as the backbone saturated, unsaturated and benzannulated *N*-heterocyclic silylenes (*vide supra*) is very similar (see Scheme 1 and 2).

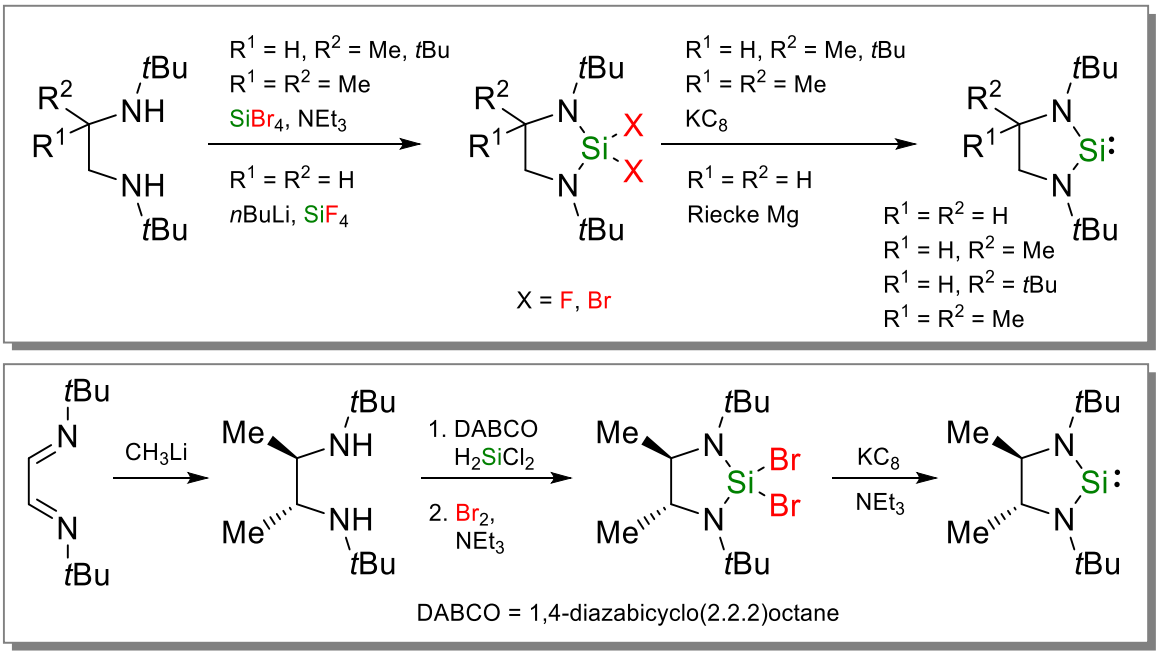

Scheme 1. Synthesis of the saturated five-membered *N*-heterocyclic silylenes **I**.

NHSis with a saturated backbone can be synthesized starting from diamines (Scheme 1, top) or diazabutadiene (Scheme 1, bottom) depending on the backbone substituents. In case of the diamines, cyclisation is achieved in a basic environment using SiF_4 (R^1 = R^2 = H) or $SiBr_4$ (R^1 = H, R^2 = Me, *t*Bu; R^1 = R^2 = Me) as a silicon source. Subsequent reduction with potassium graphite or Riecke magnesium leads to the formation of the respective free silylene which is obtained as colourless (R^1 = H, R^2 = Me) and pale yellow (R^1 = H, R^2 = *t*Bu, R^1 = R^2 = Me) liquids.[19, 20b] The racemic backbone-methylated NHSi is afforded as a pale yellow liquid by methylation of an diazabutadiene giving an enantiomeric mixture of dimethyldiamines, cyclisation *via* deprotonation of the nitrogen atoms and subsequent reaction with dichlorosilane leading to the dihydrosilane $tBu_2NHSi^{Me}(H)_2$. The dihydrosilane is brominated with elemental bromine to give the dihalosilane $tBu_2NHSi^{Me}(Cl)_2$ which is reduced to the free NHSi with potassium graphite and triethylamine to prevent over reduction.[20a]

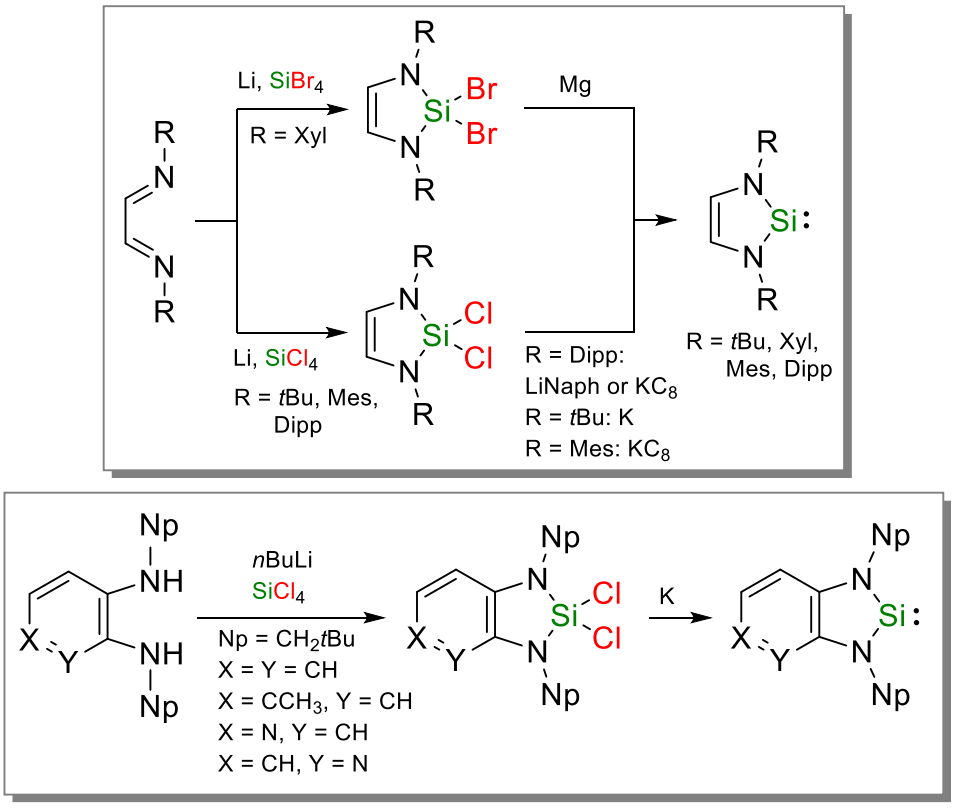

Scheme 2. Synthesis of the unsaturated five-membered *N*-heterocyclic silylenes **II**, **III** and **IV**.

The unsaturated five-membered NHSis shown in Figure 1 are synthesized in the same manner as described for the saturated compounds but in contrast are all solid at room temperature. As a first step, the diazabutadiene or diamine in case of the benzannulated and pyrido substituted silylenes is reduced with either elemental lithium or a lithium organyl and the corresponding cyclosilane is formed by adding a tetrahalosilane ($SiCl_4$ or $SiBr_4$). Finally, reduction with potassium graphite (R = Mes, Dipp), elemental potassium (R = *t*Bu, Np), lithium naphthalenide (R = Dipp) or magnesium (R = Xyl) yields the free silylenes R_2NHSi (R = Xyl, Mes, Dipp), Np_2NHSi^{benz} and Np_2NHSi^{pyr}.

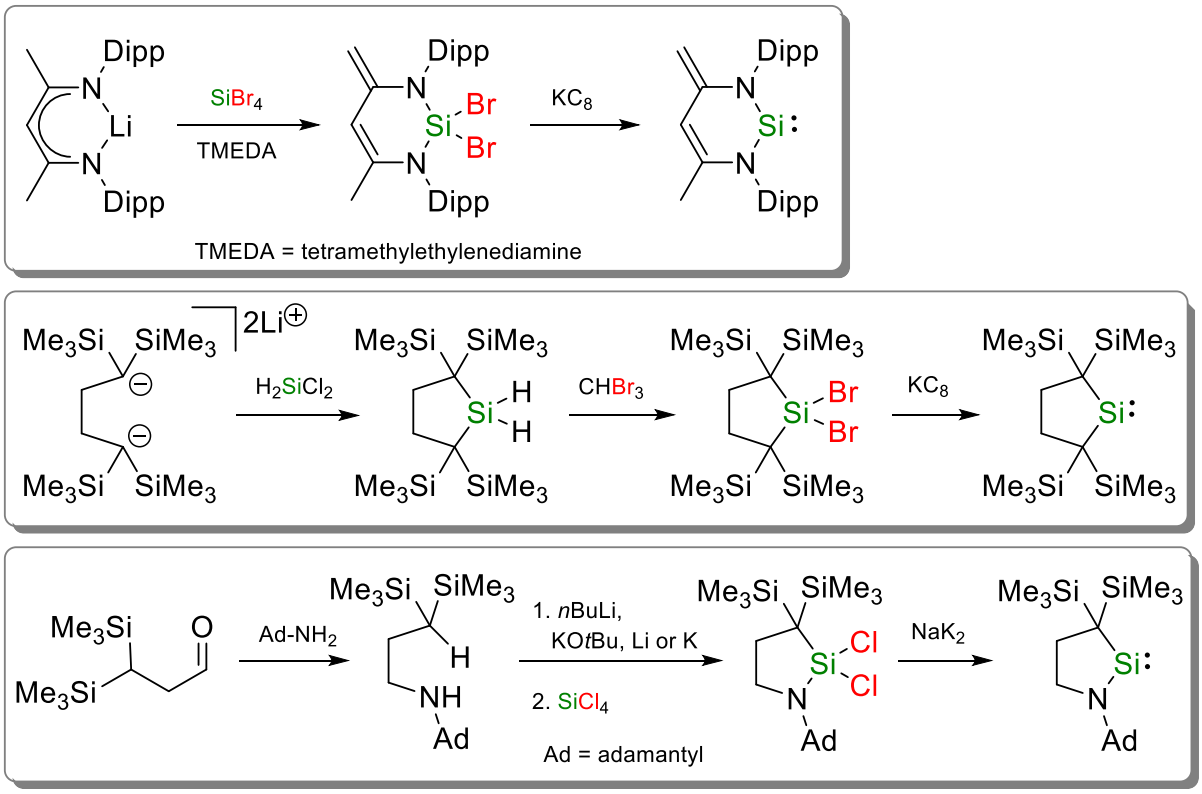

Scheme 3. Synthesis of a *β*-diketiminate silylene (**V**, top), a dialkylsilylene (**VI**, middle) and a cyclic (alkyl)(amino)silylene (**VII**, bottom).

The *β*-diketiminate silylene **V** and the dialkylsilylene **VI** are synthesized starting from anionic precursors which are reacted with a silicon source ($SiBr_4$ or H_2SiCl_2) to form the cyclic dibromo or dihydrosilane. In case of the dihydrosilane, bromoform is used for halogenation. Analogous to the previous syntheses, the free silylenes are obtained by reduction of the dihalo precursors with potassium graphite.[6d, 22] While the last step of the synthesis of the cAASi **VII** is identical to the before-mentioned syntheses

(reduction with sodium-potassium alloy to obtain the free silylene), as a starting material 3,3-bis(trimethylsilyl)propanal is used and reacted with adamantyl amine under reductive conditions to give a trimethylsilyl substituted secondary amine. Deprotonation with *Schlosser's base* (KO*t*Bu and *n*BuLi) followed by cyclisation with $SiCl_4$ afford the cyclic (alkyl)(amino)dichlorosilane, which is then reduced to the free silylene **VI**.[6i] The relatively straightforward syntheses, the good yields and mostly inexpensive starting materials as well as the stability of the compounds make NHSis (and the dialkylsilylene) an easily available source for divalent silicon.

2.1.3 Reactions of *N*-heterocyclic silylenes with element–hydrogen bonds

Carbenes like NHCs and cAACs have been studied intensively regarding their ability to activate E-H bonds in main group element compounds.[25] Examples for the activation of B–H[26], C–H[27], Si–H[28] and other bonds[29] are known. For *N*-heterocyclic silylenes, far less examples for E–H bond activations are reported. West and colleagues reported the reactions of *t*Bu$_2$NHSi with i) ethanol and ii) water lead to the activation of the O–H bonds in both cases and formation of the oxidative addition products, the ethoxysilane *t*Bu$_2$NHSi(H)(OEt) (i) and the disiloxane (μ-O)(*t*Bu$_2$NHSi(H))$_2$ (ii) *via* the silanol intermediate *t*Bu$_2$NHSi(H)(OH) (Figure 2, top).[30] In comparison, NHCs have been shown to react with water giving the hydrolysis products *t*BuN=CHCH$_2$-N(CHO)*t*Bu and *t*BuN(H)CH$_2$CH$_2$-N(CHO)*t*Bu, respectively.[31] The analogous silanes were obtained for benzannulated NHSi Np$_2$NHSi^{benz}[6b] and the Dipp substituted silylene Dipp$_2$NHSi when reacted with ethanol at room temperature giving Dipp$_2$NHSi(H)(OEt) as well as the bis(ethoxy) silane Dipp$_2$NHSi(OEt)$_2$ and the enamine {DippN(H)CH}$_2$. The weaker Si–N bond compared to the C–N bond in NHCs is assumed to be the cause for the formation of the amine.[6f]

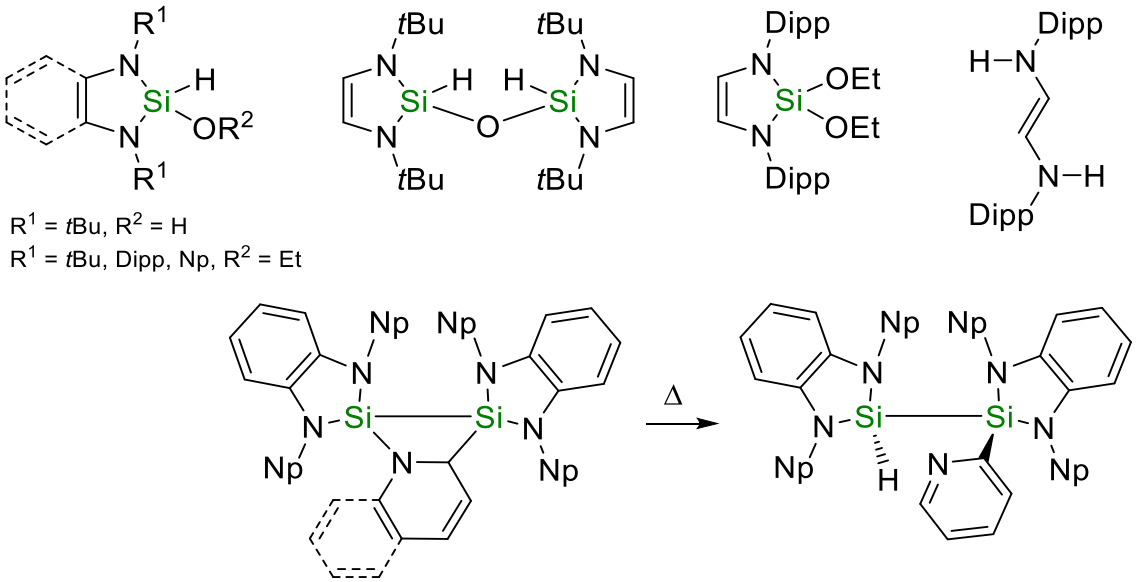

Figure 2. E–H activation products of *N*-heterocyclic silylenes.

The activation of a carbon–hydrogen bond by a *N*-heterocyclic silylene was observed by Gehrhus and co-workers who examined the reactivity of Np_2NHSi^{benz} towards pyridine and quinoline. In the case of pyridine, two equivalents of the silylene react with one molecule of pyridine and a labile cyclobutane derivative is formed which (in solution) either dissociates or proceeds to rearrange to a pyridyldisilane *via* a 1,3-H shift (Figure 2, bottom).[32] If quinoline is used, the cyclobutane is stable and no follow-up reactions are observed. Another example for C–H bond activation by a NHSi was reported by Kira *et al.* The dialkylsilylene **VII** was reacted with aromatic compounds under photochemical conditions and in case of toluene, *m*- and *p*-xylene the formation of silepin derivatives, and in case of naphthalene, mono and bis(silylene) adducts were observed. Using the sterically hindered mesitylene, no insertion into the C=C double bond occurred but activation of a methyl group and the respective silane **VII**(H)(CH_2-R) (R = 3,5-dimethylphenyl).[33]

These examples (*vide supra*) give a first impression on the distinctly different reactivity of *N*-heterocyclic carbenes and silylenes. In the following the differences between NHCs and NHSis with regard to main group element chemistry are investigated in more detail.

2.2 Results and Discussion

2.2.1 Adduct formation of $Dipp_2NHSi$ with Lewis Acids

N-heterocyclic silylenes can act as Lewis acids and bases simultaneously and thus, reacting $Dipp_2NHSi$ (**1**) with Lewis acidic alanes or boranes should lead to the formation of classical or frustrated Lewis pairs. As silylene **1** is sterically demanding[34], using an alane or borane with a huge steric bulk could favour the formation of frustrated Lewis pairs (FLP). For phosphines and *N*-heterocyclic carbenes, several FLPs containing congested boranes as Lewis acids have been synthesized and their reactivity towards small molecules such as dihydrogen[35], THF[35d, 36], C–C multiple bonds[37], carbon dioxide[38] and singlet dioxygen[39] has been studied. Alane-based adducts of NHCs have also been investigated, e.g. Dagorne *et al.* reported the activation of dihydrogen by tBu_2Im-Al(iBu)$_3$ giving $tBu_2Im(H)_2$.[40] Keeping in mind that phosphines and *N*-heterocyclic silylenes have been shown to possess similar characteristics with regard to transition metal chemistry[34], the Lewis base properties of $Dipp_2NHSi$ (**1**) with respect to typical group 13 Lewis acids were investigated and as a starting point, simple aluminium halides were used. With $AlCl_3$, no reaction or formation of an adduct could be observed. Interestingly, the reaction of silylene **1** with one equivalent of aluminium triiodide in toluene led to the clean formation of $Dipp_2NHSi{\cdot}AlI_3$ as an off-white solid in very good yields (87 % isolated yield, Scheme 4). In the ^{29}Si NMR spectrum of **2** a resonance at 42.8 ppm is detected and the aluminium atom gives rise to a signal at 40.1 ppm in the ^{27}Al NMR spectrum. In the ^{1}H NMR spectrum one set of signals for the silylene **1** can be observed, which indicates the formation of a symmetric compound and thus, no insertion into the Al–I bond but the formation of the silylene aluminium adduct $Dipp_2NHSi{\cdot}AlI_3$ (**2**, Scheme 4). The characteristic septet of the methine protons is shifted towards higher fields to 3.08 ppm (**1**: 3.25 ppm).

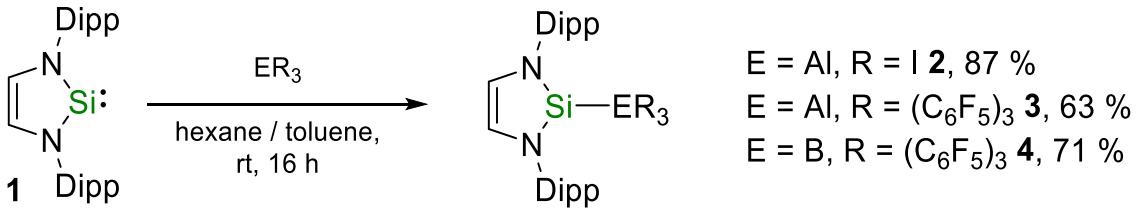

Scheme 4. Reaction of $Dipp_2NHSi_2$ with AlI_3, $Al(C_6F_5)_3$ and $B(C_6F_5)_3$ giving the silylene adducts $Dipp_2NHSi{\cdot}AlI_3$ (**2**), $Dipp_2NHSi{\cdot}Al(C_6F_5)_3$ (**3**) and $Dipp_2NHSi{\cdot}B(C_6F_5)_3$ (**4**).

Metzler reported the silylene borane adduct $t Bu_2NHSi{\cdot}B(C_6F_5)_3$, which slowly undergoes a rearrangement reaction by insertion of the silylene silicon atom into one of the B–C bonds to give $tBu_2NHSi(C_6F_5)–B(C_6F_5)_2$.[41] The reaction of $Dipp_2NHSi$ with the perfluorinated alane $Al(C_6F_5)_3$ and borane $B(C_6F_5)_3$ in a toluene / hexane mixture gives the adducts $Dipp_2NHSi{\cdot}Al(C_6F_5)_3$ (**3** 63 %) and $Dipp_2NHSi{\cdot}B(C_6F_5)_3$ (**4** 71 %) in modest to good yields. In the ^{29}Si NMR spectra the silylene silicon atoms were detected slightly shifted towards higher fields at 74.0 ppm (**3**) and 72.2 ppm (**4**) and in the ^{1}H NMR spectra one set of signals was detected for the silylene ligand and the methine protons can be assigned to the signals at 3.02 ppm (**3**) and 3.00 ppm (**4**). For adduct **3**, the aluminium atom could not be observed due to the quadrupolar nucleus and the perfluorophenyl substituents, and the boron atom of adduct **4** was detected at -19.9 ppm and therefore, at higher fields compared to the adduct $tBu_2NHSi{\cdot}B(C_6F_5)_3$ by Metzler (-14.3 ppm).[41] The fluorine substituents of the perfluorophenyl groups were observed at -123.0, -150.7 and -160.5 ppm (**3**) and at -129.0, -155.9 and -162.2 ppm (**4**). For both **3** and **4**, no Al–C / B–C insertion products were observed upon prolonged storage of **3** and **4** in benzene, toluene or hexane solutions. Single crystals of **4** suitable for X-ray diffraction were grown from a saturated hexane solution of **4** at -30 °C (Figure 3).

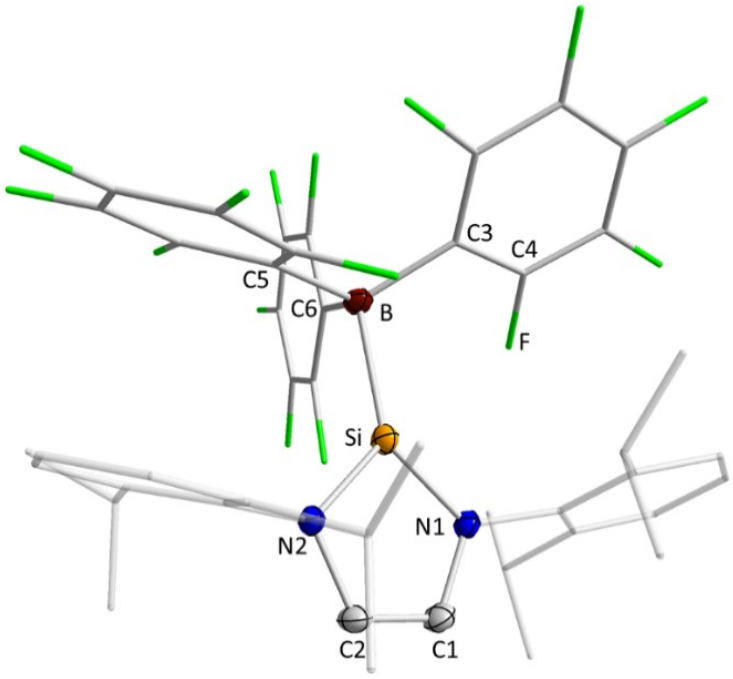

Figure 3. Molecular structure of $Dipp_2NHSi{\cdot}B(C_6F_5)_3$ (**4**) in the solid state (ellipsoids drawn at the 50 % probability level; hydrogen atoms are omitted for clarity). Selected bond lengths [Å] and angles [°] of **4**: Si–N1 1.6993(18), Si–N2 1.7085(17), Si–B 2.077(2), N1–C1 1.407(3), N2–C2 1.410(3), C1–C2 1.328(3), B–C3 1.634(3), B–C5 1.622(3), B–C6 1.627(3), C4–F 1.345(3), N1–Si–N2 92.85(9), C3–B–Si 109.15(15), C5–B–Si 100.66(13), C6–B–Si 108.59(15), (N–C1–C2–N2) / (N1–Si–N2) 3.408(81).

The solid-state structure of **4** shows that a silylene borane adduct was formed in the reaction which crystallizes in the triclinic space group $P\bar{1}$. The boron–silicon bond of Si–B 2.077(2) Å is slightly shorter than the Si–B bond observed in the amidinate chlorosilylene adduct **A** reported by Roesky and co-workers (Si–B 2.108(2) Å; Figure 4, left)[42] and significantly shorter than in the silylborate **B** observed by Krempner *et al.* (Si–B 2.167(4) Å, Figure 4, middle)[43] or the base-stabilized silylene adduct **C** presented by Braun *et al.* (Si–B 2.178(2) Å; Figure 4, right).[44] The five-membered silylene ring remains nearly planar and the perfluoroaryl substituents are oriented in a propeller-like fashion.

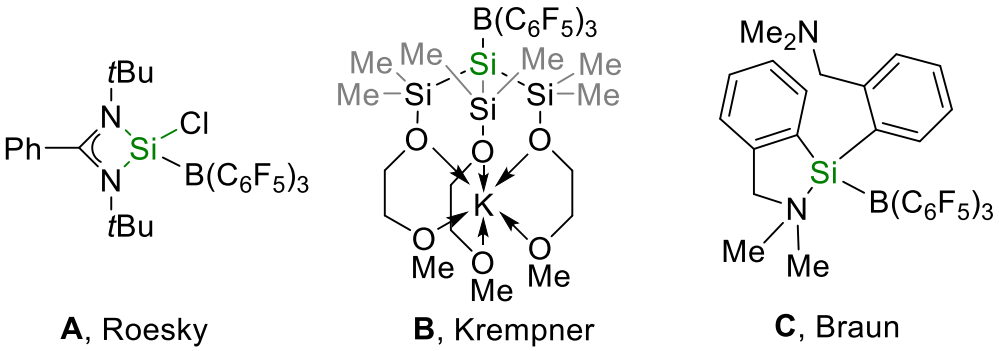

A, Roesky **B**, Krempner **C**, Braun

Figure 4. Examples of silicon containing boron adducts with a silicon–boron bond.

Following the synthesis and characterization of the perfluorinated adducts Dipp$_2$NHSi·Al(C$_6$F$_5$)$_3$ (**3**) and Dipp$_2$NHSi·B(C$_6$F$_5$)$_3$ (**4**), it was investigated whether compounds **3** and **4** react as frustrated Lewis pairs with selected substrates. To test the ability to activate small molecules, the adducts **3** and **4** were dissolved in C$_6$D$_6$ in a Young-tap NMR tube, the respective substrate was added, and the reaction progress was monitored *via* ^{1}H and ^{29}Si NMR measurements after 16 h. Dihydrogen activation by a FLP was first reported by Stephan *et al.* who used a phosphonium borate to heterolytically split H$_2$[35d], and Tamm and co-workers utilized the NHC borane adduct *t*Bu$_2$Im·B(C$_6$F$_5$)$_3$ for cleavage of the H–H bond.[35b]

The similar NHSi borane adduct **4** was reacted with dihydrogen and therefore, the argon atmosphere in the NMR tube was exchanged with dihydrogen gas but no signs of a reaction were observed. Furthermore, white phosphorus and diphenylacetylene were used as substrates but only starting material was identified in the ^{29}Si NMR spectra. In case of **3**, carbon monoxide (Figure 5) and phenylacetylene were used and no reaction could be observed after 16 h at room temperature. For B$_2$pin$_2$ (pin = pinacolato) and paraformaldehyde a reaction was observed but no defined reaction products could be identified. In contrast to the NHC adducts of alanes and boranes which readily activate small organic molecules, the silylene adducts **3** and **4** do not react as FLPs with the herein used substrates.

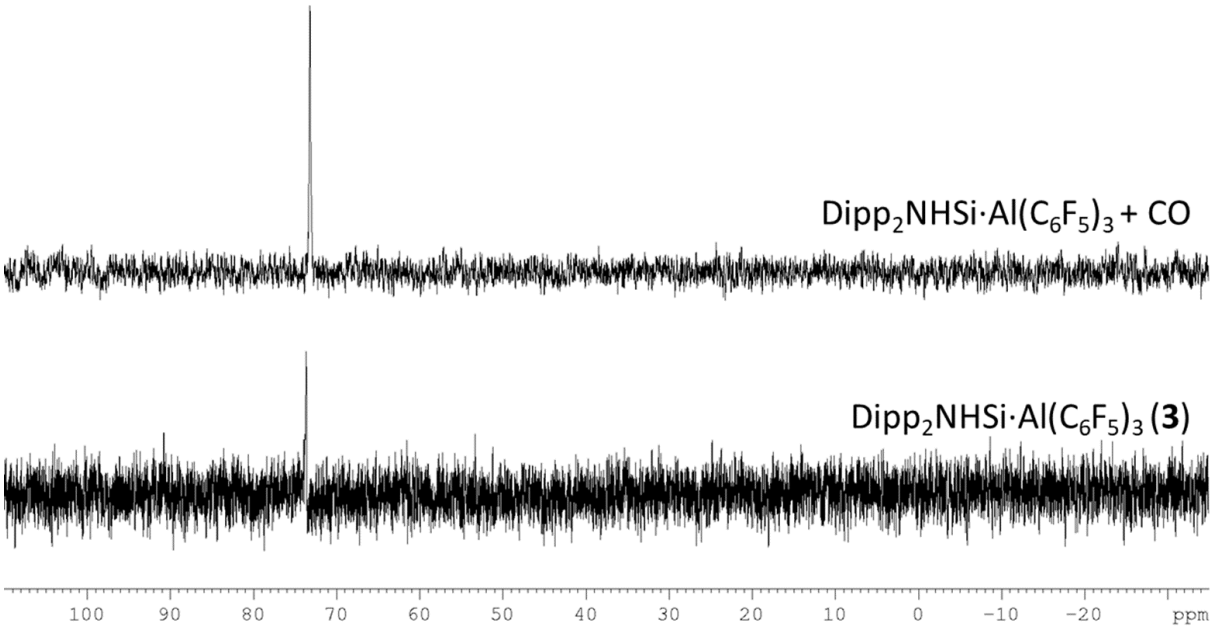

Figure 5. $^{29}Si\{^{1}H\}$ NMR spectra of $Dipp_2NHSi{\cdot}Al(C_6F_5)_3$ (**3**) (bottom) and of the reaction of $Dipp_2NHSi{\cdot}Al(C_6F_5)_3$ (**3**) with carbon monoxide in C_6D_6 after 16 h at room temperature (top).

The ability of $Dipp_2NHSi$ (**1**) to form Lewis acid-base pairs with group 13 compounds was investigated. Utilizing the simple aluminium trihalides $AlCl_3$ and AlI_3, two different reaction outcomes were observed. Whereas $Dipp_2NHSi$ does not react with aluminium trichloride, **1** readily forms the Lewis adduct $Dipp_2NHSi{\cdot}AlI_3$ (**2**) with AlI_3 and, interestingly, does not show any signs of insertion into the aluminium–iodide bond. Treatment of $Dipp_2NHSi$ (**1**) with the perfluorinated compounds $Al(C_6F_5)_3$ and $B(C_6F_5)_3$ resulted in the formation of the corresponding adducts $Dipp_2NHSi{\cdot}Al(C_6F_5)_3$ (**3**) and $Dipp_2NHSi{\cdot}B(C_6F_5)_3$ (**4**). Initial investigations regarding the ability of **3** and **4** to react as frustrated Lewis pairs and activate small molecules did not reveal such reactivity.

2.2.2 Insertion of $Dipp_2NHSi$ into element–halide bonds

Furthermore, the reactivity of the silylene **1** towards simple organic compounds was investigated. $Dipp_2NHSi$ reacts cleanly with Br_2 or I_2 in non-polar solvents like toluene, benzene or hexane to give the oxidized compounds $Dipp_2NHSiBr_2$ (**5**) and $Dipp_2NHSiI_2$ (**6**) which can be isolated from hexane as pale-yellow solids in moderate yields (**5**: 62 %, **6**: 57 %, Scheme 5).

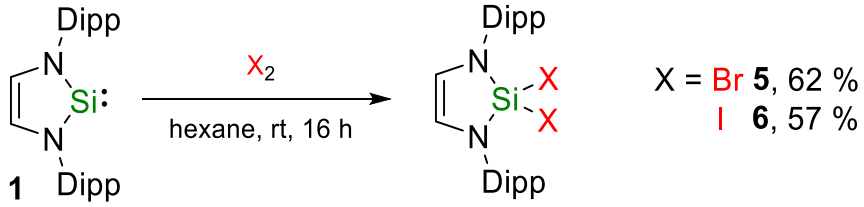

Scheme 5. Reaction of $Dipp_2NHSi$ with Br_2 and I_2.

Interestingly, compounds **5** and **6** are highly sensitive to traces of air and moisture and decompose within seconds but are well stable in solution and in the solid state if kept under an argon atmosphere. The oxidation of the silylene $Dipp_2NHSi$ leads to characteristic shifts in the ^{1}H and ^{29}Si NMR spectra. The methine protons of **5** and **6** give rise to a septet at 3.71 ppm (**5**) and 3.76 ppm (**6**) and show a significant low-field shift compared to the free silylene (3.25 ppm). The CH groups of the backbone also experience a noticeable shift to higher fields from 6.46 ppm ($Dipp_2NHSi$) to 5.74 ppm (**5**) and 5.77 ppm (**6**). In the ^{29}Si NMR spectrum a clear tendency can be observed going from $Dipp_2NHSiCl_2$ (**7**: -38.6 ppm)[45] to $Dipp_2NHSiBr_2$ (**5**: -59.3 ppm) to $Dipp_2NHSiI_2$ (**6**: -134.5 ppm). Single crystals of **5** and **6** suitable for X-ray diffraction were grown from a saturated hexane solution of **5** at -30 °C and by slow evaporation of a saturated hexane solution of **6** at room temperature and the structures in the solid state are shown in Figure 6.

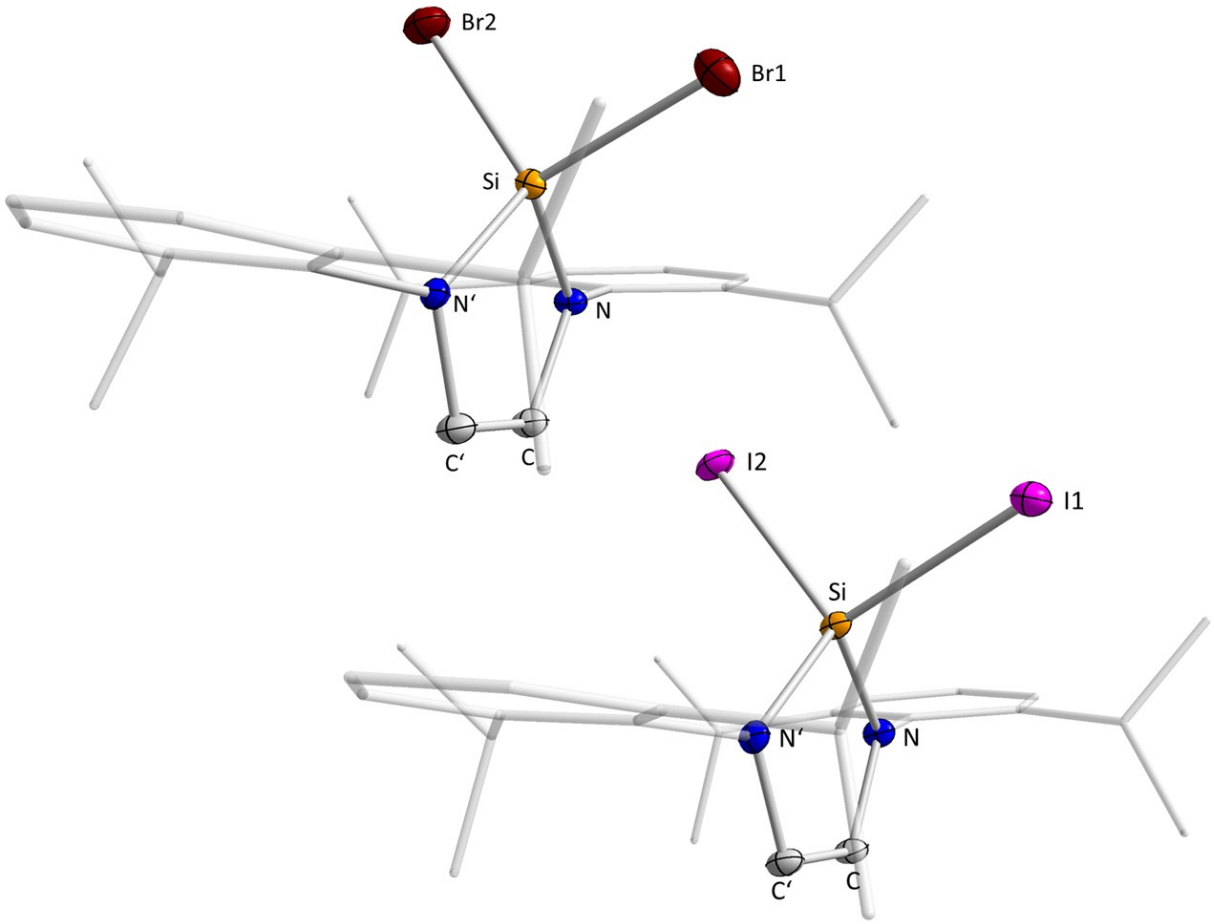

Figure 6. Molecular structure of $Dipp_2NHSiBr_2$ (**5**, top) and $Dipp_2NHSiI_2$ (**6**, bottom) in the solid state (ellipsoids drawn at 50 % probability; hydrogen atoms omitted for clarity). Selected bond lengths [Å] and angles [°] of **5**: Si–N 1.7059(19), Si–Br1 2.2239(10), Si–Br2 2.1866(9), N–C 1.417(3), C–C' 1.328(5), N–Si–N' 93.86(13), Br1–Si–Br2 102.18(4), Br1–Si–N 114.62(7), Br2–Si–N' 116.17(7), (N–C–C'–N') / (N–Si–N') 6.659(133); selected bond lengths [Å] and angles [°] of **6**: Si–N 1.711(2), Si–I1 2.4861(10), Si–I2 2.4240(9), N–C 1.420(3), C–C' 1.331(6), N–Si–N' 93.80(15), I1–Si–I2 102.99(4), I1–Si–N 113.98(8), I2–Si–N' 116.36(8), (N–C–C'–N') / (N–Si–N') 8.044(206).

$Dipp_2NHSiBr_2$ (**5**) and $Dipp_2NHSiI_2$ (**6**) crystallize in the orthorhombic space group Pnma and show a tetrahedrally coordinated silicon atom. The silylene ring is symmetry generated in part, almost planar and the silicon atom is very slightly bent out of the plane of the nitrogen atoms and the backbone (**5**: 6.659(133) °, **6**: 8.044(206) °). The silicon–halide bond lengths of 2.2239(10) (Si–Br1) and 2.1866(9) Å (Si–Br2) (**5**) and

2.4861(10) (Si–I1) and 2.4240(9) Å (Si–I2) (**6**) differ significantly due to crystal packing effects. The other bond lengths and angles are without exception compared to $Dipp_2NHSi(Cl)_2$ (**7**).[22]

Although *N*-heterocyclic silylenes are very prone to oxidation by halides and halide containing substrates[20-21, 23] and these reaction products often represent the end point of the reaction. The di-halide compounds **5**, **6** and **8** can be used as starting materials for further reactions. In a follow-up reaction to the halogenation of the free silylene, the chloride compound **6** was reacted with two equivalents of phenyl lithium in THF and $Dipp_2NHSiPh_2$ (**7**) was isolated by crystallization from hexane in excellent yields (92 %) as an off-white solid (Scheme 6).

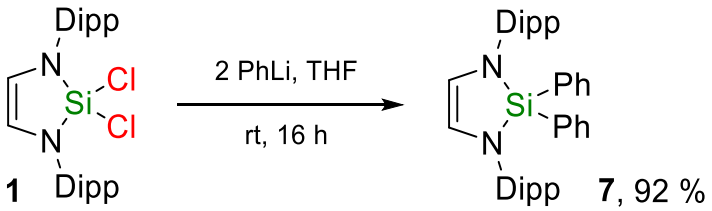

Scheme 6. Reaction of $Dipp_2NHSiCl_2$ with phenyl lithium.

In the ^1H NMR spectrum of **7**, the septet of the methine protons of the Dipp substituents were detected at 3.67 ppm and the backbone was detected as a singlet at 5.89 ppm. Both signals are shifted towards lower fields compared to the precursor ($Dipp_2NHSiI_2$: Dipp-C*H* 3.76 ppm, NC*H* 5.77 ppm). In the ^{29}Si NMR spectrum, the signal for the silicon atom was observed at -23.9 ppm and thus, also shifted towards lower fields. The composition of **7** was confirmed by elemental analysis. Crystals suitable for X-ray diffraction were grown from a saturated hexane solution of **7** at -30 °C and the structure in the solid state is shown in Figure 7.

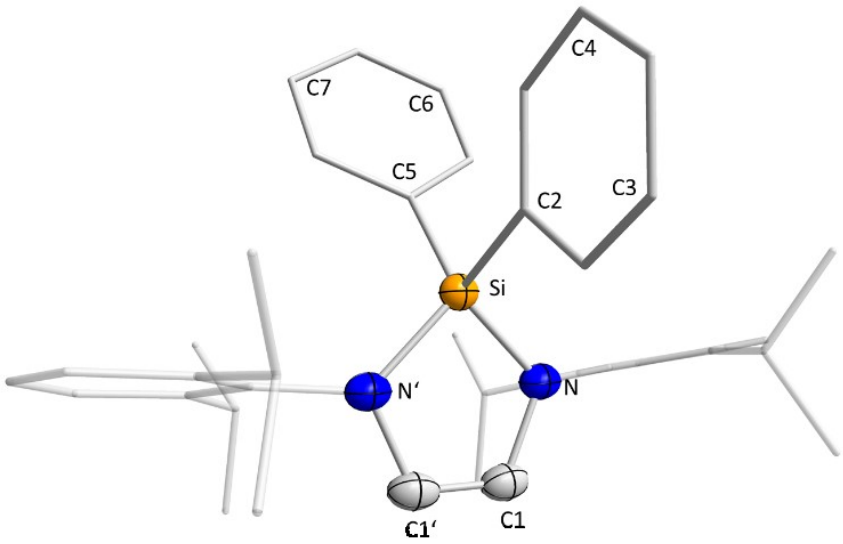

Figure 7. Molecular structure of $Dipp_2NHSiPh_2$ (**7**) in the solid state (ellipsoids drawn at the 50 % probability level; hydrogen atoms are omitted for clarity). Selected bond lengths [Å] and angles [°] of **7**: Si–N 1.744(2), Si–C2 1.876(4), Si–C5 1.861(4), N–C1 1.415(3), C1–C1' 1.329(6), N–Si–N' 91.92(14), C2–Si–C5 105.14(16), C2–Si–N 113.45(11), C5–Si–N' 116.5(1), (N–C1–C1'–N') / (N–Si–N') 10.650(91), (C2–C3–C4) / (C5–C6–C7) 90.000(95).

Compound **7** crystallizes as colourless needles in the tetragonal space group $I4_1md$ and shows the structural motif of a tetrahedrally coordinated silicon atom. The phenyl rings are arranged perfectly perpendicular towards each other and the Si–C bond lengths are almost the same with Si–C2 1.876(4) Å and Si–C3 1.861(4) Å. The silicon atom is bent out of the silylene ring plane by 10.650(91) ° and all other bond lengths and angles are unexceptional.

As only little is known about the reactivity of $Dipp_2NHSi$ (**1**) towards main group element halide compounds, investigations regarding the reaction behaviour of **1** against secondary and tertiary tin chlorides were carried out (Scheme 7).

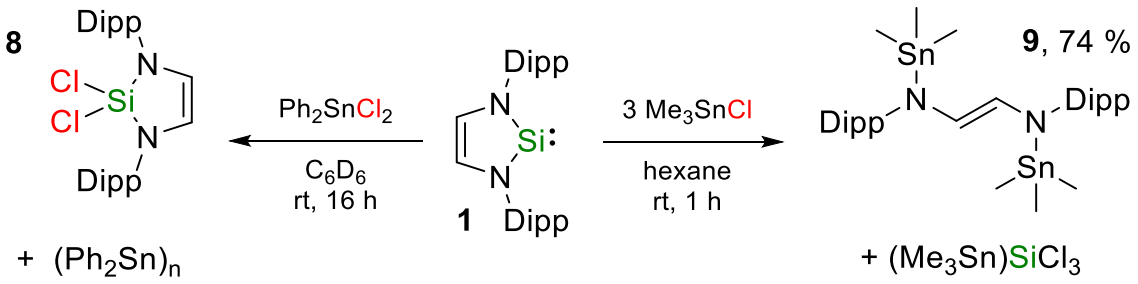

Scheme 7. The reaction of $Dipp_2NHSi$ (**1**) with the halostannanes Ph_2SnCl_2 and Me_3SnCl.

The reaction of $Dipp_2NHSi$ (**1**) with Ph_2SnCl_2 afforded the dichlorosilane $Dipp_2NHSiCl_2$ (**8**, Scheme 7, left), which was characterized by NMR spectroscopy (see Experimental Details). The silylene acts here as reducing reagent for the dichlorostannane and the thermodynamic driving force can easily be explained by the different bond enthalpies.[46] Monitoring the reaction in a Young-tap NMR tube, several signals in the range between -198.6 and -218.6 ppm in the ^{119}Sn spectrum are observed which can be assigned to cyclic poly(diphenylstannanes) like $(Ph_2Sn)_6$.[47] However, if $Dipp_2NHSi$ was reacted with trimethyltin chloride in organic solvents such as hexane, benzene, toluene or THF cleavage of the silylene ring with formation of the distannyl diazabutene **9** was observed (Scheme 7, right). The silicon atom of the silylene presumably reacts with a third equivalent of Me_3SnCl to afford the stannyl silane $(Me_3Sn)SiCl_3$. The ring opening of **1** in the reaction with three equivalents of Me_3SnCl occurs in solution spontaneously and, interestingly, also solvent-free in the solid state within a few minutes. Compound **9** was isolated from hexane in yields of 74 % and characterized by multinuclear NMR spectroscopy, elemental analysis und X-ray diffraction (Figure 8). The stannyl substituents give rise to a signal at -118.0 ppm in the ^{119}Sn NMR spectrum and the carbon atoms of the diazabutene backbone are observed at 123.8 ppm in the $^{13}C\{^1H\}$ NMR spectrum. Monitoring the reaction in a Young-tap NMR tube leads to the observation of the possible second reaction product $(Me_3Sn)SiCl_3$, which is assigned to the signal at -15.6 ppm in the ^{29}Si NMR spectrum, as well as to the second signal at 57.9 ppm in the ^{119}Sn NMR spectrum.

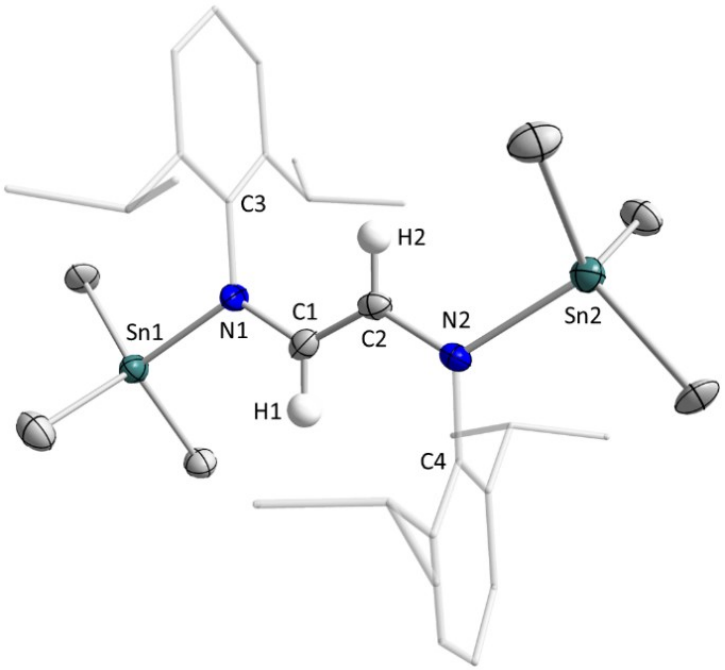

Figure 8. Molecular structure of {(Me$_3$Sn)N(Dipp)CH}$_2$ (**9**) in the solid state (ellipsoids drawn at the 50 % probability level; hydrogen atoms are omitted for clarity). Selected bond lengths [Å] and angles [°] of **9**: Sn1–N1 2.074(5), N1–C1 1.407(8), C1–C2 1.333(10), C2–N2 1.402(8), N2–Sn2 2.079(5), Sn1–N1–C1 118.9(4), Sn1–N1–C3 121.7(4). C3–N1–C1 117.7(5), N1–C1–C2 126.5(6), C1–C2–N2 126.0(6), C2–N2–Sn2 119.3(4), C2–N2–C4 118.5(5), C4–N2–Sn2 121.0(4), distance Sn1 from (N1–C1–C2–N2) 0.3497(4), distance Sn2 from (N1–C1–C2–N2) 0.3615(4).

The diazabutene fragment (N1–C1–C2–N2) is planar and the tin atoms are only very slightly bend out of the plane (Sn1 0.3497(4) Å, Sn2 0.3615(4) Å). The sum of angles around the nitrogen atoms amount to 358.3 ° (N1) and 358.8 ° (N2) and the bond between the carbon atoms of the diazabutene backbone is 1.333(10) Å and lies in the range of a C=C double bond (1.34 Å).[48]

Denk *et al.* reacted *t*Bu$_2$NHSi with tin dichloride in a 3:2 ratio and isolated the tris(chlorosilyl)stannane **D**, formed by insertion of the silylene silicon atoms into the tin–chlorine bonds, and stochiometric amounts of elemental tin (Figure 9, left).[49] Braunschweig *et al.* reported the reaction of Xyl$_2$NHSi with aryl dihaloboranes and observed the insertion of the silylene silicon atom into the boron–halogen bond to yield

silyl boranes **E** for R = Duryl and NHSi-ring expanded products **F** for R = Ph (Figure 9, middle).[50] When aryl dihalodiboranes(4) were used as boron source, diboranes **G** featuring one halosilyl and one silylene ligand were obtained (Figure 9, right).

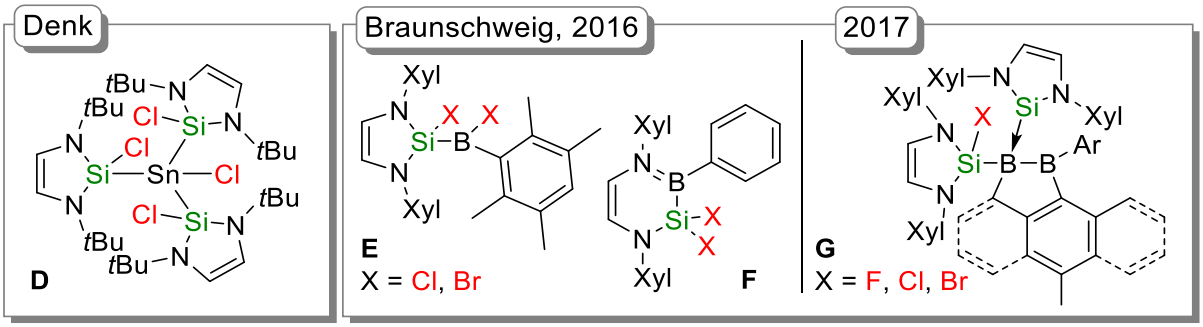

Figure 9. The reaction of *N*-heterocyclic silylenes with tin dichloride, aryl dihaloboranes and aryl dihalodiboranes(4).

Some examples of reactions of *N*-heterocyclic silylenes with halocarbons have been published so far but all of them were executed with the *tert*-butyl silylene *t*Bu$_2$NHSi. For Dipp$_2$NHSi, the reaction of **1** with the halocarbons methyl iodide, benzyl chloride and benzyl bromide leads to the insertion of the silicon atom into the C–X bond to give Dipp$_2$NHSi(I)(Me) (**10**), Dipp$_2$NHSi(Cl)(benzyl) (**11**) and Dipp$_2$NHSi(Br)(benzyl) (**12**) (Scheme 8). The insertion reaction seems to be favoured over the formation of Dipp$_2$NHSiX$_2$ (X = Cl, Br, I), as using an excess of the benzyl halides (up to three equivalents) still leads selectively to the formation of **11** and **12**. Methyl iodide can be used in up to a five-fold excess to yield **10** and not the diiodide Dipp$_2$NHSiI$_2$. The compounds **10** – **12** were isolated from hexane in good yields (**10**: 81%, **11**: 82 %, **12**: 75 %) as analytically pure, yellow (**10**, **11**) or colourless (**12**) solids. The compounds **10** – **12** are sensitive to air and moisture, well soluble in polar solvents like Et$_2$O and THF and non-polar solvents like benzene and toluene.

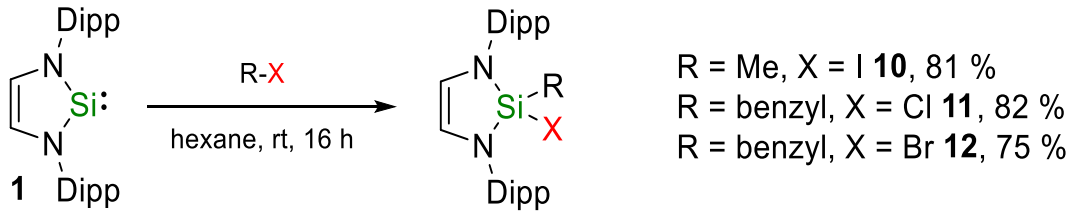

Scheme 8. Reaction of $Dipp_2NHSi_2$ with methyl iodide, benzyl chloride and benzyl bromide to yield the insertion products $Dipp_2NHSi(I)(Me)$ (**10**), $Dipp_2NHSi(Cl)(benzyl)$ (**11**) and $Dipp_2NHSi(Br)(benzyl)$ (**12**).

Due to the two different substituents at the silicon atom of **10** – **12** a doubled set of signals for the Dipp substituents at the nitrogen atoms in the ^{1}H and ^{13}C NMR spectrum can be observed (Figure 10). In the respective ^{1}H NMR spectrum of **10** – **12**, the septets of the methine protons were observed at 3.37 and 4.04 ppm (**10**), 3.51 and 3.92 ppm (**11**) and 3.52 and 3.98 ppm (**12**). The protons of the backbone are observed at 5.75 ppm (**10**), 5.74 ppm (**11**) and 5.76 ppm (**12**). In the ^{29}Si NMR spectrum, the signal of the silicon atom is shifted to higher field depending on the halide substituent (**10**: -30.3 ppm, **11**: -19.4 ppm, **12**: -20.9 ppm).

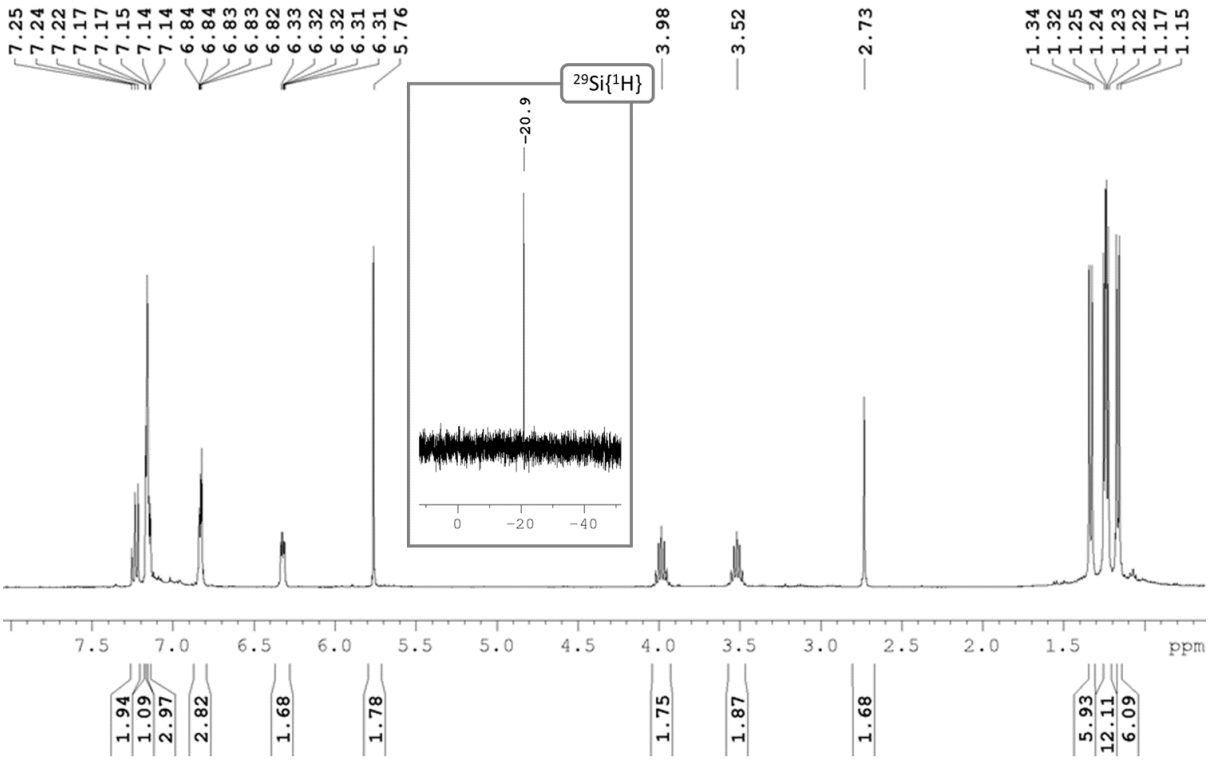

Figure 10. ^{1}H and $^{29}Si\{^{1}H\}$ NMR spectrum of compound **10**.

Single crystals of **10** suitable for X-ray diffraction were grown from a saturated hexane solution of **10** at -30 °C. Crystals of **12** were grown by vapor diffusion of hexane into a saturated solution of **12** in 1,2-difluoro benzene. The structures of **10** and **12** in the solid state are shown in Figure 11. Important ^{1}H and $^{29}Si\{^{1}H\}$ NMR resonances of the silanes **5 – 7** and **9** – **12** are summarized in Table 1.

Table 1. ^{1}H and $^{29}Si\{^{1}H\}$ NMR resonances of the silanes $Dipp_2NHSi(Cl)_2$ **8**[45], $Dipp_2NHSi(Br)_2$ **5**, $Dipp_2NHSi(I)_2$ **6**, $Dipp_2NHSi(Ph)_2$ **7**, $Dipp_2NHSi(I)(Me)$ **10**, $Dipp_2NHSi(Cl)$(benzyl) **11** and $Dipp_2NHSi(Br)$(benzyl) **12**.

Compound	δ (C*H*(CH_3)$_2$) [ppm]	δ (C*H*CH) [ppm]	δ (Si) [ppm]
$Dipp_2NHSi(Cl)_2$ **8**[45]	3.52	5.82	-38.1
$Dipp_2NHSi(Br)_2$ **5**	3.71	5.74	-59.3
$Dipp_2NHSi(I)_2$ **6**	3.76	5.77	-134.5
$Dipp_2NHSi(Ph)_2$ **7**	3.67	5.89	-23.9
$Dipp_2NHSi(I)(Me)$ **10**	3.37, 4.04	5.75	-30.4
$Dipp_2NHSi(Cl)$(benzyl) **11**	3.51, 3.92	5.74	-19.4
$Dipp_2NHSi(Br)$(benzyl) **12**	3.52, 3.98	5.76	-20.9

The silyl compounds **10** and **12** crystallize in the orthorhombic space groups Pnma and $P2_12_12_1$, respectively, and have an almost planar silylene ring with the silicon atom being bend out of the plane by 10.684(130) ° (**10**) and 10.416(343) ° (**12**). The halogen atoms in **10** and **12** have a more acute angle towards the plane generated by the five-membered silylene ring (**10**: 111.98(5) °, **12**: 112.92(14) °) than the methyl / benzyl group at the silicon atom (**10**: 118.82(7) °, **12**: 119.0(2) °). The crystal structure of the insertion product *t*Bu_2NHSi(I)(*N*-methylpiperidine) reported by Holl and co-workers was used for comparison to **10**. The silicon–iodine bond lengths are the same (**10**: Si–I 2.5220(6) Å, *t*Bu_2NHSi(I)(*N*-methylpiperidine): Si–I 2.5521(3) Å) and the silicon–carbon bond of **10** (Si–C2 1.858(2) Å) is slightly shorter than in the *tert*-butyl substituted compound *t*Bu_2NHSi(I)(*N*-methylpiperidine (Si–C11 1.9130(11) Å).

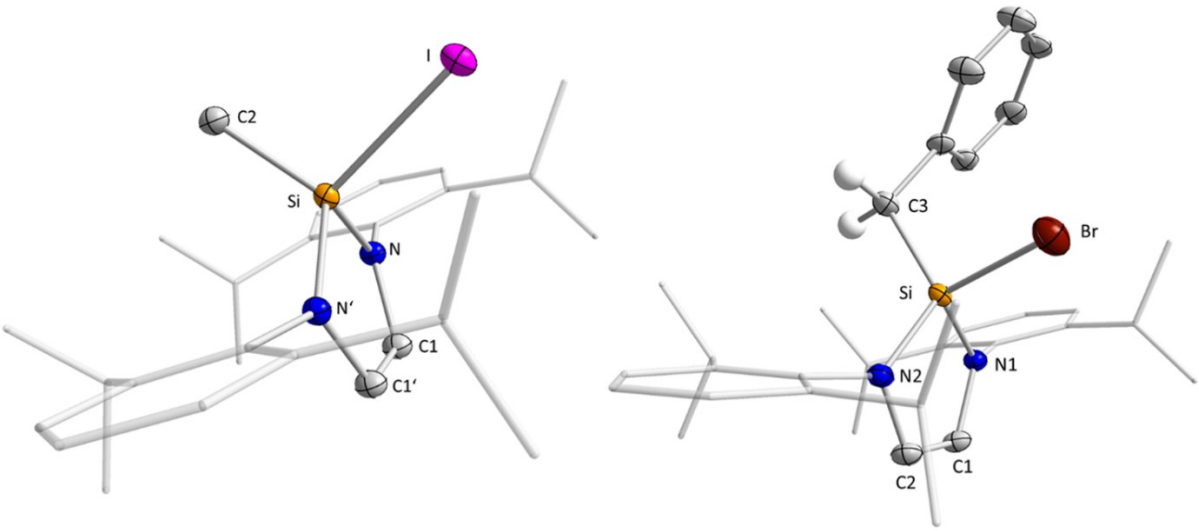

Figure 11. Molecular structure of $Dipp_2NHSi(I)(Me)$ (**10**) and $Dipp_2NHSi(Br)(benzyl)$ (**12**) in the solid state (ellipsoids drawn at the 50 % probability level; hydrogen atoms are omitted for clarity). Selected bond lengths [Å] and angles [°] of **10**: Si–N 1.7202(14), Si–I 2.5220(6), Si–C2 1.858(2), N–C1 1.420(2), C1–C1' 1.338(4), N–Si–N' 92.69(10), I–Si–C2 102.86(8), I–Si–N 111.98(5), C2–Si–N' 118.82(7), I–Si–N 111.98(5), C2–Si–N 118.82(7), (N–C1–C1'–N') / (N–Si–N') 10.684(130). Selected bond lengths [Å] and angles [°] of **12**: Si–N1 1.722(4), Si–N2 1.723(4), Si–C3 1.874(5), N–C1 1.423(6), C1–C2 1.323(7), C2–N2 1.416(6), N1–Si–N2 93.08(19) , Br–Si–C3 104.38(15), Br–Si–N1 112.92(14), Br–Si–N2 111.14(15), C3–Si–N1 116.5(2), C3–Si–N2 119.0(2), (N1–C1–C2–N2) / (N1–Si–N2) 10.416(343).

While C–Cl, C–Br and C–I bonds are readily activated by $Dipp_2NHSi$ (**1**), attempts to activate the C–F bond of fluorinated aryls using **1** were unsuccessful and only starting material was observed, even after prolonged heating. For NHCs and cAACs it has been shown previously that these carbenes activate and insert into C–F bonds of perfluorinated arenes[27, 51] or perfluorinated alkenes.[52] In these reactions, two different products have been observed: (i) insertion products into the carbon-fluorine bond[27, 51c, e, f, 52] and (ii) products from heterolytic C–F bond cleavage, especially in the presence of fluoride acceptors, which leads to arylation of the NHC and formation of a salt of the type $[R_2Im\text{-}aryl^F][X]$ ($X = F^-, HF_2^-, BF_4^-$).[51a, b, d] Arduengo *et al.* reported end of the 1990ies on C–Cl and C–I activation of chloro- and iodoalkanes.[53] If the backbone methylated carbene Me_2Im^{Me} was reacted with $CHClX_2$ (X = Cl, F) the

corresponding imidazolium salts [Me_2Im^{Me}-CHX_2][Cl] were formed.[53a] The saturated carbene Mes_2Im^{H2} reacts with CH_2Cl_2, CH_3I or CCl_4 to give the imidazolium salts [Mes_2Im^{H2}-CH_2Cl][Cl], [Mes_2Im^{H2}-CH_3][I] and [Mes_2Im^{H2}-Cl][Cl_3] as intermediates, which subsequently were transferred to the *N*-heterocyclic olefins (NHOs) Mes_2Im^{H2}=CHCl, Mes_2Im^{H2}=CH_2 and Mes_2Im^{H2}=CCl_2, respectively.[53b] Treatment of the unsaturated analogue Mes_2Im with carbon tetrachloride, on the other hand, led to substitution of the hydrogen atoms of the backbone of the NHC to give Mes_2Im^{Cl2}, which then reacts with CCl_4 to yield the salt [Mes_2Im^{Cl2}-Cl][Cl] and the NHO Mes_2Im^{Cl2}=CCl_2.[53b]

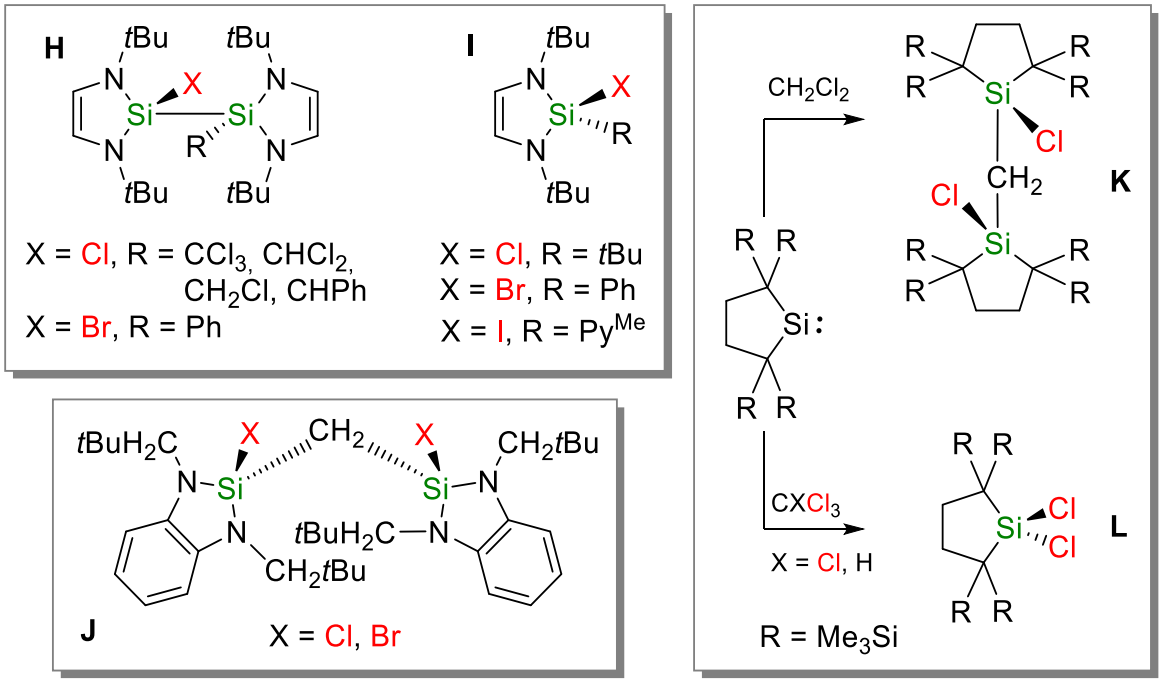

Figure 12. Examples for insertion reactions of *N*-heterocyclic silylenes into carbon–halogen bonds.

For *Arduengo*-type NHSis, a variety of examples are available for reactions of NHSis with organyl chlorides[24a, 54], bromides[54b] and iodides[24a, 55], but no studies on the reaction of NHSis with fluorocarbons have been presented so far. Roesky *et al.* and Sen *et al.* reported on the C–F activation of aryl fluorides using three coordinate silylenes PhC(N*t*Bu)$_2$SiR (R = N(SiMe$_3$)$_2$, Cl)[56] or the cyclic silylene CH[{(CH=CH$_2$)(CMe)-(Dipp)$_2$}Si,[57] which gave the insertion products PhC(N*t*Bu)$_2$Si(R)(F)(aryl^F) and CH[{(CH=CH$_2$)(CMe)-(Dipp)$_2$}Si(F)(aryl^F). As observed

for transition metal chemistry, most studies for NHSis have been conducted with the *tert*-butyl substituted NHSis *t*Bu$_2$NHSi and *t*Bu$_2$NHSi^{H2} as well as a benzannulated NHSi.[55a] These investigations reveal that *t*Bu$_2$NHSi and *t*Bu$_2$NHSi^{H2} react with a variety of chloro- or bromocarbons to yield the monosilanes **H**, disilanes **I** or mixtures of both, depending on the halocarbon and the stoichiometric ratio used (Figure 12, top left).[54b, c] Holl and co-workers reacted *t*Bu$_2$NHSi with phenyl iodide to obtain *t*Bu$_2$NHSi(I)(Ph), and subsequent addition of *N*-methyl piperidine led to the isolation of *t*Bu$_2$NHSi(I)(Py^{Me}) via a C–H activation in *ortho*-position of the piperidine nitrogen atom.[55b] Furthermore, it was shown that two molecules of the benzannulated, CH$_2$*t*Bu substituted silylene (*t*BuCH$_2$)$_2$NHSi^{benz} insert into the C–Cl (C–Br) bonds of dichloromethane or dibromomethane, respectively, to give the methylene bridged disilane **J** (Figure 12, bottom left).[55a] Dinuclear compounds **K** were also observed by Kira *et al.*, who reported studies on the reactivity of an isolable dialkylsilylene (Figure 12, right) towards halocarbons.[24a, 54a] Reaction of the dialkyl silylene with CHCl$_3$ and CCl$_4$ led to the exclusive formation of the oxidized silylene **L**, whereas the carbon–iodine insertion product was observed upon reaction with methyl iodide.[24a] For the aryl substituted stable NHSis Xyl$_2$NHSi, Mes$_2$NHSi and Dipp$_2$NHSi, no studies were reported so far concerning the reactivity towards halocarbons.

The reactivity of silylene **1** with compounds possessing an element–halide bond was investigated. The strong halophilic behaviour of silylenes was used to synthesize the dihalosilanes Dipp$_2$NHSiBr$_2$ (**5**) and Dipp$_2$NHSiI$_2$ (**6**) by treating **1** with elemental bromine or iodine. The dichloro compound Dipp$_2$NHSiCl$_2$ (**8**) was found to react with salt elimination with phenyl lithium to give the diphenyl silane Dipp$_2$NHSiPh$_2$ (**7**). NHSi **1** was reacted with the tin chlorides Ph$_2$SnCl$_2$ and Me$_3$SnCl which in both cases led to tin–chloride bond activation. In case of Ph$_2$SnCl$_2$, the oxidation product Dipp$_2$NHSiCl$_2$ (**8**) was isolated whereas the reaction with trimethyltin chloride resulted in cleavage of the silicon–nitrogen bonds of **1** giving distannyl diazabutene **9** and (Me$_3$Sn)SiCl$_3$. Furthermore, Dipp$_2$NHSi activates carbon–halide bonds giving the insertion products Dipp$_2$NHSi(I)(Me) (**10**), Dipp$_2$NHSi(Cl)(benzyl) (**11**) and Dipp$_2$NHSi(Br)(benzyl) (**12**), independently of the halide used. It could also be observed that the insertion reaction

was favoured over the formation of the dihalosilanes $Dipp_2NHSiCl_2$ (**8**), $Dipp_2NHSiBr_2$ (**5**) and $Dipp_2NHSiI_2$ (**6**).

2.2.3 $Dipp_2NHSi$ in azide chemistry

To further investigate the differences and similarities, $Dipp_2NHSi$ (**1**) was reacted with azides and the results were compared to the reaction products observed for NHCs. The first silatetrazoline was synthesized in 1978 by the oxidation of a silylated lithium hydrazide with tosyl azide.[58] In 1997, West and colleagues described the synthesis and structural studies on cyclic 1-sila-2,5-diaryltetrazenes which they obtained by the reaction of aryltetrazenes with an excess of a halosilane,[59] and several silatetrazolines have been reported to date.[60] The first stable silaimine was presented by Wiberg and co-workers in 1985.[61] *N*-heterocyclic silylene substituted silatetrazolines and silaimines have been observed as products of the reaction of *N*-heterocyclic silylenes with aryl azides.[62] In case of the Dipp substituted silylene **1**, only a few studies on the reactivity towards azides have been reported so far,[62c, g] and thus it was of interest to gain further insight into this field and to compare the results with the well examined NHSi *t*Bu_2NHSi.

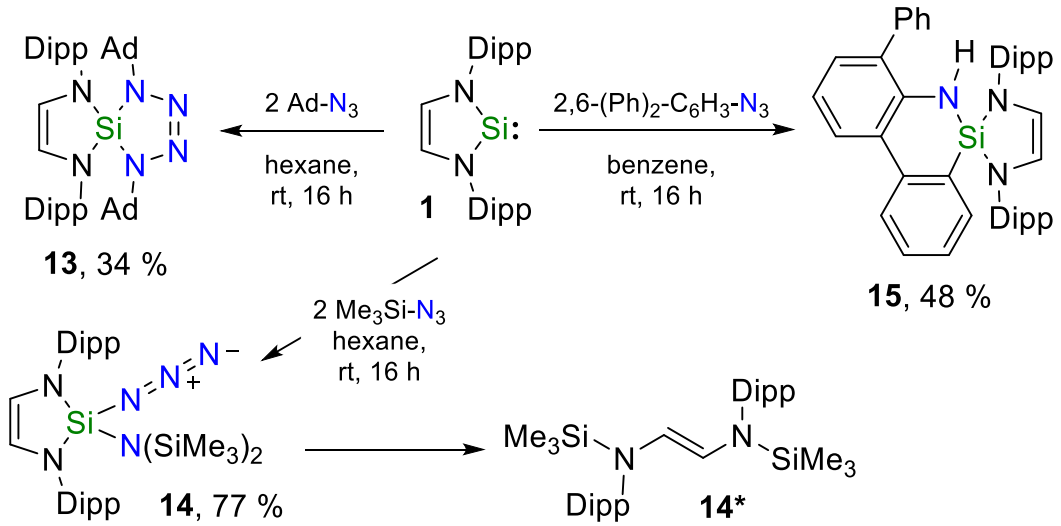

Scheme 9. Reaction of $Dipp_2NHSi$ with the azides Ad-N_3, Me_3Si-N_3 and 2,6-$(Ph)_2$-C_6H_3-N_3 giving the silatetrazoline 1-$Dipp_2NHSi$-2,5-bis(adamantyl)-tetrazoline (**13**), the azido silane (**14**), the degradation product **14*** and the cyclosilamine **15**.

The reaction of Dipp$_2$NHSi with two equivalents of adamantyl azide in hexane leads to the formation of a colourless solid which is insoluble in hexane and was identified as 1-Dipp$_2$NHSi-2,5-bis(adamantyl)-tetrazoline (**13**) by multinuclear NMR spectroscopy, single-crystal X-ray diffraction and elemental analysis (Scheme 9, left). In the ^{29}Si NMR spectra, the silylene silicon atom gives rise to a signal at -52.2 ppm (**13**) which is significantly shifted towards higher fields compared to Dipp$_2$NHSi (75.9 ppm). The methine protons give rise to one septet at 3.74 ppm, displaying the symmetry of the silatetrazoline. Single-crystals suitable for X-ray diffraction were grown by slow evaporation of a concentrated benzene solution of **13** at room temperature and the solid-state structure is shown in Figure 13.

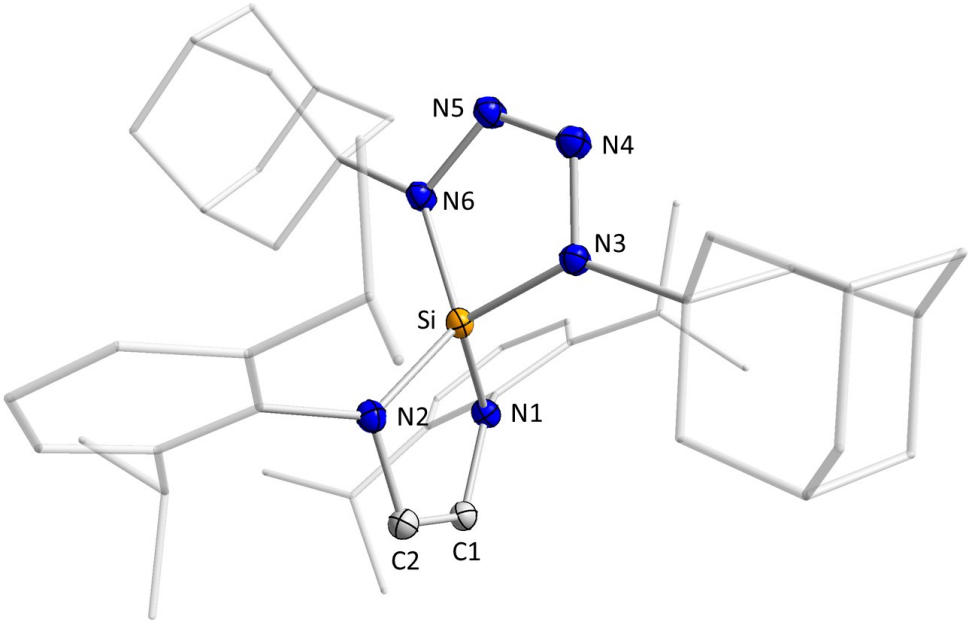

Figure 13. Molecular structure of 1-Dipp$_2$NHSi-2,5-bis(adamantyl)-tetrazoline (**13**) in the solid state (ellipsoids drawn at the 50 % probability level; hydrogen atoms are omitted for clarity). Selected bond lengths [Å] and angles [°] of **13**: Si–N1 1.7485(10), Si–N2 1.7433(10), N1–C1 1.4238(15), N2–C2 1.4269(15), C1–C2 1.3399(17), Si–N3 1.7559(10), Si–N6 1.7167(11), N3–N4 1.3823(14), N4–N5 1.2648(15), N5–N6 1.3926(14), N1–Si–N2 93.19(5), N1–Si–N3 118.58(5), N6–Si–N2 122.81(5), (N1–C1–C2–N2) / (N1–Si–N2) 21.496(58), (N1–Si–N2) / (N3–Si–N6) 88.606(45), (N3–N4–N5–N6) / (N3–Si–N6) 0.239(89).

Compound **13** crystallizes in the monoclinic space group $P2_1/c$ and consists of a spirocyclic ring system with the former silylene silicon atom being the spiro atom. The backbone-saturated *tert*-butyl silylenes *t*Bu$_2$NHSi^{tBu} and *t*Bu$_2$NHSi^{Me} which carry an additional *tert*-butyl or two methyl groups at one carbon atom of the backbone react with adamantyl azide to give the corresponding tetrazolines.[20b] The three tetrazolines show a nearly or perfectly perpendicular arrangement of the two rings (**13**: 88.606(45) °; *t*Bu$_2$NHSi^{tBu}: 87.391(71) °; *t*Bu$_2$NHSi^{Me}: 90.000(52) °). The nitrogen–nitrogen bond length of 1.3823(14) Å (N3–N4), 1.2648(15) Å (N4–N5) and 1.3926(14) Å (N5–N6) as well as the silicon–nitrogen bonds of 1.7167(11) – 1.7559(10) Å are in line with the compounds mentioned above. For NHCs, various examples are known for the reaction of *in situ* generated NHCs R$_2$Im (R = Me, *i*Pr, Mes) with alkyl and aryl azides, giving exclusively the respective mono-NHC triazines[63] and bis-NHC triazenyl imidazolium salts[64], and no NHC-tetrazolines have been observed. Lee and co-workers reported bis-NHC-supported triazenyl radicals which they obtained by reacting 2-chloroimidazolium chlorides with trimethylsilyl azide and subsequent reduction with elemental potassium.[65] A compound similar to **13** was published by Quast *et al.* who reported a 1,3-dipolar cycloaddition of a tetrazoline supported carbene with phenyl azide to give a spiro compound consisting of two five-membered rings (**M**). This closely resembles a cyclic NHC-tetrazoline.[66] Comparison of the solid state structures of **M** and **13** reveals very similar bond lengths for the nitrogen atoms in the tetrazole backbone (**13**: N3–N4 1.3823(14), N4–N5 1.2648(15), N5–N6 1.3926(14) Å; **M**: N1–N2 1.3847(31), N2–N3 1.2595(38), N3–N4 1.3743(29) Å) and the spiro angles of the two rings are also nearly identical (**13**: 88.606(45) °; **M**: 89.280(124) °). The carbon atom of the tetrazole ring of **M**, however, is bend out of the plane of the four nitrogen atoms by 12.819(138) °, whereas in **13**, the silicon atom and the nitrogen atoms are planar (0.239(89) °).

In contrast to the reaction of Dipp$_2$NHSi (**1**) with adamantyl azide (*vide supra*), the reaction of silylene **1** with one equivalent of trimethylsilyl azide in hexane resulted in a low yield conversion of **1** (Scheme 9, bottom). Using two equivalents of the azide, the bis(trimethylsilyl)amido azido silane Dipp$_2$NHSi(N(SiMe$_3$)$_2$)(N$_3$) (**14**) was isolated in good yields (77 %) as indicated by the ^{1}H, ^{29}Si and ^{13}C NMR spectra and elemental

analysis. For the *tert*-butyl NHSi *t*Bu$_2$NHSi, the analogous reaction was described by Denk *et al.* who observed the formation of a silaimine when using one equivalent of trimethylsilyl azide. Addition of a second equivalent then yielded the silyl azide *t*Bu$_2$NHSi(N(SiMe$_3$)$_2$)(N$_3$).[67] In the ^{29}Si NMR spectrum two signals are observed which can be assigned to the trimethylsilyl substituents (4.09 ppm) and to the former silylene silicon atom (**14**: -54.5 ppm; **13**: -52.2 ppm). In the ^{15}N-^{1}H HMBC NMR spectrum, the nitrogen atoms of the five-membered silylene heterocycle were observed at -299.4 ppm and the trimethylsilyl substituted nitrogen atoms of the amine substituent give rise to one signal at -327.5 ppm. The nitrogen atoms of the azide function was not observed.

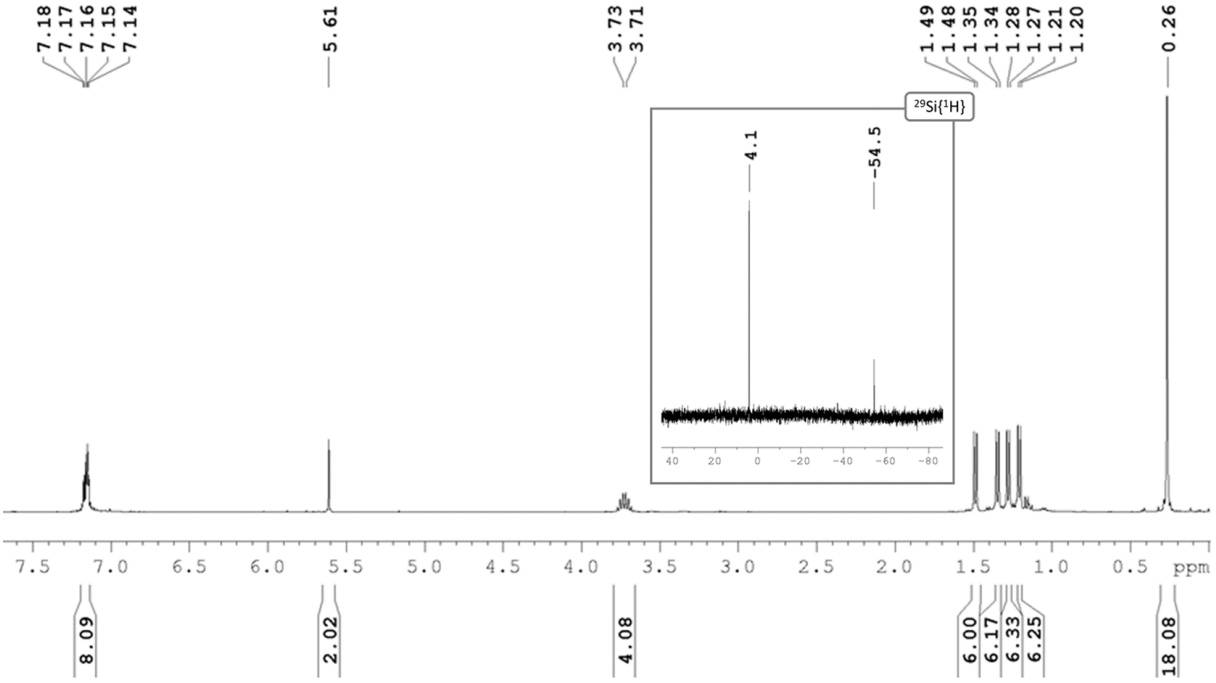

Figure 14. ^{1}H and ^{29}Si{^{1}H} NMR spectrum of azido silane **14**.

Single-crystals of **14** were obtained by storing a saturated hexane solution of **14** at -30 °C (Figure 11). Furthermore, several attempts to crystallize **14** afforded the degradation product **14*** by cleavage of the silicon–nitrogen bonds of the former silylene ring giving a diazabutene. Single-crystals of **14*** suitable for X-ray diffraction were grown by overlaying a saturated hexane solution of **14*** with acetonitrile and

storing the mixture at -30 °C and the solid state structure of the obtained colourless crystals is shown in Figure 15.

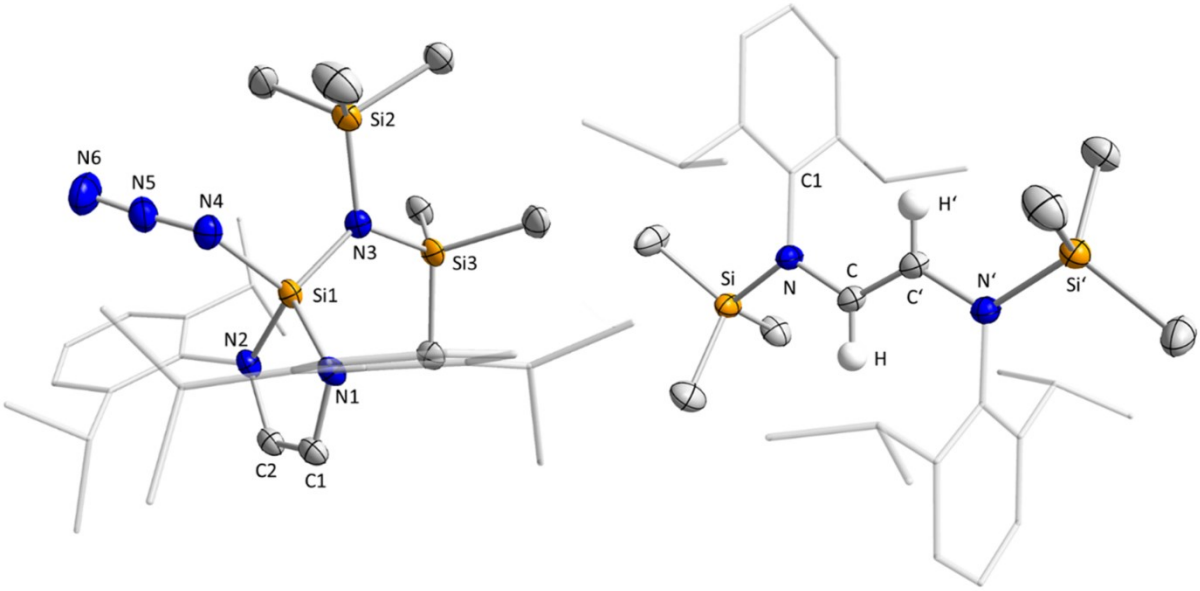

Figure 15. Molecular structure of the compounds **14** (left) and **14*** (right) in the solid state (ellipsoids drawn at the 50 % probability level; hydrogen atoms except the hydrogen atoms of the backbone are omitted for clarity). Selected bond lengths [Å] and angles [°] of **14**: Si1–N3 1.7246(14), Si1–N4 1.7480(15), N4–N5 1.222(2), N5–N6 1.136(2), N3–Si2 1.7693(14), N3–Si3 1.7765(14), C1–C2 1.327(2), Si1–N3–N4 104.22(7), Si2–N3–Si3 118.99(8), N1–Si1–N2 93.45(7). Selected bond lengths [Å] and angles [°] of **14***: Si–N 1.7479(12), N–C 1.4151(18), C–C' 1.333(3), Si–N–C 120.84(9), N–C–C' 125.81(16), Si–N–C1 121.99(9), C1–N–C 116.58(11), distance Si from (N–C–C'–N') 0.1240(4).

The silyl azide $Dipp_2NHSi(N(SiMe_3)_2)(N_3)$ (**14**) crystallizes in the triclinic space group $P\bar{1}$. The five-membered ring of the former silylene remains planar and the silicon atom is tetrahedrally coordinated by the nitrogen atoms of the NHSi ring, a bis(trimethylsilyl)amido and an azide group. The C–C bond length of the backbone of 1.327(2) Å is in accordance with a double bond.[48] The distance between the nitrogen atoms of the azido substituent are N4–N5 1.222(2) Å and N5–N6 1.136(2) Å and lie in the typical area of azide groups.[68] The crystal structure of **14*** shows a diazabutene, which is substituted by trimethylsilyl as well as Dipp groups at the nitrogen atoms. The

diazabutene backbone is, similarly to **9**, planar with the silicon atoms barely bend out of the plane (0.1240(4) Å). The distance between the carbon atoms of the former backbone of the silylene is C–C' 1.333(3) Å, which is in agreement with the value for a C=C double bond (1.34 Å).[48] The angles around the planar, sp^2-hybridized nitrogen atom are Si–N–C 120.84(9) °, Si–N–C1 121.99(9) ° and C1–N–C 116.58(11), and thus the sum of angles is 359.41 °.

While the reaction of $Dipp_2NHSi$ with adamantyl azide in the ratio 1:2 gave exclusively the corresponding silatetrazoline **13**, and with trimethysilyl azide the azido silane **14** and the decomposition product bis-silyl diazabutene **14*** were observed, the reaction of **1** with 2,6-(diphenyl)phenyl azide led to the C–H activation product **15** (Scheme 9, right). In the ^1H NMR spectrum, the resonances for the aryl groups of the nitrogen atoms of the silylene ring are split and two septets can be observed at 3.56 and 3.74 ppm, and the silicon atom was detected at -40.1 ppm in the ^{29}Si NMR spectrum. Compound **15** was isolated from hexane as a pale-yellow crystalline solid in 48 % yield and the sole formation of **15** was confirmed by elemental analysis. Presumably, a silaimine is formed initially which then undergoes a C–H activation to form the amine function as well as a silicon–carbon bond between the silicon atom and the *ortho*-carbon atom of one phenyl substituent of the former azide. X-ray diffraction was performed on single crystals of **15** grown by slow evaporation of a concentrated benzene solution of **15** at room temperature and the solid-state structure is shown in Figure 16.

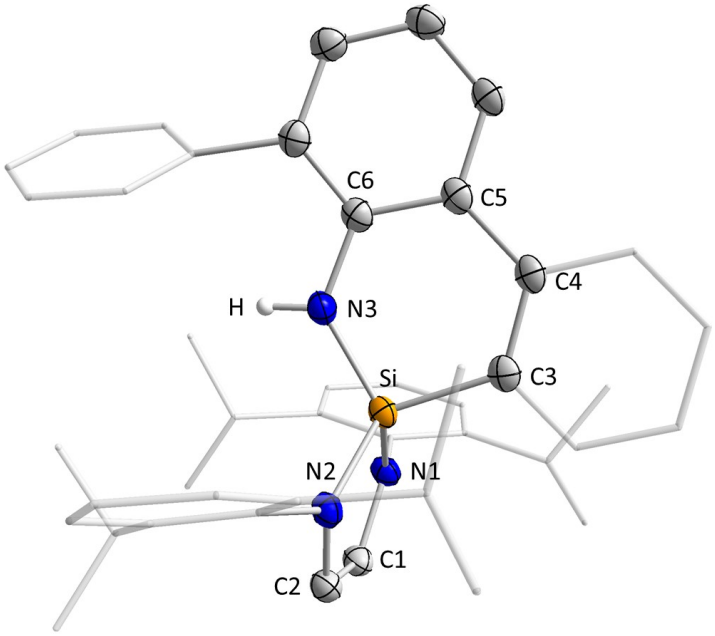

Figure 16. Molecular structure of cyclosilamine **15** in the solid state (ellipsoids drawn at the 50 % probability level; hydrogen atoms except the amine proton are omitted for clarity). Selected bond lengths [Å] and angles [°] of **15**: Si–N1 1.7372(16), Si–N2 1.7454(15), N1–C1 1.421(2), N2–C2 1.416(2), C1–C2 1.342(3), Si–C3 1.8366(19), Si–N3 1.7101(17), N3–H 0.85(3), C3–C4 1.412(3), C4–C5 1.487(3), C5–C6 1.428(2), C6–N3 1.408(2), N1–Si–N2 91.56(7), C3–Si–N1 112.30(8), N3–Si–N2 114.78(7), (N1–C1–C2–N2) / (N1–Si–N2) 6.855(101), (N1–Si–N2) / (C3–Si–N3) 85.579(79), (C3–C4–C5–C6–N3) / (C3–Si–N3) 5.789(77).

Like compound **13**, compound **15** is spirocyclic and crystallizes in the monoclinic space group $P2_1/c$. The two rings of the spiro system are the five-membered silylene ring and a newly formed six-membered ring made up of the silicon atom, the nitrogen atom of the azide and four carbon atoms of the (diphenyl)phenyl substituent of the azide. The rings are nearly perpendicular towards each other with an angle of 85.579(79) ° and the former silylene ring shows only a little bend of the silicon atom of 6.855(101) ° out of the plane.

The *N*-heterocyclic silylene **1** was treated with 1,3-dipolar compounds and was found to react with azides in different ways depending on the steric bulk of the azide (Scheme 9). Utilizing adamantyl azide, silatetrazoline **13** was isolated which was also observed for the *tert*-butyl silylene *t*Bu_2NHSi and *t*Bu_2NHSi^{H2}. The sterically less demanding trimethylsilyl azide afforded the silyl azide $Dipp_2$NHSi(N($SiMe_3$)$_2$)(N_3) (**14**) and its degradation product **14***. An interesting C–H activation was observed upon reacting 2,6-(diphenyl)phenyl azide with $Dipp_2$NHSi (**1**) which gave the cyclosilamine **15**.

Chapter II

N-Heterocyclic Silylenes as Ligands in Transition Metal Chemistry

3 *N*-Heterocyclic Silylenes as Ligands in Transition Metal Chemistry

3.1 Introduction

3.1.1 *N*-heterocyclic silylenes as ligands in transition metal chemistry

In the last decades, Arduengo-type *N*-heterocyclic carbenes (NHCs) have gained considerable interest as ligands in organometallic chemistry[69] and homogeneous catalysis.[70] Although the synthesis of the first stable isolable *N*-heterocyclic carbene[1] and *N*-heterocyclic silylene[6a] are only three years apart, considerably less *N*-heterocyclic silylene transition metal complexes have been prepared to date compared to *N*-heterocyclic carbenes complexes. In the following, the focus lies on the so called “Arduengo-type” *N*-heterocyclic silylenes (R_2NHSi) and an overview over the complexes reported to date is presented. The most studied *N*-heterocyclic silylenes in coordination and organometallic chemistry thus far are the backbone saturated and unsaturated *tert*-butyl substituted silylenes tBu$_2$NHSi^{H2} (**I**) and tBu$_2$NHSi (**II-*t*Bu**) and several transition metal complexes of **I** and **II-*t*Bu** are known. Benzannulated *N*-heterocyclic silylenes have been utilized for several years and a variety of complexes is known even though considerably less than for **I** and **II-*t*Bu**. *N*-aryl substituted *N*-heterocyclic silylene complexes bearing Mes$_2$NHSi and Dipp$_2$NHSi are considerably more scarce.

3.1.1.1 Transition metal complexes of tBu$_2$NHSi, tBu$_2$NHSi^{H2}

For the *tert*-butyl substituted NHSis tBu$_2$NHSi^{H2} (**I**) and tBu$_2$NHSi (**II-*t*Bu**), several heteroleptic transition metal carbonyl complexes have been reported, namely [M(L)$_2$(CO)$_4$] (M = Cr, Mo, W; L = tBu$_2$NHSi^{H2}, tBu$_2$NHSi), [Fe(tBu$_2$NHSi)(CO)$_4$], [Ru(tBu$_2$NHSi)$_2$(CO)$_3$] and [Ni(CO)$_2$(tBu$_2$NHSi)$_2$] (Figure 17).[71] Silylene ligated group 6 bent-metallocene complexes [(η^5-C$_5$H$_5$)$_2$M(H)(tBu$_2$NHSi)] (M = Mo, W) and [(η^5-C$_5$H$_5$)$_2$Mo(tBu$_2$NHSi)][72] have been prepared, which were obtained by irradiation or prolonged heating of a mixture of tBu$_2$NHSi and the metallocene dihydrides [(η^5-C$_5$H$_5$)$_2$M(H)$_2$], or from the reaction of the silylene with phosphine-stabilized

[(η^5-C_5H_5)$_2$Mo(PEt$_3$)].[72] Another representative of NHSi-stabilized bent-metallocene type complexes, and the only silylene lanthanide compound known to date, is [(η^5-C_5Me_5)$_2$Sm(*t*Bu$_2$NHSi)], which is seemingly not especially stable, as the silylene ligand is easily substituted by THF giving [(η^5-C_5Me_5)$_2$Sm(THF)$_2$].[73]

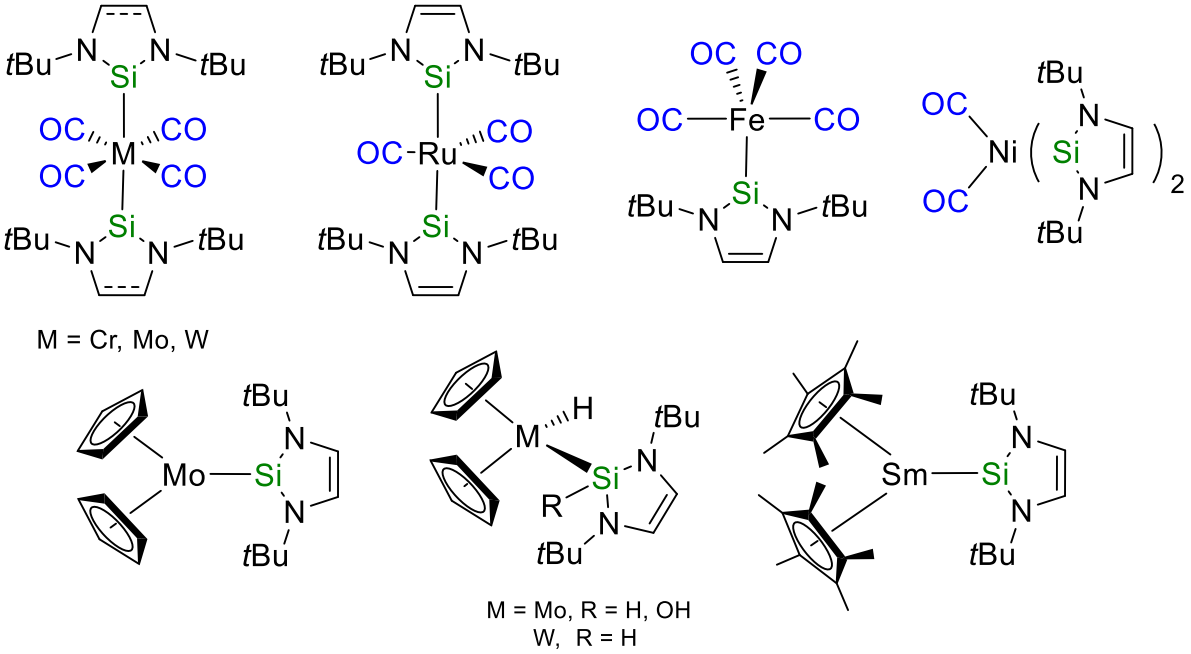

Figure 17. Metal(0) carbonyl and bent-metallocene complexes of the *N*-heterocyclic silylenes *t*Bu$_2$NHSi^{H2} (**I**) and *t*Bu$_2$NHSi (**II-tBu**).

With the d^8 and d^9 metals ruthenium and rhodium, a variety of compounds has been prepared (Figure 18). Hill and co-workers reported the coordinatively unsaturated compound [Ru(PCy$_3$)$_2$(H)(Cl)(*t*Bu$_2$NHSi)], obtained by replacement of the η^2-bound dihydrogen ligand in [Ru(PCy$_3$)$_2$(η^2-H$_2$)(H)(Cl)] with the silylene.[74] Interestingly, this reaction did not occur if the mesityl carbene Mes$_2$Im was used, as, in this case, a phosphine ligand is replaced to form [Ru(PCy$_3$)(Mes$_2$Im)(η^2-H$_2$)(H)(Cl)].[74] The complex [(η^5-C_5Me_5)Ru(*t*Bu$_2$NHSi)(Cl)] was obtained from the reaction of *t*Bu$_2$NHSi with tetranuclear [(η^5-C_5Me_5)Ru(μ-Cl)]$_4$. This mononuclear Ru complex was subsequently converted into dinuclear [{(η^5-C_5Me_5)$_2$Ru}$_2$(H)(μ-H)(μ,η^2-HSiRCl)(μ-Cl)(μ,η^2-*t*Bu$_2$NHSi)] (R = Ph, *n*hexyl, Figure 18) upon reaction with primary silanes.[74]

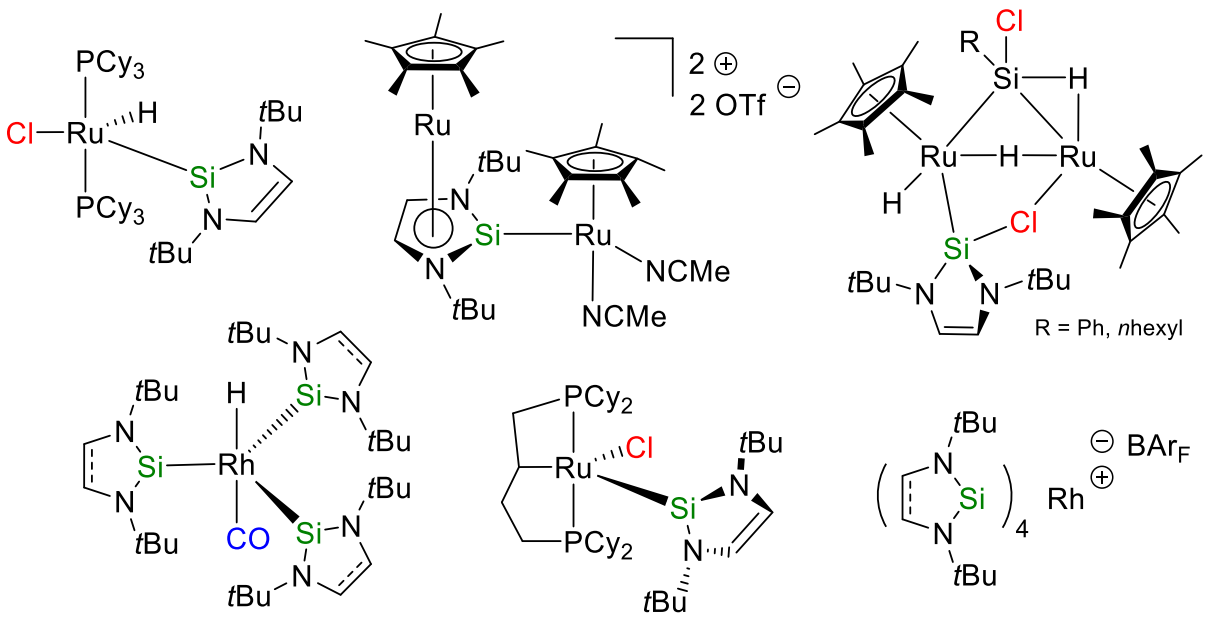

Figure 18. Neutral and ionic ruthenium and rhodium complexes of the *N*-heterocyclic silylenes *t*Bu$_2$NHSi^{H2} (**I**) and *t*Bu$_2$NHSi (**II-tBu**).

Furthermore, the ionic complex [(η^5-C$_5$Me$_5$)Ru(NCMe)$_3$][OTf] cleanly reacts with *t*Bu$_2$NHSi to afford [(η^5-C$_5$Me$_5$)Ru(NCMe)$_2$(*t*Bu$_2$NHSi)][OTf] and the solvation of this complex in THF afforded [(η^5-C$_5$Me$_5$)Ru(η^5:η^1-*t*Bu$_2$NHSi)Ru(η^5-C$_5$Me$_5$)(NCMe)$_2$][OTf]$_2$ featuring an interesting η^5:η^1-silylene ligand.[75] Another NHSi representative in Ru chemistry is the coordinatively unsaturated compound [Ru(η^3-dcypb)(Cl)(*t*Bu$_2$NHSi^{H2})] (dcypb = bis(dicyclohexyl)-1,4-phosphinobutane) which reacts promptly with small molecules such as H$_2$O, H$_2$ and CO.[76] The Rh complex [Rh(PPh$_3$)$_3$(H)(CO)] reacts with three equivalents of *t*Bu$_2$NHSi to give [Rh(H)(CO)(*t*Bu$_2$NHSi)$_3$].[77] The cationic Rh(I) compounds [Rh(L)$_4$][BAr^F] (L = *t*Bu$_2$NHSi^{H2} (**I**) *t*Bu$_2$NHSi (**II-tBu**)) were obtained by treatment of [Rh(cod)$_2$][BAr^F] (BAr^F = tetrakis(3,5-bis(trifluoromethyl)phenyl)borate; cod = 1,5-cyclooctadiene) with four equivalents of **I** or **II-*t*Bu** in hexane.[78]

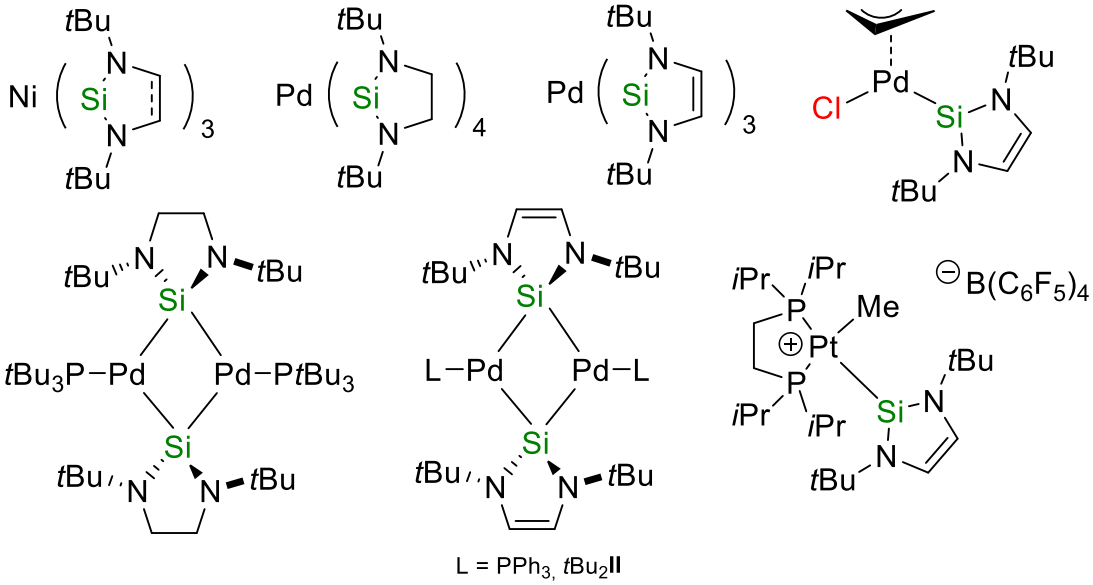

Figure 19. Neutral and ionic group 10 complexes of the *N*-heterocyclic silylenes *t*Bu$_2$NHSi^{H2} (**I**) and *t*Bu$_2$NHSi (**II-tBu**).

For the d^{10} metals Ni, Pd and Pt, a variety of NHSi complexes are known (Figure 19). Substitution of both cod ligands of [Ni(cod)$_2$] by *t*Bu$_2$NHSi^{H2} / *t*Bu$_2$NHSi (= L) in THF results in the formation of the homoleptic, trigonal planar complex [Ni(L)$_3$].[79] The allyl Pd complex [Pd(η^3-C$_3$H$_5$)(*t*Bu$_2$NHSi)(Cl)],[80] and the phosphine-stabilized silylene-bridged dimeric Pd(0) compound [Pd(PPh$_3$)(*t*Bu$_2$NHSi)]$_2$[81] are two examples of Pd NHSi complexes. The reaction of [Pd(P*t*Bu$_3$)$_2$] with *t*Bu$_2$NHSi^{H2} affords the homoleptic four-coordinate Pd(0) complex [Pd(*t*Bu$_2$NHSi^{H2})$_4$], which forms a dinuclear silylene-bridged Pd(0) complex with one phosphine at each palladium centre upon addition of P*t*Bu$_3$. Loss of two *t*Bu$_2$NHSi ligands led to the formation of a dinuclear silylene-bridged Pd(0) compound, which was further stabilized by one silylene ligand at each Pd centre. Reaction of [Pd(cod)(CH$_3$)$_2$] with six equivalents of *t*Bu$_2$NHSi^{H2} or four equivalents of *t*Bu$_2$NHSi also afforded [Pd(*t*Bu$_2$NHSi^{H2})$_4$] and [Pd(*t*Bu$_2$NHSi)$_3$], while two NHSis were consumed during the reduction of the Pd(II) precursor giving a methylated disilane from *t*Bu$_2$NHSi^{H2} or *t*Bu$_2$NHSi(CH$_3$)$_2$, respectively.[82] Element–hydrogen bond activation at a cationic platinum compound and subsequent addition of the silylene gives the complex [Pt(dippe)Me(*t*Bu$_2$NHSi)][B(C$_6$F$_5$)$_4$] (dippe = 1,2-bis(di-*iso*propylphosphino)ethane).[83]

3.1.1.2 Transition metal complexes of *N*-aryl *N*-heterocyclic silylenes

Most of the coordination chemistry of *N*-heterocyclic silylenes has been investigated using the *tert*-butyl substituted derivatives *t*Bu$_2$NHSi^{H2} and *t*Bu$_2$NHSi, as summarized above. For other silylenes, for example *N*-aryl substituted systems, only a few transition metal complexes are known (Figure 20).

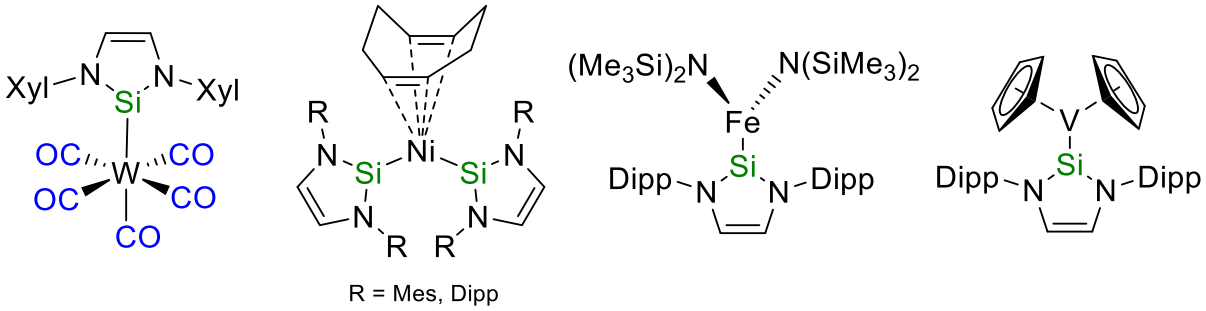

Figure 20. Transition metal complexes bearing *N*-aryl substituted *N*-heterocyclic silylenes Xyl$_2$NHSi, Mes$_2$NHSi and Dipp$_2$NHSi.

The only transition metal complex with Xyl$_2$NHSi is [W(CO)$_5$(Xyl$_2$NHSi)] which was synthesized via irradiation of [W(CO)$_6$] in THF and subsequent addition of the silylene.[6f] The number of transition metal complexes bearing Mes$_2$NHSi is limited to the heteroleptic Ni(0) complex [Ni(cod)(Mes$_2$NHSi)$_2$], for which the Dipp$_2$NHSi analogue [Ni(cod)(Dipp$_2$NHSi)$_2$] is also known. Substitution of the cod ligand by a third silylene, as observed for *t*Bu$_2$NHSi^{H2} and *t*Bu$_2$NHSi, was not successful.[6e] For the Dipp-substituted silylene, more examples exist, e. g. a three-coordinate iron(II) silylene complex [Fe(N(SiMe$_3$)$_2$)$_2$(Dipp$_2$NHSi)] reported by Layfield *et al*.[84] Another interesting example is the complex [(η^5-C$_5$H$_5$)$_2$V(Dipp$_2$NHSi)], which was obtained by reaction of the silylene with vanadocene, as it was not possible to obtain the analogous product from the corresponding carbene Dipp$_2$Im.[85]

3.1.1.3 Transition metal complexes of benzannulated *N*-heterocyclic silylenes

The homoleptic nickel complex [Ni(Np_2NHSi^{benz})$_4$] can be obtained by the reaction of [Ni(cod)$_2$] with a four-fold excess of the benzannulated silylene Np_2NHSi^{benz} or by treating [$NiCl_2(PPh_3)_2$] with a five-fold excess of the free silylene with one silylene molecule acting as a reducing agent to give $Np_2NHSi^{benz}(Cl)_2$. If [$NiCl_2(PPh_3)_2$] is reacted with four equivalents of the silylene the formation of the heteroleptic complex [Ni(PPh_3)(Np_2NHSi^{benz})$_3$] and the dichlorosilane $Np_2NHSi^{benz}(Cl)_2$ is observed (Figure 21).[86] Interestingly, the analogue reaction of four equivalents of the silylene with [$MCl_2(PPh_3)_2$] (M = Pd, Pt) afforded the M–Cl insertion products [{M(Np_2NHSi^{benz})(Np_2NHSi^{benz}-Cl)}$_2$] (M = Pd, Pt, R = CH_2tBu) which bear two silylene and two silyl ligands.[86-87] The reaction of the homoleptic Pt(0) complex [$Pt(PPh_3)_4$] with the NHSi yields the phosphine stabilized platinum complex [Pt(PPh_3)(Np_2NHSi^{benz})$_3$] by substitution of three phosphine ligands.[87] In contrast to the before-mentioned insertion of the silylene silicon atom into metal–halide bonds, the silylene does not act as a reducing agent in the reaction of [Cu(PPh_3)$_3$(I)] with Np_2NHSi^{benz} and solely gives the mono-silylene complex [Cu(PPh_3)$_2$(Np_2NHSi^{benz})(I)].[87]

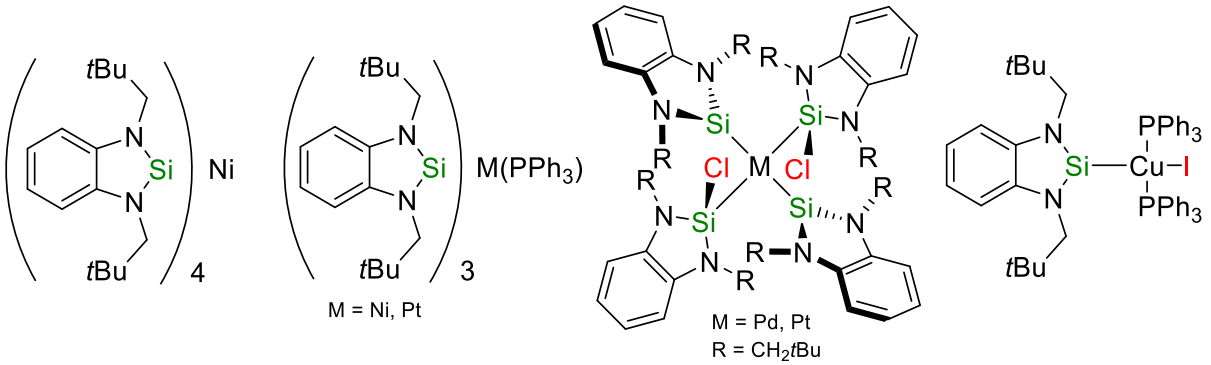

Figure 21. Complexes of d^{10} and d^{11} transition metals and benzannulated *N*-heterocyclic silylenes **III**.

Berry *et al.* reported the reaction of the chlorosilane Np_2NHSi^{benz}(H)(Cl) with a pyridine derivative (py^{N2}) stabilized ruthenium complex yielding the Ru(II) complex [Ru(py^{N2})(Np_2NHSi^{benz})(H)(Cl)] by a Si–H and Si–Cl activation (Figure 22).[88] A THF

solution of this compound is slowly converted to the silylene dinitrogen ruthenium complex [Ru(N_2)(py^{N2})(Np_2NHSi^{benz})] upon reaction with a Ru(0) complex under a nitrogen atmosphere.

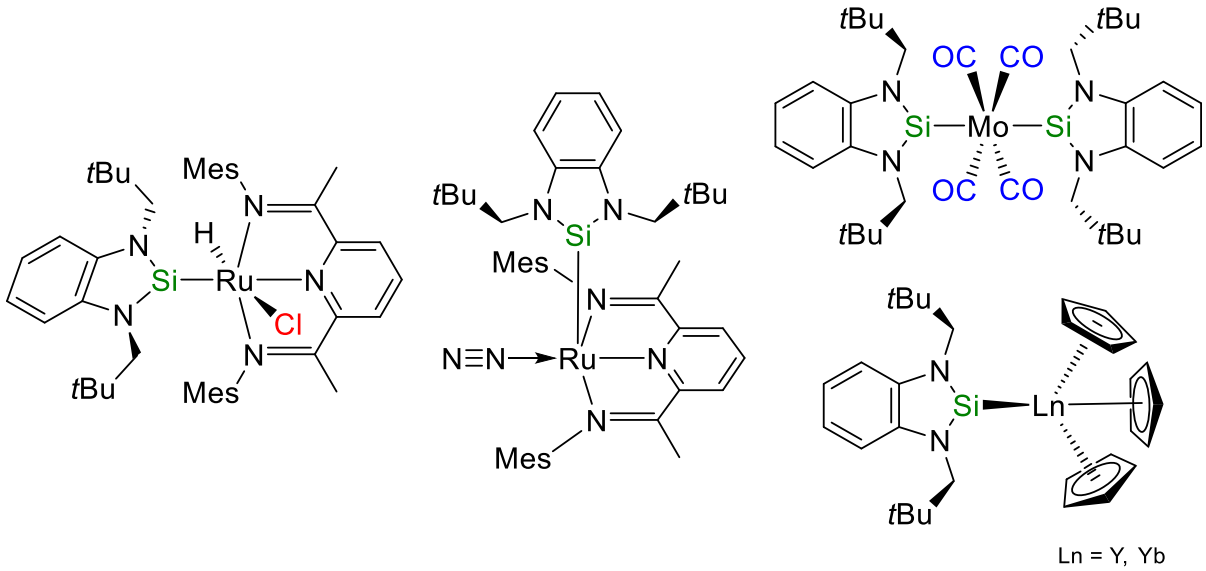

Figure 22. Complexes of benzannulated *N*-heterocyclic silylenes **III** with ruthenium, molybdenum and the early transition metals yttrium and ytterbium.

The early transition metal complex [$Mo(CO)_4(Np_2NHSi^{benz})_2$] is obtained by treating [$Mo(CO)_4$(nbd)] (nbd = norbornadiene) with the [1+4] cycloadduct obtained by reacting the triphosphabenzene $P_3C_3(tBu)_3$ with the neopentyl-substituted silylene Np_2NHSi^{benz}.[89] Similarly to the *tert*-butyl NHSi tBu_2NHSi, the number of lanthanide complexes of R_2NHSi^{benz} is very limited, namely the cyclopentadienyl complexes [(η^5-$C_5H_5)_3$Ln(Np_2NHSi^{benz})] (Ln = Y, Yb) which were synthesized by reacting an excess of the silylene ligand with [(η^5-$C_5H_5)_3$Ln] at room temperature.[90]

3.1.2 Coordination modes and halophilic behaviour of *N*-heterocyclic silylenes in transition metal chemistry

It has been shown that NHCs and NHSis adopt different coordination modes upon reaction with transition metal complexes (Figure 23). The most common coordination

mode is the *end-on* η^1-coordination of the NHC[69-70, 91] or NHSi[6e, g, j, 92] *via* coordination of the carbene carbon or silylene silicon atom to the metal centre and a multitude of transition metal complexes with terminal NHC and NHSi ligands have been observed so far (Figure 23, top left). It should be noted that NHCs coordinate almost exclusively and NHSis very often in a terminal mode. Some early examples for structurally characterized complexes with terminal NHC ligands are the cationic mercury complex $[Hg(Ph_2Im)_2][ClO_4]_2$[93] (Ph_2Im = 1,3-diphenylimidazolin-2-ylidene) and the phosphine stabilized complex *trans*-$[Pt(PEt_3)(Ph_2Im)(Cl)_2]$[94] reported in 1971 by Luger *et al.* and Lappert *et al.*, or the alkylidene amido complex $[Ni(Me_2Im^{H2})(PPh_3)_2(N{=}C(CF_3)_2)]$[95] ($Me_2Im^{H2}$ = 1,3-dimethylimidazolidin-2-ylidene) reported 1974 by Lappert *et al*.

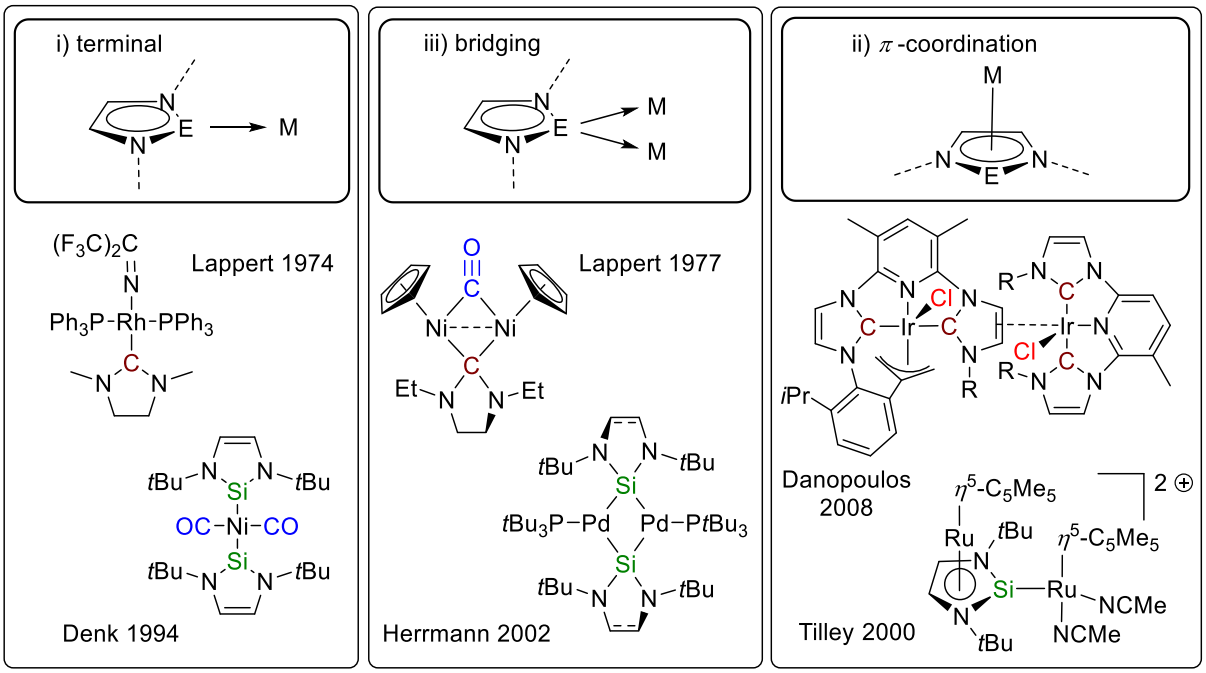

Figure 23. Coordination modes of *N*-heterocyclic carbenes and silylenes (E = C, Si).

In 1994 Denk *et al*. reported on the first structurally characterized NHSi complexes $[Ni(CO)_2(tBu_2NHSi)_2]$.[71a] Another interesting example was presented by Jutzi *et al.* in 1999 for the bent metallocenes $[(\eta^5\text{-}C_5H_5)_2M(tBu_2NHSi\text{-}H)(H)]$ (M = Mo, W), [72] in which the NHSi ligand inserts into the metal–hydride bond. There are also reports that NHCs and NHSis can act as bridging ligands between two metal centres (Figure 23, middle), although, compared to the *end-on* coordination, only few examples for a bridging coordination mode of NHCs are known so far.[96] It should be noted that the majority of

the NHC-bridged complexes is known for the coinage metals. Furthermore, the bridging coordination mode of NHCs has also been observed for the group 1 metal lithium as demonstrated by Arnold and Siebert.[97] The first example of a complex with a bridging NHC ligand was reported in 1977 by Lappert and co-workers who synthesized the dinuclear NHC-bridged nickel complex $[Ni_2(\mu\text{-}CO)(\eta^5\text{-}C_5H_5)_2(\mu\text{-}Et_2Im^{H2})]$ (Figure 23) by reacting nickelocene with $[Ni(CO)_3(Et_2Im^{H2})]$.[98] Nolan *et al.* reported the copper complexes $[Cu_6(Cy_2Im)_4(Br)_6]$ and $[\{Cu(Cy_2Im)(I)\}_3]$ (Cy = cyclohexyl), which both feature bridging as well as *end-on* coordinating NHC ligands.[96h] For *N*-heterocyclic silylenes, the bridging coordination mode of the silicon atom is observed significantly more often than for *N*-heterocyclic carbenes. In 2001, Fürstner and co-workers and in 2002 Herrmann *et al*. reported the neutral palladium complexes $[\{Pd(PPh_3)(\mu\text{-}t Bu_2NHSi)\}_2]$[81], $[\{Pd(L)(\mu\text{-}t Bu_2NHSi)\}_2]$ (L = P*t*Bu$_3$, *t*Bu$_2$NHSi) and $[\{Pd(L)(\mu\text{-}t Bu_2NHSi^{H2})\}_2]$[82] which all carry the motif of a bridging NHSi.

The rarest coordination mode for NHC and NHSi ligands is *π*-coordination. For NHCs, no structurally characterized examples are currently available in which the imidazolium core of the NHC binds to a transition metal with the *π*-system in a η^5-coordination mode. However, η^2- or η^6-coordination of the metal atom to the arene substituents at the NHC imidazoline nitrogen atoms is rather common, as observed, for example, for the low-valent, dinuclear NHC complexes $[\{M(Ar_2Im)\}_2]$[99] (Ar = Mes, M = Fe; Ar = Dipp, M = Co, Ni) and $[\{Ir(H)(Dipp_2Im)\}_2][BF_4]_2$,[100] in which each NHC ligand is *end-on* coordinated to the metal centre and one of the aryl substituents is attached *via* the *π*-system to the adjacent metal atom.[99b] Another example is the arene masked nickel silyl complex $[Ni(\eta^6\text{-}Dipp_2Im)SiCl_2(Si(SiMe_3)_2Me)]$ which also bears a NHC with an η^6-coordinated arene substituent.[101] In contrast to the quite often observed η^6-coordination, the η^2-coordination of NHCs has been observed only once. Danopoulos and co-workers described the cationic bimetallic iridium complex $[Ir_2(C_{NHC}\text{-}N^{Me}\text{-}C_{NHC})(\mu\text{-}\eta^1\text{:}\eta^2\text{-}C_{NHC}\text{-}N^{Me}\text{-}C_{NHC})(Cl)_2][PF_6]$[102] ($C_{NHC}$-$N^{Me}$-$C_{NHC}$ = 2,6-bis-(3-(2,6-di*iso*propylphenyl)imidazolin-2-ylidene)-3,5-dimethyl-pyridine) consisting of two iridium moieties which are connected by a pyridine-dicarbene pincer ligand that is η^2-coordinated to the second iridium atom *via* the unsaturated backbone (Figure 23,

right). A similar example bearing a bridging imidazoline ligand was reported by Suzuki *et al.* who synthesized the dinuclear ruthenium complex [(η^5-C_5Me_5)Ru_2(μ-H)$_2$(μ-η^1:η^2-*t*Bu_2ImH_2)].[103] The former carbene ligand is bound to the ruthenium atoms *via* one of the nitrogen atoms and the unsaturated backbone of the imidazoline ring. The π-coordination of the central five-membered ring has also been observed for a NHSi ligand. Tilley and co-workers reported the isolation of the diruthenium complex [{Ru(η^5-C_5Me_5)}(μ-η^1,η^5-*t*Bu_2NHSi){Ru(η^5-C_5Me_5)(NCMe)$_2$}][OTf] in which two ruthenium centres are bridged by a η^1:η^5-coordinating NHSi ligand.[75]

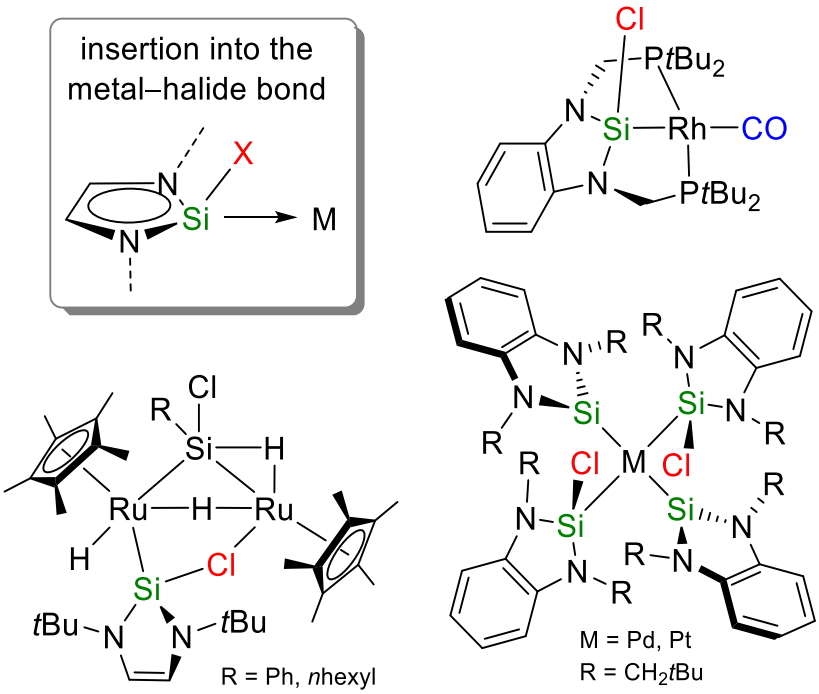

Figure 24. *N*-heterocyclic silylenes in halide complexes - insertion into the metal–halide bond.

The strong halophilicity of *N*-heterocyclic silylenes has been shown in depth in Chapter 1. This behaviour has also been observed in transition metal chemistry.[34, 49, 54b, c, 55b, 75, 104] A thorough search of the relevant literature yielded no halide transition metal complexes featuring a *N*-heterocyclic silylene which interacts with the halide ligand without inserting into the metal–halide bond. Complete insertion of the NHSi ligand into a metal–halide bond, on the other hand, has been reported more often (Figure 24). In addition to the before-mentioned chloro-silyl bridged diruthenium complex by Tilley *et*

al. (Figure 18)[75] and the complexes [{M(R_2NHSi^{benz})(R_2NHSi^{benz}-Cl)}$_2$] (M = Pd, Pt, R = CH_2*t*Bu) by Lappert *et al.* (Figure 21)[86-87], the chlorosilyl pincer complex [Rh(CO)((*t*Bu$_2$PCH$_2$)$_2$NHSi^{benz}-Cl)] was isolated from the reaction of the proligand (*t*Bu$_2$PCH$_2$)$_2$NHSi^{benz}(H)$_2$ with [Rh(CO)(PPh$_3$)$_2$(Cl)] *via* chloride migration and Si–H activation.[105]

3.2 Results and Discussion

3.2.1 Comparison of the frontier orbitals of *N*-heterocyclic silylenes and carbenes

First, the frontier orbitals suitable for coordination of the NHSi ligand with those of the NHC-type ligands are compared. DFT calculations (def2-TZVPP/B3LYP) were performed on the *N*-methyl substituted model Me_2NHSi (1,3-dimethyl-1,3-diaza-2-silacyclopent-4-ene-2-ylidene) and its NHC analogue and the molecular orbitals of these molecules and their energies are shown in Figure 25. For this purpose it is instructive to recall the main electronic features of the NHC 1,3-dimethylimidazolin-2-ylidene (Figure 25, left).[5] A quantitative MO analysis reveals that the frontier orbitals of 1,3-dimethylimidazolin-2-ylidene may be considered as those of a 6 π-electron aromatic system, superimposed on the carbene σ-type orbital $12a_1$ at -5.74 eV, which is the HOMO of the molecule. The orbitals $2b_1$, $2a_2$, $3b_1$, $3a_2$ and $4b_1$, similar to those of the well-known cyclopentadienyl anion, are the occupied orbitals of the π-system and have no nodal plane (orbital $2b_1$ in C_{2v} symmetry, at -10.26 eV) or one nodal plane ($2a_2$, -7.41 eV and $3b_1$, -6.25 eV), whereas the unoccupied π-orbitals ($3a_2$, +0.57 eV and $4b_1$, +1.08 eV) have two nodal planes. These pairs of orbitals are not degenerate due to the heteroatomic substitution of the aromatic ring and thus C_{2v} symmetry. The $4b_1$ (LUMO+1, +1.08 eV) orbital is mainly centred at the carbene carbon atom and is mostly composed of the carbene p_x-orbital (62%), while for the $3b_1$ orbital the p_x contribution is lower (22%, based on gross Mulliken contributions of AOs to the MOs). The HOMO of Me_2Im is the $12a_1$ orbital at -5.74 eV, usually referred to as the carbene σ-orbital, which contains carbene carbon p_z (49%) and s (33%) character. Within the level of theory, an energy gap of 6.82 eV between $12a_1$ and $4b_1$ is calculated.

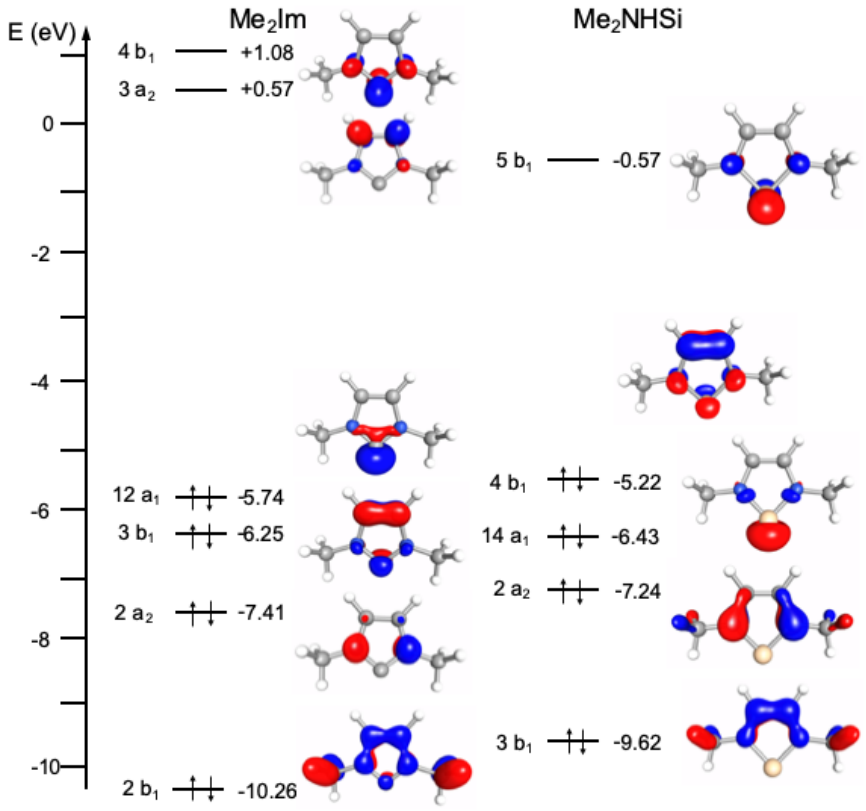

Figure 25. Main electronic features of 1,3-dimethylimidazolin-2-ylidene Me_2Im (left side) and the corresponding silylene equivalent Me_2NHSi (right side). Energies were calculated at the DFT/def2-TZVPP/B3LYP level of theory, and orbital plots are drawn at the 0.1 isosurface.

The frontier orbitals of Me_2NHSi differ considerably from those of the corresponding NHC. First, the order of the orbitals changes, as the HOMO of Me_2NHSi is not the silylene σ-orbital, but the $4b_1$ orbital, which should be weakly π-donating upon coordination to a transition metal. However, as the silicon p_x contribution is low (24%) for this orbital, the overlap of $4b_1$ with a metal centred d_π-type orbital should be rather small. The silylene σ-orbital $14a_1$ at -6.43 eV lies at much lower energy compared to the carbene σ-orbital $12a_1$ at -5.74 eV of Me_2Im and also has much more s character (48% s and 32% p_z for Me_2NHSi vs. 33% s and 49 % p_z for Me_2Im) compared to the NHC. According to the compositions and the orbital energies, one would expect that the NHSi is a much weaker σ-donor ligand compared to an NHC. On the other hand, the π-accepting orbital $5b_1$ lies much lower in energy than $4b_1$ of the NHC and has a much larger p_x contribution (76% for NHSi vs. 62% for NHC), which would be in line

with much better *π*-accepting properties of the NHSi ligand. The important frontier orbitals of the NHSis Dipp$_2$NHSi and Me$_2$NHSi with respect to those of commonly used NHC ligands are shown in Figure 26. The typical features, a *π*-donor HOMO such as 4b$_1$, a reverse orbital order of 4b$_1$ and the silylene *σ*-orbital 14a$_1$, which lies energetically much lower compared to the carbene *σ*-type orbital, and an energetically low lying *π*-acceptor orbital can also be found for the 2,6-di*iso*propyl-phenyl substituted Dipp$_2$NHSi (Figure 26).

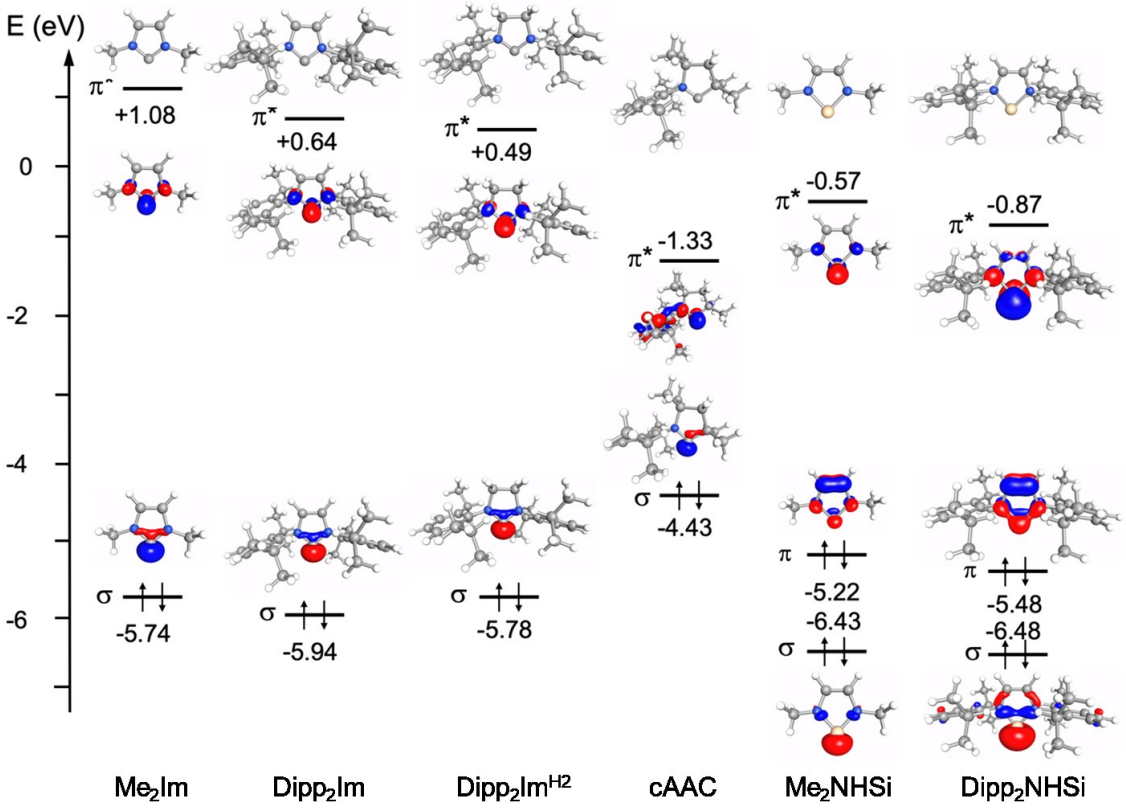

Figure 26. Important frontier orbitals of the NHSis Dipp$_2$NHSi and Me$_2$NHSi with respect to those of commonly used NHC ligands Me$_2$Im, Dipp$_2$Im, Dipp$_2$Im^{H2} and cAAC^{Me}. Energies were calculated at the DFT/def2-TZVPP/B3-LYP-D3(BJ) level of theory, orbital plots are drawn at the 0.1 isosurface.

3.2.2 Dipp$_2$NHSi as a 2-electron donor

The nature of the chemical bond between a transition metal and a carbene fragment CR$_2$ drew the attention of theoreticians soon after the first stable transition metal

carbene complex [Cr(CO)$_5${C(OMe)(Me)}] was reported in 1964 by Fischer and Maasböl.[106] Carbene complexes became particularly interesting for theoretical analyses when experimental studies suggested that there are two categories of transition metal carbene complexes which show very different properties, namely "Fischer-type" complexes,[107] which are characterized by a *π*-donor group X at the carbene ligand bound to a transition metal in a low oxidation state, and "Schrock-type" carbene complexes,[108] which have nucleophilic carbene ligands typically with hydrogen, alkyl, or aryl groups, but no *π*-donor substituents at the carbene carbon atom. For historical reasons, calculations on "Fischer"-type carbene complexes have been carried out on group 6 carbonyl complexes [M(CO)$_5$(CR$_2$)], especially those of tungsten.[109] Subsequently, the bonding of many other neutral 2-electron donor ligands was theoretically investigated with respect to the [W(CO)$_5$] complex fragment in complexes of the type [W(CO)$_5$(L)].[110] NHCs and related molecules are "Fischer"-type ligands, and calculations on [W(CO)$_5$(H$_2$Im)] in comparison with [W(CO)$_5$(H$_2$NHSi)] were reported in a theoretical study by Frenking *et al*.[109m] The bond dissociation energies of the NHC and NHSi ligand, calculated at the BP86/def2-TZVPP//BP86/def2-SVP level of theory, are, as expected, larger for the NHC complex (227.6 kJ/mol for [W(CO)$_5$(H$_2$Im)]) than for [W(CO)$_5$(H$_2$NHSi)] (185.4 kJ/mol). The calculated values for the charge transfer to [W(CO)$_5$] increase from the carbene complex [W(CO)$_5$(H$_2$Im)] (-0.47 e) to the silylene complex [W(CO)$_5$(H$_2$NHSi)] (-0.74 e), and the W–E bond order increases from [W(CO)$_5$(H$_2$Im)] (0.75) to [W(CO)$_5$(H$_2$NHSi)] (0.90). Frenking *et al.* concluded that neither the charge distributions nor the bond orders correlate with the bond dissociation energies (BDE) of the NHE ligands. The decrease in the BDEs from the carbene to the silylene is determined by the intrinsic strength of the metal–ligand bonds, ΔE_{int}, which is in the order [W(CO)$_5$(H$_2$Im)] (-243.9 kJ/mol) > [W(CO)$_5$(H$_2$NHSi)] (-201.3 kJ/mol), and the authors attributed this decrease mainly to a decrease of the Pauli repulsion for the heavier homologue. A closer inspection of the trend of the electrostatic term ΔV_{elstat} and the orbital (covalent) term ΔE_{oi} shows that the weaker bonds are mainly caused by the former term. Interestingly, Frenking *et al*. also found that the orbital interaction in [W(CO)$_5$(H$_2$NHSi)] (-256.9 kJ/mol) is even larger in magnitude than in [W(CO)$_5$(H$_2$Im)] (-223.0 kJ/mol), whereas the electrostatic term ΔV_{elstat} increases from [W(CO)$_5$(H$_2$Im)] (-538.1 kJ/mol) to [W(CO)$_5$(H$_2$NHSi)] (-438.1 kJ/mol). Thus, the authors concluded that the decrease of the bond strength going from

[W(CO)$_5$(H$_2$Im)] to [W(CO)$_5$(H$_2$NHSi)] correlates with the decrease in ΔV_{elstat}. To corroborate the results obtained for the methyl substituted NHC or NHSi ligand, calculations on the tungsten carbonyl complexes [W(CO)$_5$(Me$_2$Im)] and [W(CO)$_5$(Me$_2$NHSi)] at the TZ2P/BLYP/ZORA/D3(BJ) level of theory were performed. The results summarized in Table 2 confirm the interesting picture of the bonding of the NHSi ligand compared to the NHC ligand. Thus, (i) the intrinsic strength of the metal–ligand bonds ΔE_{int} decrease from the carbene to the silylene ligand from -273.8 kJ/mol for [W(CO)$_5$(Me$_2$Im)] to -222.9 kJ/mol for [W(CO)$_5$(Me$_2$NHSi)]. (ii) This decrease in bond strength is caused by electrostatic contributions for the Me$_2$Im complex. Whereas the contributions from Pauli repulsion remains almost constant for both complexes (538.1 kJ/mol for the Me$_2$Im complex vs. 528.7 kJ/mol for the Me$_2$NHSi complex), a significant difference of the electrostatic term ΔV_{elstat} to the bonding, i.e. -530.4 kJ/mol for [W(CO)$_5$(Me$_2$Im)] and -446.3 kJ/mol for [W(CO)$_5$(Me$_2$NHSi)] is computed. (iii) The W–Si orbital interaction in the silylene complex [W(CO)$_5$(Me$_2$NHSi)] (-253.3 kJ/mol) is larger than the W–C orbital interaction in the carbene complex [W(CO)$_5$(Me$_2$Im)] (-216.8 kJ/mol), for the methylated ligands by 36.5 kJ/mol in favor of the silylene complex.

Table 2. Energy Decomposition Analysis (kJ/mol) of the tungsten–carbene and tungsten–silylene bond in [W(CO)$_5$(Me$_2$Im)] and [W(CO)$_5$(Me$_2$NHSi)] complexes (C_{2V} symmetry). Metal–carbene/silylene bond distances are 2.282 Å (W–C) and 2.503 Å (W–Si), respectively.

L-W	ΔE_{int}	ΔE_{Pauli}	ΔV_{elstat}	ΔE_{disp}	ΔE_{oi}
Me$_2$Im	-273.8	538.1	-530.4	-64.7	-216.8
Me$_2$NHSi	-222.9	528.7	-446.3	-51.9	-253.3
L-W	ΔE_{oi}^{σ}	$\Delta E_{oi}^{\pi y}$	$\Delta E_{oi}^{\pi x}$	ΔE_{oi}^{δ}	
Me$_2$Im	-155.5	-37.3	-20.4	-3.6	
Me$_2$NHSi	-181.8	-37.7	-32.6	-1.2	

(iv) The NHSi ligand is the better *σ*-donor ligand, which is counterintuitive to the conclusions one might draw from the simple orbital picture provided in Figure 25 and Figure 26 in combination with Fukui's frontier orbital concept.[111] Calculation of the *σ*-contribution to the net orbital interaction reveals -181.8 kJ/mol for the silylene complex [W(CO)$_5$(Me$_2$NHSi)] and -155.5 kJ/mol for the carbene complex [W(CO)$_5$(Me$_2$Im)]. (v) Contributions of *π*-symmetry play only a minor role for the NHC or NHSi co-ligands in the presence of many good *π*-accepting carbonyl ligands. However, the *π*-interaction between the Me$_2$NHSi ligand and the tungsten atom is stronger compared to the Me$_2$Im ligand (-57.7 kJ/mol for [W(CO)$_5$(Me$_2$Im)] and -70.3 kJ/mol for [W(CO)$_5$(Me$_2$NHSi)]).

To provide some experimental data to support these calculations, the behaviour of Dipp$_2$NHSi towards group 6 carbonyls was investigated (Scheme 10). The group 6 silylene complexes [M(CO)$_5$(Dipp$_2$NHSi)] **16** – **18** were synthesized by reacting [M(CO)$_5$(THF)] (M = Cr, Mo, W) with Dipp$_2$NHSi in THF and isolated as red (M = Cr, **16**, 74 %, M = Mo, **17**, 75 %) and orange (M = W, **18**, 82 %) solids, respectively. Complexes **16** – **18** are well soluble in all common solvents. The tungsten silylene complex **18** decomposes very slowly in solution and in the solid state, whereas the corresponding chromium and molybdenum compounds decompose quickly in solution within 12 hours at temperatures of -30 °C, and within 7 days in the solid state.

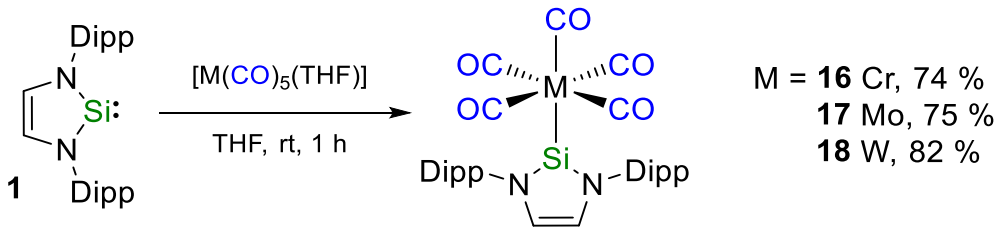

Scheme 10. Synthesis of [M(CO)$_5$(Dipp$_2$NHSi)] (M = Cr **16**, Mo **17**, W **18**).

For the carbonyl carbon atoms, a distinct upfield shift is observed in the $^{13}C\{^1H\}$ NMR spectrum going from chromium to tungsten (**16**: 215.5 ppm, 211.6 ppm, **17**: 204.1 ppm, 201.1 ppm, **18**: 196.4 ppm, 193.3 ppm). The $^{29}Si\{^1H\}$ NMR spectra of **16** – **18** reveal

sharp singlets with the resonances clearly shifting to higher fields from chromium to tungsten (**16**: 138.2 ppm, **17**: 125.4.0 ppm, **18**: 111.2 ppm, $^{1}J(^{183}W\text{-}^{29}Si)$ = 168.3 Hz; Figure 27).

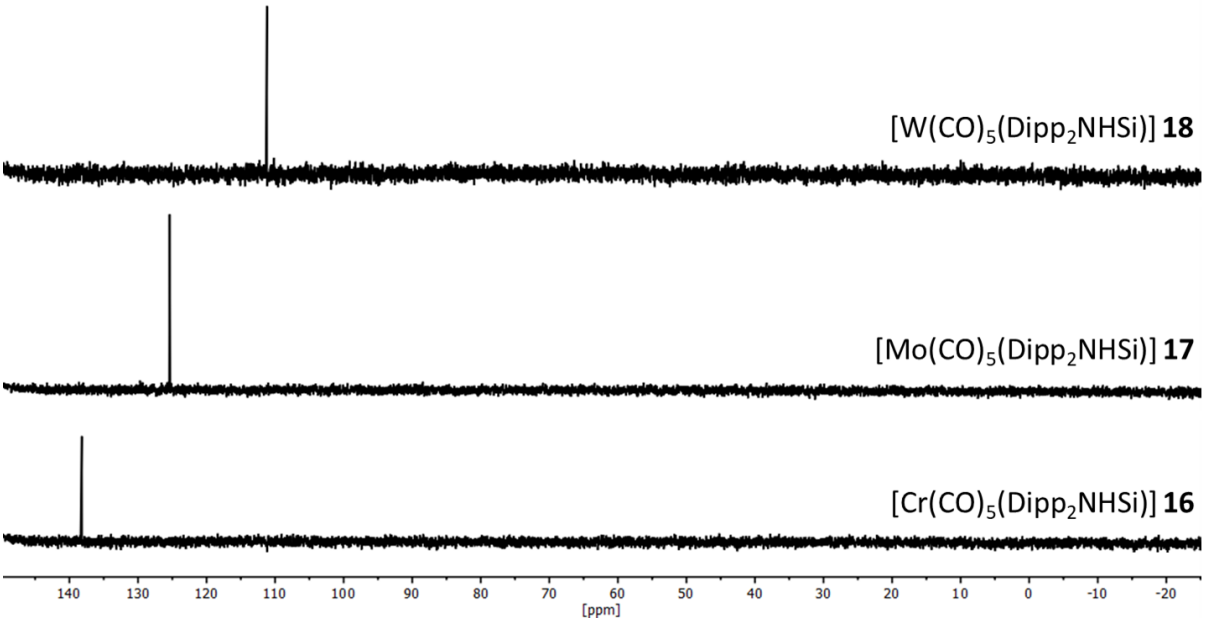

Figure 27. $^{29}Si\{^{1}H\}$ NMR spectra of compounds **16** – **18** in C_6D_6.

For comparison with common *N*-heterocyclic carbene complexes, the compounds $[W(CO)_5(iPr_2Im)]$ (**19**), $[W(CO)_5(iPr_2Im^{Me})]$ (**20**)[112] and $[W(CO)_5(Me_2Im^{Me})]$ (**21**)[112] were prepared from $[W(CO)_5(THF)]$ in good yields (**19**: 86%, **20**: 50%, **21**: 57%, Scheme 11). Complexes **20** and **21** are known, but the $^{1}J(^{183}W\text{-}^{13}C)$ coupling constants and the X-ray crystal structures of these compounds have not been reported previously.

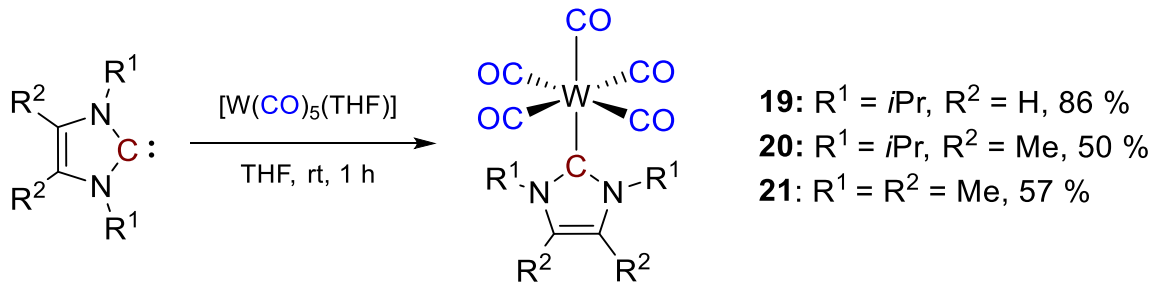

19: R^1 = *i*Pr, R^2 = H, 86 %
20: R^1 = *i*Pr, R^2 = Me, 50 %
21: R^1 = R^2 = Me, 57 %

Scheme 11. Synthesis of $[W(CO)_5(NHC)]$ (NHC = iPr_2Im **19**, iPr_2Im^{Me} **20** and Me_2Im^{Me} **21**).

Complexes **19** – **21** have been fully characterized (see Experimental Details), including the X-ray crystal structures of **19** and **20**. The molecular structures of these complexes as well as of [Mo(CO)$_5$(Dipp$_2$NHSi)] **17** and [W(CO)$_5$(Dipp$_2$NHSi)] **18**, with selected bond lengths and angles, are shown in Figure 28, and a detailed analysis of the W–C and C–O bond lengths of the tungsten complexes [W(CO)$_5$(L)] (L = Dipp$_2$NHSi **18**, *i*Pr$_2$Im **19**, *i*Pr$_2$Im^{Me} **20**) is provided in Table 3. Single crystals of **17** and **18** were grown from saturated hexane solutions at -30 °C, and those of **19** and **20** were obtained from saturated solutions of the respective complexes in toluene / hexane (1:1) mixtures at -30 °C.

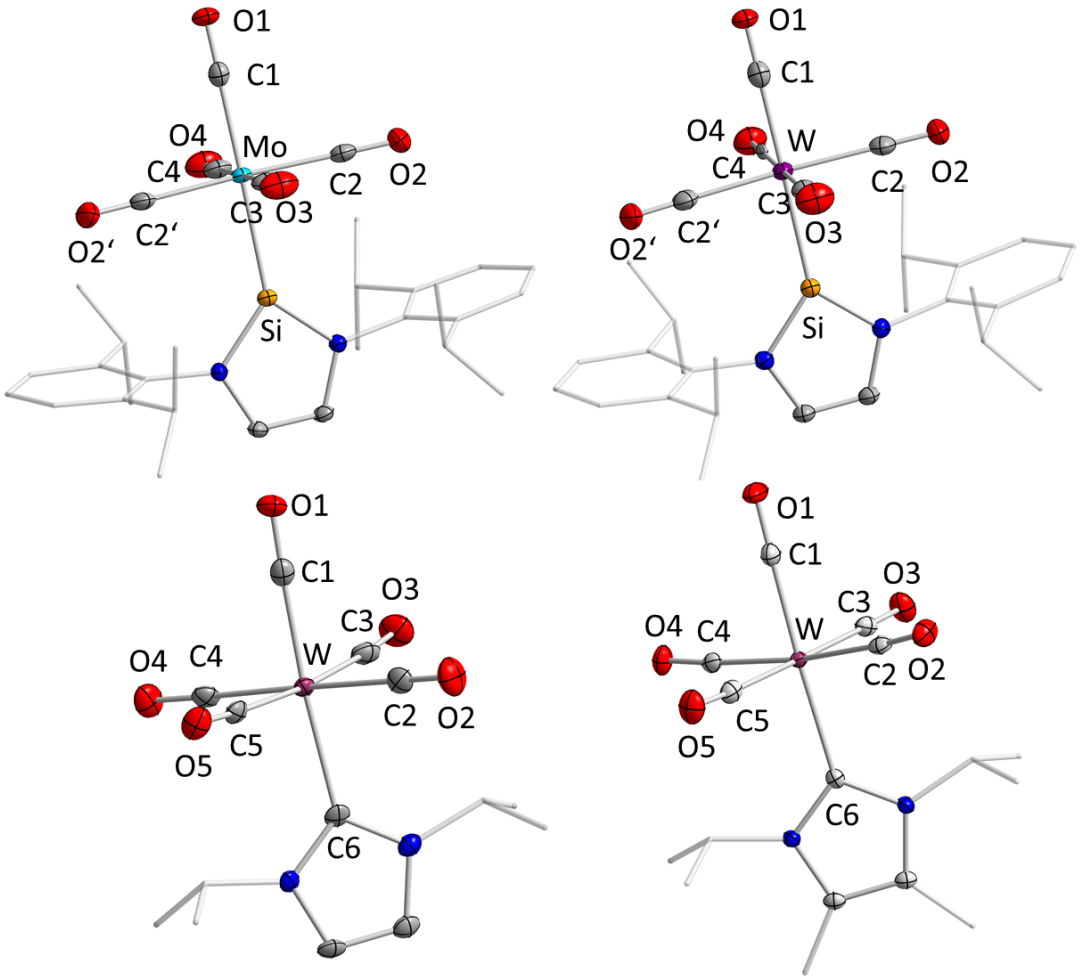

Figure 28. Molecular structures of **17** (top left), **18** (top right), **19** (bottom left) and **20** (bottom right) in the solid state (ellipsoids drawn at the 50 % probability level; hydrogen atoms are omitted for clarity). Selected bond lengths [Å]: **17**: Mo–Si 2.4594(8), Mo–C1 2.017(3), Mo–C2 2.050(2), Mo–C3 2.045(3), Mo–C4 2.053(4); **18**: W–Si 2.4576(14), W–C1 2.010(5), W–C2 2.051(4), W–C3 2.038(5), W–C4 2.021(6); **19**: W–C6 2.272(4),

W–C1 1.999(4), W–C2 2.033(4), W–C3 2.034(4), W–C4 2.049(4), W–C5 2.047(4); **20**: W–C6 2.2930(18), W–C1 1.9883(19), W–C2 2.0367(19), W–C3 2.033(2), W–C4 2.0414(19), W–C5 2.047(2).

All four complexes adopt nearly perfect octahedral structures with four carbonyl ligands arranged in the plane between the silylene and the *trans*-CO ligand. In case of the carbene complexes, a staggered conformation of the four in-plane carbonyl ligands and the NHC ligand is observed, while the silylene complexes adopt an eclipsed arrangement with two of the carbonyls pointing directly to the aryl substituents of the NHSi ligand. The silylene complexes **17** and **18** show similar M–Si (**17**: 2.4594(8) Å, **18**: 2.4576(14) Å) and M–C_{trans} (**17**: 2.017(3) Å, **18**: 2.012(6) Å) bond lengths, in agreement with distances found for [$W(CO)_5$(Xyl$_2$NHSi)] reported by Müller *et al.* (W–Si 2.4568(13) Å, W–C(*trans*) 2.058(5) Å, W–C(*cis*) 2.056 Å).[6f]

Table 3. Bond lengths of W–Si, W–C and C–O in [$W(CO)_5$(L)] (L = Dipp$_2$NHSi **18**, *i*Pr$_2$Im **19**, *i*Pr$_2$Im^{Me} **20**) complexes.

Bond lengths [Å]	**[$W(CO)_5$(Dipp$_2$NHSi)] 18**	**[$W(CO)_5$(*i*Pr$_2$Im)] 19**	**[$W(CO)_5$(*i*Pr$_2$Im^{Me})] 20**
W1–Si1 / W1–C6	2.4576(14)	2.272(4)	2.2930(18)
W1–C1	2.010(5)	1.999(4)	1.9883(19)
W1–C2	2.051(4)	2.033(4)	2.0367(19)
W1–C3	2.038(5)	2.034(4)	2.033(2)
W1–C4	2.021(6)	2.049(4)	2.0414(19)
W1–C5	-	2.047(4)	2.047(2)
C1–O1	1.147(6)	1.155(5)	1.154(2)
C2–O2	1.141(5)	1.149(5)	1.141(2)
C3–O3	1.145(6)	1.154(4)	1.144(2)
C4–O4	1.163(6)	1.138(5)	1.144(2)
C5–O5	-	1.144(4)	1.135(2)

For the NHC complexes **19** and **20**, the bond lengths between the tungsten atom and the carbene carbon atom are W–C6 2.272(4) (**19**) and W–C6 2.2930(18) Å (**20**) and, similar to those of the *n*Pr$_2$Im complex [W(CO)$_5$(*n*Pr$_2$Im)] (W–C$_{NHC}$ 2.265(4)).[113] The W–C$_{trans}$ distances of the NHC complexes **19** and **20** are shorter (e.g. **19**: W–C1 1.999(4); **20**: W–C1 1.9883(19) Å) compared to the W–C$_{cis}$ distances (**6**: W–C$_{cis}$ 2.033(4) – 2.049(4) Å; 7: W–C$_{cis}$ 2.033(2) – 2.047(2) Å), as is also the case for the molybdenum silylene complex **17** (Mo–C1 2.017(3); Mo–C$_{cis}$ 2.045(3) – 2.053(4) Å), but is only found for two of the four *cis*-situated CO ligands of the tungsten silylene complex **18** (W–C3 2.038(5), W–C4 2.021(6) Å). The bond lengths of the *cis*-carbonyl ligands of the silylene complex **18**, which are arranged directly above the aryl rings of the silylene ligand, are W–C2/C2* 2.053(4) Å and are thus significantly elongated compared to the other two *cis*-carbonyl ligands.

Utilizing the crystal structures of **18**, **19** and **20** calculation of the percent buried volume (%V_{bur}) was possible which is a useful tool to analyse the steric hindrance of a ligand in the coordination sphere of a metal centre.[114] A comparison of the calculated values for the complexes [Ni(CO)$_3$(L)] and [W(CO)$_5$(L)] is shown in Table 4. For [Ni(CO)$_3$(L)] a model compound was used. The values obtained differ quite significantly for the two central atoms nickel and tungsten which is caused by the different geometries of the [Ni(CO)$_3$(L)] and [W(CO)$_5$(L)] complexes and the distance between the central atom and the coordinating atom of the ligand used for the assessment of the percent buried volume. The values approximated from the bond lengths determined by the X-ray crystal structure analyses of the complexes was used, which is 2.0 Å for the nickel compounds and 2.5 Å for the tungsten complexes. The calculated percent buried volume of Dipp$_2$NHSi for the nickel complex is 35.5 % and for the tungsten complex it is 27.4 % which, in both cases, is notably higher than those calculated for the xylyl-substituted NHSi (W: 24.8 %) and the aryl substituted carbenes Dipp$_2$Im (Ni: 34.8 %, W: 24.7 %) and Mes$_2$Im (Ni: 32.2 %). This trend can be observed for all NHCs listed in Table 4 with exception of the extremely bulky *tert*-butyl-substituted carbene. However, it is important to note that the NHSi ligand Dipp$_2$NHSi seems to be bulkier (in terms of the volume it buries) than the NHC analogue Dipp$_2$Im, despite the larger M–Si distance in the silylene complexes compared to the M–C distance in carbene complexes.

Table 4. Percent buried volume (V_{bur}%) of the complexes [Ni(CO)$_3$(L)] (L = Dipp$_2$NHSi, Dipp$_2$Im, Mes$_2$Im, *t*Bu$_2$Im, *i*Pr$_2$Im^{Me}, *i*Pr$_2$Im) and [W(CO)$_5$(L)] (L = Dipp$_2$NHSi, Xyl$_2$NHSi, Dipp$_2$Im, Cy$_2$Im, *i*Pr$_2$Im^{Me}, *i*Pr$_2$Im). Note that V_{bur}% has been calculated for different distances for the 3d element nickel and the 5d element tungsten.

	[Ni(CO)$_3$(L)][a]	**[W(CO)$_5$(L)]**[b]
Dipp$_2$NHSi	35.5[c]	27.4
Xyl$_2$NHSi	-	24.8
Dipp$_2$Im	34.8	24.7
	31.5[c]	
Mes$_2$Im	32.2	-
Cy$_2$Im	-	19.6
***t*Bu$_2$Im**	40.4[d]	-
***i*Pr$_2$Im^{Me}**	28.8	20.2
***i*Pr$_2$Im**	28.2[e]	19.6

[a] r = 3.0 Å, d = 2.0 Å; [b] r = 3.5 Å, d = 2.5 Å; [c] optimized structure; [d] [(L)Ni(CO)$_2$]; [e] average value of L in [(L)$_2$Ni(CO)$_2$].

The ^{13}C NMR spectra of monosubstituted, octahedral tungsten carbonyl complexes [W(CO)$_5$(L)] have been used to evaluate the donor strengths of the ligand L. Buchner and Schenk established the *trans*-influence series of different ligands L toward tungsten(0) on the basis of $^1J(^{183}W\text{-}^{13}C)$ coupling constants of the carbonyl group *trans* to L. ^{13}C NMR spectra and the associated $^1J(^{183}W\text{-}^{13}C)$ coupling constants are proposed to be useful tools to gain insight into the *trans*-influence of a large variety of ligands towards tungsten(0). A good *σ*-donor ligand L, which forms a strong, short bond to the metal centre demands a high degree of metal orbitals of *n*s- and (*n-1*)d-character for this bond. Therefore, for the bond to the *trans*-ligand L', less metal s- and d-character, and more p-character remains, which results in an increase of the M–L' bond lengths and a decrease in one-bond spin coupling data, e.g. the $^1J(^{183}W\text{-}^{13}C)$ coupling constants. Thus, the reduction of one-bond spin coupling constants was rationalized and is directly related to the s-character of the hybrid orbitals used by both atoms in the formation of their bond to L and *trans*-CO.[115] The magnitude of a spin-spin coupling constant across one bond is dominated by the Fermi contact term.

In a series of closely related compounds considering the same type of bond (here W–CO), it is usually assumed that other factors change very little and that the variations in ^{1}J(A-B) are mainly due to changes in the s-character of the bonding hybrid orbitals at the metal atoms. Thus, a conclusion regarding the *σ*-donor capability of the ligand L can be made, and a series of examples are given in Table 5 which demonstrate that the stronger *σ*-donor ligand L leads to a smaller coupling constant $^{1}J(^{183}W\text{-}^{13}C)_{trans}$. In this series of complexes $[W(CO)_5(L)]$ (L = H^-, CN^-, Ph_3P, Ph_3As, Ph_3Sb, Cl^-, Br^-, I^-; Table 5) the $^{1}J(^{183}W\text{-}^{13}C)_{cis}$ coupling constant remains remarkably constant, lying between 124 and 128 Hz and shows only a small variation of 4 Hz for these very different ligands L.

Table 5. $^{1}J(^{183}W\text{-}^{13}C)$ coupling constants of $[W(CO)_5L]$ (L = H^-, CN^-, Ph_3As, Ph_3Sb, Ph_3P, Cl^-, Br^-, I^-) of the *cis* and *trans*-standing carbonyl ligands.[115]

Ligand	**H^-**	**CN^-**	**Ph_3P**	**Ph_3As**	**Ph_3Sb**	**Cl^-**	**Br^-**	**I^-**
***cis*-CO**								
***δ* [ppm],**	205.9	197.6	197.2	196.7	196.1	199.6	198.6	197.1
$^{1}J_{W\text{-}C}$ [Hz]	124	124	126	126	124	128	127	127
***trans*-CO**								
***δ* [ppm],**	210.3	200.2	199.0	199.0	198.2	201.4	201.5	201.6
$^{1}J_{W\text{-}C}$ [Hz]	149	139	140	155	162	165	171	176

On the other hand, $^{1}J(^{183}W\text{-}^{13}C)_{trans}$ reveals a variation of approximately 35 Hz and, from the data in Table 5, the ligands L may be arranged in a series of increasing $^{1}J(^{183}W\text{-}^{13}C)_{trans}$ of the axial carbonyl group and a decreasing *trans*-influence in the octahedral tungsten carbonyl complexes.

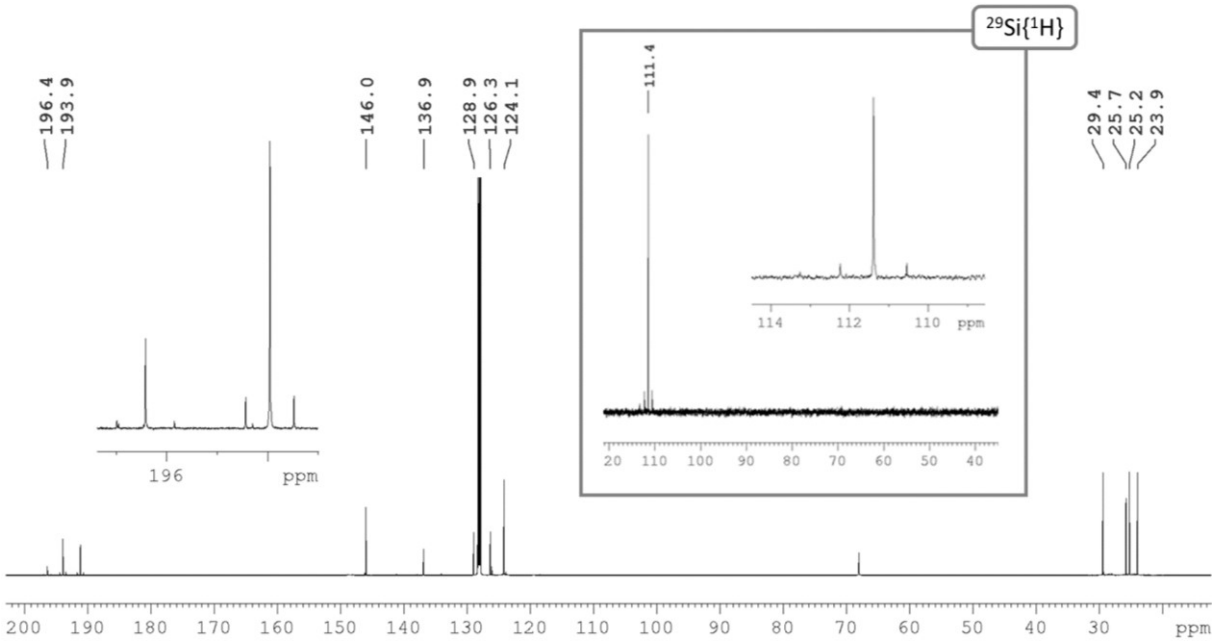

Figure 29. $^{13}C\{^{1}H\}$ (125.8 Hz) and $^{29}Si\{^{1}H\}$ NMR spectrum (99.4 Hz) of $[W(CO)_5(Dipp_2NHSi)]$ (**18**) in C_6D_6.

Evaluation of the $^{13}C\{^{1}H\}$ NMR spectrum of **18** revealed tungsten satellites for the *trans*- and *cis*-CO resonances with $^{1}J(^{183}W\text{-}^{13}C)$ coupling constants of 144 Hz (*trans*-CO) and 121 Hz (*cis*-CO, Figure 29), which fit well with the data presented in Table 6. Furthermore, $^{1}J(^{183}W\text{-}^{13}C)_{trans}$ obtained for **18** is close to $^{1}J(^{183}W\text{-}^{13}C)_{trans}$ of other silylene tungsten pentacarbonyl complexes reported previously, i.e., $[W(CO)_5(Xyl_2NHSi)]$ **II-Xyl**[6f] with a coupling constant $^{1}J(^{183}W\text{-}^{13}C)_{trans}$ of 144 Hz and $[W(CO)_5(amid_2NHSi)]$ **IX**[116] ($amid_2NHSi$ = bis(amidinato)silylene) with a coupling constant of 145 Hz. The $^{1}J(^{183}W\text{-}^{13}C)_{trans}$ coupling constants of these complexes lie between the values found for $[W(CO)_5(PPh_3)]$ (140 Hz) and $[W(CO)_5(PMe_3)]$ (145 Hz).[115] For the carbene complexes **19** – **21** as well as for $[W(CO)_5(Dipp_2Im)]$ **X**[117] reported previously, the values of $^{1}J(^{183}W\text{-}^{13}C)_{trans}$ lie in a range between 126 and 132 Hz and, thus, are much lower than those of the silylene complexes. These values demonstrate that NHCs are superior net donors (including electrostatic and orbital contributions) and reveal a stronger *trans*-influence compared to the silylene (and phosphine) ligands. They lie in the region of the excellent donor ligand hydride (i.e. $[W(CO)_5(H)]^-$, $^{1}J(^{183}W\text{-}^{13}C)_{trans}$ = 149 Hz).

Table 6. $^{1}J(^{183}W\text{-}^{13}C)$ coupling constants of $[M(CO)_5(L)]$ (L = $Dipp_2NHSi$, Xyl_2NHSi, $amid_2NHSi$, $i Pr_2Im$, $i Pr_2Im^{Me}$, Me_2Im^{Me}, $Dipp_2Im$) of the *cis*- and *trans*-standing carbonyl ligands.

	$Dipp_2NHSi$ 18	**Xyl_2NHSi II-Xyl**	**$amid_2NHSi$ IX**
***cis*-CO**			
δ [ppm],	193.6	193.7	203.7
$^{1}J_{W\text{-}C}$ [Hz]	120.5	120.8	123.1
***trans*-CO**			
δ [ppm],	196.6	196.6	203.3
$^{1}J_{W\text{-}C}$ [Hz]	143.9	144.3	145.0
***v(CO)* [cm^{-1}]**	1935, 2068	1980, 2011,	-

	$i Pr_2Im$ 19	**$i Pr_2Im^{Me}$ 20**	**Me_2Im^{Me} 21**	**$Dipp_2Im$ X**
***cis*-CO**				
δ [ppm],	198.4	197.9	198.5	197.2
$^{1}J_{W\text{-}C}$ [Hz]	125.8	126.2	125.9	125.8
***trans*-CO**				
δ [ppm],	201.5	201.9	201.6	200.8
$^{1}J_{W\text{-}C}$ [Hz]	131.3	131.9	131.6	127.2
***v(CO)* [cm^{-1}]**	1961, 2056	1998, 2058	1864, 2058	1916, 2053[a]

[a] in $CHCl_3$

The better net donor properties of the NHC ligands are also reflected in the IR spectra of the complexes. The C–O stretching frequencies of different tungsten complexes with *N*-heterocyclic carbenes and *N*-heterocyclic silylenes are shown in Table 6. In complexes of the type $[W(CO)_5(L)]$ with the idealized C_{4v} symmetry, A_1^{I}, E and A_1^{II} stretching vibrations are IR-active. The A_1^{I} vibration is the symmetric stretching mode of all carbonyl groups in *cis* and *trans* positions and can thus be used as a probe of the total charge density at the tungsten atom. The E and A_1^{II} stretches are close in energy and often not resolved in the IR spectra of the compounds. For the silylene complexes, the A_1^{I} frequencies are slightly higher (Table 6, **18**: 2068 cm^{-1}; $amid_2NHSi$: 2069 cm^{-1}) than those observed for the corresponding carbene compounds (2053 – 2058 cm^{-1}),

which indicates that less electron density is located at the tungsten atom due to the poorer net donor properties and/or better net acceptor properties of the NHSi ligand. Analysis of the $^{1}J(^{183}W\text{-}^{13}C)$ coupling constants thus reveals that the net donor properties of the NHSi ligand should be similar to phosphines, but not to NHCs; the latter can be classified as excellent (*σ*-)donors such as hydride or methyl. However, it should be noted that several mechanisms, which are not independent from each other, may contribute to the *trans*-influence which includes orbital energy separation between the tungsten acceptor orbital and the ligand donor orbital, changes in overlap population, interaction with tungsten *n*p orbitals and *π*-contributions, etc.

Table 7. A_1 IR stretching frequencies (in cm^{-1}) of $[W(CO)_5(Me_2Im)]$ and $[W(CO)_5(Me_2NHSi)]$ complexes and Voronoi deformation density (VDD) charges (as fraction of one electron) of W. Negative VDD charge values signify accumulation of electrons (C_{2V} symmetry).

L	VDDC (W)	*v(CO)*
Me_2Im	+0.131	1902 (s), 1916 (m), 2023 (w)
Me_2NHSi	+0.100	1938 (s), 2033 (m)

To support these findings, the tungsten carbonyl model complexes $[W(CO)_5(Me_2Im)]$ and $[W(CO)_5(Me_2NHSi)]$ at the TZ2P/BLYP/ZORA/D3(BJ) level of theory were analysed more closely. Calculated IR stretching frequencies of the complexes $[W(CO)_5(Me_2Im)]$ and $[W(CO)_5(Me_2NHSi)]$ and Voronoi deformation density (VDD) charges of tungsten are given in Table 7, and the energy decomposition analysis (kJ/mol) of the axial tungsten–carbonyl bond in the complexes $[W(CO)_5(Me_2Im)]$ and $[W(CO)_5(Me_2NHSi)]$ is given in Table 8.

Table 8. Energy Decomposition Analysis (kJ/mol) of the axial tungsten–carbonyl bond in $[W(CO)_5(Me_2Im)]$ and $[W(CO)_5(Me_2NHSi)]$ complexes.

L-W	ΔE_{int}	ΔE_{Pauli}	ΔV_{elstat}	ΔE_{disp}	ΔE_{oi}	ΔE_{oi}^{σ}	ΔE_{oi}^{π}	ΔE_{oi}^{δ}
Me_2Im	-242.1	+592.9	-429.7	-24.8	-380.5	-162.5	-218.0	0.0
Me_2NHSi	+229.2	+580.8	-421.1	-23.8	-365.1	-164.5	-200.7	0.0

Inspection of the calculated IR stretching vibrations of *pseudo*-A_1 symmetry reveals the same trend, i.e., that the symmetric stretching frequency for the NHSi complexes lies 10 cm^{-1} higher in energy and supports the idea that the NHC ligand is the better net donor ligand (Table 7). The EDA of the *trans*-CO ligand (Table 8) reveals that the W–C orbital interaction is stronger for $[W(CO)_5(Me_2Im)]$ (-380.5 kJ/mol) than for $[W(CO)_5(Me_2NHSi)]$ (-365.1 kJ/mol), which in turn supports the idea of a larger orbital interaction of the *trans*-NHSi ligand. Interestingly, the calculation showed for both complexes similar contributions from σ-symmetry (-162.5 kJ/mol for $[W(CO)_5(Me_2Im)]$ and -165.5 kJ/mol for $[W(CO)_5(Me_2NHSi)]$), whereas π-back-bonding is more efficient for the NHC complex (-218.0 kJ/mol vs. -200.7 kJ/mol for the Me_2NHSi complex), which is in line with the observed and calculated IR spectra.

In summary, the main electronic features of the *N*-heterocyclic silylenes in general and of $Dipp_2NHSi$ in particular were calculated and compared to similar carbene ligands. The calculations revealed significant differences in the frontier orbital region of these compounds, which affect the ligation properties of NHSis. (i) The orbital order changes, as the HOMO of NHSis is a π-orbital. (ii) The σ-orbital of NHSis lies at much lower energy than those of NHC's and has a higher degree of s-orbital character. (iii) The π-accepting LUMO of NHSis is much lower in energy than those of NHCs and reveals a large silicon p_x-contribution. These differences are responsible for a significantly different behaviour of NHSis compared to NHCs in transition metal chemistry which can be explained by the frontier orbitals of NHSis. Especially, one energetically low lying π-acceptor orbital has a strong impact on the coordination chemistry of this class

of compounds. The calculations were experimentally supported by the synthesis of the silylene complexes [M(CO)$_5$(Dipp$_2$NHSi)] (M = Cr **16**, Mo **17**, W **18**) which were synthesized from Dipp$_2$NHSi and [M(CO)$_6$] (M= Cr, Mo, W). The tungsten NHSi complex **18** and similar NHSi complexes [W(CO)$_5$(NHSi)] were compared to the NHC complexes [W(CO)$_5$(*i*Pr$_2$Im)] (**19**), [W(CO)$_5$(*i*Pr$_2$Im^{Me})] (**20**)[112] and [W(CO)$_5$(Me$_2$Im^{Me})] (**21**).[112]

3.2.3 Dipp$_2$NHSi as a bridging ligand

The *Tolman Electronic Parameter* (TEP) is a widely used method to determine the electronic characteristics of a ligand. This parameter is based on measurement of the C–O stretching vibration of a$_1$ symmetry in complexes of the type [Ni(CO)$_3$(L)].[118] This stretching frequency allows one to draw conclusions regarding electron density at the metal centre of the nickel carbonyl complex and, therefore, of the donor properties of the ligand.[119] In order to determine the TEP for Dipp$_2$NHSi and to synthesize a complex of the type [Ni(CO)$_3$(NHSi)], [Ni(CO)$_4$] was reacted with one equivalent of Dipp$_2$NHSi in toluene at room temperature. This reaction led to a colourless solution which turned purple upon removal of the solvent, and a deep purple solid was isolated in moderate yield (**22**, 41 %; Scheme 12).

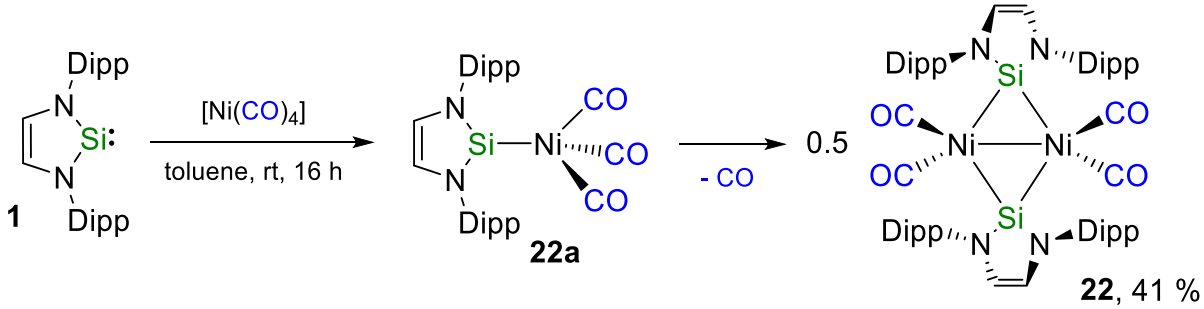

Scheme 12. Synthesis of the [{Ni(CO)$_2$(*μ*-Dipp$_2$NHSi)}$_2$] (**22**).

Compound **22** was characterized by ^{1}H, ^{13}C and ^{29}Si NMR spectroscopy in solution and *via* IR spectroscopy and single-crystal X-ray diffraction in the solid state. In the ^{1}H NMR spectrum, the expected signals of the silylene ligand were shifted slightly

downfield compared to the free NHSi. The $^{13}C\{^1H\}$ NMR spectra also displayed a shift of the resonances for the NHSi ligand as well as one resonance for the carbonyl carbon atoms at 195.7 ppm. In the $^{29}Si\{^1H\}$ NMR spectrum, a resonance at 121.9 ppm also indicated the formation of a silylene transition metal complex. Two carbonyl stretching bands at 1971 and 2010 cm^{-1} were observed in the IR spectrum at rather low energies compared to other complexes of the type $[Ni(CO)_3(L)]$.[98, 118b, 120] The X-ray crystal structure (Figure 30) of the product **22** revealed that the reaction of $[Ni(CO)_4]$ with one equivalent of $Dipp_2NHSi$ leads to the dimeric, silylene-bridged complex $[\{Ni(CO)_2(\mu\text{-}Dipp_2NHSi)\}_2]$ (**22**), which was, most probably, formed from the colourless intermediate $[Ni(CO)_3(Dipp_2NHSi)]$ (**22a**) (Scheme 12) upon CO elimination and subsequent dimerization. The dimer is built from two $[Ni(CO)_2(Dipp_2NHSi)]$ moieties, which are connected by a nickel–nickel bond (Ni–Ni' 2.5218(5) Å) of a similar length to those in bridged dinuclear nickel complexes (2.36 – 2.54 Å).[120c, 121] The molecules lie on an inversion centre located between the Ni atoms. Both the silicon and the nickel atoms are tetrahedrally coordinated. The silylene ligands are each bonded to the nickel atoms *via* one longer (2.3090(5) Å) and one shorter (2.2798(5) Å) Ni–Si bond, and the nickel atoms are thus slightly unsymmetrically bridged by the silylene ligands. The nickel carbon distances are unexceptional.

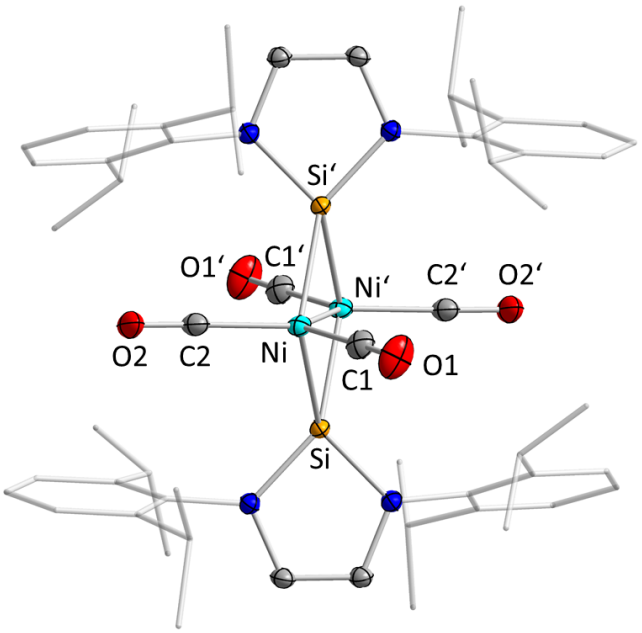

Figure 30. Molecular structure of $[\{Ni(CO)_2(\mu\text{-}Dipp_2NHSi)\}_2]$ (**22**) in the solid state (ellipsoids drawn at the 50 % probability level; hydrogen atoms are omitted for clarity). Selected bond lengths [Å] and angles [°] of **22**: Ni–Ni' 2.5218(5), Ni–Si 2.2798(5), Ni–

Si' 2.3090(5), Ni'–Si' 2.2798(5), Ni'–Si 2.3090(5), Ni–C1 1.7760(19), Ni–C2 1.8079(18), C1–O1 1.146(2), C2–O2 1.132(2), Ni–Si–Ni' 66.672(16), N1–Si–N2 88.22(6), C1–Ni1–C2 115.55(8), C1–Ni–Ni' 127.72(6), C2–Ni–Ni' 116.64(6), Si–Ni–Si' 113.327(16), Si–Ni–C1 113.18(6), Si–Ni–C2 102.61(5).

The corresponding NHC complexes [Ni(CO)$_3$(NHC)], which are ligated with Mes$_2$Im or Dipp$_2$Im, are reluctant to replace a carbonyl ligand to give three-coordinate complexes.[98, 118b, 120d-f] Bis-carbene complexes of the type [Ni(CO)$_2$(NHC)$_2$] have been accessible either by carbonylation of bis-NHC complex precursors, by reaction of [Ni(CO)$_4$] with sterically less demanding NHCs, or by addition of a carbene to coordinatively unsaturated complexes bearing a bulky NHC ligand, such as [Ni(CO)$_2$(*t*Bu$_2$Im)].[98, 118b, 120] Cyclic (alkyl)(amino)carbenes react with [Ni(CO)$_4$] to give the 18 VE complexes [Ni(CO)$_3$(cAAC)] and complexes [Ni(CO)(cAAC)$_2$] which are available by further substitution of [Ni(CO)$_3$(cAAC)] with additional cAAC or from the reaction of suitable NHC precursors such as [Ni(CO)$_2$(*t*Bu$_2$Im)] with two equivalents of the cAAC.[122] Carbene-bridged, dinuclear nickel complexes have rarely been observed, and the only example of an NHC-bridged nickel complex was prepared by Lappert *et al*. in 1977.[98] To shed more light on the energetics of this reaction, DFT (TURBOMOLE/def2-SV(P)/BP86) calculations were performed on the dimerization of [Ni(CO)$_2$(Dipp$_2$Im)] and [Ni(CO)$_2$(Dipp$_2$NHSi)] (Figure 31).

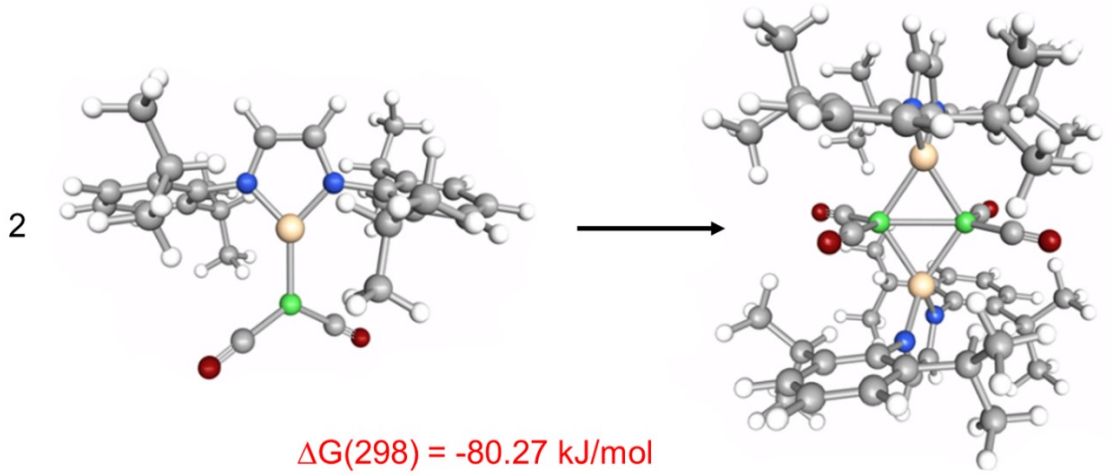

Figure 31. DFT calculations (TURBOMOLE/def2-SV(P)/BP86) on the dimerization of [Ni(CO)$_2$(NHSi)] (**22a**) to give the dimer [{Ni(CO)$_2$(*μ*-NHSi)}$_2$] (**22**).

The optimized geometry of [{Ni(CO)$_2$(*μ*-Dipp$_2$NHSi)}$_2$] is similar to the experimentally observed structure (distances (calc.) Ni–Ni: 2.5348 Å, Ni–Si: 2.2946 – 2.2968 Å; Ni–C: 1.7724 – 1.7861 Å; Figure 30), and the calculated CO stretching vibrations (1975 and 2001 cm^{-1}) agree well with the experimentally observed frequencies (1971 and 2010 cm^{-1}). Whereas the dimerization of [Ni(CO)$_2$(Dipp$_2$Im)] is highly repulsive on the energy hypersurface, for which a *ΔG(298)* of +275.03 kJ/mol is calculated, the dimerization of the NHSi complex [Ni(CO)$_2$(Dipp$_2$NHSi)] *via* the bridging of the NHSi ligand is favourable by *ΔG(298)* = -80.27 kJ/mol. The strong interaction of the *π*-accepting orbitals of the NHSi ligand with occupied d-orbitals of the planar [(OC)$_2$Ni–Ni(CO)$_2$] dimer is considered as one of the main driving forces for the dimerization process.

Furthermore, it seemed to be interesting to compare the bonding in Ni–NHSi vs. Ni–NHC with that in classical phosphine complexes. To focus on the interaction of one d^{10} nickel atom with the NHSi and NHC ligands, respectively, DFT calculations were performed at the TZ2P/BLYP/ZORA/D3(BJ) level of theory on the mono-ligated model complexes [Ni(Me$_2$Im)] and [Ni(Me$_2$NHSi)]. The results of the detailed energy decomposition analysis of the Ni–C and Ni–Si bonds (in C_{2V} symmetry) in the mono-coordinated complexes [Ni(L)], [Ni(Me$_2$Im)] and [Ni(Me$_2$NHSi)] are given in Table 9 and are compared to the Ni–P bond (in C_{3v} symmetry) in [Ni(PPh$_3$)].

Table 9. Energy Decomposition Analysis (kJ/mol) of the Ni–C and Ni–Si bonds (C_{2V} symmetry) and of the Ni–P bond (C_{3v} symmetry) in [Ni(L)] complexes. Metal–carbene, –phosphine and –silylene bond distances are 1.753 Å (Ni–C), 2.020 Å (Ni–P) and 2.002 Å (Ni–Si), respectively.

L-Ni	ΔE_{int}	ΔE_{Pauli}	ΔV_{elstat}	ΔE_{disp}	ΔE_{oi}	ΔE_{oi}^{σ}	$\Delta E_{oi}^{\pi y}$	$\Delta E_{oi}^{\pi x}$	ΔE_{oi}^{δ}
Me$_2$Im	-479.5	+890.7	-824.6	-24.5	-521.0	-336.2	-146.6	-38.6	+0.4
Ph$_3$P	-431.3	+737.1	-704.0	-41.0	-423.5	-218.8	-204.6		0.0
Me$_2$NHSi	-426.5	+665.0	-679.1	-17.7	-394.8	-165.9	-128.3	-99.8	-0.9

In C_{2v} symmetry $\Delta E_{oi}^{\pi y}$ corresponds to b_2 and $\Delta E_{oi}^{\pi x}$ to b_1. In C_{3v} symmetry ΔE_{oi}^{π} corresponds to the e representation.

The metal–carbene, –phosphine and –silylene bond distances were fixed at the equilibrium distances of 1.753 Å (Ni–C), 2.020 Å (Ni–P) and 2.002 Å (Ni–Si), respectively. These results reveal that the electronic properties of the silylene ligand are probably more similar to those of the phosphine ligand than to those of the NHC ligand. The interaction energy ΔE_{int} between the neutral ligands L and the nickel atom decreases in the order Me_2Im (-479.5 kJ/mol) > PPh_3 (-431.3 kJ/mol) ≈ Me_2NHSi (-426.5 kJ/mol), and a decrease in the orbital interaction ΔE_{oi} of -521.0 kJ/mol (Me_2Im) >> -423.5 kJ/mol (PPh_3) > -394.8 kJ/mol (Me_2NHSi) was calculated, in which the orbital interactions between the PPh_3 and the Me_2NHSi are close in energy. The NHC ligand is certainly the strongest *σ*-donor ligand among these three ligands, with a *σ*-orbital interaction of -336.2 kJ/mol (64.5 % of ΔE_{oi}) and a *π*-orbital interaction energy of -185.2 kJ/mol (35.5 % of ΔE_{oi}). For the NHSi ligand, -165.9 kJ/mol (42.0 %) arises from *σ*-donor contribution and -228.1 kJ/mol (57.8 %) from the *π*-interaction. Although it cannot be differentiated here between *π*-donation and *π*-acceptance, it is interesting to note that: (i) *σ*-interaction is much weaker for the NHSi ligand compared to NHC; and (ii) *π*-interaction prevails for the NHSi ligand.

This is in line with the general orbital picture of the ligands (Figure 25 and Figure 26) in which both the *σ*-donor and the *π*-acceptor orbital of the NHSi ligand lie at much lower energies compared to the NHC ligand, whereas a *π*-donating orbital of the NHSi ligand, the HOMO, lies at higher energy compared to the carbene ligand. The calculations on the phosphine ligated complex [Ni(L)] provide a rather balanced picture concerning *σ*- and *π*-contributions to the orbital interaction, i.e. -218.8 kJ/mol (51.7%) for the *σ*-interaction and -204.6 kJ/mol (48.3%) for the *π*-interaction. According to the calculated Voronoi deformation density charges (Table 10), in all cases net charge is transferred to the nickel atom in the order NHC (-0.103 e^-) > NHSi (-0.081 e^-) > PPh_3 (-0.068 e^-).

Table 10. Voronoi deformation density (VDD) charges (as fraction of one electron) of Ni in the complexes [Ni(L)] and [Ni(CO)$_3$(L)] complexes and corrected TEP values of [Ni(CO)$_3$(L)] (in cm^{-1}, available experimental values in curly brackets). Positive VDD charge (VDDC) values signify depletion of electrons. Metal–carbene, –phosphine and –silylene bond distances are 1.997 Å (Ni–C), 2.251 Å (Ni–P) and 2.219 Å (Ni–Si), respectively.

L	VDDC (L–Ni)	VDDC (L–Ni(CO)$_3$)	TEP (L–Ni(CO)$_3$)
Me$_2$Im	-0.103	+0.166	2053 {2051}[123]
Ph$_3$P	-0.068	+0.121	2066 {2069}[118a]
Me$_2$NHSi	-0.081	+0.100	2076

Thus, there is a slightly larger charge transfer to the nickel for the silylene compared to the phosphine ligand, due to a larger *π*-donation or weaker *π*-acceptor interaction (or both), which compensates the stronger *π*-interaction found for PPh$_3$. A similar analysis was performed for [Ni(L)(CO)$_3$] using Me$_2$Im, Me$_2$NHSi and PPh$_3$ as the ligand (Table 11). Compared to [Ni(L)], three good *σ*-donating and excellent *π*-accepting carbonyl ligands have been added to the complex. As a consequence, the whole M–L interaction should be weaker, and much of the *π*-contributions should be located at the M–C bond to the carbonyl ligands, i.e. contributions of the NHC, NHSi and PPh$_3$ ligand should be much less developed. This stabilization can be traced to the relative energies of the acceptor and donor orbitals of the transition metal component. The *σ*-bonding a$_1$ acceptor orbital of [Ni(CO)$_3$] is 0.84 eV lower in energy compared to that of [Ni]. This trend is even more pronounced for the occupied d-orbitals, for which stabilization by the three carbonyl ligands is essential. These [Ni(CO)$_3$] donor orbitals, responsible for *π*-back donation to the ligand, are stabilized by almost 6.17 eV compared to the d-orbital level of the Ni atom in its d^{10}s^0 electron configuration.

Table 11. Energy Decomposition Analysis (kJ/mol) of the Ni–C and Ni–Si bonds (C_s symmetry) and the Ni–P bond (C_{3v}) in [Ni(CO)$_3$(L)] complexes. Metal–carbene, –phosphine and –silylene bond distances are 1.997 Å (Ni–C), 2.249 Å (Ni–P) and 2.219 Å (Ni–Si), respectively.

L-Ni	ΔE_{int}	ΔE_{Pauli}	ΔV_{elstat}	ΔE_{disp}	ΔE_{oi}	ΔE_{oi}^{σ}	ΔE_{oi}^{π}	ΔE_{oi}^{δ}
Me$_2$Im	-202.4	+570.5	-513.2	-44.3	-215.4	-194.0	-21.4	-
Ph$_3$P	-161.2	379.8	-306.9	-64.8	-169.3	-112.4	-56.4	-0.4
Me$_2$NHSi	-170.5	+524.6	-438.6	-34.2	-222.3	-189.6	-32.6	-

For [Ni(L)(CO)$_3$], this difference is reflected in the lower interaction energy ΔE_{int} of -202.4 kJ/mol (Me$_2$Im) > -170.5 kJ/mol (Me$_2$NHSi) > 161.2 kJ/mol (PPh$_3$) between L and [Ni(CO)$_3$]. Interestingly, the largest orbital interaction ΔE_{oi} was calculated for the silylene ligand, i.e. -222.3 kJ/mol for Me$_2$NHSi, compared to -215.4 kJ/mol for Me$_2$Im and -169.3 kJ/mol for PPh$_3$. The electrostatic contributions are thus largest for the NHC complex. As the orbital interaction in [Ni(Me$_2$Im)(CO)$_3$] (-215.4 kJ/mol) is even weaker than that in [Ni(Me$_2$NHSi)(CO)$_3$] (-222.3 kJ/mol), the decrease in ΔE_{int} is attributed to the decrease in the electrostatic term ΔV_{elstat} from -513.2 kJ/mol for [Ni(Me$_2$Im)(CO)$_3$] to -438.6 kJ/mol for [Ni(Me$_2$NHSi)(CO)$_3$]. The more stabilizing ΔE_{oi} for [Ni(Me$_2$NHSi)(CO)$_3$] can be mainly attributed to superior π-bonding, as the interaction with Me$_2$Im reveals a larger σ-contribution ΔE_{oi}^{σ} for Me$_2$Im (-194.0 kJ/mol; 90.0 % of ΔE_{oi}), than for Me$_2$NHSi (-189.6 kJ/mol; 85.3 % of ΔE_{oi}) and PPh$_3$ (-112.4 kJ/mol; 66.4% of ΔE_{oi}) whereas π-contributions ΔE_{oi}^{π} are larger for Me$_2$NHSi (-32.6 kJ/mol; 14.7% of ΔE_{oi}) compared to Me$_2$Im (-21.4 kJ/mol; 10.0 % of ΔE_{oi}; cf. -56.4 kJ/mol 33.3 % of ΔE_{oi} for PPh$_3$). Although the formation of the dimer [{Ni(CO)$_2$(μ-Dipp$_2$NHSi)}$_2$] **22** prevents the experimental determination of Tolman's electronic parameter (TEP), these values were calculated for [Ni(CO)$_3$(L)] (Table 10), and clearly show that Me$_2$NHSi is the weakest donating ligand in this series: Me$_2$Im: TEP = 2053 cm^{-1}; PPh$_3$: TEP = 2066 cm^{-1}, Me$_2$NHSi: TEP = 2076 cm^{-1}. These TEP values correlate with the Voronoi deformation density charges of Ni in the complexes [Ni(CO)$_3$(L)] (Me$_2$Im: +0.166; PPh$_3$: +0.121, Me$_2$NHSi: +0.100). In conclusion, considering the orbital interaction in [Ni(L)(CO)$_3$], Me$_2$NHSi has good σ-donor properties similar to those of

Me_2Im, but (i) beneficial electrostatic contributions to the Me_2Im–Ni interaction as well as (ii) *π*-accepting contributions of the NHSi ligand reduce the electron density on the central metal.

The coordination chemistry of NHCs in transition metal half-sandwich complexes is well studied[124] whereas only a few examples of NHSi half-sandwich complexes are known.[72-75, 85] Therefore, the reactivity of *N*-heterocyclic silylenes with half-sandwich transition metal complexes was examined. A common and easily accessible precursor for the synthesis of nickel half-sandwich complexes is nickelocene. For *N*-heterocyclic carbenes the neutral complexes $[(\eta^5\text{-}C_5H_5)Ni(NHC)(X)]$[125] and $[(\eta^5\text{-}C_5H_5)Ni(\eta^1\text{-}C_5H_5)(NHC)]$[126] as well as the cationic complexes of the type $[(\eta^5\text{-}C_5H_5)Ni(NHC)_2][X]$[124d, 125b, c, 126-127] ($X = Cl^-$, Br^-, I^-, PF_6^-, BF_4^-, $\eta^5\text{-}C_5H_5^-$) were synthesized by reaction of nickelocene with the free carbenes or the imidazolium salts of the corresponding NHC. Wolf *et al*. reported the synthesis of interesting $[(\eta^5\text{-}C_5H_5)Ni(NHC)]$ nickel(I) metal radicals by reducing $[(\eta^5\text{-}C_5H_5)Ni(NHC)(Cl)]$ (NHC = Mes_2Im, $Dipp_2Im$) with KC_8. $[(\eta^5\text{-}C_5H_5)Ni(Dipp_2Im)]$ reacts with P_4, S_8, Se_∞ and Te_∞ to afford nickel tetraphosphide and chalcogenide complexes and transformations with phenyl isothiocyanate led to the formation of new nickel-heterocycles.[128] Based on this work, attempts were made to synthesize the novel, neutral nickel(I) metal radical $[(\eta^5\text{-}C_5H_5)Ni(Dipp_2NHSi)]$ or $[(\eta^5\text{-}C_5H_5)Ni(Dipp_2NHSi)_2]$ *via* the reaction of nickelocene with one equivalent $Dipp_2NHSi$ in the presence of lithium naphthalenide in Et_2O (Scheme 13). After workup, $[\{(\eta^5\text{-}C_5H_5)Ni(\mu\text{-}Dipp_2NHSi)\}_2]$ (**23**) was isolated as a dark red solid in good yield (75%). This diamagnetic complex is well soluble in all common organic solvents and was characterized by using ^1H, ^{13}C and ^{29}Si NMR spectroscopy, elemental analysis and single-crystal X-ray diffraction.

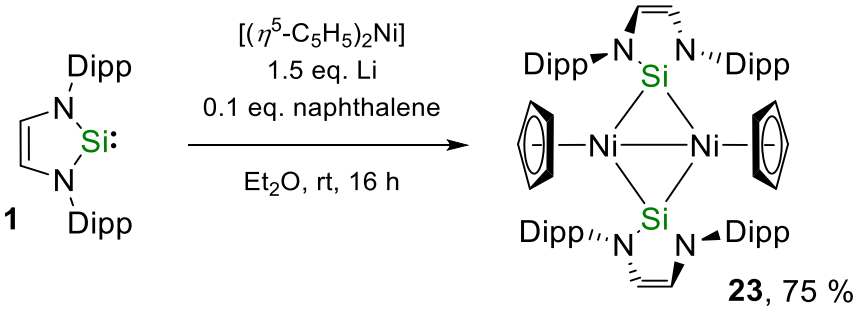

Scheme 13. Synthesis of $[\{(\eta^5\text{-}C_5H_5)Ni(\mu\text{-}Dipp_2NHSi)\}_2]$ (**23**).

The ^{1}H and ^{13}C NMR spectrum show a single set of signals for the silylene ligand with the characteristic septet of the methine proton of the Dipp-substituent at 3.64 ppm, shifted slightly downfield compared to the starting material (3.25 ppm)[6f] and a singlet at 5.26 ppm for the cyclopentadienyl protons (Figure 32). The $^{29}Si\{^{1}H\}$ NMR spectrum reveals a resonance at 124.2 ppm, significantly shifted compared to uncoordinated NHSi (75.9 ppm).[6f] The elemental analysis confirmed that one cyclopentadienyl ligand was successfully removed in course of the reaction and that the ratio of NHSi to cyclopentadienyl ligand was 1:1.

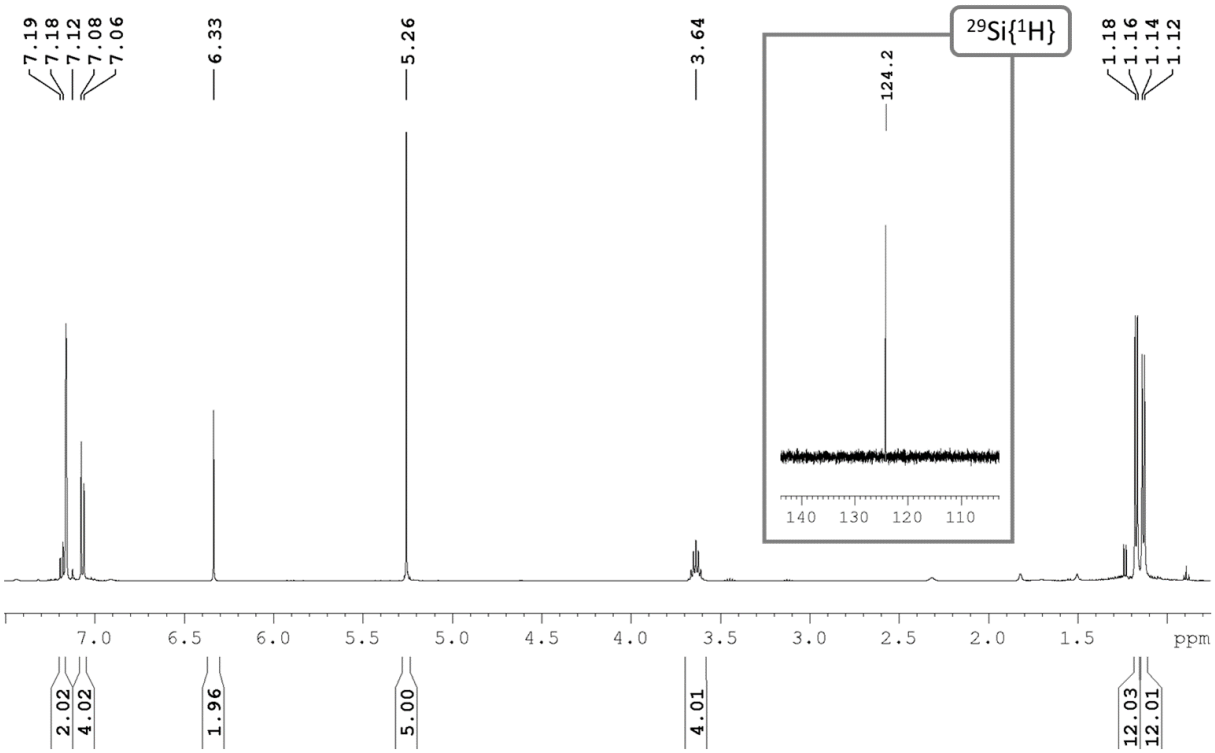

Figure 32. ^{1}H (500.1 Hz) and $^{29}Si\{^{1}H\}$ NMR spectrum (99.4 Hz) of [{(η^5-C_5H_5)Ni(μ-Dipp$_2$NHSi)}$_2$] (**23**) in C_6D_6.

Crystals of complex **23** suitable for single-crystal X-ray diffraction were grown from a saturated solution of **23** in hexane at -30°C. The X-ray diffraction analysis reveales that the reduction of [(η^5-C_5H_5)$_2$Ni] in the presence of Dipp$_2$NHSi leads to the formation of a dimeric nickel complex in which the nickel centers, similarly to complex **22**, are stabilized by two bridging silylene ligands and two η^5-coordinated cyclopentadienyl ligands (Figure 33).

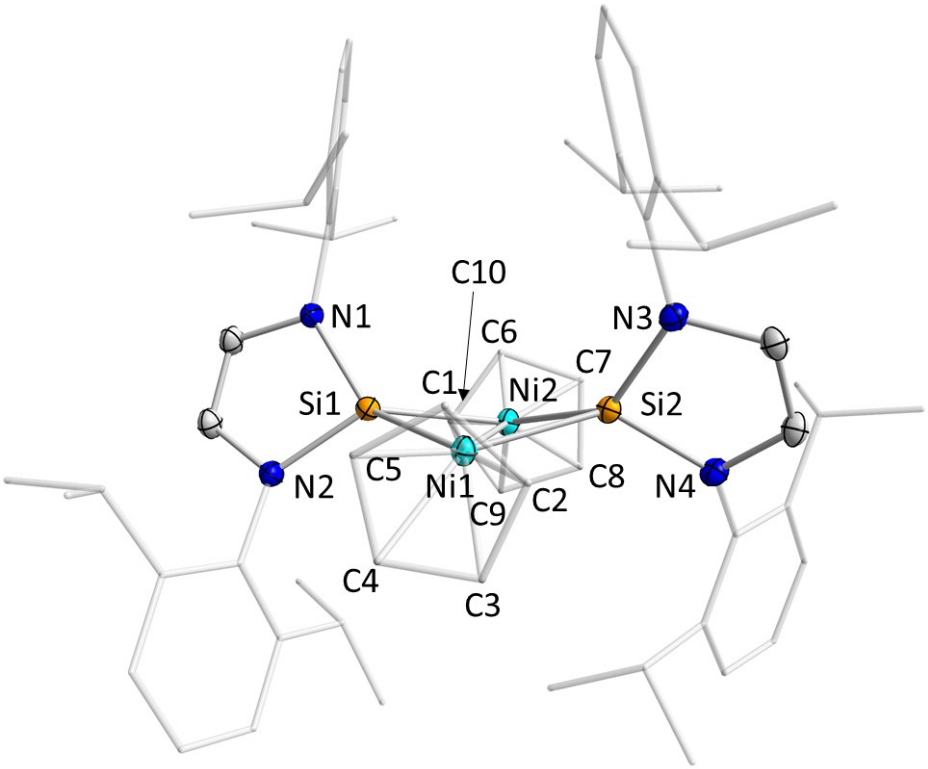

Figure 33. Molecular structure of [{(η^5-C_5H_5)Ni(μ-Dipp$_2$NHSi)}$_2$] (**23**) in the solid state (ellipsoids drawn at the 50 % probability level; hydrogen atoms are omitted for clarity). Selected bond lengths [Å] and angles [°] of **23**: Ni1–Ni2 2.5025(3), Ni1–Si1 2.2100(4), Ni1–Si2 2.2555(4), Ni2–Si1 2.2615(4), Ni2–Si2 2.2020(4), Ni1–C1 2.0732(16), Ni1–C2 2.1103(15), Ni1–C3 2.2167(15), Ni1–C4 2.1873(15), Ni1–C5 2.0665(16), Ni2–C6 2.0715(15), Ni2–C7 2.0874(15), Ni2–C8 2.1863(15), Ni2–C9 2.2049(15), Ni2–C10 2.0881(15); Ni1–Si1–Ni2 68.053(14), Ni1–Si2–Ni2 68.297(14), Si1–Ni1–Si2 108.020(17), Si1–Ni2–Si2 108.085(17), (Ni1–Si1–Ni2) and (Ni1–Si2–Ni2) 24.533(10), (N1–Si1–N2) and (N3–Si2–N4) 40.023(52).

Formation of the diamagnetic complex **23** (in comparison with the existence of paramagnetic [(η^5-C_5H_5)Ni(Dipp$_2$Im)]) can be explained by a preferential bridging coordination mode adopted by the NHSi ligand as compared to NHCs (*vide supra*). Compound **23** crystallizes in the orthorhombic space group Pbca and consists of two {(η^5-C_5H_5)Ni} moieties which are connected by two Ni–Si–Ni bridges. This results in a nickel–nickel bond of Ni1–Ni2 2.5025(3) Å, which is similar to nickel–nickel bond lengths observed before for other bridged dinuclear nickel complexes (2.36 –

2.54 Å).[120c, 121a, c, 129] The comparison with unbridged dinuclear nickel complexes corroborates the assumption of a nickel–nickel bond in complex **23**. The cofacial nickel-dimer [{Ni($C_{10}H_{14}N_8$)}$_2$][130] ($C_{10}H_{14}N_8$ = dihydrooctaaza[14]annulene) and the cyclopentadienyl-coordinated phosphine-stabilized complex [{(η^5-C_5H_5)Ni(PEt_3)}$_2$][131] feature nickel–nickel bonds of 2.788(2) Å and 2.407(1) Å, respectively, with **23** lying in the middle of this range of bond lengths. The distorted tetrahedral environment at the NHSi silicon atoms is spanned by the nitrogen atoms of the five-membered silylene ring and both nickel atoms. The silicon and nickel atoms span a butterfly with angles Ni1–Si1–Ni2 of 68.053(14)° and Ni1–Si2–Ni2 of 68.297(14)° at silicon and angles Si1–Ni1–Si2 of 108.020(17)° and Si1–Ni2–Si2 of 108.085(17)° at nickel. The five-membered silylene rings are twisted against each other by 40.023(52) °.

Lappert and co-workers described the reaction of [{(η^5-C_5H_5)Fe(CO)$_2$}$_2$] with R_2Im^{H2} (R = Me, Et) in xylene at 140°C which led to the isolation of a dark green solid. The reaction product was identified as [(η^5-C_5H_5)$_2$Fe$_2$(CO)$_3$(R_2Im^{H2})], formed by substitution of one carbonyl ligand with a terminal coordinating NHC. According to Lappert *et al.*, all attempts for a further replacement of CO ligands by using an excess of the NHC failed.[98]

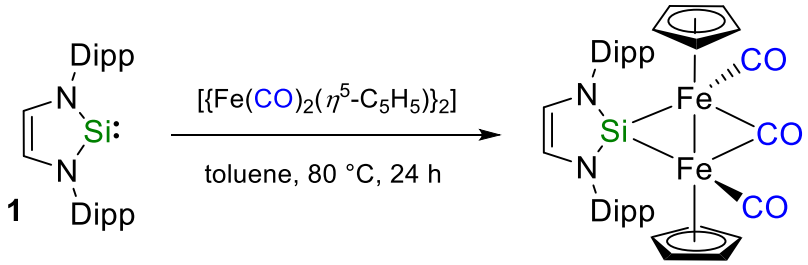

24, 68 %

Scheme 14. Synthesis of the NHSi-bridged iron complex [{(η^5-C_5H_5)Fe(CO)}$_2$(μ-CO)(μ-$Dipp_2$NHSi)] (**24**).

Based on this work, the dimeric compound [{(η^5-C_5H_5)Fe(CO)$_2$}$_2$] was reacted with two equivalents of $Dipp_2$NHSi in toluene at elevated temperatures (80 °C) to afford [{(η^5-C_5H_5)Fe(CO)}$_2$(μ-CO)(μ-$Dipp_2$NHSi)] (**24**) as a dark green solid (Scheme 14). Raising the reaction temperature up to 100 °C or higher led to decomposition of the

starting materials. Up to date, there is no evidence of what happens with the second equivalent of Dipp$_2$NHSi, but the reaction with one equivalent of the silylene ligand leads to a low-yield conversion of the precursor. Complex **24** is soluble in organic solvents like THF, Et$_2$O and toluene and very little soluble in hexane from which it was crystallized and isolated in 68 % yield. Elemental analysis confirmed the equimolar reaction and the loss of one CO ligand and thus reinforces the assumption of the formation of [{(η^5-C$_5$H$_5$)Fe(CO)}$_2$(μ-CO)(μ-Dipp$_2$NHSi)] (**24**). Two very broad signals for the methine protons at 3.80 and 4.28 ppm and one singlet for the cyclopentadienyl ligand at 4.54 ppm were observed in the ^{1}H NMR spectrum of **24**. The silicon silylene atom gives rise to a resonance at 147.2 ppm in the ^{29}Si{^{1}H} NMR spectrum and the CO ligands were detected at 210.4 and 215.4 ppm in the ^{13}C{^{1}H} NMR spectrum. The IR spectrum reveals two strong bands at 1772 and 1937 cm^{-1} in the region for the carbonyl stretching frequencies. Single-crystals suitable for X-ray diffraction were grown from an at room temperature saturated solution of **24** in hexane at –30 °C and the molecular structure in the solid state is shown in Figure 34.

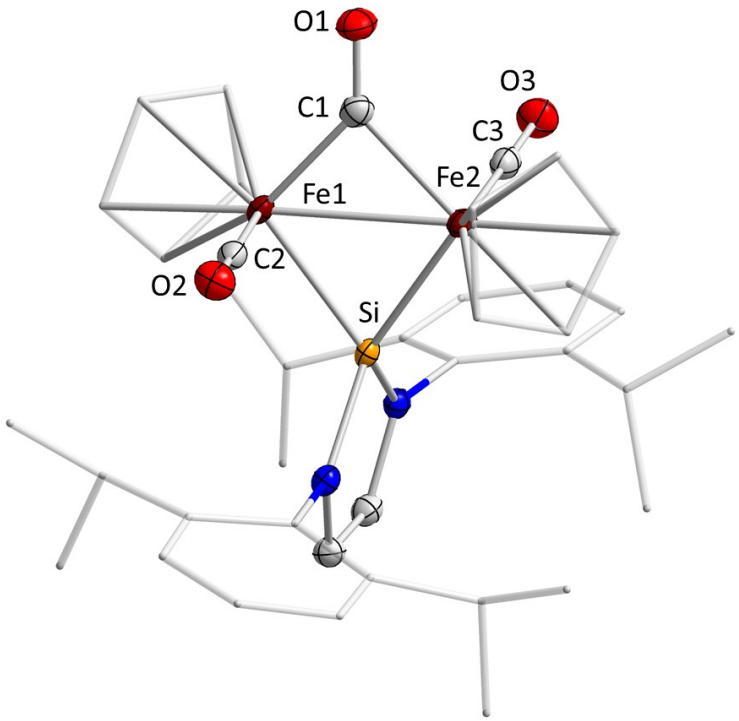

Figure 34. Molecular structure of [{(η^5-C$_5$H$_5$)Fe(CO)}$_2$(μ-CO)(μ-Dipp$_2$NHSi)] (**24**) in the solid state (ellipsoids drawn at the 50 % probability level; hydrogen atoms are omitted for clarity). Selected bond lengths [Å] and angles [°] of **24**: Fe1–Fe2 2.6165(4), Fe1–Si 2.3140(5), Fe2–Si 2.3014(5), Fe1–C1 1.9018(18), Fe2–C1 1.9468(17), Fe1–C2

1.7550(18), Fe2–C3 1.7546(18), C1–O1 1.175(2), C2–O2 1.151(2), C3–O3 1.152(2), Fe1–Si–Fe2 69.070(15), Fe1–C1–Fe2 85.66(7), Si–Fe1–C1 103.00(5), Si–Fe2–C1 102.02(5).

The solid state structure confirms the loss of one CO ligand and reveals a tetrahedral coordination at the silicon atom which connects the two {(η^5-C_5H_5)Fe(CO)} moieties. Furthermore, the iron centers are connected by a bridging carbonyl ligand, which is arranged directly above the iron–iron vector in plane with the Fe–Si–Fe unit. The iron–iron distance of 2.6165(4) Å lies slightly above the range typically observed for cyclopentadienyl-stabilized iron carbonyl dimers (2.465(1) – 2.5603(16) Å, depending on the bridging unit),[132] but is slightly shorter compared to the cationic silylene-bridged complexes [(η^5-C_5H_5)$_2$Fe$_2$(CO)$_3$(μ-Si(*t*Bu)(NMI))][I]•CD_3CN **N** (Fe–Fe 2.626(2) Å) and [Fe$_2$(CO)$_3$(η^5-C_5H_5)$_2$(μ-Si(*t*Bu)(DMAP))][I] **O** (Fe–Fe 2.633(2) Å) (NMI = *N*-methylimidazole, DMAP = 4-(dimethylamino)pyridine) reported by Ogino *et al*.[133] The {(η^5-C_5H_5)Fe(CO)} moieties are twisted by 180 °C to each other with the terminal CO ligands perpendicular aligned to the Fe–Fe–μSi–μC plane, pointing in opposite directions. Both bridging ligands are not symmetrically arranged inbetween the iron centers as the Fe1–Si bond (2.3140(5) Å) is slightly longer compared to Fe2–Si (2.3014(5) Å). The iron–carbon bonds to the bridging carbonyl ligand are in reverse order as found for the bridging silylene, i.e. the Fe1–C1 of 1.9018(18) Å is slightly shorter than Fe2–C2 of 1.9468(17) Å. The iron–carbon bond lengths are in the same range as observed in the complexes presented by Ogino (**N**: Fe–C 1.913(8) Å; **O**: Fe–C 1.912(9) Å). The bridging carbonyl and silylene ligand are a returning motif in *N*-heterocyclic silylene chemistry and are in contrast to the NHC iron complex [(η^5-C_5H_5)$_2$Fe$_2$(CO)$_3$(R_2Im)], reported by Lappert and co-workers. It was assumed that the NHC complex consists of two different Fe–Fe connected iron complex fragments {(η^5-C_5H_5)Fe(CO)$_2$} and {(η^5-C_5H_5)Fe(CO)(R_2Im^{H2})} in which the NHC is η^1-coordinated to an iron atom.[98]

The model systems [Ni(L)], [Ni(CO)$_3$(L)], and [W(CO)$_5$(L)] (see 3.2.2 and 3.2.3) have been used to assess the bonding situation of Me_2Im and Me_2NHSi (= L) in transition

metal complexes. Regardless of the model system, some differences in the bonding in M–NHSi and M–NHC were observed: (i) NHCs are the better net donor ligands. (ii) The intrinsic M–L interaction energy typically decreases going from M–NHC to M–NHSi. (iii) This decrease is mainly caused by favourable electrostatic contributions to the M–NHC bond. (iv) The orbital interaction in the carbonyl complexes was typically larger for M–NHSi than for M-NHC. (iv) The contribution of *σ*- and *π*-interactions depends significantly on the system under investigation. Interestingly, the M–NHSi *π*-interaction is often stronger compared to that in M–NHC. (v) The electronic properties of NHSi ligands are closer to those of phosphines than to NHCs. (vi) Calculation of the percent buried volume (V_{bur}%) show that $Dipp_2$NHSi is slightly bulkier than $Dipp_2$Im. Comparing NHCs and NHSis, it was found that *N*-heterocyclic silylenes possess a stronger tendency to act as bridging ligands between two metal centres which was demonstrated on three different examples. The nickel complexes [{$Ni(CO)_2$(*μ*-$Dipp_2$NHSi)}$_2$] (**22**) and [(*η*^{5}-C_5H_5)Ni(*μ*-$Dipp_2$NHSi)]$_2$ (**23**) were obtained by reacting $Dipp_2$NHSi with [$Ni(CO)_4$] forming the colourless intermediate [$Ni(CO)_3$($Dipp_2$NHSi)] (**22a**), which dimerizes to the NHSi-bridged compound **22**, and by reduction of nickelocene with lithium naphthalenide in the presence of $Dipp_2$NHSi yielding **23**. The formation of complex **23** is in contrast to the formation of [(*η*^{5}-C_5H_5)Ni(NHC)] (NHC = Mes_2Im, $Dipp_2$Im) metal radicals upon reduction of [(*η*^{5}-C_5H_5)Ni(NHC)(Cl)] with KC_8, as presented by Wolf and co-workers earlier. The silylene-bridged iron complex [(*η*^{5}-C_5H_5)$_2$$Fe_2$$(CO)_2$(*μ*-CO)(*μ*-$Dipp_2$NHSi)] (**24**) was afforded by treating Dipp2NHSi with the dimeric half-sandwich complex [{(*η*^{5}-C_5H_5)$Fe(CO)_2$}$_2$]. The similar reaction utilizing the *N*-heterocyclic carbenes R_2Im^{H2} (R = Me, Et) was described by Lappert *et al*. and afforded complexes [(*η*^{5}-C_5H_5)$_2$$Fe_2$$(CO)_3$($R_2Im^{H2}$)] which are unsymmetrically substituted at the iron centres and feature a non-bridging carbene ligand. These three examples exemplify that *N*-heterocyclic silylenes are good metal–metal bridging ligands as compared to NHC ligands.

3.2.4 $Dipp_2NHSi$ as a metal–halide activator

Silylenes reveal a considerable affinity towards halogens and halogen-containing compounds with examples being mainly in main group element chemistry[49, 55b, 104] which has been covered in detail in Chapter 1. This behavior can also be observed in transition metal chemistry, as exemplified by Tilley and co-workers in the reactivity of the previously mentioned dinuclear ruthenium complex [{(η^5-C_5Me_5)$_2$Ru}$_2$(H)(μ-H)(μ,η^2-HSiRCl)(μ-Cl)(μ,η^2-*t*Bu_2NHSi)] (R = Ph, *n*-hexyl), in which an NHSi-Cl ligand bridges two ruthenium atoms *via* the silicon and chloride atoms (Figure 18). After the reactions of NHSi with suitable carbonyl precursors [$M(CO)_5$(THF)] (M = Cr, Mo, W) leading to NHSi carbonyl complexes, it should be tested how this reaction pattern changes if the transition metal complex contains a halide ligand in addition to the carbonyl ligands. Natural starting materials for such studies are group 7 metal carbonyl halide complexes [$Mn(CO)_5$(X)]. Interestingly, there are only a few publications on analogous manganese complexes bearing *N*-heterocyclic carbene ligands. In 1977, Lappert *et al.* reported that the reaction of [$Mn(CO)_5$(Br)] with the *N*-heterocyclic carbene dimer $(Me_2Im^{H2})_2$ led to oxidation of the manganese compound instead of the formation of the desired complex [$Mn(CO)_3(Me_2Im^{H2})_2$(Br)].[98] By using the manganese bis-phosphine precursor [$Mn(CO)_3(PPh_3)_2$(Br)], the bis-carbene complex *fac*-[$Mn(CO)_3(Me_2Im)_2$(Br)] was obtained in very low yields *via* substitution of both phosphine ligands. Whittlesey and co-workers reported the reaction of two equivalents of the backbone-methylated NHC iPr_2Im^{Me} with [$Mn(CO)_5$(Br)] which afforded the bis-NHC complex *fac*-[$Mn(CO)_3(iPr_2Im^{Me})_2$(Br)]. The reaction of one equivalent of the sterically more demanding NHC $Dipp_2Im$ led to the mono-NHC complex [$Mn(CO)_4(Dipp_2Im)$(Br)][134] which is also known for the *N*-mesityl-substituted NHC Mes_2Im.[135]

$Dipp_2NHSi$ was reacted with the pentacarbonyl manganese complexes [$Mn(CO)_5$(X)] (X = I, Br, Cl) and the bis-silylene complexes [$Mn(CO)_3(Dipp_2NHSi)_2$(I)] (**25**), [$Mn(CO)_3(Dipp_2NHSi)_2$(Br)] (**26**) and the silylene silyl complex [$Mn(CO)_4(Dipp_2NHSi)(Dipp_2NHSi\text{-}Cl)$] (**27**) were isolated as a yellow solids (**25**: 57 %, **26**: 63 %, **27**: 52 %; Scheme 15). Complexes **25** – **27** are very soluble in common

organic solvents such as THF and toluene, but only sparingly soluble in non-polar solvents such as hexane. $[Mn(CO)_3(Dipp_2NHSi)_2(I)]$ **25**, $[Mn(CO)_3(Dipp_2NHSi)_2(Br)]$ **26** and $[Mn(CO)_4(Dipp_2NHSi)(Dipp_2NHSi\text{-}Cl)]$ **27** were characterized by IR, multinuclear NMR spectroscopy, elemental analysis and single-crystal X-ray diffraction.

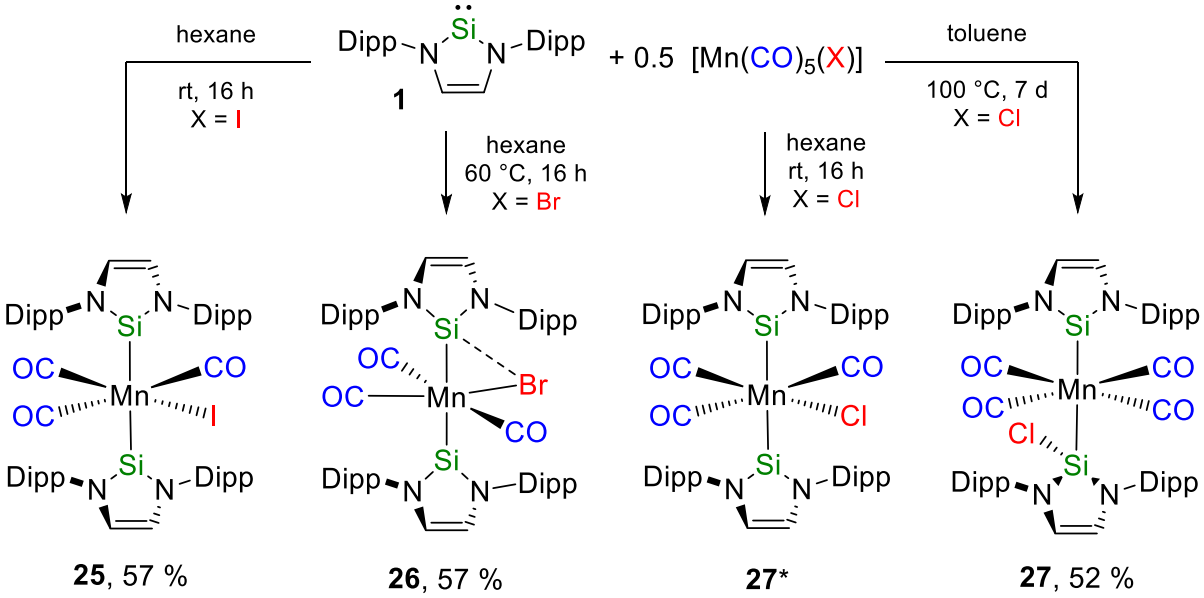

Scheme 15. Synthesis of the bis-silylene complexes $[Mn(CO)_3(Dipp_2NHSi)_2(I)]$ (**25**), $[Mn(CO)_3(Dipp_2NHSi)_2(Br)]$ (**26**) and $[Mn(CO)_3(Dipp_2NHSi)_2(Cl)]$ (**27***) and the silylene silyl complex $[Mn(CO)_4(Dipp_2NHSi)(Dipp_2NHSi\text{-}Cl)]$ (**27**).

For $[Mn(CO)_5(I)]$, the reaction was carried out in hexane at room temperature, whereas $Dipp_2NHSi$ was reacted with $[Mn(CO)_5(Br)]$ at elevated temperatures (60 °C) in hexane, and dark yellow solids were isolated by filtration of the respective precipitates formed in this solvent. Elemental analysis performed on crystals of **25** and **26** led to the assumption that two of the carbonyls of the manganese complex were replaced by NHSi ligands. As the IR spectrum revealed only two absorptions for the CO stretching modes at 1929 and 1960 cm^{-1} (**25**) and 1927 and 1962 cm^{-1} (**26**) this assumption was confirmed by the loss of two carbonyl ligands. One set of signals was observed for the NHSi silylene ligands of $[Mn(CO)_3(Dipp_2NHSi)_2(I)]$ (**25**) and $[Mn(CO)_3(Dipp_2NHSi)_2(Br)]$ (**26**) in the ^1H and $^{13}C\{^1H\}$ NMR spectra and one resonance for the NHSi silicon atoms at 125.2 ppm (**25**) in the $^{29}Si\{^1H\}$ NMR spectrum, which indicates that both NHSi ligands are equivalent. The $^{29}Si\{^1H\}$ NMR spectrum of **26** recorded at -40 °C reveals a

single resonance at 121.5 ppm which is in line with a dynamic behavior of this complex in solution, caused by an oscillating movement of the bromine atom between the two silicon silylene atoms and explained in detail in the next paragraph (see also Figure 37). In case of the chloride substituted manganese complex $[Mn(CO)_5(Cl)]$, the analogous reaction in hexane or toluene at room temperature leads in both cases to a mixture of two manganese complexes as indicated by multinuclear NMR spectroscopy, which were identified as the complexes $[Mn(CO)_3(Dipp_2NHSi)_2(Cl)]$ **27*** and $[Mn(CO)_4(Dipp_2NHSi)(Dipp_2NHSi\text{-}Cl)]$ **27** (Figure 35).

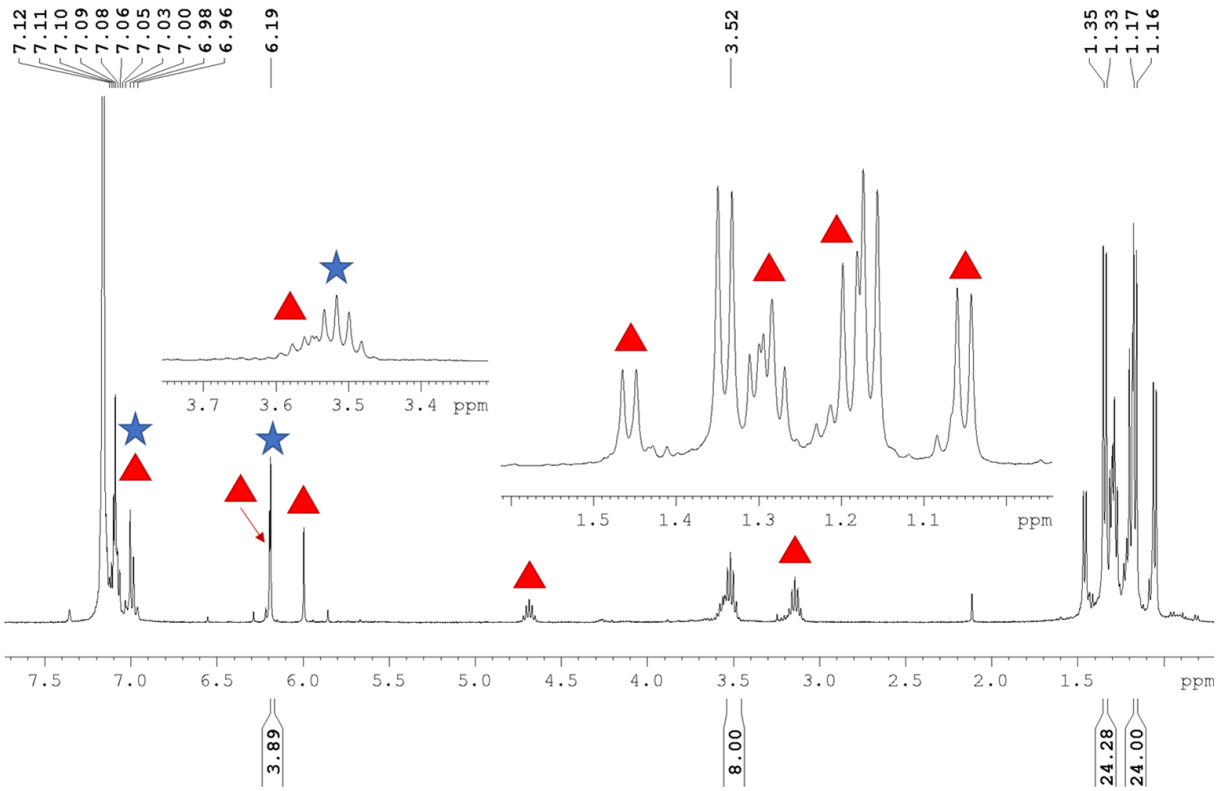

Figure 35. ^1H NMR spectrum (400.3 Hz) of the reaction of $Dipp_2NHSi$ with $[Mn(CO)_5(Cl)]$ giving $[Mn(CO)_4(Dipp_2NHSi)(Dipp_2NHSi\text{-}Cl)]$ (**27**, red) and $[Mn(CO)_3(Dipp_2NHSi)_2(Cl)]$ (**27***, blue) in C_6D_6.

By executing the reaction at higher temperatures (100 °C) and for a prolonged period of time (7 days), the formation of a single manganese silylene species can be observed. After crystallization from a mixture of hexane / toluene (1:1) a pale-yellow solid was obtained in 52 % yields. In the ^1H and $^{13}C\{^1H\}$ NMR spectra two sets of signals were observed for the Dipp-substituents of the silylene ligands, and two

resonances in the $^{29}Si,^{1}H$ HMQC NMR spectrum at 28.9 and 135.9 ppm corroborated the assumption that two silylene species are involved (^{1}H NMR spectrum pictured in Figure 36).

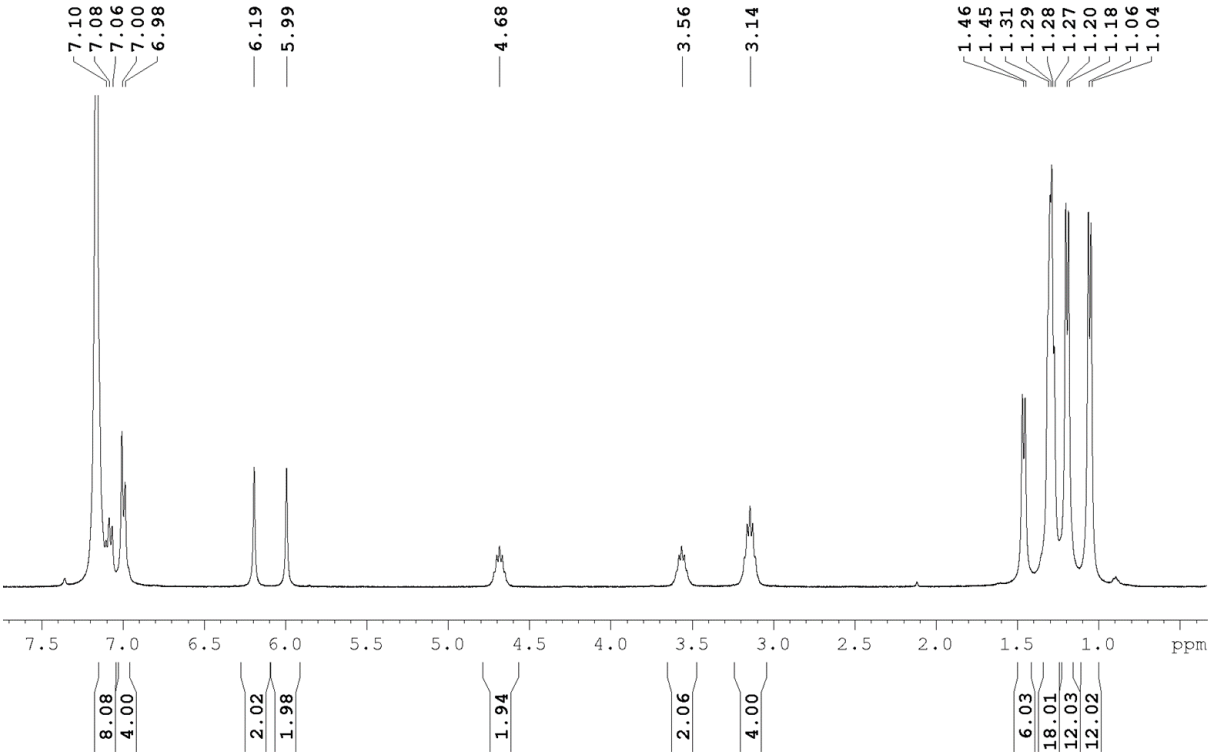

Figure 36. ^{1}H NMR spectrum (400.3 Hz) of $[Mn(CO)_4(Dipp_2NHSi)(Dipp_2NHSi\text{-}Cl)]$ (**27**) in C_6D_6.

Crystals suitable for X-ray diffraction of the complexes **25** and **27** were grown from storing at room temperature saturated solutions of **25** and **27** in a hexane / toluene mixture (1:1) at –30 °C and the solid state structures are shown in Figure 37.

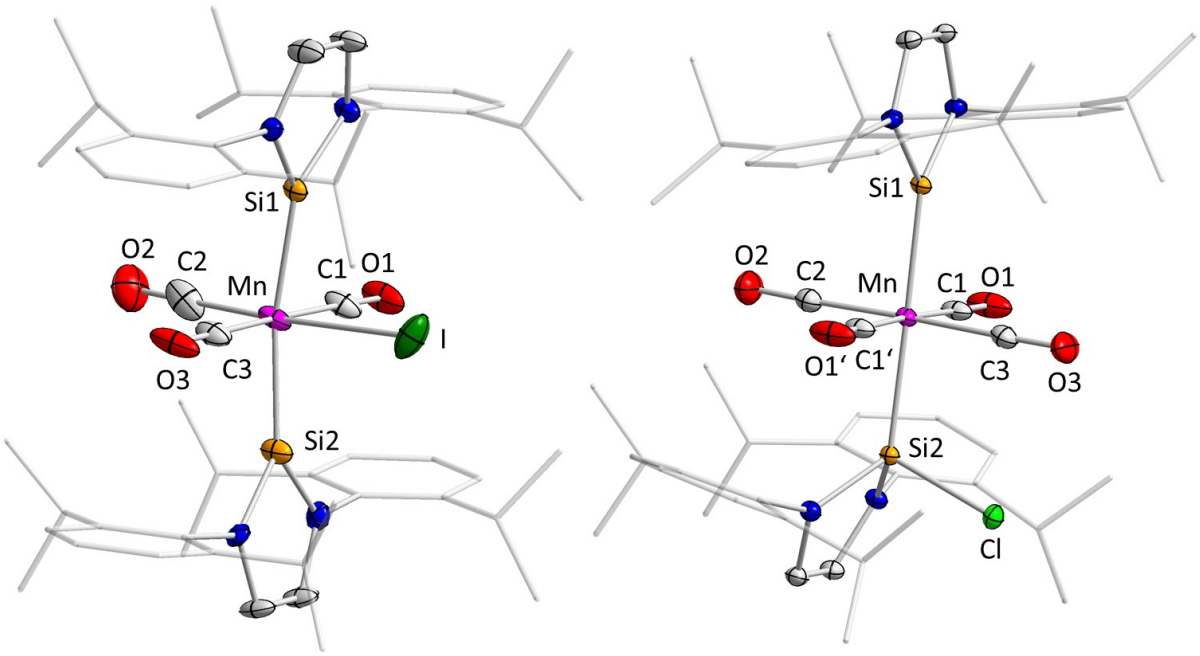

Figure 37. Molecular structure of $[Mn(CO)_3(Dipp_2NHSi)_2(I)]$ (**25,** left) and $[Mn(CO)_4(Dipp_2NHSi)(Dipp_2NHSi\text{-}Cl)]$ (**27**, right) in the solid state (ellipsoids drawn at the 50 % probability level; hydrogen atoms are omitted for clarity). Selected bond lengths [Å] and angles [°] of **25**: Mn–Si1 2.223(2), Mn–Si2 2.214(2), Mn–I 2.7134(13), Mn–C1 1.863(8), Mn–C2 1.825(10), Mn–C3 1.854(8), C1–O1 1.128(9), C2–O2 1.126(11), C3–O3 1.13(1), Si1–Mn–Si2 167.75(10). Selected bond lengths [Å] and angles [°] of **27**: Mn–Si1 2.2563(4), Mn–Si2 2.3716(4), Si2–Cl 2.1675(5), Mn–C1 1.8517(11), Mn–C2 1.8418(16), Mn–C3 1.8490(16), C1–O1 1.1403(14), C2–O2 1.140(2), C3–O3 1.139(2), Si1–I 3.2065(20), Si2–I 3.4241(23), Si1–Mn–Si2 179.084(16), Si1–Mn–I 80.35(6), Si2–Mn–I 87.43(7).

The complexes **25** and **27** crystallize in the orthorhombic space groups $P2_12_12_1$ and Pnma, respectively, and both complexes show an octahedral arrangement (Figure 37). The silylene ligands in complex $[Mn(CO)_3(Dipp_2NHSi)_2(I)]$ (**25**) are in *trans*-position to each other, adopt a staggered conformation with the iodide ligand in-plane with the carbonyl ligands. The silylenes are slightly bend towards the iodide with angles Si1–Mn–I of 80.35(6) ° and Si2–Mn–I of 87.43(7) ° (angle Si1–Mn–Si2 of 167.75(10) °). The slightly different Si–Mn–I angles are also reflected in different silicon–iodide distances Si1–I 3.2065(20) Å and Si2–I 3.4241(23) Å. The Mn–Si distances amount to

2.223(2) and 2.214(2) Å. The larger and softer iodide ligand causes an almost symmetrical interaction of the silylene ligands with the iodide atom as compared to the bromide analogue. The molecular structure of [Mn(CO)$_4$(Dipp$_2$NHSi)(Dipp$_2$NHSi-Cl)] (**27**) clearly reveals the insertion of one of the NHSi ligands into the manganese–chloride bond, which leads to the formation of a chloro silyl ligand. As this happens to only one of the silylene ligands, the other one stays intact and acts as a neutral 2 VE donor. The silyl and the silylene ligand are in *trans*-position to each other and four additional carbonyl ligands span the octahedral environment at the manganese central atom. The Mn–Si bond lengths of Mn–Si1 2.2563(4) and Mn–Si2 2.3716(4) Å are expectedly longer to the silyl silicon atom Si2 than to the silylene silicon atom Si1.

Single-crystals of complex **26** were grown by slow evaporation of a benzene solution at room temperature, and the molecular structure of **26** was established by X-ray diffraction (Figure 38).

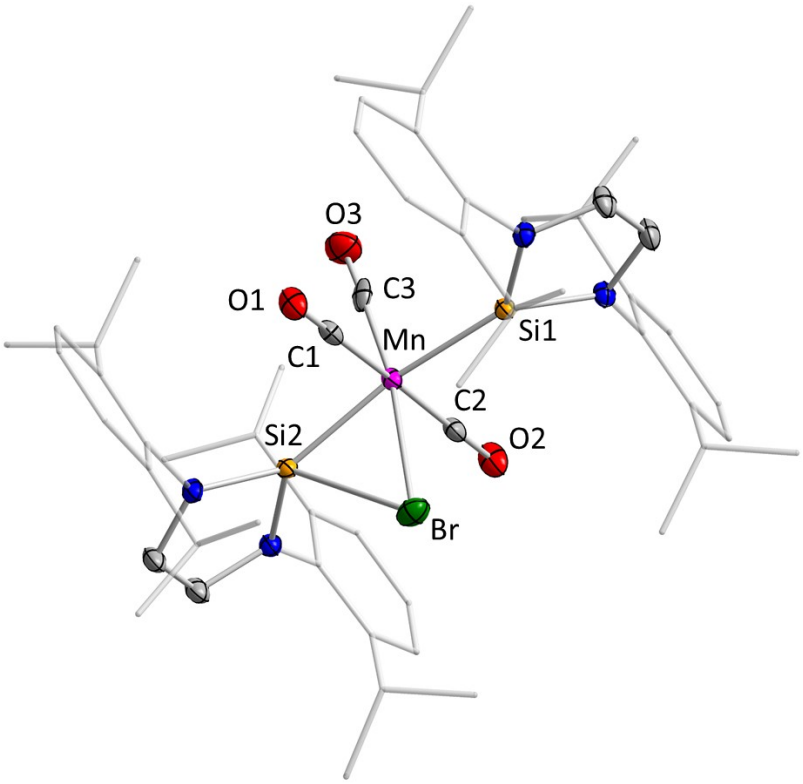

Figure 38. Molecular structure of [Mn(CO)$_3$(Dipp$_2$NHSi)$_2$(Br)] (**26**) in the solid state (ellipsoids drawn at the 50 % probability level; hydrogen atoms are omitted for clarity).

Selected bond lengths [Å] and angles [°] of **26**: Mn1–C1 1.854(3), C1–O1 1.133(4), Mn1–C2 1.852(3), C2–O2 1.142(4), Mn1–C3 1.839(3), C3–O3 1.084(4), Mn1–Br1 2.5585(5), Si1–Br1 3.6315(9), Si2–Br 2.7583(8), Si2–Mn1–Br1 69.95(2), Si1–Mn1–Br1 98.34(3), Si2–Br1–Mn1 49.43(2), Br1–Si2–Mn1 60.62(2), Si1–Mn1–Si2 168.23(4), plane (Mn1–C1–C2–C3) / plane (C1–C2–Br) 10.372(14)°.

Compound **26** crystallizes in the orthorhombic space group $P2_12_12_1$ and has a distorted octahedral structure with the silylene ligands *trans* to one another and the three CO ligands and the bromine atom lying in a plane between them. The silylenes are simultaneously bent towards the bromine atom which lies slightly out of the plane formed by the three carbonyl groups (10.37(14)°). Despite the interaction of one silylene ligand with the bromine atom, nearly the same bond lengths for Mn–Si1 (2.2329(9) Å) and Mn–Si2 (2.2304(9) Å) are observed and are similar to those of complex **27** (2.223(2) and 2.214(2) Å). The Si2–Br1 distance is 2.7583(8) Å whereas the Si1–Br1 distance is 3.6315(9) Å. The distortion of the complex is caused by an interaction of the lone pair orbitals at the bromide ligand with the unoccupied silicon p_π-orbital. DFT calculations on **26** show that the Si–Br interaction contributes to the stability of the complex and that the bromide ligand should oscillate between the two silylene silicon atoms (Figure 39).

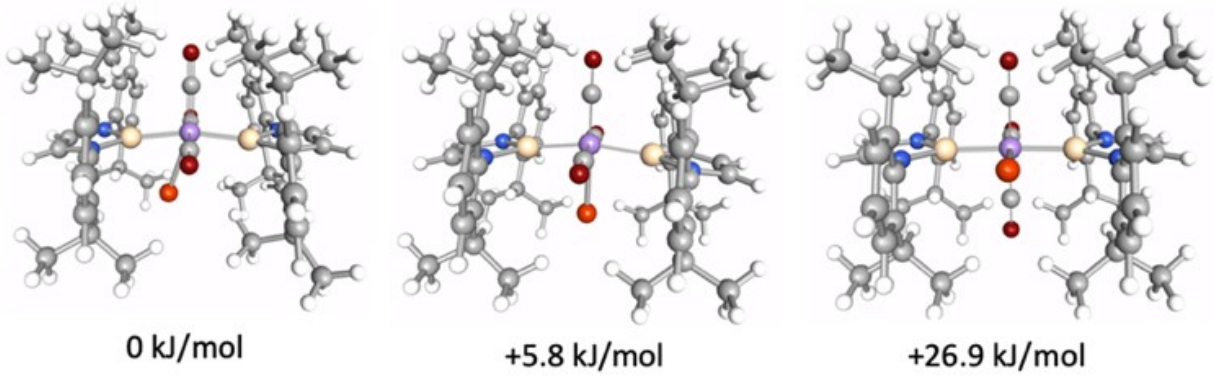

Figure 39. DFT calculations (TURBOMOLE/def2-TZVP(Mn,Si,Br)/def2-SV(P)/BP86-D3(BJ)) on $[Mn(CO)_3(Dipp_2NHSi)_2(Br)]$ **26**.

A more symmetrical arrangement with the bromide ligand in the manganese carbonyl plane (i.e. without significant interaction with the silicon atom) is energetically unfavorable by 5.8 kJ/mol (TURBOMOLE/def2-TZVP(Mn,Si,Br)/def2-SV(P)/BP86-D3(BJ)) and represents a transition state (Figure 39). However, it should be noted that the relative position of the bromide ligand with respect to the five-membered ring of the silylene ligand is also crucial for stabilization of the complex. If the bromide atom lies perpendicular to the plane spanned by the five-membered NHSi rings and interaction with the silicon atom p_{π}-orbital is enabled, the complex is stabilized, whereas if the bromide lies in the NHSi plane, such an interaction is not possible, leading to a destabilization of 26.9 kJ/mol with respect to the minimum energy structure.

In order to synthesize a mononuclear nickel NHSi complex of the type [(η^5-C_5H_5)Ni(NHSi)(Cl)] for studies by NHSi / PPh_3 ligand exchange, [(η^5-C_5H_5)Ni(PPh_3)(Cl)] was reacted with $Dipp_2$NHSi (Scheme 16). However, different other likely reaction products might arise from i) the coordination of the silylene ligand to the nickel center with simultaneous change of the hapticity of the cyclopentadienyl ligand to afford [Ni(NHSi)(PPh_3)(η^1-C_5H_5)(Cl)], ii) substitution of the phosphine ligand to give [(η^5-C_5H_5)Ni(NHSi)(Cl)]; and iii) insertion of the silicon silylene atom into the Ni–Cl bond to afford [(η^5-C_5H_5)Ni(PPh_3)($Dipp_2$NHSi-Cl)] (**28**). The reaction of $Dipp_2$NHSi with [(η^5-C_5H_5)Ni(PPh_3)(Cl)] takes place already at room temperature and the insertion product [(η^5-C_5H_5)Ni(PPh_3)($Dipp_2$NHSi-Cl)] (**28**) was isolated as a light brown solid in 75 % yield (Scheme 16).

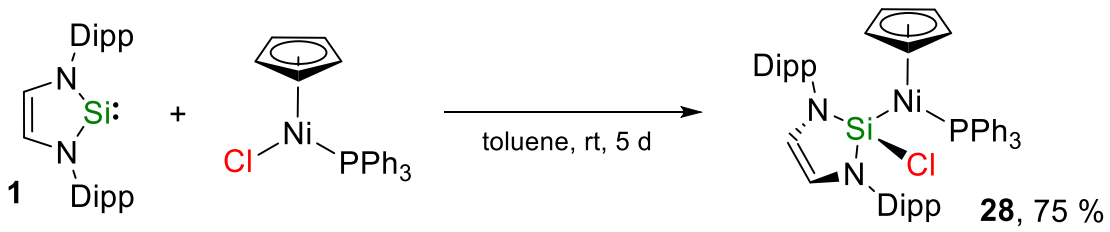

Scheme 16. Synthesis of [(η^5-C_5H_5)Ni(PPh_3)($Dipp_2$NHSi-Cl)] **28**.

Complex **28** is well soluble in polar solvents like THF and Et_2O while it is moderately soluble in toluene and only poorly soluble in hexane. Furthermore, **28** is air stable but very hygroscopic, which led to the appearance of the characteristic band of H_2O in the IR spectrum (see Experimental Details), but shows no signs of hydrolysis when stored under air for several weeks. The ^{1}H and $^{13}C\{^{1}H\}$ NMR spectra of **28** reveal a doubled set of resonances for the NHSi Dipp-substituents, which indicates an unsymmetrical environment of the silyl ligand as provided by the chloride and the {(η^5-C_5H_5)Ni(PPh_3)} substituent (Figure 40). The silicon atom gives rise to a doublet at δ = –5.59 ppm in the $^{29}Si\{^{1}H\}$ NMR spectrum of **28** with a $^{2}J(^{29}Si\text{-}^{31}P)$ coupling constant of 48 Hz, which confirms that the phosphine ligand still coordinates to the nickel atom.

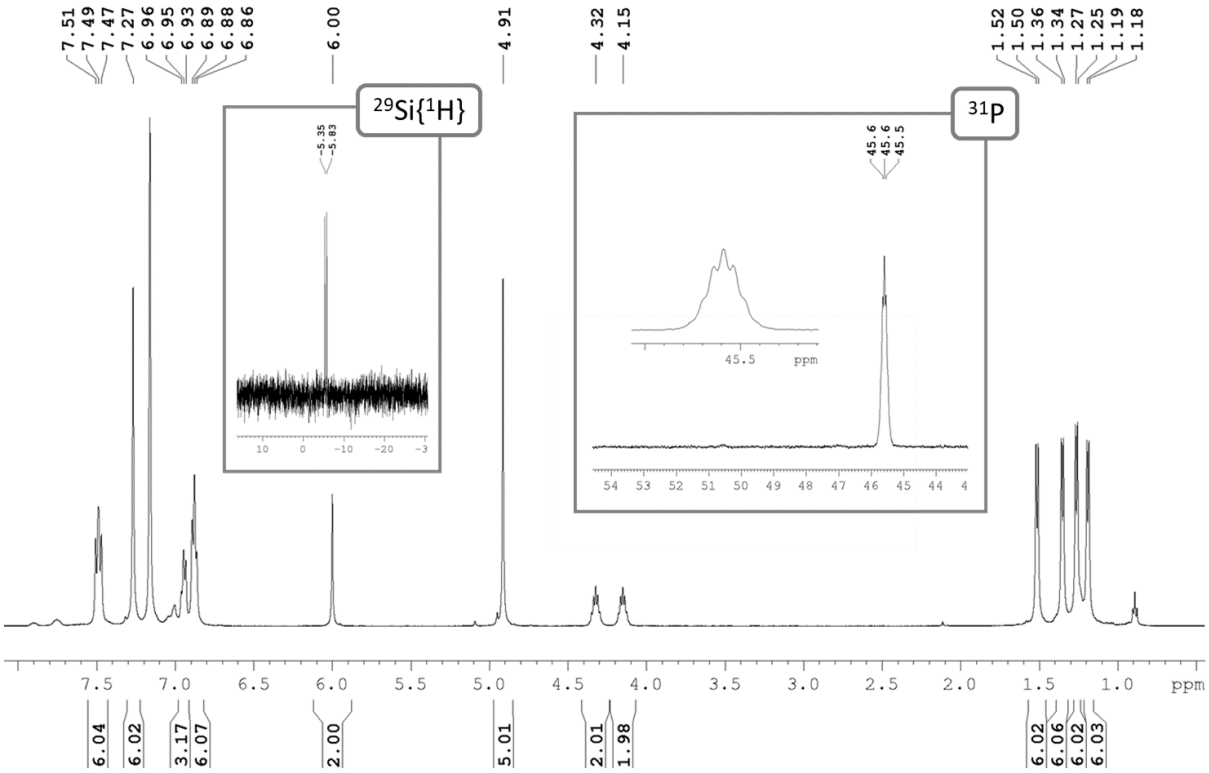

Figure 40. ^{1}H (500.1 Hz), $^{29}Si\{^{1}H\}$ (99.4 Hz) and ^{31}P NMR spectrum (202.5 Hz) of [(η^5-C_5H_5)Ni(PPh_3)($Dipp_2NHSi$-Cl)] (**28**) in C_6D_6.

Crystals of complex **28** suitable for single-crystal X-ray diffraction were grown by slow evaporation of a saturated solution of **28** in hexane / toluene at room temperature (Figure 41).

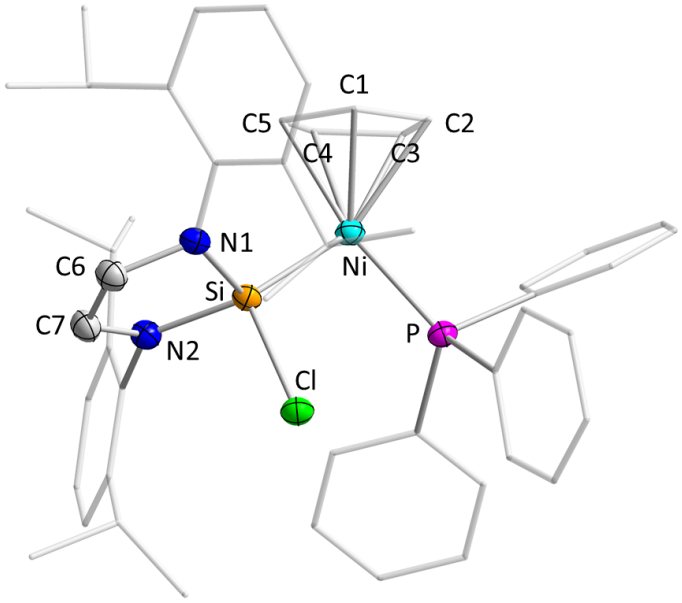

Figure 41. Molecular structure of [(η^5-C_5H_5)Ni(PPh_3)($Dipp_2NHSi$-Cl)] (**28**) in the solid state (ellipsoids drawn at the 50 % probability level; hydrogen atoms are omitted for clarity). Selected bond lengths [Å] and angles [°] of **28**: Ni–P 2.1559(7), Ni–Si 2.2247(7), Si–Cl 2.1477(8), Ni–Cl 3.5794(8), Ni–C1 2.116(2), Ni–C2 2.151(2), Ni–C3 2.144(2), Ni–C4 2.142(2), Ni–C5 2.041(2), Si–Ni–P 102.37(3), N1–Si–N2 90.18(9), Cl–Si–Ni 109.88(3), (N1–C6–C7–N2) and (N1–Si–N2) 19.694(99).

The molecular structure of **28** confirms the insertion of the silylene silicon atom into the nickel–chloride bond and that the silylene did not substitute the phosphine ligand. The nickel–silicon and nickel–phosphine distances Ni–Si of 2.2247(7) Å and Ni–P of 2.1559(7) Å are in accordance with single bonds. The Ni–P bond in **28** of 2.1559(7) Å is slightly shorter compared to the Ni–P distance found in the precursor [(η^5-C_5H_5)Ni(PPh_3)(Cl)] (2.1599(11) Å).[136] The cyclopentadienyl ligand is η^5-coordinated to the nickel atom and the nickel–carbon distances are unexceptional. Due to insertion of the NHSi into the nickel chloride bond, the former silylene acts in **28** as a tetrahedral silyl ligand, in which the N1–Si–N2 plane is bent (19.694(99) °) out of the N1–C6–C7–N2 plane.

Similarly, the reaction of $Dipp_2NHSi$ with $[(\eta^5\text{-}C_5H_5)Fe(CO)_2(I)]$ in hexane at room temperature led to formation of the iron complex $[(\eta^5\text{-}C_5H_5)Fe(CO)_2(Dipp_2NHSi\text{-}I)]$ (**29**), which is formally the product of an insertion of the silylene into the Fe–I bond (Scheme 17). There is no evidence to indicate that initial substitution of CO by $Dipp_2NHSi$ is involved in the course of this reaction. After purification, complex **29** was obtained as a red-brown solid in 60 % yield, and was characterized by IR and NMR spectroscopy and single-crystal X-ray diffraction. The IR spectrum revealed two absorptions for the symmetric and asymmetric stretches of the CO ligands at 1974 and 2021 cm^{-1}, respectively, which confirms that no carbonyl ligand was lost.

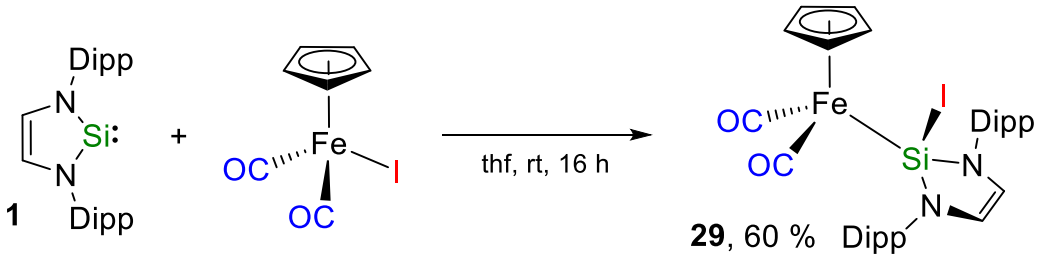

Scheme 17. Synthesis of $[(\eta^5\text{-}C_5H_5)Fe(CO)_2(Dipp_2NHSi\text{-}I)]$ **29**.

The shift of the stretching modes of complex **29** from those of the starting material $[(\eta^5\text{-}C_5H_5)Fe(CO)_2(I)]$ (1986 and 1941 cm^{-1})[137] displays the altered electronic environment at the iron atom. By symmetry (maximum = C_s), the aryl-substituents of the silylene ligand are chemically inequivalent which leads to a splitting of their resonances in the ^1H and ^{13}C NMR spectra. The CO ligands give rise to one resonance at 212.2 ppm, and the resonance of the silicon atom was detected at 17.2 ppm in the $^{29}Si\{^1H\}$ NMR spectrum, significantly shifted (59 ppm) to higher fields compared to the free NHSi. The reaction of $[(\eta^5\text{-}C_5H_5)Fe(CO)_2(I)]$ with *N*-heterocyclic carbenes leads to formation of the ionic complexes $[(\eta^5\text{-}C_5H_5)Fe(CO)_2(NHC)][I]$ (NHC = Me_2Im, iPr_2Im, Mes_2Im, etc.) by displacement of iodide.[138] In contrast to the formation of **29**, the carbene ligands are not prone to nucleophilic attack by iodide, which is in line with the properties of the NHSi as discussed prior.

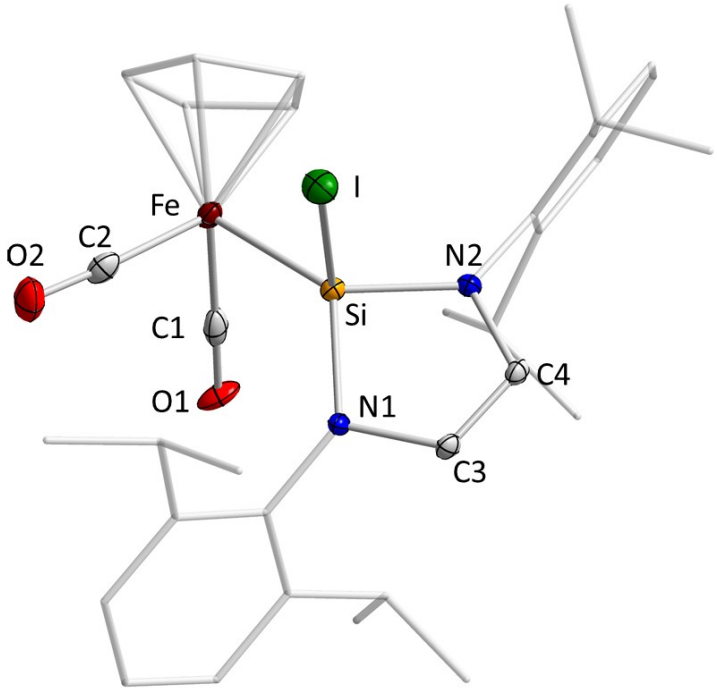

Figure 42. Molecular structure of [(η^5-C_5H_5)Fe(CO)$_2$(Dipp$_2$NHSi-I)] **29** in the solid state (ellipsoids drawn at the 50 % probability level; hydrogen atoms are omitted for clarity). Selected bond lengths [Å] and angles [°] of **29**: Fe–Si1 2.2461(9), Si1–I1 2.6443(9), Si1–N1 1.746(3), Si1–N2 1.744(3), Fe1–C32 1.767(4), Fe1–C33 1.760(4), C1–O1 1.105(4), C2–O2 1.135(4); plane (N2–C3–C4–N2) / plane (N1–Si1–N2) 20.970(139)°.

Compound **29** crystallizes as dark red crystals in the monoclinic space group P2$_1$/n (Figure 42). The X-ray diffraction analysis confirmed the insertion of the silicon atom into the iron–iodine bond leading to an oxidized silylene ligand which no longer acts as a neutral two-electron donor but as a silyl ligand, i.e., an anionic 2-VE donor ligand, which gives complex **29** an 18 electron count. The silyl ligand is tetrahedrally surrounded by iron, iodine and two nitrogen atoms with a silicon–iodine distance of 2.6443(9) Å and a silicon–iron bond length of 2.2461(9). The tetrahedral coordination at silicon leads to a twist out of the (former) NHSi plane containing the nitrogen atoms and the backbone by 20.97(14) °). There is no significant geometrical change at the [(η^5-C_5H_5)Fe(CO)$_2$] unit.

The insertion of the silylene atom of **1** with regard to different metal–halide bonds was examined. First, the influence of the halide ligand in the manganese complexes $[Mn(CO)_5(X)]$ (X = Cl, Br, I) on the reactivity of $Dipp_2NHSi$ (**1**) was investigated and two equivalents of silylene **1** were reacted with $[Mn(CO)_5(I)]$ and $[Mn(CO)_5(Br)]$ affording tricarbonyl complexes $[Mn(CO)_3(Dipp_2NHSi)_2(I)]$ (**25**) and $[Mn(CO)_3(Dipp_2NHSi)_2(Br)]$ (**26**). Whereas in **25**, the iodide ligand is symmetrically located in the $\{Mn(CO)_3\}$ plane between the silylene ligands, the bromide ligand in **26** shows a distortion out of the $\{Mn(CO)_3\}$ plane towards one silicon atom. The distortion in **26** was confirmed by X-ray analysis and DFT calculations. In case of the manganese complex $[Mn(CO)_5(Cl)]$, the reaction with $Dipp_2NHSi$ at room temperature leads to the formation of the complexes $[Mn(CO)_3(Dipp_2NHSi)_2(Cl)]$ (**27***) and $[Mn(CO)_4(Dipp_2NHSi)(Dipp_2NHSi\text{-}Cl)]$ (**27**). Raising the reaction temperature to 100 °C, the insertion product **27** is obtained as the main product and the insertion of one of the NHSi ligands into the manganese–chloride bond was verified by the spectroscopic data and molecular structure of **27**. In this series of manganese halide complexes a clear trend could be discovered. With the large and well polarizible iodide ligand a symmetrical arrangement of the halide ligand between the silylene silicon atoms is achieved. Using the smaller bromide ligand leads to a distortion of the complex and an interaction between the halide ligand and the silicon atoms of the silylene ligands. Finally, the smallest and least polarizible in this row causes the insertion of one silylene ligand into the manganese–chlorine bond. Similary, $Dipp_2NHSi$ was shown to react with the half-sandwich complexes $[(\eta^5\text{-}C_5H_5)Ni(PPh_3)(Cl)]$ and $[(\eta^5\text{-}C_5H_5)Fe(CO)_2(I)]$ *via* insertion into metal–halide bonds to give the silyl complexes $[(\eta^5\text{-}C_5H_5)Ni(PPh_3)(Dipp_2NHSi\text{-}Cl)]$ (**28**) and $[(\eta^5\text{-}C_5H_5)Fe(CO)_2(Dipp_2NHSi\text{-}I)]$ (**29**). For the good σ-donating NHCs, the substitution of the phosphine ligand in $[(\eta^5\text{-}C_5H_5)Ni(PPh_3)(Cl)]$ is the favored reaction pathway and examples for insertion reactions of NHCs into nickel–halide bonds are unknown to date.

4 Experimental Details

4.1 General procedures

All reactions and subsequent manipulations, unless otherwise stated, were performed under an argon atmosphere in an Innovative Technology Inc. glovebox or BRAUN Uni Lab or using standard Schlenk techniques. Argon was dried over silica gel and P_4O_{10}. All solvents were either HPLC grade (Honeywell), further treated to remove traces of water using an Innovative Technology Inc. Pure-Solv 400 Solvent Purification System and deoxygenated using the freeze-pump-thaw method or dried using standard procedures[139], deoxygenated and stored under an argon atmosphere. Tetrahydrofuran (THF), diethyl ether (Et_2O), toluene and benzene were dried over sodium / benzophenone and freshly distilled before use. *n*-Hexane was dried over lithium aluminium hydride and freshly distilled before use. d^8-THF, $CDCl_3$, CD_2Cl_2, d^8-toluene and C_6D_6 were obtained from Sigma Aldrich, dried over sodium or calcium dihydride, respectively, distilled and stored under an argon atmosphere over 4 Å molecular sieves.

Safety precautions in handling [Ni(CO)$_4$]

Special care has been taken while manipulating the extremely toxic, flammable and volatile (b.p. 43°C) [Ni(CO)$_4$]. All manipulations were carried out in a well-ventilated fume hood or in a glovebox. Safety glasses, an apron and gloves using additional protective gloves should be worn when handling this reagent. [Ni(CO)$_4$] should be maintained at temperatures below 0 °C. Traces of [Ni(CO)$_4$] can be disposed of by treatment with concentrated nitric acid diluted 1:1 with water and all glassware used should be treated with the nitric acid solution.

UV irradiation

For irradiation, a mercury vapor lamp with a wavelength of λ = 254 nm was used.

Starting materials

All starting materials were purchased from ABCR, Sigma Aldrich and the chemical distribution center of the University of Würzburg and usually used without further

purification. The following reagents were prepared according to literature procedures: $B(C_6F_5)_3$[140], $Al(C_6F_5)_3$[141], $[Mn(CO)_5(Cl)]$[142], $[Mn(CO)_5(Br)]$[143], $[Mn(CO)_5(I)]$[142], $[\{(\eta^5\text{-}C_5H_5)Fe(CO)_2\}_2]$[144] and $Dipp_2NHSi$[6f, 45]. The following reagents were available in the working group: $[Ni(\eta^5\text{-}C_5H_5)_2]$, $[(\eta^5\text{-}C_5H_5)_2Ni(PPh_3)(Cl)]$.

4.2 Analytical methods

Elemental analysis

Elemental analyses were performed in the micro analytical laboratory of the Institute of Inorganic Chemistry at the University of Würzburg with an Elementar vario MICRO cube and are reported in wt%.

4.3 Spectroscopic methods

IR spectroscopy

Infrared spectra were recorded on solid samples at room temperature on a Bruker Alpha FT-IR spectrometer using an ATR unit and are reported in cm^{-1}. In dependence of the intensity of the vibration bands the following abbreviations were used: very strong (vs), strong (s), middle (m), weak (w) and very weak (vw).

NMR spectroscopy

NMR spectra were recorded on Bruker Avance 300 (^1H: 300.1 MHz, $^{13}C\{^1H\}$: 75.5 MHz, $^{29}Si\{^1H\}$: 59.6 MHz), Bruker NEO 400 (^1H: 400.3 MHz, $^{13}C\{^1H\}$: 100.7 MHz, $^{19}F\{^1H\}$: 376.6 , $^{29}Si\{^1H\}$: 79.5, $^{31}P\{^1H\}$: 162.0 MHz), Bruker Avance 400 (^1H: 400.1 MHz, $^{13}C\{^1H\}$: 100.7 MHz, $^{27}Al\{^1H\}$: 104.4 MHz, $^{29}Si\{^1H\}$: 79.6 MHz) or Bruker Avance 500 (^1H: 500.1 MHz, $^{11}B\{^1H\}$: 160.5 MHz, $^{19}F\{^1H\}$: 470.6 MHz, $^{13}C\{^1H\}$: 125.8 MHz, $^{29}Si\{^1H\}$: 99.4 MHz, $^{31}P\{^1H\}$: 202.5 MHz, $^{119}Sn\{^1H\}$: 186.5 MHz) spectrometers in d^8-THF, $CDCl_3$, CD_2Cl_2, d^8-toluene and C_6D_6 solutions at room temperature if not stated differently. Chemical shifts are listed in parts per million (ppm) and were calibrated

against the residual solvent signals (δ (^{1}H): d^7-THF 3.58, C(D/H)Cl$_3$ 7.26, CDHCl$_2$ 5.32, d^7-toluene 2.08, C$_6$D$_5$H 7.16; δ (^{13}C): d^8-THF 67.21, CDCl$_3$ 77.16, CD$_2$Cl$_2$ 53.84, d^8-toluene 20.43, C$_6$D$_6$ 128.06). Coupling constants (J) are quoted in Hertz (Hz) without consideration of the sign. For multiplicities, the following abbreviations are used: s = singlet, d = doublet, t = triplet, sept = septet, m = multiplet, br = broad, v = very.

4.4 Synthesis of the starting material Dipp$_2$NHSi

1,4-Bis(2,6-diisopropylphenyl)-1,3-diazabutadiene[145]

2,6-Di*iso*propylphenyl amine (94.0 g, 100 mL, 530 mmol) and glyoxal (15.4 g, 30.6 mL, 265 mmol, 40% in H$_2$O) were dissolved in ethanol (500 mL), treated with formic acid (2 drops) and stirred at room temperature for 16 h. The precipitate was filtered off, washed with *n*-propanol (3x 100 mL) and dried *in vacuo* to yield a yellow solid (84.7 g, 225 mmol, 85 %).

^{1}H-NMR (400.3 MHz, CDCl$_3$, 298 K): δ [ppm] = 1.21 (d, 24H, $^3J_{H\text{-}H}$ = 6.8 Hz, *i*Pr-C*H*$_3$), 2.99 (sept, 4H, $^3J_{H\text{-}H}$ = 6.8 Hz, *i*Pr-C*H*), 7.08 – 7.30 (m, 6H, aryl-C*H*), 8.10 (s, 2H, C*H*).

^{13}C{^{1}H} NMR (100.7 MHz, CDCl$_3$, 298 K): δ [ppm] = 23.5 (*i*Pr-*C*H$_3$), 28.2 (*i*Pr-*C*H), 123.3 (aryl-*C*H), 125.3 (aryl-*C*H), 136.9 (aryl-*C*), 148.1 (aryl-*C*), 163.2 (N*CC*N).

1,3-Bis(2,6-diisopropylphenyl)-1,3-diaza-2,2-dichlor-2-silacyclopent-4-ene[45]

1,4-Bis(2,6-di*iso*propylphenyl)-1,3-diazabutadiene (10.0 g, 26.6 mmol) and DABCO (20.9 g, 186 mmol, 7.0 eq.) were dissolved in CH$_2$Cl$_2$ (100 mL), cooled to –78 °C and treated with HSiCl$_3$ (4.43 g, 3.31 mL, 32.7 mmol, 1.2 eq.). The reaction mixture was slowly warmed up to room temperature and stirred for 16 h. All volatiles were removed under reduced pressure, the remaining solid was suspended in hexane (60 mL) and filtered through a pad of Celite. The solvent was removed *in vacuo* and residual DABCO was removed *via* sublimation at $1 \cdot 10^{-3}$ mbar at 50 – 60 °C to yield a colourless solid (10.3 g, 21.7 mmol, 82 %).

^{1}H-NMR (500.1 MHz, CD_2Cl_2, 298 K): δ [ppm] = 1.20 (d, 12H, $^{3}J_{H-H}$ = 6.9 Hz, *i*Pr-C*H*$_3$), 1.31 (d, 12H, $^{3}J_{H-H}$ = 6.9 Hz, *i*Pr-C*H*$_3$), 3.48 (sept, 4H, $^{3}J_{H-H}$ = 6.9 Hz, *i*Pr-C*H*), 5.83 (s, 2H, NC*H*CHN), 7.21 – 7.33 (m, 6H, aryl-C*H*).

^{13}C{^{1}H} NMR (125.8 MHz, CD_2Cl_2, 298 K): δ [ppm] = 23.9 (*i*Pr-*C*H$_3$), 26.0 (*i*Pr-*C*H$_3$), 28.7 (*i*Pr-*C*H$_3$), 119.9 (N*C*CN), 124.5 (aryl-*C*$_{para}$), 128.2 (aryl-*C*$_{meta}$), 135.3 (aryl-*C*$_{ortho}$), 148.8 (aryl-*C*$_{ipso}$).

^{29}Si{^{1}H} NMR (99.4 MHz, CD_2Cl_2, 298 K): δ [ppm] = 38.6.

*1,3-Bis(2,6-diisopropylphenyl)-1,3-diaza-2-silacyclopent-4-en-2-ylidene (**1**)*[6f]

Lithium (128 mg, 18.5 mmol, 2.2 eq.) and naphthalene (237 mg, 1.85 mmol, 0.1 eq.) in THF (40 mL) were irradiated in an ultrasonic bath for 30 minutes. The obtained dark green solution was treated with 1,3-bis(2,6-di*iso*propylphenyl)-1,3-diaza-2,2-dichlor-2-silacyclopent-4-ene (4.00 g, 8.41 mmol) in THF (40 mL) in several portions and stirred at room temperature for 16 h. All volatiles were removed *in vacuo*, the remaining solid was suspended in hexane (50 mL) and filtered through a pad of Celite. The filtrate was evaporated to dryness and naphthalene was removed *via* sublimation at $1 \cdot 10^{-3}$ mbar at 50 – 60 °C to yield **1** as an orange solid (3.30 g, 8.15 mmol, 97 %).

^{1}H-NMR (300.1 MHz, C_6D_6, 298 K): δ [ppm] = 1.20 (d, 12H, $^{3}J_{H-H}$ = 6.9 Hz, *i*Pr-C*H*$_3$), 1.28 (d, 12H, $^{3}J_{H-H}$ = 6.9 Hz, *i*Pr-C*H*$_3$), 3.28 (sept, 4H, $^{3}J_{H-H}$ = 6.9 Hz, *i*Pr-C*H*), 6.46 (s, 2H, NC*H*CHN), 7.15 – 7.26 (m, 6H, aryl-C*H*).

^{13}C{^{1}H} NMR (75.5 MHz, C_6D_6, 298 K): δ [ppm] = 24.4 (*i*Pr-*C*H$_3$), 25.7 (*i*Pr-*C*H$_3$), 28.8 (*i*Pr-*C*H), 123.7 (aryl-*C*$_{meta}$), 125.5 (N*C*CN), 127.9 (aryl-*C*$_{para}$), 139.3 (aryl-*C*$_{ipso}$), 146.1 (aryl-*C*$_{ortho}$).

^{29}Si{^{1}H} NMR (59.6 MHz, C_6D_6, 298 K): δ [ppm] = 76.1.

4.5 N-Heterocyclic Silylenes as ambiphilic Reagents in Main Group Chemistry

4.5.1 Adduct formation of $Dipp_2NHSi$ with Lewis Acids

*$Dipp_2NHSi{\cdot}AlI_3$ (**2**)*

1,3-Bis(2,6-di*iso*propylphenyl)-1,3-diaza-2-silacyclopent-4-en-2-ylidene (50.0 mg, 124 *µ*mol) and AlI_3 (51.0 mg, 124 *µ*mol) were dissolved in benzene (3 mL) and stirred at room temperature for 16 h. All volatiles were removed *in vacuo*, the remaining solid was washed with hexane (3x 2 mL) and evacuated to dryness to yield **2** as an off-white solid (84.5 mg, 108 *µ*mol, 87 %).

^{1}H NMR (400.3 MHz, C_6D_6, 298 K): *δ* [ppm] = 1.08 (d, 12H, $^{3}J_{H\text{-}H}$ = 6.8 Hz, *i*Pr-C*H*$_3$), 1.41 (d, 12H, $^{3}J_{H\text{-}H}$ = 6.8 Hz, *i*Pr-C*H*$_3$), 3.08 (sept, 4H, $^{3}J_{H\text{-}H}$ = 6.8 Hz, *i*Pr-C*H*), 6.16 (s, 2H, NC*H*CHN), 7.08 – 7.10 (d, 4H, aryl-C*H*), 7.18 – 7.20 (d, 2H, aryl-C*H*).

^{13}C{^{1}H} NMR (100.7 MHz, C_6D_6, 298 K): *δ* [ppm] = 24.5 (*i*Pr-*C*H$_3$), 25.2 (*i*Pr-*C*H$_3$), 29.4 (*i*Pr-*C*H), 124.4 (aryl-*C*$_{meta}$), 126.3 (N*C*CN), 129.6 (aryl-*C*$_{para}$), 136.0 (aryl-*C*$_{ipso}$), 145.0 (aryl-*C*$_{ortho}$).

^{27}Al NMR (104.4 MHz, C_6D_6, 298 K): *δ* [ppm] = 40.1.

^{29}Si{^{1}H} NMR (79.5 MHz, C_6D_6, 298 K): *δ* [ppm] = 42.8.

Elemental analysis (%) calcd. for $C_{26}H_{36}N_2SiAlI_3$: C 39.82, H 4.63, N 3.57; found C 23.89, H 3.65, N 1.55. Despite repeated attempts, satisfactory elemental analysis of **2** was not possible, due to very high sensitivity of **2** towards air and moisture.

*$Dipp_2NHSi{\cdot}Al(C_6F_5)_3$ (**3**)*

1,3-Bis(2,6-di*iso*propylphenyl)-1,3-diaza-2-silacyclopent-4-en-2-ylidene (50.0 mg, 124 *µ*mol) and $Al(C_6F_5)_3$ (65.3 mg, 124 *µ*mol) were dissolved in hexane (4 mL) and toluene (2 mL) and stirred at room temperature for 16 h. All volatiles were removed *in*

vacuo, the remaining solid was washed with hexane (3x 2 mL) and evacuated to dryness to yield **3** as a yellow solid (72.3 mg, 77.5 *µ*mol, 63 %).

^{1}H NMR (400.3 MHz, C_6D_6, 298 K): *δ* [ppm] = 1.03 (d, 12H, $^{3}J_{H\text{-}H}$ = 6.9 Hz, *i*Pr-C*H*$_3$), 1.12 (d, 12H, $^{3}J_{H\text{-}H}$ = 6.9 Hz, *i*Pr-C*H*$_3$), 3.02 (sept, 4H, $^{3}J_{H\text{-}H}$ = 6.9 Hz, *i*Pr-C*H*), 6.26 (s, 2H, NC*H*CHN), 6.99 (d, 4H, $^{3}J_{H\text{-}H}$ = 7.7 Hz, aryl-C*H*), 7.15 (t, 2H, $^{3}J_{H\text{-}H}$ = 7.7 Hz, aryl-C*H*).

^{13}C{^{1}H} NMR (125.8 MHz, C_6D_6, 298 K): *δ* [ppm] = 22.7 (*i*Pr-*C*H$_3$), 25.8 (*i*Pr-*C*H$_3$), 29.3 (*i*Pr-*C*H), 124.0 (aryl-*C*), 126.1 (N*C*CN), 127.2 (aryl-*C*), 129.4 (aryl-*C*), 135.4 (aryl-*C*), 144.9 (aryl-*C*). The signals of the carbon atoms of the pentafluorophenyl substituents could not be detected.

^{19}F NMR (376.6 MHz, C_6D_6, 298 K): *δ* [ppm] = -123.0 (dm, 6F, $^{3}J_{F\text{-}F}$ = 29.3 Hz, aryl-C*F*), -150.7 (tt, 3F, $^{3}J_{F\text{-}F}$ = 20.0 Hz, $^{4}J_{F\text{-}F}$ = 2.6 Hz, aryl-CF_{para}), -160.5 (m, 6F, aryl-C*F*).

^{27}Al NMR: The signal of the aluminium atom could not be detected.

^{29}Si{^{1}H} NMR (79.5 MHz, C_6D_6, 298 K): *δ* [ppm] = 74.0.

Elemental analysis (%) calcd. for $C_{44}H_{36}N_2Si\,AlF_{15}$: C 56.65, H 3.89, N 3.00; found C 56.65, H 4.60, N 3.13.

*Dipp$_2$NHSi·B(C$_6$F$_5$)$_3$ (**4**)*

1,3-Bis(2,6-di*iso*propylphenyl)-1,3-diaza-2-silacyclopent-4-en-2-ylidene (50.0 mg, 124 *µ*mol) and $B(C_6F_5)_3$ (63.3 mg, 124 *µ*mol) were dissolved in hexane (4 mL) and toluene (2 mL) and stirred at room temperature for 16 h. All volatiles were removed *in vacuo*, the remaining solid was washed with hexane (3x 2 mL) and evacuated to dryness to yield **4** as a pale-yellow solid (80.4 mg, 87.7 *µ*mol, 71 %). Crystals suitable for X-ray diffraction were grown from an at room temperature saturated hexane solution of **4** at -30 °C.

^{1}H NMR (500.1 MHz, C_6D_6, 298 K): *δ* [ppm] = 0.96 (d, 12H, $^{3}J_{H\text{-}H}$ = 6.8 Hz, *i*Pr-C*H*$_3$), 1.07 (d, 12H, $^{3}J_{H\text{-}H}$ = 6.8 Hz, *i*Pr-C*H*$_3$), 3.00 (sept, 4H, $^{3}J_{H\text{-}H}$ = 6.8 Hz, *i*Pr-C*H*), 6.02 (s,

2H, NC*H*CHN), 6.90 (d, 4H, $^{3}J_{H\text{-}H}$ = 7.8 Hz, aryl-C*H*$_{meta}$), 7.08 (t, 2H, $^{3}J_{H\text{-}H}$ = 7.8 Hz, aryl-C*H*$_{para}$).

^{11}B{^{1}H} NMR (160.5 MHz, C_6D_6, 298 K): *δ* [ppm] = -19.9.

^{13}C NMR (125.8 MHz, C_6D_6, 298 K): *δ* [ppm] = 21.9 (qm, $^{1}J_{C\text{-}H}$ = 126 Hz, *i*Pr-*C*H$_3$), 26.1 (qm, $^{1}J_{C\text{-}H}$ = 126 Hz, *i*Pr-*C*H$_3$), 29.5 (dm, $^{1}J_{C\text{-}H}$ = 126 Hz, *i*Pr-*C*H), 123.4 (m, N*C*CN), 124.2 (d, $^{1}J_{C\text{-}H}$ = 10.7 Hz, aryl-*C*), 124.7 (m, aryl-*C*), 125.7 (d, $^{1}J_{C\text{-}H}$ = 10.7 Hz, aryl-*C*), 127.7 (s, aryl-*C*), 128.4 (s, aryl-*C*), 129.0 (s, aryl-*C*), 129.6 (s, aryl-*C*), 136.4 (m, aryl-*C*), 136.9 (m, aryl-*C*), 138.4 (m, aryl-*C*), 144.5 (s, aryl-*C*), 147.3 (m, aryl-*C*), 149.2 (m, aryl-*C*).

^{19}F NMR (160.5 MHz, C_6D_6, 298 K): *δ* [ppm] = -129.0 (s, 6F, aryl-C*F*), -155.9 (s, 3F, aryl-C*F*$_{para}$), -162.2 (s, 6F, aryl-C*F*).

^{29}Si{^{1}H} NMR (99.4 MHz, C_6D_6, 298 K): *δ* [ppm] = 72.2.

Elemental analysis (%) calcd. for $C_{44}H_{36}N_2SiBF_{15}$: C 57.65, H 3.96, N 3.06; found C 56.87, H 4.77, N 2.87.

*General procedure for reactions of Dipp$_2$NHSi·Al(C$_6$F$_5$)$_3$ (**3**) and Dipp$_2$NHSi·B(C$_6$F$_5$)$_3$ (**4**) in a Young-tap NMR tube*

Dipp$_2$NHSi·E(C$_6$F$_5$)$_3$ (E = B, Al; 24.7 *μ*mol) was dissolved in C_6D_6 (0.6 mL) and the respective substrate (24.7 *μ*mol, 1 eq.) was added. In case of gases, the freeze-pump-thaw method was used to change the atmosphere in the NMR tube. The reaction mixture was measured using multinuclear NMR spectroscopy after 16 h at room temperature. For Dipp$_2$NHSi·Al(C$_6$F$_5$)$_3$ (**3**), carbon monoxide, phenylacetylene, B$_2$pin$_2$ and paraformaldehyde were examined. For Dipp$_2$NHSi·B(C$_6$F$_5$)$_3$ (**4**), dihydrogen, white phosphorus and diphenylacetylene were used.

4.5.2 Insertion of $Dipp_2NHSi$ into element–halide bonds

*1,3-Bis(2,6-diisopropylphenyl)-1,3-diaza-2,2-dibromo-2-silacyclopent-4-ene (**5**)*

1,3-Bis(2,6-di*iso*propylphenyl)-1,3-diaza-2-silacyclopent-4-en-2-ylidene (100 mg, 247 *µ*mol) was dissolved in toluene (5 mL), Br_2 (21.7 mg, 7.00 *µ*L, 272 *µ*mol, 1.1 eq.) was added to the reaction mixture and stirred at room temperature for 16 h. All volatiles were removed *in vacuo*, the remaining solid was suspended in hexane (3 mL) and stored at -30 °C to yield **5** as a pale-yellow solid (86.4 mg, 153 *µ*mol, 62 %). Crystals suitable for X-ray diffraction were grown from an at room temperature saturated hexane solution of **5** at -30 °C.

^{1}H NMR (300.1 MHz, C_6D_6, 298 K): *δ* [ppm] = 1.18 (d, 12H, $^3J_{H\text{-}H}$ = 6.8 Hz, *i*Pr-C*H*$_3$), 1.37 (d, 12H, $^3J_{H\text{-}H}$ = 6.8 Hz, *i*Pr-C*H*$_3$), 3.71 (sept, 4H, $^3J_{H\text{-}H}$ = 6.8 Hz, *i*Pr-C*H*), 5.74 (s, 2H, NC*H*CHN), 7.11 – 7.22 (m, 6H, aryl-C*H*).

^{13}C{^{1}H} NMR (100.7 MHz, C_6D_6, 298 K): *δ* [ppm] = 24.1 (*i*Pr-*C*H$_3$), 26.2 (*i*Pr-*C*H$_3$), 28.8 (*i*Pr-*C*H), 120.7 (aryl-*C*$_{meta}$), 124.6 (N*C*CN), 128.6 (aryl-*C*$_{para}$), 135.4 (aryl-*C*$_{ipso}$), 148.5 (aryl-*C*$_{ortho}$).

^{29}Si{^{1}H} NMR (79.5 MHz, C_6D_6, 298 K): *δ* [ppm] = -59.3.

Elemental analysis (%) calcd. for $C_{26}H_{36}N_2SiBr_2$: C 55.32, H 6.43, N 4.96; found C 55.58, H 6.66, N 4.54.

*1,3-Bis(2,6-diisopropylphenyl)-1,3-diaza-2,2-diiodo-2-silacyclopent-4-ene (**6**)*

1,3-Bis(2,6-di*iso*propylphenyl)-1,3-diaza-2-silacyclopent-4-en-2-ylidene (100 mg, 247 *µ*mol) was dissolved in toluene (5 mL), I_2 (34.5 mg, 272 *µ*mol, 1.1 eq.) was added to the reaction mixture and stirred at room temperature for 16 h. All volatiles were removed *in vacuo*, the remaining solid was suspended in hexane (3 mL) and stored at -30 °C to yield **6** as a pale-yellow solid (92.9 mg, 141 *µ*mol, 57 %). Crystals suitable for X-ray diffraction were grown by slow evaporation of a saturated hexane solution of **6** at room temperature.

^{1}H NMR (300.1 MHz, C_6D_6, 298 K): δ [ppm] = 1.17 (d, 12H, $^{3}J_{H\text{-}H}$ = 6.8 Hz, *i*Pr-C*H*$_3$), 1.42 (d, 12H, $^{3}J_{H\text{-}H}$ = 6.8 Hz, *i*Pr-C*H*$_3$), 3.76 (sept, 4H, $^{3}J_{H\text{-}H}$ = 6.8 Hz, *i*Pr-C*H*), 5.77 (s, 2H, NC*H*CHN), 7.13 – 7.27 (m, 6H, aryl-C*H*).

^{13}C{^{1}H} NMR (100.7 MHz, C_6D_6, 298 K): δ [ppm] = 24.3 (*i*Pr-*C*H$_3$), 26.5 (*i*Pr-*C*H$_3$), 29.2 (*i*Pr-*C*H), 121.6 (aryl-*C*$_{meta}$), 124.8 (N*C*CN), 128.6 (aryl-*C*$_{para}$), 135.7 (aryl-*C*$_{ipso}$), 148.6 (aryl-*C*$_{ortho}$).

^{29}Si{^{1}H} NMR (79.5 MHz, C_6D_6, 298 K): δ [ppm] = -134.5.

Elemental analysis (%) calcd. for $C_{26}H_{36}N_2SiI_2$: C 47.43, H 5.51, N 4.25; found C 45.12, H 5.61, N 4.14. Despite repeated attempts, satisfactory elemental analysis of **6** was not possible, due to very high sensitivity of **6** towards air and moisture.

*1,3-Bis(2,6-diisopropylphenyl)-1,3-diaza-2,2-diphenyl-2-silacyclopent-4-ene (**7**)*

1,3-Bis(2,6-di*iso*propylphenyl)-1,3-diaza-2,2-dichlor-2-silacyclopent-4-ene (1.00 g, 2.10 mmol) was dissolved in THF (50 mL) and phenyllithium (3.18 mL, 4.20 mmol, 2.0 eq.) was added to the yellow solution. The reaction mixture was stirred at room temperature for 16 h. All volatiles were removed *in vacuo*, the remaining solid was suspended in hexane (3 mL) and filtered through a pad of Celite. The filtrate was concentrated and stored at -30 °C to yield **6** as an off-white crystalline solid (1.08 g, 1.93 mmol, 92 %). Crystals suitable for X-ray diffraction were grown from an at room temperature saturated hexane solution of **7** at -30 °C.

^{1}H NMR (400.3 MHz, C_6D_6, 298 K): δ [ppm] = 0.79 (d, 6H, $^{3}J_{H\text{-}H}$ = 6.9 Hz, *i*Pr-C*H*$_3$), 1.26 (d, 6H, $^{3}J_{H\text{-}H}$ = 6.9 Hz, *i*Pr-C*H*$_3$), 3.67 (sept, 2H, $^{3}J_{H\text{-}H}$ = 6.9 Hz, *i*Pr-C*H*), 5.89 (s, 2H, NC*H*CHN), 6.91 – 6.95 (m, 4H, aryl-C*H*), 7.01 – 7.05 (m, 2H, aryl-C*H*), 7.13 – 7.15 (m, 4H, aryl-C*H*), 7.20 – 7.23 (m, 2H, aryl-C*H*), 7.38 – 7.40 (m, 4H, aryl-C*H*).

^{13}C{^{1}H} NMR (100.7 MHz, C_6D_6, 298 K): δ [ppm] = 23.3 (*i*Pr-*C*H$_3$), 26.0 (*i*Pr-*C*H$_3$), 28.7 (*i*Pr-*C*H), 121.3 (aryl-*C*), 124.4 (N*C*CN), 127.2 (aryl-*C*), 127.7 (aryl-*C*), 130.3 (aryl-*C*), 134.9 (aryl-*C*), 135.2 (aryl-*C*), 140.1 (aryl-*C*), 148.7 (aryl-*C*).

^{29}Si{^{1}H} NMR (79.5 MHz, C_6D_6, 298 K): δ [ppm] = -23.9.

Elemental analysis (%) calcd. for $C_{38}H_{46}N_2Si$: C 81.67, H 8.30, N 5.01; found C 81.67, H 8.79, N 5.00.

*Reaction of Dipp$_2$NHSi (**1**) with Ph$_2$SnCl$_2$*

1,3-Bis(2,6-di*iso*propylphenyl)-1,3-diaza-2-silacyclopent-4-en-2-ylidene (25.0 mg, 61.8 *µ*mol) and diphenyltin dichloride (21.2 mg, 61.8 *µ*mol, 1 eq.) were dissolved in C_6D_6 (0.6 mL) in a Young-tap NMR tube. After 16 h at room temperature, the reaction mixture was measured using multinuclear NMR spectroscopy comprising a mixture of compounds.

^{1}H NMR (500.1 MHz, C_6D_6, 298 K): *δ* [ppm] = 1.19 (d, 12H, $^3J_{H\text{-}H}$ = 6.9 Hz, *i*Pr-C*H*$_3$), 1.35 (d, 12H, $^3J_{H\text{-}H}$ = 6.9 Hz, *i*Pr-C*H*$_3$), 3.67 (sept, 2H, $^3J_{H\text{-}H}$ = 6.9 Hz, *i*Pr-C*H*), 5.72 (s, 2H, NC*H*CHN), 6.99 – 7.01 (m, 6H, aryl-C*H*), 7.11 – 7.12 (m, 7H, aryl-C*H*), 7.17 – 7.20 (m, 2H, aryl-C*H*), 7.37 – 7.39 (m, 1H, aryl-C*H*), 7.55 – 7.57 (m, 1H, aryl-C*H*), 7.62 – 7.67 (m, 2H, aryl-C*H*).

^{13}C{^{1}H} NMR (125.8 MHz, C_6D_6, 298 K): *δ* [ppm] = 24.0 (*i*Pr-*C*H$_3$, Dipp$_2$NHSi(Cl)$_2$), 26.1 (*i*Pr-*C*H$_3$, Dipp$_2$NHSi(Cl)$_2$), 28.7 (*i*Pr-*C*H, Dipp$_2$NHSi(Cl)$_2$), 119.9 (aryl-*C*$_{meta}$, Dipp$_2$NHSi(Cl)$_2$), 124.6 (N*C*CN, Dipp$_2$NHSi(Cl)$_2$), 126.1 (aryl-*C*), 128.4 (aryl-*C*), 128.5 (aryl-*C*), 129.4 (aryl-*C*$_{para}$, Dipp$_2$NHSi(Cl)$_2$), 129.8 (aryl-*C*), 130.6 (aryl-*C*), 131.7 (aryl-*C*), 135.3 (aryl-*C*$_{ipso}$, Dipp$_2$NHSi(Cl)$_2$), 136.5 (aryl-*C*), 148.5 (aryl-*C*$_{ortho}$, Dipp$_2$NHSi(Cl)$_2$).

^{29}Si{^{1}H} NMR (99.4 MHz, C_6D_6, 298 K): *δ* [ppm] = -38.2.

^{119}Sn{^{1}H} NMR (186.5 MHz, C_6D_6, 298 K): *δ* [ppm] = -218.6, -207.2 ((Ph$_2$Sn)$_6$), -201.5, -201.3, -200.7, -200.2, -200.0, -199.9, -199.8, -199.5, -199.2, -198.6.

*1,4-Bis(2,6-diisopropylphenyl)-1,4-bis(trimethylstannyl)-1,4-diazabut-2-ene (**9**)*

1,3-Bis(2,6-di*iso*propylphenyl)-1,3-diaza-2-silacyclopent-4-en-2-ylidene (50.0 mg, 124 *µ*mol) and trimethyltin chloride (74.1 mg, 372 *µ*mol, 3 eq.) were dissolved in hexane (5 mL) and stirred at room temperature for 1 h. All volatiles were removed *in*

vacuo, the remaining solid was suspended in hexane (3 mL) and stored at -30 °C to yield **9** as a colourless solid (65 mg, 92.3 *µ*mol, 74 %). Crystals suitable for X-ray diffraction were grown by slow evaporation of a saturated benzene solution of **9** at room temperature.

^{1}H NMR (400.3 MHz, C_6D_6, 298 K): *δ* [ppm] = 0.05 (s, 18H, SnC*H*$_3$), 1.20 (d, 12H, $^{3}J_{H\text{-}H}$ = 6.9 Hz, *i*Pr-C*H*$_3$), 1.44 (d, 12H, $^{3}J_{H\text{-}H}$ = 6.9 Hz, *i*Pr-C*H*$_3$), 3.57 (sept, 2H, $^{3}J_{H\text{-}H}$ = 6.9 Hz, *i*Pr-C*H*), 5.28 (s, 2H, NC*H*CHN), 7.14 – 7.19 (m, 6H, aryl-C*H* overlaid by solvent peak).

^{13}C{^{1}H} NMR (100.7 MHz, C_6D_6, 298 K): *δ* [ppm] = -6.13 (Sn*C*H$_3$), 24.8 (*i*Pr-*C*H$_3$), 25.3 (*i*Pr-*C*H$_3$), 27.8 (*i*Pr-*C*H), 121.6 (aryl-*C*$_{meta}$), 123.8 (N*C*CN), 125.8 (aryl-*C*$_{para}$), 143.8 (aryl-*C*$_{ipso}$), 148.4 (aryl-*C*$_{ortho}$).

^{119}Sn{^{1}H} NMR (186.5 MHz, C_6D_6, 298 K): *δ* [ppm] = -118.0.

Elemental analysis (%) calcd. for $C_{32}H_{54}N_2Sn_2$: C 54.58, H 7.73, N 3.98; found C 53.63, H 7.90, N 3.53.

*1,3-Bis(2,6-diisopropylphenyl)-1,3-diaza-2-iodo-2-methyl-2-silacyclopent-4-en-silane (**10**)*

1,3-Bis(2,6-di*iso*propylphenyl)-1,3-diaza-2-silacyclopent-4-en-2-ylidene (179 mg, 442 *µ*mol) and methyl iodide (144 mg, 50.0 *µ*L, 803 *µ*mol, 1.8 eq.) were dissolved in hexane (7 mL) and stirred at room temperature for 16 h. All volatiles were removed *in vacuo* and the remaining solid was evacuated to dryness to yield **10** as a colourless solid (195 mg, 357 *µ*mol, 81 %). Crystals suitable for X-ray diffraction were grown from an at room temperature saturated hexane solution of **10** at -30 °C.

^{1}H NMR (400.3 MHz, C_6D_6, 298 K): *δ* [ppm] = 0.90 (s, 3H, Si-C*H*$_3$), 1.16 (d, 6H, $^{3}J_{H\text{-}H}$ = 6.8 Hz, *i*Pr-C*H*$_3$), 1.19 (d, 6H, $^{3}J_{H\text{-}H}$ = 6.8 Hz, *i*Pr-C*H*$_3$), 1.19 (d, 6H, $^{3}J_{H\text{-}H}$ = 6.8 Hz, *i*Pr-C*H*$_3$), 1.48 (d, 6H, $^{3}J_{H\text{-}H}$ = 6.8 Hz, *i*Pr-C*H*$_3$), 3.37 (sept, 2H, $^{3}J_{H\text{-}H}$ = 6.8 Hz, *i*Pr-C*H*), 4.04 (sept, 2H, $^{3}J_{H\text{-}H}$ = 6.8 Hz, *i*Pr-C*H*), 5.75 (s, 2H, NC*H*CHN), 7.07 (d, 1H, $^{3}J_{H\text{-}H}$ = 2.3 Hz, aryl-C*H*), 7.09 (d, 1H, $^{3}J_{H\text{-}H}$ = 2.3 Hz, aryl-C*H*), 7.16 – 7.20 (m, 4H, aryl-C*H*).

$^{13}C\{^1H\}$ NMR (100.7 MHz, C_6D_6, 298 K): δ [ppm] = 11.5 (Si-*C*H_3), 23.1 (*i*Pr-*C*H_3), 25.2 (*i*Pr-*C*H_3), 26.2 (*i*Pr-*C*H_3), 26.5 (*i*Pr-*C*H_3), 28.8 (*i*Pr-*C*H), 28.9 (*i*Pr-*C*H), 120.5 (N*C*CN), 124.0 (aryl-*C*H), 125.2 (aryl-*C*H), 128.1 (aryl-*C*H) 136.7 (aryl-*C*H), 148.1 (aryl-*C*), 149.0 (aryl-*C*).

$^{29}Si\{^1H\}$ NMR (79.5 MHz, C_6D_6, 298 K): δ [ppm] = -30.4.

Elemental analysis (%) calcd. for $C_{27}H_{39}N_2SiI$: C 59.33, H 7.19, N 5.13; found C 59.28, H 7.21, N 5.01.

*1,3-Bis(2,6-diisopropylphenyl)-1,3-diaza-2-chloro-2-benzyl-2-silacyclopent-4-en-silane (**11**)*

1,3-Bis(2,6-di*iso*propylphenyl)-1,3-diaza-2-silacyclopent-4-en-2-ylidene (100 mg, 247 *µ*mol) and *α*-chlorotoluene (31.3 mg, 28.5 *µ*L, 247 *µ*mol) were dissolved in hexane (5 mL) and stirred at room temperature for 16 h. The reaction mixture was concentrated to precipitate a colourless solid. The solvent was decanted, the remaining solid was washed with hexane (2x 1 mL) and dried *in vacuo* to yield **11** as a pale-yellow solid (108 mg, 203 *µ*mol, 82 %).

^1H NMR (400.3 MHz, C_6D_6, 298 K): δ [ppm] = 1.16 (d, 6H, $^3J_{H\text{-}H}$ = 6.9 Hz, *i*Pr-C*H*$_3$), 1.18 (d, 6H, $^3J_{H\text{-}H}$ = 6.8 Hz, *i*Pr-C*H*$_3$), 1.26 (d, 6H, $^3J_{H\text{-}H}$ = 6.8 Hz, *i*Pr-C*H*$_3$), 1.34 (d, 6H, $^3J_{H\text{-}H}$ = 6.9 Hz, *i*Pr-C*H*$_3$), 2.62 (s, 2H, C*H*$_2$), 3.51 (sept, 2H, $^3J_{H\text{-}H}$ = 6.9 Hz, *i*Pr-C*H*), 3.92 (sept, 2H, $^3J_{H\text{-}H}$ = 6.8 Hz, *i*Pr-C*H*), 5.74 (s, 2H, NC*H*CHN), 6.31 – 6.33 (m, 2H, aryl-C*H*), 6.82 – 6.83 (m, 2H, aryl-C*H*), 6.94 – 7.03 (m, 4H, aryl-C*H*), 7.11 – 7.14 (m, 2H, aryl-C*H*), 7.21 – 7.25 (m, 2H, aryl-C*H*).

$^{13}C\{^1H\}$ NMR (100.7 MHz, C_6D_6, 298 K): δ [ppm] = 23.3 (*i*Pr-*C*H_3), 24.3 (*i*Pr-*C*H_3), 25.8 (*i*Pr-*C*H_3), 26.1 (*C*H_2), 26.6 (*i*Pr-*C*H_3), 28.4 (*i*Pr-*C*H), 28.8 (*i*Pr-*C*H), 119.8 (N*C*CN), 124.1 (aryl-*C*H), 124.9 (aryl-*C*H), 125.4 (aryl-*C*H), 128.0 (aryl-*C*H), 128.4 (aryl-*C*H), 129.9 (aryl-*C*H), 134.9 (aryl-*C*), 137.6 (aryl-*C*), 148.1 (aryl-*C*), 149.0 (aryl-*C*).

$^{29}Si\{^1H\}$ NMR (79.5 MHz, C_6D_6, 298 K): δ [ppm] = -19.4.

Elemental analysis (%) calcd. for $C_{33}H_{43}N_2SiCl$: C 74.61, H 8.16, N 5.27; found C 74.02, H 8.20, N 5.16.

*1,3-Bis(2,6-diisopropylphenyl)-1,3-diaza-2-bromo-2-benzyl-2-silacyclopent-4-en-silane (**12**)*

1,3-Bis(2,6-di*iso*propylphenyl)-1,3-diaza-2-silacyclopent-4-en-2-ylidene (100 mg, 247 *µ*mol) and *α*-bromotoluene (42.2 mg, 29.3 *µ*L, 247 *µ*mol) were dissolved in hexane (5 mL) and stirred at room temperature for 16 h. The reaction mixture was concentrated to precipitate a colourless solid. The solvent was decanted, the remaining solid was washed with hexane (2x 1 mL) and dried in vacuo to yield **12** as a pale-yellow solid (107 mg, 186 *µ*mol, 75 %). Crystals suitable for X-ray diffraction were grown by vapor diffusion of hexane into a saturated solution of **12** in 1,2-difluorobenzene.

^{1}H NMR (400.3 MHz, C_6D_6, 298 K): *δ* [ppm] = 1.16 (d, 6H, $^3J_{H\text{-}H}$ = 6.9 Hz, *i*Pr-C*H*$_3$), 1.23 (d, 6H, $^3J_{H\text{-}H}$ = 6.9 Hz, *i*Pr-C*H*$_3$), 1.24 (d, 6H, $^3J_{H\text{-}H}$ = 6.9 Hz, *i*Pr-C*H*$_3$), 1.33 (d, 6H, $^3J_{H\text{-}H}$ = 6.9 Hz, *i*Pr-C*H*$_3$), 2.73 (s, 2H, C*H*$_2$), 3.52 (sept, 2H, $^3J_{H\text{-}H}$ = 6.9 Hz, *i*Pr-C*H*), 3.98 (sept, 2H, $^3J_{H\text{-}H}$ = 6.9 Hz, *i*Pr-C*H*), 5.76 (s, 2H, NC*H*CHN), 6.31 – 6.33 (m, 2H, aryl-C*H*), 6.82 – 6.84 (m, 2H, aryl-C*H*), 7.14 – 7.16 (m, 3H, aryl-C*H*), 7.17 – 7.17 (m, 1H, aryl-C*H*), 7.22 – 7.25 (m, 2H, aryl-C*H*).

^{13}C{^{1}H} NMR (100.7 MHz, C_6D_6, 298 K): *δ* [ppm] = 23.2 (*i*Pr-*C*H$_3$), 24.5 (*i*Pr-*C*H$_3$), 26.0 (*i*Pr-*C*H$_3$), 26.7 (*i*Pr-*C*H$_3$), 28.3 (*C*H$_2$), 28.5 (*i*Pr-*C*H), 28.8 (*i*Pr-*C*H), 120.1 (N*C*CN), 124.1 (aryl-*C*H), 125.1 (aryl-*C*H), 125.6 (aryl-*C*H), 128.4 (aryl-*C*H), 130.2 (aryl-*C*H), 134.8 (aryl-*C*), 137.5 (aryl-*C*), 148.1 (aryl-*C*), 149.1 (aryl-*C*).

^{29}Si{^{1}H} NMR (79.5 MHz, C_6D_6, 298 K): *δ* [ppm] = -20.9.

Elemental analysis (%) calcd. for $C_{33}H_{43}N_2SiBr$: C 68.85, H 7.53, N 4.87; found C 68.85, H 8.00, N 4.63.

4.5.3 $Dipp_2NHSi$ in azide chemistry

*1-$Dipp_2NHSi$-2,5-bis(adamantyl)-tetrazoline (**13**)*

1,3-Bis(2,6-di*iso*propylphenyl)-1,3-diaza-2-silacyclopent-4-en-2-ylidene (50.0 mg, 124 *µ*mol) and 1-azidoadamantane (43.8 mg, 247 *µ*mol, 2.0 eq.) were dissolved in hexane (7 mL) and stirred at room temperature for 16 h. The precipitate was filtered off, washed with hexane (3x 3 mL) and dried *in vacuo* to yield **13** as a colourless solid (30.8 mg, 42.1 *µ*mol, 34 %). Crystals suitable for X-ray diffraction were grown by slow evaporation of a concentrated benzene solution of **13** at room temperature.

^{1}H NMR (400.3 MHz, C_6D_6, 298 K): *δ* [ppm] = 1.27 (d, 24H, $^3J_{H\text{-}H}$ = 6.6 Hz, *i*Pr-C*H*$_3$), 1.50 (s, 12H, Ad-C*H*$_2$), 1.95 (s, 6H, Ad-C*H*), 2.12 (s, 12H, $^3J_{H\text{-}H}$ = 6.9 Hz, Ad-C*H*$_2$), 3.74 (sept, 4H, $^3J_{H\text{-}H}$ = 6.6 Hz, *i*Pr-C*H*), 5.66 (s, 2H, NC*H*CHN), 7.10 – 7.18 (m, 6H, aryl-C*H*, overlaid by solvent peak).

^{13}C{^{1}H} NMR (100.7 MHz, C_6D_6, 298 K): *δ* [ppm] = 24.9 (*i*Pr-*C*H$_3$), 26.9 (*i*Pr-*C*H$_3$), 28.6 (*i*Pr-*C*H), 36.5 (Ad-*C*H$_2$), 42.4 (Ad-*C*H$_2$), 55.8 (Ad-*C*H), 117.9 (aryl-*C*$_{meta}$), 125.6 (N*C*CN), 125.8 (aryl-*C*$_{para}$), 139.4 (aryl-*C*$_{ipso}$), 145.4 (aryl-*C*$_{ortho}$).

^{29}Si{^{1}H} NMR (99.4MHz, C_6D_6, 298 K): *δ* [ppm] = -52.2.

Elemental analysis (%) calcd. for $C_{46}H_{66}N_6Si$: C 75.57, H 9.10, N 11.49; found C 75.36, H 9.39, N 11.58.

*Bis(trimethylsilyl)amino azido silane (**14**)*

1,3-Bis(2,6-di*iso*propylphenyl)-1,3-diaza-2-silacyclopent-4-en-2-ylidene (50.0 mg, 124 *µ*mol) and trimethylsilyl azide (28.6 mg, 32.9 *µ*L, 248 *µ*mol, 2 eq.) were dissolved in hexane (5 mL) and stirred at room temperature for 16 h. All volatiles were removed *in vacuo* to yield **14** as a yellow solid (58.6 mg, 96.5 *µ*mol, 77 %). Crystals suitable for X-ray diffraction were grown from an at room temperature saturated hexane solution of **14** at -30 °C.

^{1}H NMR (400.3 MHz, C_6D_6, 298 K): δ [ppm] = 0.26 (s, 18H, Si-CH_3), 1.21 (d, 6H, $^{3}J_{H\text{-}H}$ = 6.7 Hz, *i*Pr-CH_3), 1.28 (d, 6H, $^{3}J_{H\text{-}H}$ = 6.7 Hz, *i*Pr-CH_3), 1.35 (d, 6H, $^{3}J_{H\text{-}H}$ = 6.8 Hz, *i*Pr-CH_3), 1.49 (d, 6H, $^{3}J_{H\text{-}H}$ = 6.7 Hz, *i*Pr-CH_3), 3.71 (sept, 2H, $^{3}J_{H\text{-}H}$ = 6.7 Hz, *i*Pr-C*H*), 3.73 (sept, 2H, $^{3}J_{H\text{-}H}$ = 6.8 Hz, *i*Pr-C*H*), 5.61 (s, 2H, NC*H*CHN), 7.11 – 7.20 (m, 6H, aryl-C*H*).

^{13}C{^{1}H} NMR (100.7 MHz, C_6D_6, 298 K): δ [ppm] = 5.35 (Si-*C*H_3), 24.3 (*i*Pr-*C*H_3), 26.6 (*i*Pr-*C*H_3), 27.1 (*i*Pr-*C*H_3), 28.4 (*i*Pr-*C*H), 29.0 (*i*Pr-*C*H), 120.2 (aryl-*C*), 124.2 (N*C*CN), 125.6 (aryl-*C*), 127.2 (aryl-*C*), 138.9 (aryl-*C*), 148.1 (aryl-*C*), 148.6 (aryl-*C*).

^{15}N, ^{1}H HMBC NMR (50.7 Hz / 500.1 Hz, C_6D_6, 298 K): δ [ppm] = -327.5 (*N*-SiMe_3), -299.4 (*N*-Dipp).

^{29}Si{^{1}H} NMR (79.5 MHz, C_6D_6, 298 K): δ [ppm] = -54.4 (N-*Si*-N), 4.09 (*Si*-CH_3).

Elemental analysis (%) calcd. for $C_{32}H_{54}N_6Si_2$: C 63.31, H 8.97, N 13.84; found C 61.73, H 8.88, N 11.60. Despite repeated attempts, satisfactory elemental analysis of **14** was not possible, presumably due to incomplete combustion.

*Cyclosilamine (**15**)*

1,3-Bis(2,6-di*iso*propylphenyl)-1,3-diaza-2-silacyclopent-4-en-2-ylidene (30.0 mg, 74.1 *µ*mol) and 2,6-(diphenyl)phenylazide (20.1 mg, 74.1 *µ*mol) were dissolved in benzene (5 mL) and stirred at room temperature for 16 h. All volatiles were removed *in vacuo*, the remaining solid was dissolved in hexane (3 mL) and stored at -30 °C to yield **15** as a light yellow crystalline solid (22.8 mg, 35.2 *µ*mol, 48 %). Crystal suitable for X-ray diffraction were grown by slow evaporation of a concentrated benzene solution of **15** at room temperature.

^{1}H NMR (500.1 MHz, C_6D_6, 298 K): δ [ppm] = 0.67 (d, 6H, $^{3}J_{H\text{-}H}$ = 6.8 Hz, *i*Pr-CH_3), 0.89 (t, 3H, $^{3}J_{H\text{-}H}$ = 7.2 Hz, *i*Pr-CH_3), 0.92 (d, 6H, $^{3}J_{H\text{-}H}$ = 6.8 Hz, *i*Pr-CH_3), 1.24 (d, 6H, $^{3}J_{H\text{-}H}$ = 7.3 Hz, *i*Pr-CH_3), 1.25 (d, 6H, $^{3}J_{H\text{-}H}$ = 7.3 Hz, *i*Pr-CH_3), 3.57 (sept, 2H, $^{3}J_{H\text{-}H}$ = 6.8 Hz, *i*Pr-C*H*), 3.75 (sept, 2H, $^{3}J_{H\text{-}H}$ = 6.8 Hz, *i*Pr-C*H*), 5.39 (s, 1H, N*H*), 5.75 (s, 2H, NC*H*CHN), 6.72 (dd, 1H, $^{3}J_{H\text{-}H}$ = 8.1 Hz, aryl-C*H*), 6.88 (dd, 1H, $^{3}J_{H\text{-}H}$ = 7.3 Hz, $^{4}J_{H\text{-}H}$ = 1.5 Hz, aryl-C*H*), 6.96 (dd, 2H, $^{3}J_{H\text{-}H}$ = 7.3 Hz, $^{4}J_{H\text{-}H}$ = 2.0 Hz, aryl-C*H*), 7.00 (m, 1H,

aryl-C*H*), 7.02 (m, 1H, aryl-C*H*), 7.05 (m, 3H, aryl-C*H*), 7.08 (m, 1H, aryl-C*H*), 7.09 (m, 1H, aryl-C*H*), 7.11 (m, 1H, aryl-C*H*), 7.12 (m, 1H, aryl-C*H*), 7.14 (m, 1H, aryl-C*H*), 7.76 (dm, 1H, $^{3}J_{H\text{-}H}$ = 8.1 Hz, aryl-C*H*), 7.83 (d, 1H, $^{3}J_{H\text{-}H}$ = 8.1 Hz, aryl-C*H*), 8.35 (dd, 1H, $^{3}J_{H\text{-}H}$ = 8.1 Hz, $^{4}J_{H\text{-}H}$ = 1.5 Hz, aryl-C*H*).

^{13}C{^{1}H} NMR (125.8 MHz, C_6D_6, 298 K): *δ* [ppm] = 14.4, 23.1 (*i*Pr-*C*H$_3$), 24.0 (*i*Pr-*C*H$_3$), 24.3, 25.4 (*i*Pr-*C*H$_3$), 26.2 (*i*Pr-*C*H$_3$), 28.5 (*i*Pr-*C*H), 28.7 (*i*Pr-*C*H), 32.0, 119.2, 119.2 (N*C*CN), 121.7 (aryl-*C*H), 124.13 (aryl-*C*H), 124.15 (aryl-*C*H), 124.3 (aryl-*C*H), 125.76 (aryl-*C*H), 125.77 (aryl-*C*H), 126.9 (aryl-*C*H), 127.7 (aryl-*C*H), 128.4 (aryl-*C*H), 128.7 (aryl-*C*H), 129.5 (aryl-*C*H), 130.2 (aryl-*C*H), 131.16 (aryl-*C*H), 131.22 (aryl-*C*H), 132.0 (aryl-*C*), 136.3 (aryl-*C*H), 138.9 (aryl-*C*), 139.9 (aryl-*C*), 140.0 (aryl-*C*), 142.9 (aryl-*C*), 147.6 (aryl-*C*), 148.0 (aryl-*C*).

^{29}Si{^{1}H} NMR (79.5 MHz, C_6D_6, 298 K): *δ* [ppm] = -40.1.

Elemental analysis (%) calcd. for $C_{44}H_{49}N_3Si$: C 81.56, H 7.62, N 6.48; found C 81.28, H 7.91, N 6.50.

4.6 N-Heterocyclic Silylenes as Ligands in Transition Metal Chemistry

4.6.1 Dipp$_2$NHSi as a 2-electron donor

*[Cr(CO)$_5$(Dipp$_2$NHSi)] (**16**)*

[Cr(CO)$_6$] (70.0 mg, 318 *μ*mol) dissolved in THF (10 mL) was irradiated at room temperature for 3 h. After addition of Dipp$_2$NHSi (129 mg, 318 *μ*mol) in THF (5 mL), the reaction mixture was stirred at room temperature for 1 h. All volatiles were removed under reduced pressure and the residue was washed with hexane and dried *in vacuo* yielding **16** (140 mg, 235 *μ*mol, 74 %) as an orange solid.

^{1}H NMR (400.3 MHz, C_6D_6, 298 K): *δ* [ppm] = 1.17 (d, 12H, $^{3}J_{H\text{-}H}$ = 6.8 Hz, *i*Pr-C*H*$_3$), 1.38 (d, 12H, $^{3}J_{H\text{-}H}$ = 6.8 Hz, *i*Pr-C*H*$_3$), 3.34 (sept, 4H, $^{3}J_{H\,H}$ = 6.8 Hz, *i*Pr-C*H*), 6.32 (s, 2H, NC*H*CHN), 7.11 – 7.21 (m, 6H, aryl-C*H*).

$^{13}C\{^1H\}$ NMR (100.7 MHz, C_6D_6, 298 K): δ [ppm] = 23.7 (*i*Pr-*C*H_3), 25.5 (*i*Pr-*C*H_3), 29.3 (*i*Pr-*C*H), 124.1 (N*C*CN), 126.8 (aryl-C_{para}), 129.0 (aryl-C_{meta}), 137.1 (aryl-C_{ortho}), 146.0 (aryl-C_{ipso}), 211.6 (*C*O), 215.5 (*C*O).

$^{29}Si\{^1H\}$ NMR (79.5 MHz, C_6D_6, 298 K): δ [ppm] = 138.2.

IR ([cm^{-1}]): 1937 (vs, $\nu_{CO,str}$), 2060 (m, $\nu_{CO,str}$), 2867 (w, $\nu_{CH,str}$), 2927 (w, $\nu_{CH,str}$), 2961 (m, $\nu_{CH,str}$).

Elemental analysis (%) calcd. for $C_{31}H_{36}N_2SiO_5Cr$: C 62.40, H 6.08, N 4.69; found C 62.39, H 6.93, N 4.44.

*[Mo(CO)$_5$(Dipp$_2$NHSi)] (**17**)*

[Mo(CO)$_6$] (75.0 mg, 284 μmol) dissolved in THF (10 mL) was irradiated at room temperature for 3 h. After addition of Dipp$_2$NHSi (115 mg, 284 μmol) in THF (5 mL), the reaction mixture was stirred at room temperature for 1 h. All volatiles were removed under reduced pressure and the residue was washed with hexane and dried *in vacuo* yielding **17** (136 mg, 212 μmol, 75 %) as an orange solid. Crystals suitable for X-ray diffraction were grown from a saturated hexane solution of **17** at -30 °C.

^1H NMR (400.3 MHz, $CDCl_3$, 298 K): δ [ppm] = 1.26 (d, 12H, $^3J_{H\text{-}H}$ = 6.9 Hz, *i*Pr-C*H*$_3$), 1.34 (d, 12H, $^3J_{H\text{-}H}$ = 6.9 Hz, *i*Pr-C*H*$_3$), 3.21 (sept, 4H, $^3J_{H\,H}$ = 6.9 Hz, *i*Pr-C*H*), 6.58 (s, 2H, NC*H*CHN), 7.27 – 7.38 (m, 6H, aryl-C*H*).

$^{13}C\{^1H\}$ NMR (100.7 MHz, $CDCl_3$, 298 K): δ [ppm] = 23.8 (*i*Pr-*C*H_3), 25.2 (*i*Pr-*C*H_3), 29.1 (*i*Pr-*C*H), 123.8 (N*C*CN), 126.2 (aryl-C_{para}), 128.3 (aryl-C_{meta}), 136.8 (aryl-C_{ortho}), 146.0 (aryl-C_{ipso}), 201.1 (*C*O), 204.1 (*C*O).

$^{29}Si\{^1H\}$ NMR (79.5 MHz, $CDCl_3$, 298 K): δ [ppm] = 125.4.

IR ([cm^{-1}]): 1946 (vs, $\nu_{CO,str}$), 2070 (m, $\nu_{CO,str}$), 2866 (w, $\nu_{CH,str}$), 2927 (w, $\nu_{CH,str}$), 2961 (m, $\nu_{CH,str}$).

Elemental analysis (%) calcd. for $C_{31}H_{36}N_2SiO_5Mo$: C 58.12, H 5.66, N 4.37; found C 58.77, H 6.63, N 4.03.

*[W(CO)$_5$(Dipp$_2$NHSi)] (**18**)*

[W(CO)$_6$] (87.0 mg, 247 *µ*mol) dissolved in THF (10 mL) was irradiated at room temperature for 3 h. After addition of Dipp$_2$NHSi (100 mg, 247 *µ*mol) in THF (5 mL), the reaction mixture was stirred at room temperature for 1 h. All volatiles were removed under reduced pressure and the residue was washed with hexane and dried *in vacuo* yielding **18** (148 mg, 203 *µ*mol, 82 %) as a yellow solid. Crystals suitable for X-ray diffraction were grown from a saturated hexane solution of **18** at -30 °C.

^{1}H NMR (500.1 MHz, C_6D_6, 298 K): *δ* [ppm] = 1.17 (d, 12H, $^3J_{H\text{-}H}$ = 6.9 Hz, *i*Pr-C*H*$_3$), 1.38 (d, 12H, $^3J_{H\text{-}H}$ = 6.9 Hz, *i*Pr-C*H*$_3$), 3.31 (sept, 4H, $^3J_{H\text{-}H}$ = 6.9 Hz, *i*Pr-C*H*), 6.32 (s, 2H, NC*H*CHN), 7.12 – 7.14 (m, 4H, aryl-C*H*), 7.19 – 7.22 (m, 2H, aryl-C*H*).

^{13}C{^{1}H} NMR (125.8 MHz, C_6D_6, 298 K): *δ* [ppm] = 23.9 (*i*Pr-*C*H$_3$), 25.2 (*i*Pr-*C*H$_3$), 29.4 (*i*Pr-*C*H), 124.1 (N*C*CN), 126.3 (aryl-*C*$_{para}$), 128.9 (aryl-*C*$_{meta}$), 136.9 (aryl-*C*$_{ortho}$), 146.0 (aryl-*C*$_{ipso}$), 193.9 ($^1J_{W\text{-}C}$ = 120.5 Hz, *cis*-*C*O), 196.4 ($^1J_{W\text{-}C}$ = 144.0 Hz, *trans*-*C*O).

^{29}Si{^{1}H} NMR (99.4 MHz, $CDCl_3$, 298 K): *δ* [ppm] = 111.2 ($^1J_{W\text{-}Si}$ = 168.3 Hz).

IR ([cm^{-1}]): 1935 (vs, *ν*$_{CO,str}$), 2068 (m, *ν*$_{CO,str}$), 2867 (w, *ν*$_{CH,str}$), 2927 (w, *ν*$_{CH,str}$), 2963 (m, *ν*$_{CH,str}$).

Elemental analysis (%) calcd. for $C_{31}H_{36}N_2O_5SiW$: C 51.11, H 4.98, N 3.85; found C 50.98, H 4.86, N 3.64.

*[W(CO)$_5$(*i*Pr$_2$Im)] (**19**)*

[W(CO)$_6$] (100 mg, 284 *µ*mol) dissolved in THF (10 mL) was irradiated for 3 h at room temperature. After addition of *i*Pr$_2$Im (43.2 mg, 284 *µ*mol) in THF (5 mL), the reaction mixture was stirred at room temperature for 1 h. All volatiles were removed under reduced pressure and the residue was washed with hexane and dried *in vacuo* yielding **19** (116 mg, 244 *µ*mol, 86%) as a yellow solid. Crystals suitable for X-ray diffraction were grown from a saturated hexane/toluene solution of **19** at -30 °C.

^{1}H NMR (300.1 MHz, d^8-THF, 298 K): *δ* [ppm] = 1.75 (d, 12H, $^3J_{H\text{-}H}$ = 6.7 Hz, *i*Pr-C*H*$_3$), 5.49 (sept, 2H, $^3J_{H\text{-}H}$ = 6.7 Hz, *i*Pr-C*H*), 7.72 (s, 2H, NC*H*CHN).

$^{13}C\{^1H\}$ NMR (75.5 MHz, d^8-THF, 298 K): δ [ppm] = 23.5 (*i*Pr-*C*H_3), 54.9 (*i*Pr-*C*H), 119.4 (N*C*CN), 175.4 (N*C*N), 198.4 ($^1J_{W\text{-}C}$ = 125.8 Hz, *cis*-CO), 201.5 ($^1J_{W\text{-}C}$ = 131.3 Hz, *trans*-CO).

^1H NMR (400.3 MHz, C_6D_6, 298 K): δ [ppm] = 0.93 (d, 12H, $^3J_{H\text{-}H}$ = 6.7 Hz, *i*Pr-C*H*$_3$), 5.09 (sept, 2H, $^3J_{H\text{-}H}$ = 6.7 Hz, *i*Pr-C*H*), 6.25 (s, 2H, NC*H*CHN).

$^{13}C\{^1H\}$ NMR (100.7 MHz, C_6D_6, 298 K): δ [ppm] = 23.3 (*i*Pr-*C*H_3), 54.1 (*i*Pr-*C*H), 117.8 (N*C*CN), 176.4 (N*C*N), 198.2 (*cis*-CO), 201.3 (*trans*-CO).

IR ([cm^{-1}]): 1961 (m, $\nu_{CO,str}$), 2056 (m, $\nu_{CO,str}$), 2935 (w, $\nu_{CH,str}$), 2972 (w, $\nu_{CH,str}$).

Elemental analysis (%) calcd. for $C_{14}H_{16}N_2O_5W$: C 35.32, H 3.39, N 5.88; found C 34.96, H 3.44, N 5.95.

*[W(CO)$_5$(iPr_2Im^{Me})] (**20**)*

[W(CO)$_6$] (60.0 mg, 171 µmol) dissolved in THF (10 mL) was irradiated at room temperature for 3 h. After addition of *i*Pr_2Im^{Me} (30.7 mg, 171 µmol) in THF (5 mL), the reaction mixture was stirred at room temperature for 1 h. All volatiles were removed under reduced pressure and the residue was washed with hexane and dried *in vacuo* yielding **20** (43.1 mg, 85.9 µmol, 50%) as a yellow solid. Crystals suitable for X-ray diffraction were grown from a saturated hexane/toluene solution of **20** at -30 °C.

^1H NMR (500.1 MHz, $CDCl_3$, 298 K): δ [ppm] = 1.51 (d, 12H, $^3J_{H\text{-}H}$ = 7.1 Hz, *i*Pr-C*H*$_3$), 2.24 (s, 6H, C(C*H*$_3$)), 5.57 (sept, 2H, $^3J_{H\text{-}H}$ = 7.1 Hz, *i*Pr-C*H*).

$^{13}C\{^1H\}$ NMR (125.8 MHz, $CDCl_3$, 298 K): δ [ppm] = 10.8 (C(*C*H_3)), 21.9 (*i*Pr-*C*H_3), 55.7 (*i*Pr-*C*H), 126.5 (N*C*CN), 177.7 (N*C*N), 197.9 ($^1J_{W\text{-}C}$ = 126.2 Hz, *cis*-*C*O), 201.9 ($^1J_{W\text{-}C}$ = 131.9 Hz, *trans*-*C*O).

IR ([cm^{-1}]): 1998 (m, $\nu_{CO,str}$), 2058 (m, $\nu_{CO,str}$), 2934 (w, $\nu_{CH,str}$), 2977 (w, $\nu_{CH,str}$).

Elemental analysis (%) calcd. for $C_{16}H_{20}N_2O_5W$: C 38.12, H 4.00, N 5.63; found C 37.92, H 3.99, N 5.56.

*[W(CO)$_5$(Me$_2$Im^{Me})] (**21**)*

[W(CO)$_6$] (60.0 mg, 171 *µ*mol) dissolved in THF (10 mL) was irradiated at room temperature for 3 h. After addition of Me$_2$Im^{Me} (21.2 mg, 171 *µ*mol) in THF (5 mL), the reaction mixture was stirred at room temperature for 1 h. All volatiles were removed under reduced pressure and the residue was washed with hexane and dried *in vacuo* yielding **21** (43.6 mg, 97.3 *µ*mol, 57%) as a yellow solid.

^{1}H NMR (500.1 MHz, $CDCl_3$, 298 K): *δ* [ppm] = 2.15 (s, 6H, NC(C*H*$_3$)), 3.74 (s, 6H, NC*H*$_3$).

^{13}C{^{1}H} NMR (125.8 MHz, $CDCl_3$, 298 K): *δ* [ppm] = 10.1 (NC(C*H*$_3$)), 37.7 (NC*H*$_3$), 125.7 (N*C*CN), 177.1 ($^1J_{W\text{-}C}$ = 100 Hz, N*C*N), 198.5 ($^1J_{W\text{-}C}$ = 125.9 Hz, *cis*-*C*O), 201.6 ($^1J_{W\text{-}C}$ = 131.6 Hz, *trans*-*C*O).

IR ([cm^{-1}]): 1864 (vs, $\nu_{CO,str}$), 2058 (m, $\nu_{CO,str}$), 2961 (w, $\nu_{CH,str}$).

Elemental analysis (%) calcd. for $C_{12}H_{12}N_2O_5W$: C 32.17, H 2.70, N 6.25; found C 31.87, H 2.74, N 6.05.

4.6.2 Dipp$_2$NHSi as a bridging ligand

*[{Ni(CO)$_2$(µ-Dipp$_2$NHSi)}$_2$] (**22**)*

Dipp$_2$NHSi (150 mg, 370 *µ*mol) dissolved in toluene (10 mL) was cooled to 0°C and Ni(CO)$_4$ (69.5 mg, 53.0 *µ*L, 407 *µ*mol, 1.1 eq.) was added. The reaction mixture was allowed to warm to room temperature and the resulting light yellow solution stirred for 16 h. All volatiles were removed under reduced pressure yielding **22** (83.0 mg, 160 *µ*mol, 43 %) as a dark violet solid. Crystals suitable for X-ray diffraction were grown by slow evaporation of a saturated benzene solution of **22** at room temperature.

^{1}H NMR (300.1 MHz, C_6D_6, 298 K): *δ* [ppm] = 1.18 (d, 12H, $^3J_{H\text{-}H}$ = 6.9 Hz, *i*Pr-C*H*$_3$), 1.33 (d, 12H, $^3J_{H\text{-}H}$ = 6.9 Hz, *i*Pr-C*H*$_3$), 3.30 (sept, 4H, $^3J_{H\text{-}H}$ = 6.9 Hz, *i*Pr-C*H*), 6.38 (s, 2H, NC*H*CHN), 7.12 – 7.23 (m, 6H, aryl-C*H*).

$^{13}C\{^1H\}$ NMR (75.5 MHz, C_6D_6, 298 K): δ [ppm] = 24.2 (*i*Pr-*C*H_3), 24.9 (*i*Pr-*C*H_3), 29.1 (*i*Pr-*C*H), 123.9 (N*C*CN), 125.4 (aryl-C_{para}), 128.5 (aryl-C_{meta}), 137.5 (aryl-C_{ortho}), 146.0 (aryl-C_{ipso}), 195.7 (*C*O).

$^{29}Si\{^1H\}$ NMR (59.6 MHz, C_6D_6): δ [ppm] = 121.9.

IR (CH_2Cl_2 [cm^{-1}]): 1971 (s, $\nu_{CO,str}$), 2010 (vs, $\nu_{CO,str}$), 2962 (m, $\nu_{CH,str}$).

Elemental analysis (%) calcd. for $C_{56}H_{72}N_4Si_2Ni_2O_4$: C 64.75, H 6.99, N 5.39; found C 63.97, H 6.92, N 5.30.

*[{(η^5-C_5H_5)Ni(μ-Dipp$_2$NHSi)}$_2$] (**23**)*

[Ni(η^5-C_5H_5)]$_2$ (93.3 mg, 494 μmol), Dipp$_2$NHSi (200 mg, 494 μmol), lithium (5.14 mg, 741 μmol, 1.5 eq.) and naphthalene (9.50 mg, 374.1 μmol) were dissolved in Et_2O (10 mL), stirred in the ultrasonic bath for 15 min and subsequently at room temperature for 16 h. All volatiles were removed *in vacuo* and the remaining solid was suspended in hexane (10 mL). After filtration over a pad of Celite, the filtrate was concentrated and stored at –30 °C to yield **23** (181 mg, 343 μmol, 69 %) as a dark red solid. Crystals suitable for X-ray diffraction were grown from a saturated hexane solution of **23** at -30 °C.

^1H NMR (500.1 MHz, C_6D_6, 298 K): δ [ppm] = 1.13 (d, 12H, $^3J_{H\text{-}H}$ = 6.9 Hz, *i*Pr-CH_3), 1.17 (d, 12H, $^3J_{H\text{-}H}$ = 6.9 Hz, *i*Pr-CH_3), 3.64 (sept, 4H, $^3J_{H\text{-}H}$ = 6.9 Hz, *i*Pr-C*H*), 5.26 (s, 5H, η^5-C_5H_5), 6.33 (s, 2H, NC*H*CHN), 7.06 – 7.19 (m, 6H, aryl-C*H*).

$^{13}C\{^1H\}$ NMR (125.8 MHz, C_6D_6, 298 K): δ [ppm] = 23.4 (*i*Pr-*C*H_3), 26.9 (*i*Pr-*C*H_3), 29.0 (*i*Pr-*C*H_3), 89.8 (η^5-C_5H_5), 124.6 (N*C*CN), 126.2 (aryl-C_{para}), 126.9 (aryl-C_{meta}), 142.9 (aryl-C_{ortho}), 145.8 (aryl-C_{ipso}).

$^{29}Si\{^1H\}$ NMR (99.4 MHz, C_6D_6, 298 K): δ [ppm] = 124.2.

Elemental analysis (%) calcd. for $C_{62}H_{82}N_4Ni_2Si_2$: C 70.46, H 7.82, N 5.30; found C 70.72, H 8.32, N 5.22.

[{(η^5-C_5H_5)Fe(CO)}$_2$(μ-CO)(μ-Dipp$_2$NHSi)] (***24***)

Dipp$_2$NHSi (175.3 mg, 186 *µ*mol) and [Fe(CO)$_2$(η^5-C_5H_5)]$_2$ (64.0 mg, 186 *µ*mol) were dissolved in toluene (10 mL) and stirred at 80 °C for 24 h. All volatiles were removed *in vacuo* and the remaining solid was suspended in hexane (20 mL). The solid was filtered on to a pad of Celite, washed with hexane (2x 5 mL) and afterwards the filter cake was eluted with toluene into a new flask (3x 10 mL). Toluene was removed under reduced pressure yielding **24** (51.5 mg, 70.5 *µ*mol) as a green solid. The hexane solution was concentrated and stored at –30 °C yielding additional 28.2 mg of **24** (overall 79.9 mg, 126 *µ*mol, 68 %). Crystals suitable for X-ray diffraction were grown from a saturated hexane solution of **24** at –30 °C.

^{1}H NMR (500.1 MHz, C_6D_6, 298 K): *δ* [ppm] = 1.29 (br. d, 12H, $^3J_{H\text{-}H}$ = 6.8 Hz, *i*Pr-C*H*$_3$), 1.33 (br. d, 12H, $^3J_{H\text{-}H}$ = 6.1 Hz, *i*Pr-C*H*$_3$), 3.79 (br. s, 2H, *i*Pr-C*H*), 4.36 (br. s, 2H, *i*Pr-C*H*), 4.54 (s, 5H, η^5-C_5H_5), 6.38 (s, 2H, NC*H*CHN), 7.16 (overlaid by solvent peak, 6H, aryl-C*H*).

^{13}C{^{1}H} NMR (100.7 MHz, C_6D_6, 298 K): *δ* [ppm] = 14.3 (*i*Pr-*C*H$_3$), 23.1 (*i*Pr-*C*H$_3$), 32.0 (*i*Pr-*C*H), 86.1 (η^5-*C*$_5$H$_5$), 124.1 (*C*$_{aryl}$), 126.1 (N*C*CN), 141.8 (aryl-*C*), 210.4 (*C*O), 215.4 (*C*O).

^{29}Si{^{1}H} NMR (79.5 MHz, C_6D_6, 298 K): *δ* [ppm] = 147.2.

IR ([cm^{-1}]): 1772 (s, $\nu_{CO,str}$), 1937 (vs, $\nu_{CO,str}$), 2861 (vw, $\nu_{CH,str}$), 2939 (w, $\nu_{CH,str}$), 2967 (w, $\nu_{CH,str}$).

Elemental analysis (%) calcd. for $C_{31}H_{42}N_2SiO_3Fe_2$: C 64.12, H 6.35, N 3.83; found C 64.02, H 6.43, N 3.75.

4.6.3 $Dipp_2NHSi$ as a metal–halide activator

*$[Mn(CO)_3(Dipp_2NHSi)_2(I)]$ (**25**)*

$Dipp_2NHSi$ (214 mg, 528 *µ*mol, 2.0 eq.) and $[Mn(CO)_5(I)]$ (85.0 mg, 264 *µ*mol) were dissolved in hexane (10 mL) and stirred at room temperature for 16 h. The precipitate was filtered on to a pad of Celite, washed with hexane (2x 5 mL) and afterwards the filter cake was eluted with toluene into a new flask (4x 5 mL). The solvent was removed under reduced pressure yielding **25** (162 mg, 151 *µ*mol, 57 %) as a dark yellow solid. Crystals suitable for X-ray diffraction were grown by diffusion of hexane into a saturated toluene solution of **25** at room temperature.

^{1}H NMR (400.3 MHz, C_6D_6, 298 K): *δ* [ppm] = 1.15 (d, 12H, $^3J_{H\text{-}H}$ = 6.8 Hz, *i*Pr-C*H*$_3$), 1.40 (d, 12H, $^3J_{H\text{-}H}$ = 6.8 Hz, *i*Pr-C*H*$_3$), 3.57 (sept, 4H, $^3J_{H\text{-}H}$ = 6.8 Hz, *i*Pr-C*H*), 6.23 (s, 2H, NC*H*CHN), 7.06 (s, 6H, aryl-C*H*).

^{13}C{^{1}H} NMR (125.8 MHz, C_6D_6, 298 K): *δ* [ppm] = 23.8 (*i*Pr-*C*H$_3$), 25.9 (*i*Pr-*C*H), 29.2 (*i*Pr-*C*H$_3$), 124.0 (aryl-*C*$_{meta}$), 125.7 (N*C*CN), 128.4 (aryl-*C*$_{ipso}$), 128.7 (aryl-*C*$_{ipso}$), 137.9 (aryl-*C*$_{para}$), 146.5 (aryl-*C*$_{ortho}$), 211.7 (*C*O), 221.4 (*C*O).

^{29}Si{^{1}H} NMR (79.5 MHz, C_6D_6, 298 K): *δ* [ppm] = 125.2.

IR ([cm^{-1}]): 1929 (vs, *ν*$_{CO,str}$), 1960 (vs, *ν*$_{CO,str}$), 2863 (w, *ν*$_{CH,str}$), 2923 (w, *ν*$_{CH,str}$), 2957 (m, *ν*$_{CH,str}$).

Elemental analysis (%) calcd. for $C_{55}H_{72}IMnN_4O_3Si_2$: C 61.44, H 6.75, N 5.21; found C 60.87, H 6.87, N 5.10.

*$[Mn(CO)_3(Dipp_2NHSi)_2(Br)]$ (**26**)*

$Dipp_2NHSi$ (60.0 mg, 148 *µ*mol, 2.0 eq.) and $[Mn(CO)_5(Br)]$ (20.4 mg, 74.2 *µ*mol) were dissolved in hexane (5 mL) and stirred at 60 °C for 16 h. The precipitate was collected by filtration, washed with hexane (2x 2 mL) and dried *in vacuo* yielding **26** (47.9 mg,

46.6 *µ*mol, 63 %) as a yellow solid. Crystals suitable for X-ray diffraction were grown from a saturated hexane solution of **26** at -30 °C.

^{1}H NMR (500.1 MHz, d^{8}-toluene, -40 °C): *δ* [ppm] = 1.15 (d, 12H, $^{3}J_{H\text{-}H}$ = 6.6 Hz, *i*Pr-C*H*$_3$), 1.37 (d, 12H, $^{3}J_{H\text{-}H}$ = 6.6 Hz, *i*Pr-C*H*$_3$), 3.53 (sept, 4H, $^{3}J_{H\text{-}H}$ = 6.6 Hz, *i*Pr-C*H*), 6.16 (s, 2H, NC*H*CHN), 7.05 (s, 3H, aryl-C*H*), 7.13 (s, 3H, aryl-C*H*).

^{13}C{^{1}H} NMR (125.8 MHz, d^{8}-toluene, -40 °C): *δ* [ppm] = 23.6 (*i*Pr-*C*H$_3$), 25.7 (*i*Pr-*C*H$_3$), 29.1 (*i*Pr-*C*H), 123.8 (N*C*CN), 128.2 (aryl-*C*$_{para}$), 129.1 (aryl-*C*$_{meta}$), 137.1 (aryl-*C*$_{ortho}$), 146.0 (aryl-*C*$_{ipso}$), 213.1 (CO).

^{29}Si{^{1}H} NMR (99.4 MHz, d^{8}-toluene, -40 °C): *δ* [ppm] = 121.5.

IR ([cm^{-1}]): 1927 (vs, *ν*$_{CO,str}$), 1962 (m, *ν*$_{CO,str}$), 2865 (w, *ν*$_{CH,str}$), 2925 (w, *ν*$_{CH,str}$), 2959 (m, *ν*$_{CH,str}$).

Elemental analysis (%) calcd. for $C_{55}H_{72}BrMnN_4O_3Si_2$: C 64.25, H 7.06, N 5.45; found C 64.28, H 6.98, N 5.31.

*[Mn(CO)$_4$(Dipp$_2$NHSi)(Dipp$_2$NHSi-Cl)] (**27**)*

Dipp$_2$NHSi (50.0 mg, 124 *µ*mol 2.0 eq.) and [Mn(CO)$_5$(Cl)] (14.2 mg, 61.8 *µ*mol) were dissolved in toluene (10 mL) and stirred at 100 °C for 7 d. All volatiles were removed *in vacuo*, the remaining solid was dissolved in a mixture of hexane (4 mL) and toluene (1 mL) and stored at -30 °C yielding **27** (32.6 mg, 32.2 *µ*mol, 52 %) as a pale yellow solid. Crystals suitable for X-ray diffraction were grown from a saturated hexane solution of **27** at -30 °C.

^{1}H NMR (400.3 MHz, C_6D_6, 298 K): *δ* [ppm] = 1.05 (d, 12H, $^{3}J_{H\text{-}H}$ = 6.6 Hz, *i*Pr-C*H*$_3$), 1.19 (d, 12H, $^{3}J_{H\text{-}H}$ = 6.6 Hz, *i*Pr-C*H*$_3$), 1.27 – 1.31 (m, 18H, *i*Pr-C*H*$_3$), 1.46 (d, 6H, $^{3}J_{H\text{-}H}$ = 6.6 Hz, *i*Pr-C*H*$_3$), 3.14 (sept, 4H, $^{3}J_{H\text{-}H}$ = 6.6 Hz, *i*Pr-C*H*), 3.56 (sept, 2H, $^{3}J_{H\text{-}H}$ = 6.6 Hz, *i*Pr-C*H*), 4.68 (sept, 2H, $^{3}J_{H\text{-}H}$ = 6.6 Hz, *i*Pr-C*H*), 5.99 (s, 2H, C*H*), 6.19 (s, 2H, NC*H*CHN), 6.98 – 7.14 (s, 12H, aryl-C*H*).

$^{13}C\{^1H\}$ NMR (125.8 MHz, C_6D_6, 298 K): δ [ppm] = 23.4 (*i*Pr-*C*H_3), 23.9 (*i*Pr-*C*H_3), 23.9 (*i*Pr-*C*H_3), 25.5 (*i*Pr-*C*H_3), 26.1 (*i*Pr-*C*H_3), 28.0 (*i*Pr-*C*H), 28.7 (*i*Pr-*C*H_{ox}), 29.0 (*i*Pr-*C*H_{ox}), 29.3 (*i*Pr-*C*H), 122.0 (N*C*CN), 123.6 (aryl-*C*H), 124.2 (aryl-*C*H), 124.3 (aryl-*C*H), 127.08 (N*C*CN), 127.1 (aryl-*C*H), 128.4 (aryl-*C*H), 129.2 (aryl-*C*H), 136.4 (aryl-*C*), 141.1 (aryl-*C*), 145.7 (aryl-*C*), 148.7 (aryl-*C*), 149.4 (aryl-*C*), 211.6 (*C*O). The subscript "ox" refers to the silyl ligand.

^{29}Si, ^1H HMQC NMR (79.5 MHz, C_6D_6, 298 K): δ [ppm] = 28.9 (Mn-Si-Cl), 135.9 (Si-Mn).

IR ([cm^{-1}]): 1925 (m, $\nu_{CO,str}$), 1962 (vs, $\nu_{CO,str}$), 1976 (s, $\nu_{CO,str}$), 2865 (w, $\nu_{CH,str}$), 2925 (w, $\nu_{CH,str}$), 2961 (m, $\nu_{CH,str}$).

Elemental analysis (%) calcd. for $C_{55}H_{72}ClMnN_4O_3Si_2$: C 66.48, H 7.17, N 5.54; found C 65.26, H 7.07, N 5.35. Due to the high sensitivity towards air and moisture no satisfying elemental analysis could be obtained and the samples significantly changed their weight during the measurement.

*$[Mn(CO)_3(Dipp_2NHSi)_2(Cl)]$ (**27***)*

$Dipp_2NHSi$ (80.0 mg, 198 μmol, 2.0 eq.) and $[Mn(CO)_5(Cl)]$ (22.8 mg, 99.0 μmol) were dissolved in toluene (10 mL) and stirred at room temperature for 3 d. All volatiles were removed *in vacuo* and the remaining solid was suspended in hexane (5 mL). The solid was filtered on to a pad of Celite, washed with hexane (2x 3 mL) and afterwards the filter cake was eluted with toluene into a new flask (3x 6 mL). Toluene was removed under reduced pressure yielding a mixture of **27** and **27*** (1:2) as a yellow solid.

^1H NMR (400.3 MHz, C_6D_6, 298 K): δ [ppm] = 1.16 (d, 24H, $^3J_{H\text{-}H}$ = 6.8 Hz, *i*Pr-CH_3), 1.34 (d, 24H, $^3J_{H\text{-}H}$ = 6.8 Hz, *i*Pr-CH_3), 3.52 (sept, 4H, $^3J_{H\text{-}H}$ = 6.8 Hz, *i*Pr-C*H*), 6.19 (s, 4H, NC*H*CHN), 6.96 – 7.12 (m, 12H, aryl-C*H*).

^{13}C{^{1}H} NMR (100.7 MHz, C_6D_6, 298 K): δ [ppm] = 23.8 (*i*Pr-*C*H$_3$), 25.7 (*i*Pr-*C*H$_3$), 29.2 (*i*Pr-*C*H), 123.9 (aryl-*C*H), 124.6 (N*C*CN), 138.0 (aryl-*C*H), 146.6 (aryl-*C*H). The carbon atoms of the carbonyl groups could not be detected and one of the aromatic signals was presumably overlaid by the solvent peak.

^{29}Si, ^{1}H HMQC NMR (99.4 MHz, C_6D_6, 298 K): δ [ppm] = 125.5.

*[(η^5-C_5H_5)Ni(Dipp$_2$NHSi-Cl)(PPh$_3$)] (**28**)*

[(η^5-C_5H_5)Ni(PPh$_3$)(Cl)] (378 mg, 897 μmol) was dissolved in toluene (10 mL), mixed with a solution of Dipp$_2$NHSi (362 mg, 895 μmol) in toluene (10 mL) and the resulting solution was stirred at room temperature for 5 d. All volatiles were removed *in vacuo* and the remaining solid was suspended in hexane (8 mL). The solid was filtered off, washed with hexane (3x 6 mL) and dried under reduced pressure to yield **28** (555 mg, 672 μmol, 75 %) as a light brown solid. Crystals suitable for X-ray diffraction were grown by slow evaporation of a saturated solution of **28** in hexane / toluene at room temperature.

^{1}H NMR (500.1 MHz, C_6D_6, 298 K): δ [ppm] = 1.19 (d, 6H, $^{3}J_{H\text{-}H}$ = 6.6 Hz, *i*Pr-C*H*$_3$), 1.26 (d, 6H, $^{3}J_{H\text{-}H}$ = 6.6 Hz, *i*Pr-C*H*$_3$), 1.35 (d, 6H, $^{3}J_{H\text{-}H}$ = 6.6 Hz, *i*Pr-C*H*$_3$), 1.51 (d, 6H, $^{3}J_{H\text{-}H}$ = 6.6 Hz, *i*Pr-C*H*$_3$), 4.15 (sept, 2H, *i*Pr-C*H*), 4.32 (sept, 2H, *i*Pr-C*H*), 4.91 (s, 5H, η^5-C_5H_5), 6.00 (s, 2H, NC*H*CHN), 6.86 – 6.89 (m, 6H, aryl-C*H*), 6.93 – 6.96 (m, 3H, aryl-C*H*), 7.27 (s, 6H, aryl-C*H*), 7.47 – 7.51 (m, 6H, aryl-C*H*).

^{13}C{^{1}H} NMR (100.7 MHz, C_6D_6, 298 K): δ [ppm] = 23.3 (*i*Pr-*C*H$_3$), 24.5 (*i*Pr-*C*H$_3$), 25.8 (*i*Pr-*C*H$_3$), 26.8 (*i*Pr-*C*H$_3$), 29.1 (*i*Pr-*C*H), 29.2 (*i*Pr-*C*H), 92.5 (d, $^{2}J_{C\text{-}P}$ = 1.7 Hz, η^5-C_5H_5), 122.6 (N*C*CN), 124.0 (aryl-*C*H), 124.8 (aryl-*C*H), 126.3 (aryl-*C*H), 128.2 (aryl-*C*H), 128.4 (aryl-*C*H), 129.7 (d, $^{2}J_{C\text{-}P}$ = 2.3 Hz, aryl-*C*H), 134.1 (aryl^{P}-*C*H), 134.1 (aryl^{P}-*C*H), 135.8 (aryl-*C*H), 136.2 (aryl-*C*H), 144.3 (aryl-*C*), 147.1 (aryl-*C*), 148.3 (aryl-*C*).

^{29}Si{^{1}H} NMR (99.4 MHz, C_6D_6, 298 K): δ [ppm] = -5.59 (d, $^{2}J_{Si\text{-}P}$ = 48 Hz).

^{31}P NMR (202.5 MHz, C_6D_6, 298 K): δ [ppm] = 45.6 (sept, $^{2}J_{P\text{-}H}$ = 11 Hz).

IR ([cm^{-1}]): 1598 (vw, $\nu_{CC,str}$), 1627 (vw, $\nu_{CC,str}$), 2865 (w, $\nu_{CH,str}$), 2923 (w, $\nu_{CH,str}$), 2962 (w, $\nu_{CH,str}$), 3059 (vw, $\nu_{CH,str}$), 3433 (w, $\nu_{OH,str}$).

Elemental analysis (%) calcd. for $C_{49}H_{55}N_2SiClNiP*2\ H_2O$: C 68.34, H 6.91, N 3.25; found C 68.03, H 6.58, N 3.05.

*[(η^5-C_5H_5)Fe(CO)$_2$(Dipp$_2$NHSi-I)] (**29**)*

Dipp$_2$NHSi (100 mg, 247 μmol) and [(η^5-C_5H_5)Fe(CO)$_2$(I)] (75.1 mg, 247 μmol) were dissolved in THF (10 mL) and stirred at room temperature for 16 h. After all volatiles were removed under reduced pressure the residue was dissolved in hexane and cooled to -30 °C yielding **29** (104 mg, 147 μmol, 60 %) as a red-brown solid. Crystals suitable for X-ray diffraction were grown from a saturated hexane solution of **29** at -30 °C.

^{1}H NMR (400.3 MHz, C_6D_6, 298 K): δ [ppm] = 1.23 (d, 6H, $^3J_{H-H}$ = 4.7 Hz, *i*Pr-C*H*$_3$), 1.30 (d, 6H, $^3J_{H-H}$ = 4.7 Hz, *i*Pr-C*H*$_3$), 1.37 (d, 6H, $^3J_{H-H}$ = 4.7 Hz, *i*Pr-C*H*$_3$), 1.58 (d, 6H, $^3J_{H-H}$ = 4.7 Hz, *i*Pr-C*H*$_3$), 3.60 (s, 2H, *i*Pr-C*H*), 4.06 (s, 5H, η^5-C_5H_5), 4.78 (s, 2H, *i*Pr-C*H*), 6.14 (s, 2H, NC*H*CHN), 7.12 – 7.25 (m, 6H, aryl-C*H*).

^{13}C{^{1}H} NMR (100.7 MHz, C_6D_6, 298 K): δ [ppm] = 22.9 (*i*Pr-*C*H$_3$), 24.1 (*i*Pr-*C*H$_3$), 26.9 (*i*Pr-*C*H$_3$), 28.1 (*i*Pr-*C*H$_3$), 29.3 (*i*Pr-*C*H), 29.9 (*i*Pr-*C*H), 86.9 (η^5-*C*$_5$H$_5$), 123.1 (N*C*CN), 123.4 (aryl-*C*$_{para}$), 125.3 (aryl-*C*$_{meta}$), 140.2 (aryl-*C*$_{ortho}$), 148.3 (aryl-*C*$_{ortho}$), 149.7 (aryl-*C*$_{ipso}$), 212.2 (*C*O).

^{29}Si{^{1}H} NMR (79.5 MHz, C_6D_6, 298 K): δ [ppm] = 17.2.

IR (CH_2Cl_2 [cm^{-1}]): 1974 (vs, $\nu_{CO,str}$), 2021 (m, $\nu_{CO,str}$), 2865 (w, $\nu_{CH,str}$), 2925 (w, $\nu_{CH,str}$), 2961 (m, $\nu_{CH,str}$).

Elemental analysis (%) calcd. for $C_{33}H_{41}N_2SiO_2IFe$: C 55.94, H 5.83, N 3.95; found C 55.84, H 6.06, N 5.16.

5 Crystallographic Details

5.1 Collection parameters

Crystal data were collected with a Bruker D8 Apex-2 diffractometer equipped with an Oxford Cryosystems low-temperature device using a CCD area detector and graphite monochromated Mo-K_α radiation or a Rigaku XtaLAB Synergy-DW diffractometer equipped with an Oxford Cryo 800 using a HyPix-6000HE detector and copper monochromated Cu-K_α radiation. Crystals were immersed in a film of perfluoropolyether oil on a MicroMount™ and data were collected at 100 K. The images were processed with the Bruker or CrySalis software packages and the structures solved using the ShelXTL software package.[146] All non-hydrogen atoms were refined anisotropically. Hydrogen atoms were included in structure factor calculations and assigned to idealized positions. Diamond software was used for graphical representation.

Crystallographic data for the compounds **17** – **20** and **22** – **29** have been deposited with the Cambridge Crystallographic Data Centre as supplementary publication nos. CCDC-1987080 (**17**), CCDC-1987077 (**18**), CCDC-1987081 (**19**), CCDC-1987079 (**20**), CCDC-1987076 (**22**), CCDC-2004651 (**23**), CCDC-2004652 (**24**), CCDC-2004650 (**25**), CCDC-1987082 (**26**), CCDC-2004653 (**27**), CCDC-2004654 (**28**), and CCDC-1987078 (**29**). These data can be obtained free of charge from The Cambridge Crystallographic Data Centre *via* www.ccdc.cam.ac.uk/data_request/cif.

5.2 Crystallographic data

5.2.1 *N*-Heterocyclic Silylenes as ambiphilic Reagents in Main Group Chemistry

5.2.1.1 Adduct formation of $Dipp_2NHSi$ with Lewis Acids

Crystal data for $Dipp_2NHSi{\cdot}B(C_6F_5)_3$ (4): $C_{44}H_{36}BF_{15}N_2Si$, M_r = 1426.27, T = 100.00(10) K, λ = 0.71073 Å, yellow block, 0.100x0.146x0.359 mm^3, triclinic space group P-1, a = 13.6485(10), b = 17.6582(12) Å, c = 18.8693(13) Å, α = 106.855(3) °, β

= 107.231(3) °, γ = 92.482(3) °, V = 4115.2(5) Å^3, Z = 4, ρ_{calcd} = 1.480 Mg/m^3, μ = 0.161 mm^{-1}, F(000) = 1872, 94302 reflections, -18 ≤ h ≤ 18, -23 ≤ k ≤ 23, -25 ≤ l ≤ 25, 1.191 < θ < 28.494 °, completeness 99.5 %, 20757 independent reflections, 12424 reflections observed with [I > 2σ(I)], 1151 parameters, 0 restraints, R indices (all data) R_1 = 0. 1127, wR_2 = 0.1256, final R indices [I > 2σ(I)] R_1 = 0.0530, wR_2 = 0.1074, largest difference peak and hole 0.760 and -0.446 eA^{-3}, GooF = 1.015.

5.2.1.2 Insertion of Dipp$_2$NHSi into element–halide bonds

Crystal data for 1,3-Bis(2,6-di*iso*propylphenyl)-1,3-diaza-2,2-dibromo-2-silacyclopent-4-ene (5): $C_{26}H_{36}N_2Br_2Si$, M_r = 564.48, T = 100(0) K, λ = 0.71073 Å, yellow plate, 0.120x0.257x0.704 mm^3, orthorhombic space group Pnma, *a* = 12.0901(7) Å, *b* = 21.0717(13) Å, *c* = 10.4566(7) Å, V = 2663.9(3) Å^3, Z = 4, ρ_{calcd} = 1.407 Mg/m^3, μ = 3.104 mm^{-1}, F(000) = 1160, 40509 reflections, -16 ≤ h ≤ 16, -28 ≤ k ≤ 28, -13 ≤ l ≤ 13, 1.933 < θ < 28.309 °, completeness 99.9 %, 3392 independent reflections, 2745 reflections observed with [I > 2σ(I)], 149 parameters, 0 restraints, R indices (all data) R_1 = 0.0454, wR_2 = 0.1047, final R indices [I > 2σ(I)] R_1 = 0.0340, wR_2 = 0.0976, largest difference peak and hole 0.556 and -1.247 eA^{-3}, GooF = 1.030.

Crystal data for 1,3-Bis(2,6-di*iso*propylphenyl)-1,3-diaza-2,2-diiodo-2-silacyclopent-4-ene (6): $C_{26}H_{36}N_2I_2Si$, M_r = 638.46, T = 100.00(11) K, λ = 1.54184 Å, yellow block, 0.178x0.224x0.280 mm^3, orthorhombic space group Pnma, *a* = 12.36420(10) Å, *b* = 21.01450(10) Å, *c* = 10.48310(10) Å, V = 2723.80(4) Å^3, Z = 8, ρ_{calcd} = 1.606 Mg/m^3, μ = 18.662 mm^{-1}, F(000) = 1304, 54381 reflections, -14 ≤ h ≤ 15, -25 ≤ k ≤ 25, -12 ≤ l ≤ 11, 4.208 < θ < 72.127 °, completeness 100 %, 2753 independent reflections, 2743 reflections observed with [I > 2σ(I)], 150 parameters, 0 restraints, R indices (all data) R_1 = 0.0277, wR_2 = 0.0748, final R indices [I > 2σ(I)] R_1 = 0.0277, wR_2 = 0.0748, largest difference peak and hole 1.142 and -1.094 eA^{-3}, GooF = 1.051.

Crystal data for 1,3-Bis(2,6-di*iso*propylphenyl)-1,3-diaza-2,2-diphenyl-2-silacyclopent-4-ene (7): $C_{38}H_{46}N_2Si$, M_r = 564.48, T = 100.00(10) K, λ = 1.54184 Å, colourless plate, 0.056x0.204x0.314 mm^3, tetragonal space group $I4_1md$, a = b = 26.0207(3) Å, c = 10.6846(2) Å, V = 7234.3(2) Å^3, Z = 16, ρ_{calcd} = 1.026 Mg/m^3, μ = 0.748 mm^{-1}, F(000) = 2416, 22565 reflections, -32 ≤ h ≤ 31, -30 ≤ k ≤ 32, -12 ≤ l ≤ 13, 3.397 < θ < 78.620 °, completeness 1.75/0.93 %, 3772 independent reflections, 3651 reflections observed with [I > 2σ(I)], 204 parameters, 1 restraint, R indices (all data) R_1 = 0.0426, wR_2 = 0.1102, final R indices [I > 2σ(I)] R_1 = 0.0406, wR_2 = 0.1077, largest difference peak and hole 0.294 and -0.318 eA^{-3}, GooF = 1.089.

Crystal data for 1,4-Bis(2,6-di*iso*propylphenyl)-1,4-bis(trimethylstannyl)-1,4-diazabut-2-ene (9): $C_{32}H_{54}N_2Sn_2$, M_r = 704.15, T = 100.01(10) K, λ = 1.54184 Å, colourless block, 0.059x0.071x0.266 mm^3, orthorhombic space group $P2_12_12_1$, a = 8.6820(2) Å, b = 17.5960(3) Å, c = 21.9586(5) Å, V = 3354.58(12) Å^3, Z = 4, ρ_{calcd} = 1.394 Mg/m^3, μ = 11.979 mm^{-1}, F(000) = 1440, 66727 reflections, -10 ≤ h ≤ 10, -19 ≤ k ≤ 21, -26 ≤ l ≤ 27, 3.218 < θ < 72.123 °, completeness 1.77/1.00, 6613 independent reflections, 6452 reflections observed with [I > 2σ(I)], 339 parameters, 0 restraints, R indices (all data) R_1 = 0.0418, wR_2 = 0.1039, final R indices [I > 2σ(I)] R_1 = 0.0405, wR_2 = 0.1034, largest difference peak and hole 1.868 and -1.387 eA^{-3}, GooF = 1.036.

Crystal data for 1,3-Bis(2,6-di*iso*propylphenyl)-1,3-diaza-2-iodo-2-methyl-2-silacyclopent-4-en-silane (10): $C_{27}H_{39}N_2ISi$, M_r = 437.27, T = 100(2) K, λ = 1.54184 Å, colourless plate, 0.042x0.076x0.385 mm^3, orthorhombic space group Pnma, a = 12.23390(10), b = 21.0553(2) Å, c = 10.49910(10) Å, V = 2704.45(4) Å^3, Z = 5, ρ_{calcd} = 1.342 Mg/m^3, μ = 9.831 mm^{-1}, F(000) = 1128, 53020 reflections, -15 ≤ h ≤ 11, -25 ≤ k ≤ 25, -12 ≤ l ≤ 12, 4.199 < θ < 72.122 °, completeness 100 %, 2729 independent reflections, 2652 reflections observed with [I > 2σ(I)], 144 parameters, 0 restraints, R indices (all data) R_1 = 0. 0219, wR_2 = 0.0564, final R indices [I > 2σ(I)] R_1 = 0.0213, wR_2 = 0.0561, largest difference peak and hole 0.917 and -0.378 eA^{-3}, GooF = 1.062.

Crystal data for 1,3-bis(2,6-di*iso*propylphenyl)-1,3-diaza-2-bromo-2-benzyl-2-silacyclopent-4-en-silane (12): $C_{33}H_{43}N_2BrSi$, M_r = 575.69, T = 100.00(10) K, λ = 1.54184 Å, colourless plate, 0.042x0.096x0.304 mm^3, orthorhombic space group $P2_12_12_1$, a = 9.1730(2), b = 16.9984(3) Å, c = 19.4498(4) Å, V = 3032.74(11) Å^3, Z = 4, ρ_{calcd} = 1.261 Mg/m^3, μ = 2.389 mm^{-1}, F(000) = 1216, 17331 reflections, -10 ≤ h ≤ 11, -20 ≤ k ≤ 12, -23 ≤ l ≤ 24, 3.453 < θ < 72.125 °, completeness 1.72/0.97, 5786 independent reflections, 5481 reflections observed with [I > 2σ(I)], 342 parameters, 6 restraints, R indices (all data) R_1 = 0.0525, wR_2 = 0.1388, final R indices [I > 2σ(I)] R_1 = 0.0499, wR_2 = 0.1369, largest difference peak and hole 0.552 and -0.859 eA^{-3}, GooF = 1.052.

5.2.1.3 Dipp$_2$NHSi in azide chemistry

Crystal data for 1-Dipp$_2$NHSi-2,5-bis(adamantyl)-tetrazene (13): $C_{46}H_{66}N_6Si$, M_r = 916.65, T = 100.00(10) K, λ = 1.54184 Å, colourless block, 0.057x0.123x0.226 mm^3, monoclinic space group $P2_1/c$, a = 20.27630(10), b = 40.3564(3) Å, c = 10.10800(10) Å, β = 102.5260(10) °, V = 8074.29(11) Å^3, Z = 4, ρ_{calcd} = 1.203 Mg/m^3, μ = 0.811 mm^{-1}, F(000) = 3184, 96524 reflections, -25 ≤ h ≤ 25, -49 ≤ k ≤ 49, -10 ≤ l ≤ 12, 2.486 < θ < 72.127 °, completeness 99.9 %, 15903 independent reflections, 13964 reflections observed with [I > 2σ(I)], 971 parameters, 0 restraints, R indices (all data) R_1 = 0.0442, wR_2 = 0.1089, final R indices [I > 2σ(I)] R_1 = 0.0383, wR_2 = 0.1021, largest difference peak and hole 0.313 and -0.380 eA^{-3}, GooF = 1.037.

Crystal data for bis(trimethylsilyl)amino azido silane (14): $C_{32}H_{54}N_6Si_3$, M_r = 607.08, T = 100.00(10) K, λ = 1.54184 Å, colourless block, 0.105x0.194x0.290 mm^3, triclinic space group P-1, a = 9.1235(2), b = 9.8699(2) Å, c = 20.0995(2) Å, α = 79.6860(10) °, β = 88.1520(10) °, γ = 83.612(2) °, V = 1769.48(6) Å^3, Z = 2, ρ_{calcd} = 1.139 Mg/m^3, μ = 1.454 mm^{-1}, F(000) = 660, 66230 reflections, -11 ≤ h ≤ 11, -12 ≤ k ≤ 12, -24 ≤ l ≤ 24, 2.234 < θ < 72.129 °, completeness 99.7 %, 6964 independent reflections, 6445 reflections observed with [I > 2σ(I)], 384 parameters, 0 restraints, R indices (all data) R_1 = 0.0465, wR_2 = 0.1314, final R indices [I > 2σ(I)] R_1 = 0.0442, wR_2 = 0.1294 largest difference peak and hole 0.688 and -0.315 eA^{-3}, GooF = 1.047.

Crystal data for 1,4-Bis(di*iso*propylphenyl)-1,4-bis(trimethylsilyl)-1,4-diazabut-2-ene (14*): $C_{32}H_{34}N_2Si_2$, M_r = 522.94, T = 100.01(10) K, λ = 1.54184 Å, colourless block, 0.142x0.180x0.252 mm^3, triclinic space group P-1, a = 8.7119(2), b = 9.4161(2) Å, c = 11.2448(2) Å, α = 103.215(2) °, β = 91.540(2) °, γ = 114.401(2) °, V = 810.10(3) Å^3, Z = 2, ρ_{calcd} = 1.072 Mg/m^3, μ = 1.135 mm^{-1}, F(000) = 288, 16069 reflections, -10 ≤ h ≤ 10, -11 ≤ k ≤ 9, -13 ≤ l ≤ 13, 4.077 < θ < 72.110 °, completeness 99.7 %, 3172 independent reflections, 2987 reflections observed with [I > 2σ(I)], 170 parameters, 0 restraints, R indices (all data) R_1 = 0.0542, wR_2 = 0.1417, final R indices [I > 2σ(I)] R_1 = 0.0525, wR_2 = 0.1400 largest difference peak and hole 0.895 and -0.340 eA^{-3}, GooF = 1.056.

Crystal data for cyclosilamine 15: $C_{50}H_{55}N_3Si$, M_r = 726.06, T = 100.00(10) K, λ = 1.54184 Å, colourless block, 0.058x0.162x0.205 mm^3, monoclinic space group $P2_1/c$, a = 16.0677(2), b = 19.3165(3) Å, c = 13.16640(10) Å, β = 94.6510(10) °, V = 4073.02(9) Å^3, Z = 4, ρ_{calcd} = 1.184 Mg/m^3, μ = 0.788 mm^{-1}, F(000) = 1560, 47944 reflections, -19 ≤ h ≤ 19, -23 ≤ k ≤ 23, -15 ≤ l ≤ 16, 2.759 < θ < 72.123 °, completeness 100 %, 8023 independent reflections, 7078 reflections observed with [I > 2σ(I)], 499 parameters, 0 restraints, R indices (all data) R_1 = 0.0600, wR_2 = 0.1463, final R indices [I > 2σ(I)] R_1 = 0.0529, wR_2 = 0.1381, largest difference peak and hole 0.557 and -0.414 eA^{-3}, GooF = 1.009.

5.2.2 *N*-Heterocyclic Silylenes as Ligands in Transition Metal Chemistry

5.2.2.1 Dipp$_2$NHSi as a 2-electron donor

Crystal data for [Mo(CO)$_5$(Dipp$_2$NHSi)] (17): $C_{31}H_{36}N_2MoO_5Si$, M_r = 640.68, T = 100(2) K, λ = 0.71073 Å, blue plate, 0.066x0.201x0.373 mm^3, monoclinic space group $P2_1/m$, a = 9.1296(6) Å, b = 19.4397(13) Å, c = 9.5888(6) Å, β = 110.248(3) °, V = 1596.62(18) Å^3, Z = 1, ρ_{calcd} = 1.333 Mg/m^3, μ = 0.487 mm^{-1}, F(000) = 664, 17161 reflections, -11 ≤ h ≤ 11, -24 ≤ k ≤ 23, -12 ≤ l ≤ 12, 2.264 < θ < 26.777 °, completeness 99.8%, 3511 independent reflections, 2900 reflections observed with [I > 2σ(I)], 197

parameters, 0 restraints, R indices (all data) R_1 = 0.0478, wR_2 = 0.0634, final R indices [I > 2σ(I)] R_1 = 0.0334, wR_2 = 0.0592, largest difference peak and hole 0.450 and -0.485 eA^{-3}, GooF = 1.032.

Crystal data for [W(CO)$_5$(Dipp$_2$NHSi)] (18): $C_{31}H_{36}N_2WO_5Si$, M_r = 728.56, T = 100(2) K, λ = 0.71073 Å, yellow block, 0.079x0.182x0.192 mm^3, monoclinic space group P2(1)/m, *a* = 9.1098(10) Å, *b* = 19.486(2) Å, *c* = 9.5658(11) Å, β = 110.252(4) °, V = 1593.1(3) Å^3, Z = 1, ρ_{calcd} = 1.519 Mg/m^3, μ = 3.702 mm^{-1}, F(000) = 728, 23543 reflections, -11 ≤ h ≤ 11, -24 ≤ k ≤ 24, -12 ≤ l ≤ 12, 2.662 < θ < 26.820 °, completeness 99.3%, 3500 independent reflections, 3167 reflections observed with [I > 2σ(I)], 265 parameters, 0 restraints, R indices (all data) R_1 = 0. 0338, wR_2 = 0.0641, final R indices [I > 2σ(I)] R_1 = 0.0281, wR_2 = 0.0618, largest difference peak and hole 2.361 and -0.812 eA^{-3}, GooF = 1.048.

Crystal data for [W(CO)$_5$(*i*Pr$_2$Im)] (19): $C_{14}H_{16}N_2WO_5$, M_r = 476.13, T = 100(2) K, λ = 0.71073 Å, yellow block, 0.062x0.346x0.561 mm^3, orthorhombic space group Pbca, *a* = 13.6965(14) Å, *b* = 12.8373(13) Å, *c* = 18.3680(18) Å, V = 3229.6(6) Å^3, Z = 8, ρ_{calcd} = 1.959 Mg/m^3, μ = 7.177 mm^{-1}, F(000) = 1824, 22302 reflections, -17 ≤ h ≤ 17, -16 ≤ k ≤ 15, -20 ≤ l ≤ 23, 2.441 < θ < 26.809 °, completeness 99.7%, 3448 independent reflections, 2951 reflections observed with [I > 2σ(I)], 203 parameters, 0 restraints, R indices (all data) R_1 = 0.0336, wR_2 = 0.0994, final R indices [I > 2σ(I)] R_1 = 0.0268, wR_2 = 0.0874, largest difference peak and hole 0.911 and -0.2142 eA^{-3}, GooF = 0.805.

Crystal data for [W(CO)$_5$(*i*Pr$_2$Im^{Me})] (20): $C_{16}H_{20}N_2WO_5$, M_r = 504.19, T = 100(2) K, λ = 0.71073 Å, yellow block, 0.164x0.243x0.491 mm^3, monoclinic space group P2$_1$/n, *a* = 9.4325(8) Å, *b* = 12.7850(10) Å, *c* = 14.6688(12) Å, β = 94.558(2) °, V = 1763.4(2) Å^3, Z = 4, ρ_{calcd} = 1.899 Mg/m^3, μ = 6.578 mm^{-1}, F(000) = 976, 28450 reflections, -11 ≤ h ≤ 11, -16 ≤ k ≤ 16, -18 ≤ l ≤ 18, 2.116 < θ < 26.857 °, completeness 99.9%, 3789 independent reflections, 3666 reflections observed with [I > 2σ(I)], 223 parameters, 0 restraints, R indices (all data) R_1 = 0.0134, wR_2 = 0.0337, final R indices [I > 2σ(I)] R_1

= 0.0129, wR_2 = 0.0334, largest difference peak and hole 0.681 and -0.629 eA^{-3}, GooF = 1.110.

5.2.2.2 Dipp$_2$NHSi as a bridging ligand

Crystal data for [{Ni(CO)$_2$(μ-Dipp$_2$NHSi)}$_2$] (22): $C_{56}H_{72}N_4Ni_2O_4Si_2$, M_r = 1038.77, T = 100.00(10) K, λ = 1.54184 Å, purple plate, 0.039×0.12×0.215 mm^3, triclinic space group $P\bar{1}$, a = 10.5548(2) Å, b = 11.9880(3) Å, c = 12.4406(2) Å, α = 104.912(2) °, β = 113.089(2) °, γ = 97.345(2) °, V = 1352.12(5) $Å^3$, Z = 2, ρ_{calcd} = 1.276 Mg/m^3, μ = 1.660 mm^{-1}, F(000) = 552, 32636 reflections, -13 ≤ h ≤ 13, -14 ≤ k ≤ 15,-13 ≤ l ≤ 15, 3.949 < θ < 77.633 °, completeness 97.7 %, 5635 independent reflections, 5193 reflections observed with [I > 2σ(I)], 315 parameters, 0 restraints, R indices (all data) R_1 = 0.0399, wR_2 = 0.0964, final R indices [I > 2σ(I)] R_1 = 0.0350, wR_2 = 0.0908, largest difference peak and hole 0.390 and -0.477 eA^{-3}, GooF = 1.132.

Crystal data for [{(η^5-C$_5$H$_5$)Ni(μ-Dipp$_2$NHSi)}$_2$] (23): $C_{62}H_{82}Ni_2N_4Si_2$, M_r = 1056.91, T = 100.00(10) K, λ = 1.54184 Å, red plate, 0.047x0.085x0.092 mm^3, orthorhombic space group Pbca, a = 19.4427(2) Å, b = 21.4500(2) Å, c = 26.5765(2) Å, V = 11083.62(18) $Å^3$, Z = 8, ρ_{calcd} = 1.267 Mg/m^3, μ = 1.572 mm^{-1}, F(000) = 4528, 61257 reflections, -24 ≤ h ≤ 24, -26 ≤ k ≤ 26, -32 ≤ l ≤ 32, 3.326 < θ < 72.127 °, completeness 100 %, 10907 independent reflections, 9687 reflections observed with [I > 2σ(I)], 647 parameters, 0 restraints, R indices (all data) R_1 = 0.0372, wR_2 = 0.0867, final R indices [I > 2σ(I)] R_1 = 0.0322, wR_2 = 0.0839, largest difference peak and hole 0.367 and -0.438 eA^{-3}, GooF = 1.041.

Crystal data for [{(η^5-C$_5$H$_5$)Fe(CO)}$_2$(μ-CO)(μ-Dipp$_2$NHSi)] (24): $C_{39}H_{46}Fe_2N_2O_3Si$, M_r = 730.57, T = 99.9(4) K, λ = 1.54184 Å, green block, 0.090x0.145x0.159 mm^3, monoclinic space group P2(1)/c, a = 16.5028(2) Å, b = 10.50880(10) Å, c = 20.1633(2) Å, β = 90.5550(10) °, V = 3496.65(6) $Å^3$, Z = 4, ρ_{calcd} = 1.388 Mg/m^3, μ = 7.294 mm^{-1},

F(000) = 1536, 66528 reflections, -19 ≤ h ≤ 20, -12 ≤ k ≤ 12, -24 ≤ l ≤ 24, 2.678 < θ < 72.128 °, completeness 99.8 %, 6875 independent reflections, 6491 reflections observed with [I > 2σ(I)], 432 parameters, 0 restraints, R indices (all data) R_1 = 0.0348, wR_2 = 0.0861, final R indices [I > 2σ(I)] R_1 = 0.0328, wR_2 = 0.0846, largest difference peak and hole 0.794 and -0.517 eA^{-3}, GooF = 1.043.

5.2.2.3 $Dipp_2NHSi$ as a metal–halide activator

Crystal data for $[Mn(CO)_3(Dipp_2NHSi)_2(I)]$ (25): $C_{55}H_{72}MnIN_4O_3Si_2$, M_r = 1075.18, T = 99.9(4) K, λ = 1.54184 Å, yellow block, 0.092x0.126x0.241 mm^3, orthorhombic space group $P2_12_12_1$, *a* = 12.07693(8) Å, *b* = 19.13451(15) Å, *c* = 23.8649(2) Å, V = 5514.86(7) $Å^3$, Z = 4, ρ_{calcd} = 1.295 Mg/m^3, μ = 7.096 mm^{-1}, F(000) = 2240, 32227 reflections, -12 ≤ h ≤ 14, -23 ≤ k ≤ 14, -27 ≤ l ≤ 29, 2.960 < θ < 72.104 °, completeness 1.69/0.93, 10124 independent reflections, 9856 reflections observed with [I > 2σ(I)], 612 parameters, 0 restraints, R indices (all data) R_1 = 0.0622, wR_2 = 0.1356, final R indices [I > 2σ(I)] R_1 = 0.0608, wR_2 = 0.1356, largest difference peak and hole 3.619 and -2.286 eA^{-3}, GooF = 1.033.

Crystal data for $[Mn(CO)_3(Dipp_2NHSi)_2(Br)]$ (26): $C_{55}H_{72}N_4MnO_3Si_2Br_1$, M_r = 1028.22, T = 100(2) K, λ = 0.71073 Å, orange block, 0.16×0.405×0.449 mm^3, orthorhombic space group $P2_12_12_1$, a = 12.1025(3) Å, b = 19.0741(4) Å, c = 23.6608(6) Å, V = 5462.0(2) $Å^3$, Z = 4, ρ_{calcd} = 1.250 Mg/m^3, μ = 1.061 mm^{-1}, F(000) = 2168, 62019 reflections, -16 ≤ h ≤ 15, -25 ≤ k ≤ 25, -31 ≤ l ≤ 31, 1.371 < θ < 28.357 °, completeness 1.82/1.00, 13621 independent reflections, 11762 reflections observed with [I > 2σ(I)], 613 parameters, 0 restraints, R indices (all data) R_1 = 0.0445, wR_2 = 0.0819, final R indices [I > 2σ(I)] R_1 = 0.0348, wR_2 = 0.0790, largest difference peak and hole 1.547 and -0.561 eA^{-3}, GooF = 1.006.

Crystal data for [Mn(CO)$_4$(Dipp$_2$NHSi)(Dipp$_2$NHSi-Cl)] (27): $C_{56}H_{72}MnClN_4O_4Si_2$, M_r = 1011.74, T = 100.00(10) K, λ = 0.71073 Å, yellow block, 0.093x0.141x0.166 mm^3, orthorhombic space group Pnma, a = 23.5397(3) Å, b = 21.8828(3) Å, c = 10.7153(2) Å, V = 5519.61(15) Å^3, Z = 8, ρ_{calcd} = 1.218 Mg/m^3, μ = 0.378 mm^{-1}, F(000) = 2152, 108938 reflections, -29 ≤ h ≤ 29, -27 ≤ k ≤ 27, -13 ≤ l ≤ 13, 1.965 < θ < 26.022 °, completeness 100 %, 5579 independent reflections, 5210 reflections observed with [I > 2σ(I)], 327 parameters, 0 restraints, R indices (all data) R_1 = 0.0291, wR_2 = 0.0777, final R indices [I > 2σ(I)] R_1 = 0.0270, wR_2 = 0.0765, largest difference peak and hole 0.333 and -0.262 eA^{-3}, GooF = 1.132.

Crystal data for [(η^5-C$_5$H$_5$)Ni(PPh$_3$)(Dipp$_2$NHSi-Cl)] (28): $C_{49}H_{56}ClN_2NiPSi$, M_r = 826.18, T = 100.00(11) K, λ = 1.54184 Å, orange-brown block, 0.052x0.086x0.133 mm^3, monoclinic space group $P2_1/n$, a = 9.99460(10) Å, b = 21.8775(2) Å, c = 39.3253(5) Å, β = 89.4930(10) °, V = 8598.41(16) Å^3, Z = 4, ρ_{calcd} = 1.276 Mg/m^3, μ = 2.106 mm^{-1}, F(000) = 3504, 49913 reflections, -12 ≤ h ≤ 8, -27 ≤ k ≤ 26, -49 ≤ l ≤ 49, 2.311 < θ < 77.509 °, completeness 90.6 %, 16578 independent reflections, 13562 reflections observed with [I > 2σ(I)], 1007 parameters, 0 restraints, R indices (all data) R_1 = 0.0594, wR_2 = 0.1385, final R indices [I > 2σ(I)] R_1 = 0.0478, wR_2 = 0.1309, largest difference peak and hole 0.708 and -0.459 eA^{-3}, GooF = 1.064.

Crystal data for [(μ^5-C$_5$H$_5$)Fe(CO)$_2$(Dipp$_2$NHSi-I)] (29): $C_{33}H_{41}N_2FeIO_2Si$, M_r = 708.54, T = 100(2) K, λ = 0.71073 Å, orange block, 0.175x0.211x0.242 mm^3, monoclinic space group P2(1)/n, a = 17.6210(11) Å, b = 10.6925(6) Å, c = 18.1746(11) Å, β = 110.295(2) °, V = 3211.7(3) Å^3, Z = 4, ρ_{calcd} = 1.465 Mg/m^3, μ = 1.499 mm^{-1}, F(000) = 1448, 56480 reflections, -23 ≤ h ≤ 23, -14 ≤ k ≤ 14, -24 ≤ l ≤ 24, 1.992 < θ < 28.360 °, completeness 99.7%, 8020 independent reflections, 6976 reflections observed with [I > 2σ(I)], 369 parameters, 0 restraints, R indices (all data) R_1 = 0.0521, wR_2 = 0.1158, final R indices [I > 2σ(I)] R_1 = 0.0438, wR_2 = 0.1117, largest difference peak and hole 2.891 and -0.896 eA^{-3}, GooF = 1.094.

6 Computational Details

Calculations on the NHCs, NHSis and the complexes [{Ni(CO)$_2$(μ-NHSi)}$_2$] were carried out using the TURBOMOLE V7.2 2017 program suite, a development of the University of Karlsruhe and the Forschungszentrum Karlsruhe GmbH, 1989-2007, TURBOMOLE GmbH, since 2007; available from http://www.turbomole.com.[147] Geometry optimizations were performed using (RI-)DFT calculations[148] on an m4 grid employing the BP86[149] functional and a def2-SV(P)[150] basis set for all atoms or employing the B3LYP[149, 151] functional and a def2-TZVPP[150] basis set for selected or all atoms. Vibrational frequencies were calculated at the same level with the AOFORCE[152] module and all structures represented true minima without imaginary frequencies.

All calculations for the energy decomposition analysis were carried out using the Amsterdam Density Functional (ADF) program.[153] The numerical integration was performed using a procedure developed by Becke *et al.*[154] The molecular orbitals (MOs) were expanded in a large uncontracted set of Slater-type orbitals (STOs) containing diffuse functions: a triple-ζ quality basis set was used for all atoms,[155] augmented with two sets of polarization functions for H (2p, 3d), C, N, O, Si, (3d, 4f), Ni (4p, 4f) and W (6p, 5f). An auxiliary set of s, p, d, f and g STOs was used to fit the molecular density and to represent the Coulomb and exchange potentials accurately in each self-consistent field (SCF) cycle. All electrons were included in the variational treatment (no frozen-core approximation was used). The generalized gradient approximation (GGA) at the BLYP level was used where exchange is described by Slater Xα potential,[156] with non-local corrections due to Becke[149, 151b] added self-consistently, and where correlation was treated by using the Lee-Yang-Parr gradient-corrected functional.[151c, 157] Relativistic effects were included with the scalar-zero-order-regular-approximation (ZORA).[158] In addition, the D3(BJ) dispersion correction was used.[159] This level of theory is denoted as TZ2P/BLYP/ZORA/D3(BJ) throughout the text. Energy minima have been verified by vibrational analysis.[160] Voronoi *deformation* density (VDD) charges[161] were calculated for the optimized gas-phase structures at the same level of theory.

The interaction energy (ΔE_{int}) between Ni ($d^{10}s^0$) and the NHC^{Me}/$NHSi^{Me}$ fragments can be decomposed into the following terms:

$$\Delta E_{int} = \Delta E_{Pauli} + \Delta V_{elstat} + \Delta E_{disp} + \Delta E_{oi} \qquad (\mathbf{1})$$

This energy decomposition analysis (EDA)[69] quantifies the Pauli-repulsive orbital interactions (ΔE_{Pauli}) between same-spin electrons, the electrostatic interaction (ΔV_{elstat}), the interaction due to dispersion forces (ΔE_{disp}) and orbital interactions (ΔE_{oi}), that emerge from charge transfer (interaction between occupied orbitals on one fragment with unoccupied orbitals on the other fragment, including donor-acceptor interactions) and polarization (empty-occupied orbital mixing on one fragment due to the presence of the other fragment). It can be further divided into contributions from each irreducible representation Γ of the interacting system (Equation 2).

$$\Delta E_{oi}(\zeta) = \sum_{\Gamma} \Delta E_{oi}^{\Gamma}(\zeta) \qquad (\mathbf{2})$$

The percentage AO contribution to MOs is based on gross Mulliken contributions.[162] The Tolman electronic parameter (TEP) was calculated by simulating the IR-spectra of $[Ni(NHC^{Me})(CO)_3]$ and $[Ni(NHSi^{Me})(CO)_3]$, respectively. The frequencies obtained were corrected by using an empirical formula:

$$TEP = 0.8609x + 376.28 \qquad (\mathbf{3})$$

7 Summary

This thesis reports on the applications of a particular *N*-heterocyclic silylene, $Dipp_2NHSi$ (**1**), as an ambiphilic reagent in main group chemistry and as a ligand in transition metal chemistry. One focus of the work lies in the evaluation of the differences in the reactivity of *N*-heterocyclic silylenes in main group element and transition metal chemistry in comparison with the in these areas nowadays ubiquitous *N*-heterocyclic carbenes (NHCs). The first chapter gives an insight into the reactivity of $Dipp_2NHSi$ with respect to different types of main group element compounds (Scheme 18). In the course of this study, silylene **1** was reacted with selected group 13 compounds (Scheme 18, top).

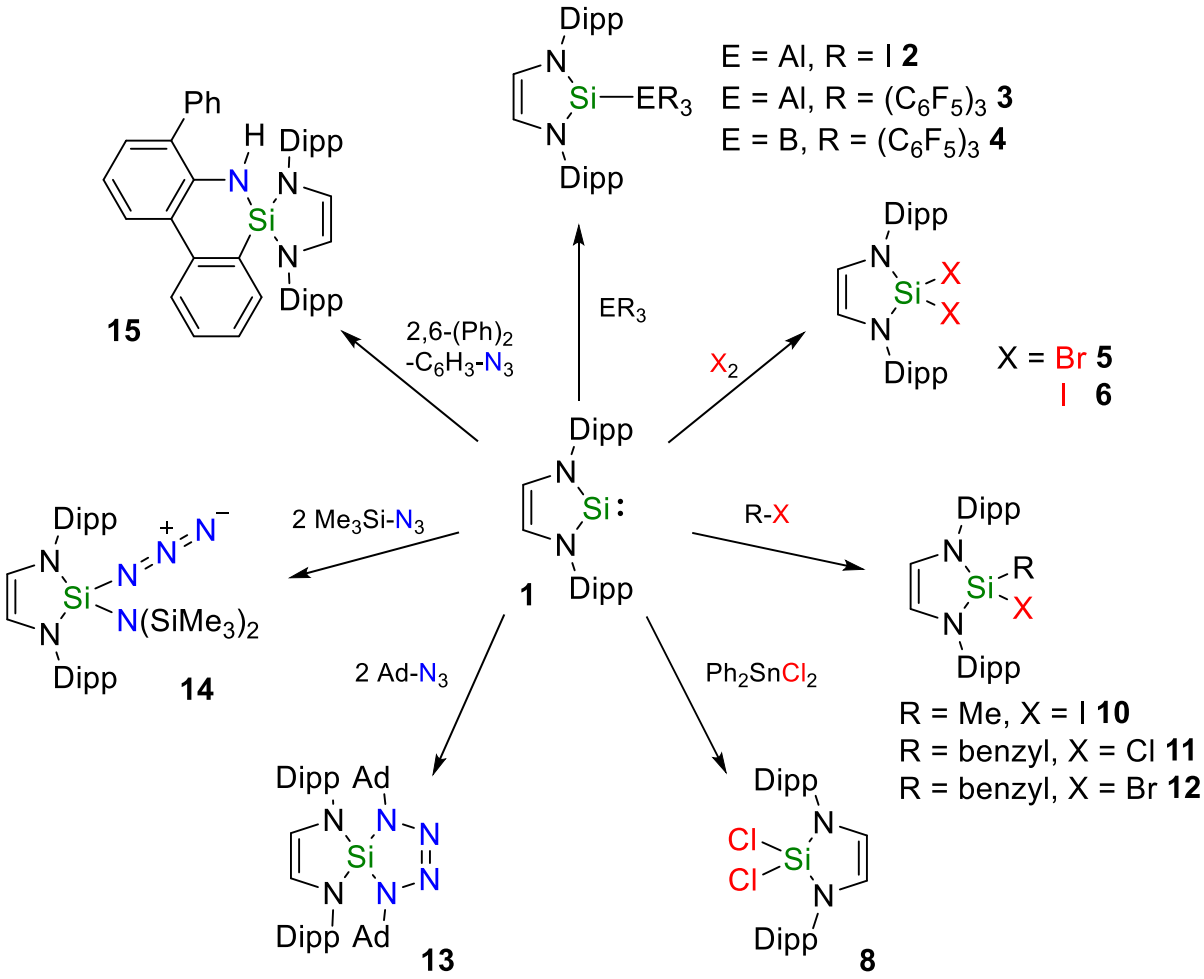

Scheme 18. Reactivity of the silylene **1** towards the group 3 compounds AlI_3, $Al(C_6F_5)_3$ and $B(C_6F_5)_3$, elemental halides, carbon–halide and tin–chloride bonds of aryl and alkyl halides as well as azides of different steric bulk.

Adduct formation was observed with the Lewis acids AlI_3, $Al(C_6F_5)_3$ and $B(C_6F_5)_3$ which led to isolation of $Dipp_2NHSi{\cdot}AlI_3$ (**2**), $Dipp_2NHSi{\cdot}Al(C_6F_5)_3$ (**3**) and $Dipp_2NHSi{\cdot}B(C_6F_5)_3$ (**4**). Compound **4** reveals a high thermal stability, which is in contrast to the literature-known adduct $tBu_2NHSi{\cdot}B(C_6F_5)_3$. The latter slowly undergoes B–C bond activation to give a silyl borane. The adducts **3** and **4** do not seem to form a frustrated Lewis pair and no such reactivity was observed upon reaction with several small organic molecules.

Furthermore, the reactivity of $Dipp_2NHSi$ (**1**) with respect to different element–halide bonds was investigated. The reaction with elemental bromine and iodine leads to the dihalosilanes $Dipp_2NHSiBr_2$ (**5**) and $Dipp_2NHSiI_2$ (**6**) (Scheme 18, top right). The dihalosilanes further react with organolithium compounds as demonstrated for the example of the reaction of $Dipp_2NHSiCl_2$ (**8**) with phenyl lithium to give $Dipp_2NHSiPh_2$ (**7**). Utilizing the halocarbons methyl iodide, benzyl chloride and benzyl bromide, it was demonstrated that the insertion into the carbon–halide bond occurs, leading to the insertion products $Dipp_2NHSi(I)(Me)$ (**10**), $Dipp_2NHSi(Cl)(benzyl)$ (**11**) and $Dipp_2NHSi(Br)(benzyl)$ (**12**). Thus, insertion is preferred to reductive coupling with formation of $RH_2C–CH_2R$ (R = H, Ph) and the corresponding dihalosilane (Scheme 18, middle right). The reaction of **1** with the Me_3SnCl in a 1:3 ratio leads to cleavage of the NHSi and oxidation of the silicon atom to yield the diazabutene $\{(Me_3Sn)N(Dipp)CH\}_2$ (**9**) and $(Me_3Sn)SiCl_3$. The reaction of **1** with one equivalent of Ph_2SnCl_2 gives exclusively the dichlorosilane $Dipp_2NHSiCl_2$ (**8**) and cyclic polystannanes $(Ph_2Sn)_n$ (Scheme 18, bottom right).

The reactivity of **1** towards selected 1,3-dipolar compounds was also examined. Thus, $Dipp_2NHSi$ (**1**) was reacted with azides of different size (Scheme 18, left). The reaction with two equivalents of the sterically demanding adamantyl azide led to the formation of the tetrazoline **13**. For the reaction with the sterically less demanding trimethylsilyl azide the azido silane $Dipp_2NHSi(N(SiMe_3)_2)(N_3)$ (**14**) and the degradation product **14***, which is formed by loss of the silylene silicon atom, was isolated. The cyclosilamine **15** was formed from the reaction of **1** with 2,6-(diphenyl)phenyl azide, presumably *via* a silaimine which then is transformed to **15** by a C–H bond activation step.

The bonding situation and ligation properties of $Dipp_2NHSi$ (**1**) in transition metal complexes was assessed in the second part of the thesis by means of theoretical calculations and experimental investigations. Surprisingly, the silylene ligand $Dipp_2NHSi$ is much less reactive compared to similar NHC ligands. Calculations on the main electronic features of Me_2Im / Me_2NHSi and $Dipp_2NHSi$ / $Dipp_2Im$ revealed significant differences in the frontier orbital region of these compounds, which affect the ligation properties of NHSis in general. It was demonstrated that *N*-heterocyclic silylenes show significantly different behaviour concerning their coordination chemistry, which can largely be explained by a simple MO picture of the NHSis. In particular, one energetically low lying π-acceptor orbital seems to determine the coordination chemistry of these ligands. To provide experimental support for these calculations, the silylene complexes $[M(CO)_5(Dipp_2NHSi)]$ (M = Cr **16**, Mo **17**, W **18**) were synthesized from $Dipp_2NHSi$ and $[M(CO)_6]$ (M = Cr, Mo, W) (Scheme 19, left) and the tungsten NHSi complex **18** was compared to the NHC complexes $[W(CO)_5(iPr_2Im)]$ (**19**), $[W(CO)_5(iPr_2Im^{Me})]$ (**20**) and $[W(CO)_5(Me_2Im^{Me})]$ (**21**).

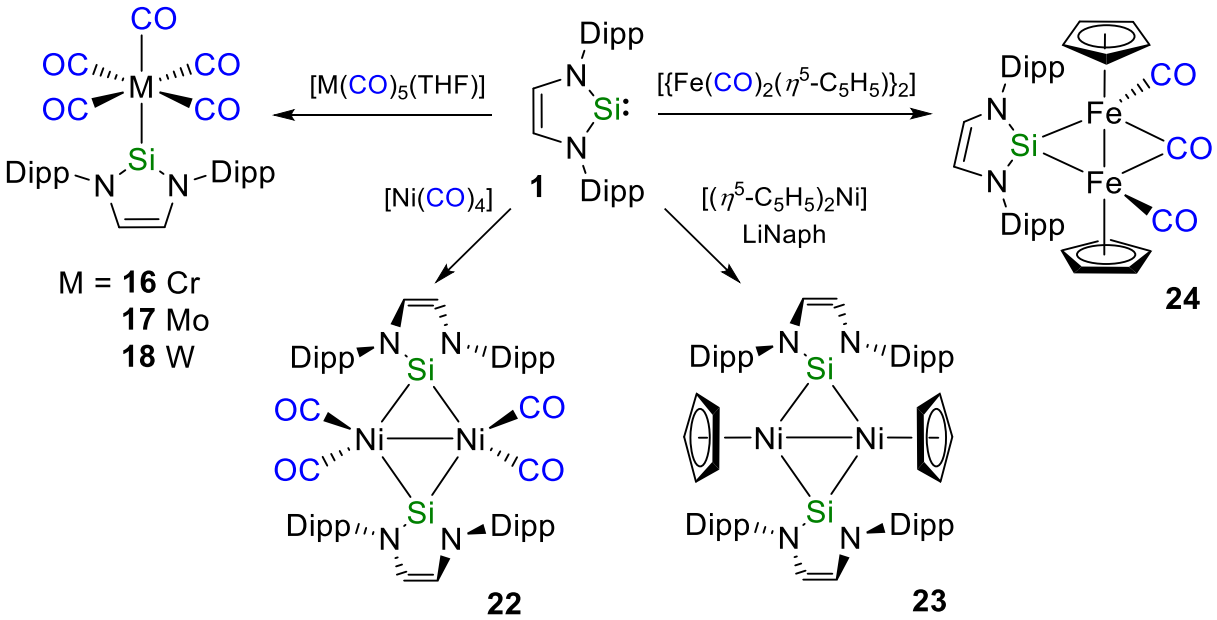

Scheme 19. Synthesis of the silylene complexes $[M(CO)_5(Dipp_2NHSi)]$ (M = Cr **16**, Mo **17**, W **18**) and the silylene-bridged complexes $[\{Ni(CO)_2(\mu\text{-}Dipp_2NHSi)\}_2]$ (**22**), $[\{(\eta^5\text{-}C_5H_5)Ni(\mu\text{-}Dipp_2NHSi)\}_2]$ (**23**) and $[\{(\eta^5\text{-}C_5H_5)Fe(CO)\}_2(\mu\text{-}CO)(\mu\text{-}Dipp_2NHSi)]$ (**24**).

The bonding of Me_2Im and Me_2NHSi (= L) to transition metal complexes has been assessed with DFT calculations for several model systems, i.e., [Ni(L)], $[Ni(CO)_3(L)]$, and $[W(CO)_5(L)]$. These studies revealed some common features in the difference between M–NHSi and M–NHC bonding which largely affect the bonding situation in transition metal complexes. In contrast to NHCs, *N*-heterocyclic silylenes show a propensity for bridging two metal atoms which was demonstrated on three different examples (Scheme 19, right and bottom). $Dipp_2NHSi$ (**1**) reacts with $[Ni(CO)_4]$ to form the colourless intermediate $[Ni(CO)_3(Dipp_2NHSi)]$ (**22a**), which led to the isolation of the dinuclear silylene-bridged complex $[\{Ni(CO)_2(\mu\text{-}Dipp_2NHSi)\}_2]$ (**22**) upon CO elimination. The reduction of $[Ni(\eta^5\text{-}C_5H_5)_2]$ with lithium naphthalenide (LiNaph) in the presence of $Dipp_2NHSi$ yielded the NHSi-bridged, diamagnetic Ni(I) dimer $[\{(\eta^5\text{-}C_5H_5)Ni(\mu\text{-}Dipp_2NHSi)\}_2]$ (**23**). The dimeric half-sandwich complex $[\{(\eta^5\text{-}C_5H_5)Fe(CO)_2\}_2]$ led upon reaction with $Dipp_2NHSi$ to the formation of the dinuclear, NHSi-bridged iron complex $[\{(\eta^5\text{-}C_5H_5)Fe(CO)\}_2(\mu\text{-}CO)(\mu\text{-}Dipp_2NHSi)]$ (**24**).

Furthermore, the insertion of $Dipp_2NHSi$ into metal halide bonds M–X was investigated in a series of manganese complexes $[Mn(CO)_5(X)]$ (X = Cl, Br, I) (Scheme 20, top). The reaction of two equivalents of $Dipp_2NHSi$ with the manganese precursors $[Mn(CO)_5(I)]$ led to substitution of two carbonyl ligands with $Dipp_2NHSi$ (**1**) to afford the tricarbonyl complex $[Mn(CO)_3(Dipp_2NHSi)_2(I)]$ (**25**). In **25**, the iodide ligand is aligned in the $\{Mn(CO)_3\}$ plane, located between both NHSi silicon atoms. Similarly, treatment of $[Mn(CO)_5(Br)]$ with two equivalents of $Dipp_2NHSi$ afforded the complex $[Mn(CO)_3(Dipp_2NHSi)_2(Br)]$ (**26**), in which according to the X-ray molecular structure and DFT calculations the bromide ligand is distorted towards one of the NHSi ligands. The reaction of the silylene ligand with $[Mn(CO)_5(Cl)]$ at room temperature afforded a mixture of two products, $[Mn(CO)_3(Dipp_2NHSi)_2(Cl)]$ (**27***) and the insertion product $[Mn(CO)_4(Dipp_2NHSi)(Dipp_2NHSi\text{-}Cl)]$ (**27**). Using higher temperatures (100 °C) and prolonged reaction times (7 days) afforded complex **27** preferentially. Spectroscopic data and the molecular structure of **27** reveal the insertion of one of the NHSi ligands into the manganese–chloride bond.

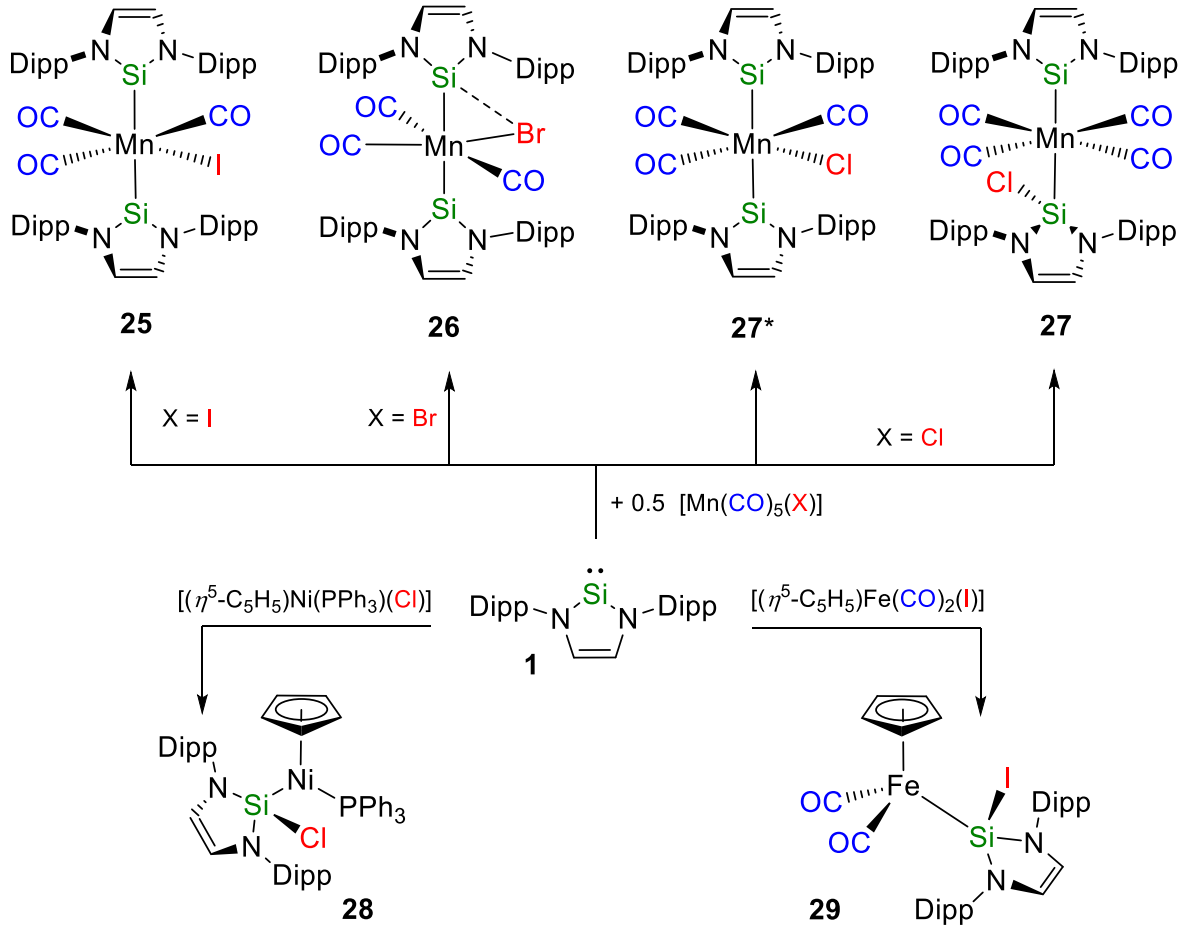

Scheme 20. Reactivity of Dipp$_2$NHSi (**1**) towards [Mn(CO)$_5$(X)] (X = Cl, Br, I) giving the bis-silylene complexes [Mn(CO)$_3$(Dipp$_2$NHSi)$_2$(I)] (**25**), [Mn(CO)$_3$(Dipp$_2$NHSi)$_2$(Br)] (**26**) and [Mn(CO)$_3$(Dipp$_2$NHSi)$_2$(Cl)] (**27***) and the silyl complexes [Mn(CO)$_4$(Dipp$_2$NHSi)(Dipp$_2$NHSi-Cl)] (**27**), [(η^5-C$_5$H$_5$)Ni(PPh$_3$)(Dipp$_2$NHSi-Cl)] (**28**) and [(η^5-C$_5$H$_5$)Fe(CO)$_2$(Dipp$_2$NHSi-I)] (**29**).

Thus, these experiments show a trend for the different halide ligands employed: i) the large and well polarizable iodide ligand prefers a symmetrical interaction of the halide ligand with the NHSi silicon atoms. ii) The smaller, less polarizable bromide ligand distorts towards one of the NHSi ligands in order to maximize the silicon-halide interaction. iii) For the smallest and less polarizable chloride ligand, the halide with the highest Si–X affinity in this row, complete transfer to the NHSi silylene atom occurs, which leads to insertion of the NHSi into the manganese–chlorine bond and formation of [Mn(CO)$_4$(Dipp$_2$NHSi)(Dipp$_2$NHSi-Cl)] (**27**). Thus, the manganese–halide bond

activation of $[Mn(CO)_5(X)]$ (X = Cl, Br, I) with **1** is feasible at high temperatures for the Mn–Cl bond due to the formation of the strong Si–Cl bond whereas the Mn–Br bond in **26** is elongated but still intact and the Mn–I bond in **25** is nearly unaffected by silylene **1**. Complete transfer of a halide to the silylene was achieved for the reaction of $Dipp_2NHSi$ with $[(\eta^5\text{-}C_5H_5)Ni(PPh_3)(Cl)]$, which did not lead to the substitution of the phosphine as might be expected, but insertion of the NHSi into the Ni–Cl bond occurs to yield $[Ni(PPh_3)(\eta^5\text{-}C_5H_5)(Dipp_2NHSi\text{-}Cl)]$ (**28**) (Scheme 20, bottom left). Similarly, the reaction with $[(\eta^5\text{-}C_5H_5)Fe(CO)_2(I)]$ led to the formation of $[(\eta^5\text{-}C_5H_5)Fe(CO)_2(Dipp_2NHSi\text{-}I)]$ (**29**) (Scheme 20, bottom right). Both complexes **28** and **29** no longer feature silylene ligands but contain silyl ligands due to the oxidation of the silicon atom.

In this thesis the reactivity of *N*-heterocyclic silylenes with respect to a variety of examples from main group element and transition metal chemistry was examined and compared to the reaction behaviour of *N*-heterocyclic carbenes. It was found that i) the frontier orbital region of NHSis differs considerably from that of NHCs which results in a significantly different reaction behaviour of NHSis. ii) NHSis readily activate a variety of element–halide bonds and react with azides in a manner unknown for NHCs. iii) NHSis have a strong tendency to act as bridging ligands between two metal centres whereas no such NHCs complexes have been prepared to date and iv) due to the strong halophilic behaviour, the insertion into metal–halide bonds readily occurs which has not been observed for NHC halide complexes.

8 Zusammenfassung

Diese Arbeit beschäftigt sich mit den Anwendungen des *N*-heterocyclischen Silylens Dipp$_2$NHSi (**1**) als ambiphiles Reagenz in der Hauptgruppenchemie und als Ligand in der Übergangsmetallchemie. Ein Schwerpunkt dieser Arbeit ist die Beurteilung der Unterschiede in der Reaktivität von *N*-heterocyclischen Silylenen in der Hauptgruppen- und Übergangsmetallchemie im Vergleich zu den heutzutage allgegenwärtigen *N*-heterocyclischen Carbenen (NHCs). Das erste Kapitel dieser Arbeit gibt einen Einblick in die Reaktivität von Dipp$_2$NHSi in Bezug auf verschiedene Hauptgruppenelement-verbindungen (Schema 21).

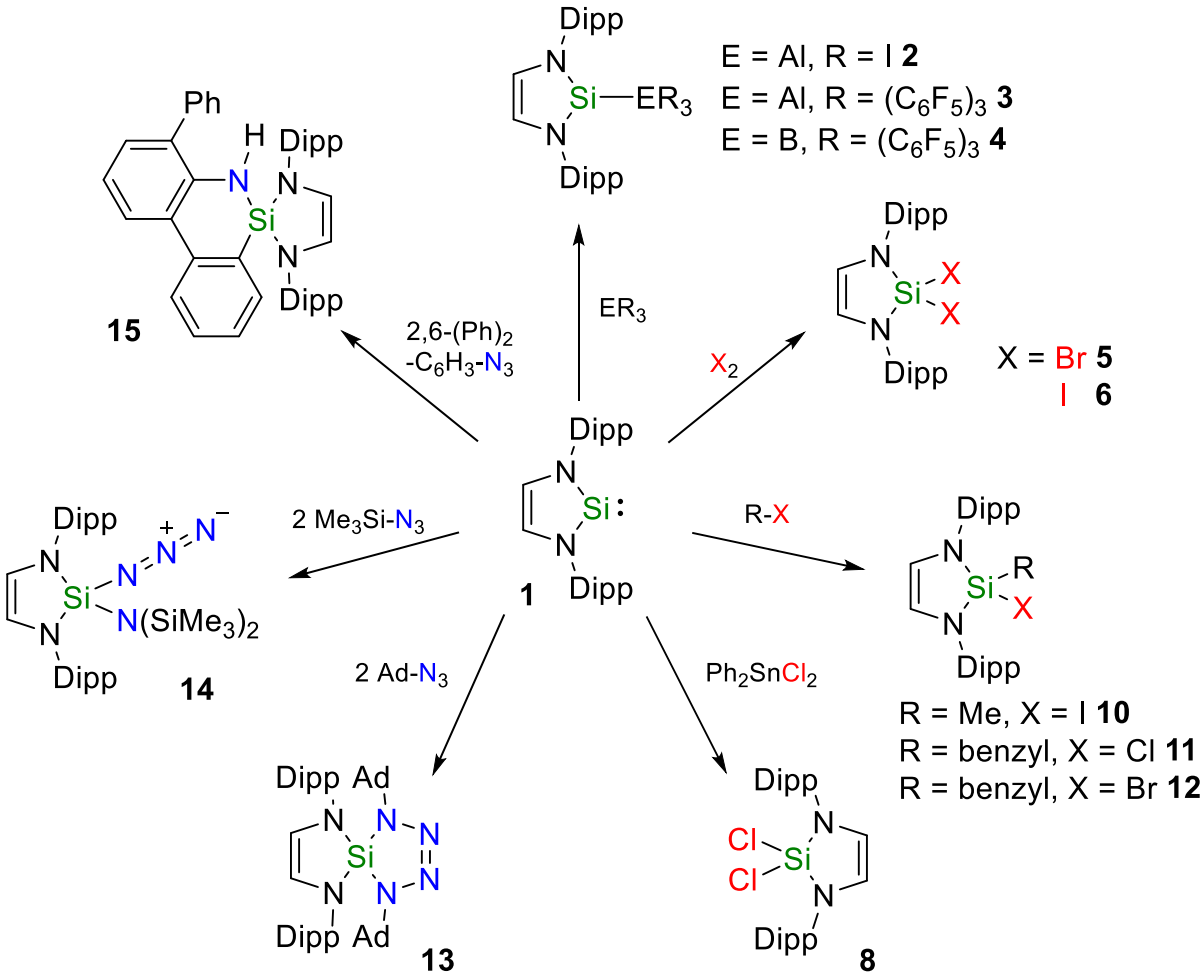

Schema 21. Umsetzung von Silylen **1** mit den Gruppe 3 Verbindungen AlI_3, $Al(C_6F_5)_3$ und $B(C_6F_5)_3$, elementaren Halogenen, Kohlenstoff–Halogenid- und Zinn–Chlorid-Bindungen von Aryl- und Alkylhalogeniden sowie Aziden mit unterschiedlichem sterischen Anspruch.

Im Verlauf dieser Studie wurde Silylen **1** mit ausgewählten Verbindungen der Gruppe 13 umgesetzt. Mit den Lewis-Säuren AlI_3, $Al(C_6F_5)_3$ und $B(C_6F_5)_3$ wurde die Adduktbildung beobachtet und die Addukte $Dipp_2NHSi{\cdot}AlI_3$ (**2**), $Dipp_2NHSi{\cdot}Al(C_6F_5)_3$ (**3**) und $Dipp_2NHSi{\cdot}B(C_6F_5)_3$ (**4**) isoliert. Verbindung **4** weist im Gegensatz zum literaturbekannten Addukt $tBu_2NHSi{\cdot}B(C_6F_5)_3$ eine hohe thermische Stabilität auf. Letzteres wird langsam durch eine B–C Aktivierung in ein Silylboran umgewandelt. Die Addukte **3** und **4** scheinen kein frustriertes Lewis-Paar zu bilden und zeigen bei Umsetzungen mit mehreren kleinen organischen Molekülen keine derartige Reaktivität. Weiterhin wurde die Reaktivität von $Dipp_2NHSi$ (**1**) in Bezug auf Element–Halogen-Bindungen verschiedener Hauptgruppenelement-Verbindungen untersucht. Die Umsetzung mit elementarem Brom und Iod führt zu den Dihalogensilanen $Dipp_2NHSiBr_2$ (**5**) und $Dipp_2NHSiI_2$ (**6**) (Schema 21, rechts oben). Die Dihalogensilane reagieren mit Organolithiumverbindungen, wie exemplarisch anhand der Reaktion von $Dipp_2NHSiCl_2$ (**8**) mit Phenyllithium zu $Dipp_2NHSiPh_2$ (**7**) gezeigt wurde. Unter Verwendung der Alkyl- und Arylhalogenide Methyliodid, Benzylchlorid und Benzylbromid konnte gezeigt werden, dass die Insertion in die Kohlenstoff–Halogen-Bindung erfolgt und die Insertionsprodukte $Dipp_2NHSi(I)(Me)$ (**10**), $Dipp_2NHSi(Cl)(benzyl)$ (**11**) und $Dipp_2NHSi(Br)(benzyl)$ (**12**) gebildet werden (Schema 21, rechts). Die Insertion ist somit gegenüber der reduktiven Kupplung unter Ausbildung von $RH_2C–CH_2R$ (R = H, Ph) und dem Dihalosilan bevorzugt. Die Umsetzung von **1** mit dem Zinnchlorid Me_3SnCl in einem Verhältnis von 1:3 führt zur Spaltung des NHSis durch die Oxidation des Siliciumatoms und zur Bildung des Diazabutens $\{(Me_3Sn)N(Dipp)CH\}_2$ (**9**) und $(Me_3Sn)SiCl_3$. Die Reaktion mit Ph_2SnCl_2 hingegen ergibt ausschließlich das Dichlorsilan $Dipp_2NHSiCl_2$ (**8**) sowie cyclische Polystannane der Form $(Ph_2Sn)_n$ (Schema 21, unten rechts).

Außerdem wurde die Reaktivität von **1** gegenüber ausgewählten 1,3-dipolaren Verbindungen untersucht und $Dipp_2NHSi$ mit Aziden unterschiedlichen sterischen Anspruchs umgesetzt (Schema 21, links). Die Reaktion mit zwei Äquivalenten des sterisch anspruchsvollen Adamantylazids führt zur Bildung des Tetrazolins **13**. Das sterisch weniger anspruchsvolle Trimethylsilylazid reagiert mit $Dipp_2NHSi$ unter Bildung des Silylazids $Dipp_2NHSi(N(SiMe_3)_2)(N_3)$ (**14**) und, durch Verlust des Silylen-

Siliciumatoms, zum Zersetzungsprodukt **14***. Das Cyclosilamin **15** wird durch die Reaktion von **1** mit 2,6-(Diphenyl)phenylazid gebildet, wobei zunächst vermutlich ein Silaimin entsteht, welches durch eine C–H Aktivierung zu **15** abreagiert (Schema 21, rechts).

Im zweiten Teil der Arbeit wurden die Bindungssituation und die Ligandeneigenschaften von $Dipp_2NHSi$ (**1**) in Übergangsmetallkomplexen mithilfe von theoretischen Rechnungen und experimentellen Untersuchungen beleuchtet. Überraschenderweise weist der Silylenligand $Dipp_2NHSi$ eine deutlich verminderte Reaktivität im Vergleich zu ähnlichen NHC-Liganden auf. DFT-Rechnungen zu den grundlegenden elektronischen Eigenschaften von Me_2Im / Me_2NHSi und $Dipp_2Im$ / $Dipp_2NHSi$ ergaben signifikante Unterschiede im Bereich der Grenzorbitale, welche die Bindungssituation von NHSis im Allgemeinen beeinflussen. Es wurde gezeigt, dass *N*-heterocyclische Silylene hinsichtlich ihrer Koordinationschemie ein signifikant unterschiedliches Verhalten aufweisen, was weitgehend durch ein einfaches MO-Schema der NHSis erklärt werden kann. Insbesondere ein energetisch tiefliegendes *π*-Orbital scheint die Koordinationschemie dieser Liganden zu bestimmen.

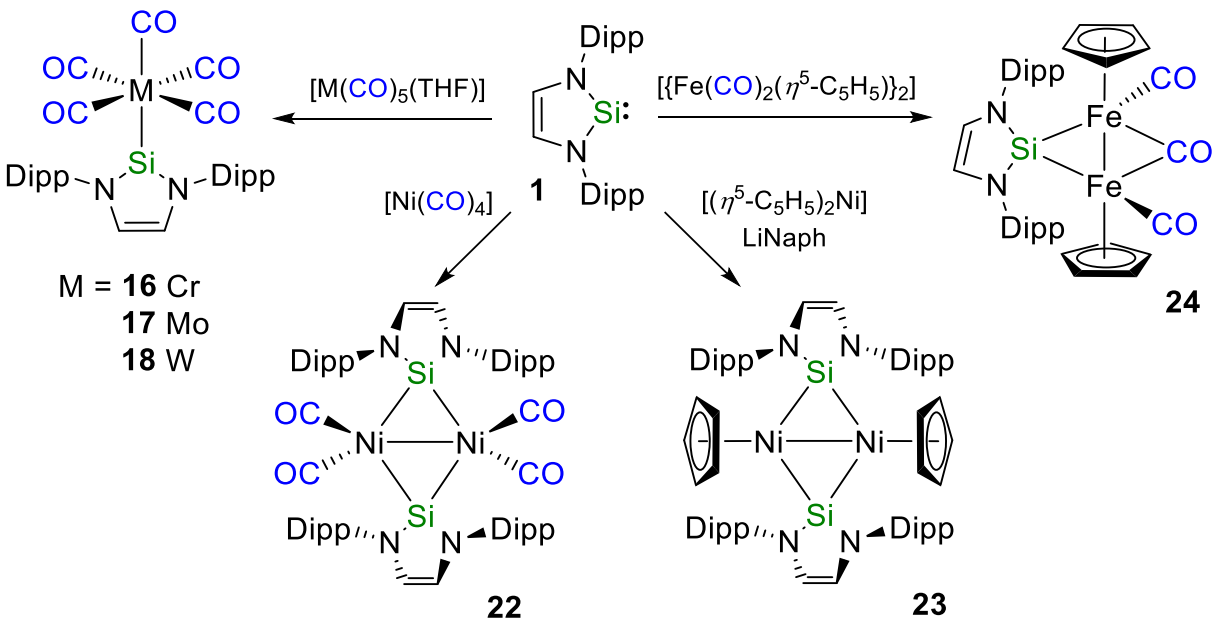

Schema 22. Synthese der Silylen-Komplexe $[M(CO)_5(Dipp_2NHSi)]$ (M = Cr **16**, Mo **17**, W **18**) und und der Silylen-verbrückten Komplexe $[\{Ni(CO)_2(\mu\text{-}Dipp_2NHSi)\}_2]$ (**22**), $[\{(\eta^5\text{-}C_5H_5)Ni(\mu\text{-}Dipp_2NHSi)\}_2]$ (**23**) und $[\{(\eta^5\text{-}C_5H_5)Fe(CO)\}_2(\mu\text{-}CO)(\mu\text{-}Dipp_2NHSi)]$ (**24**).

Zur Unterstützung der theoretischen Befunde wurden die Silylen-Komplexe $M(CO)_5(Dipp_2NHSi)]$ (M = Cr **16**, Mo **17**, W **18**) durch Umsetzung von $Dipp_2NHSi$ und $[M(CO)_6]$ (M= Cr, Mo, W) dargestellt (Schema 22, links) und der Wolframkomplex **18** mit den NHC-Komplexen $[W(CO)_5(i Pr_2Im)]$ (**19**), $[W(CO)_5(i Pr_2Im^{Me})]$ (**20**)[112] und $[W(CO)_5(Me_2Im^{Me})]$ (**21**)[112] verglichen. Die Bindung von Me_2Im und Me_2NHSi (= L) und Übergangsmetallkomplexen wurde weiterhin für die verschiedenen Modellverbindungen [Ni(L)], $[Ni(CO)_3(L)]$ und $[W(CO)_5(L)]$ mittels DFT Rechnungen untersucht, wobei einige Unterschiede zwischen den M–NHSi und M–NHC Bindungen festgestellt wurden, welche die Bindungssituation in Übergangsmetallkomplexen stark beeinflussen. Im Unterschied zu NHCs zeigen *N*-heterocyclische Silylene eine Neigung zur Verbrückung zweier Metallzentren und dieses Verhalten konnte anhand dreier Beispielen belegt werden (Schema 22). $Dipp_2NHSi$ (**1**) reagiert mit $[Ni(CO)_4]$ intermediär zum farblosen Tricarbonylkomplex $[Ni(CO)_3(Dipp_2NHSi)]$ (**22a**), welcher unter Verlust eines Carbonylliganden den Silylen-verbrückten Nickelkomplex $[\{Ni(CO)_2(\mu\text{-}Dipp_2NHSi)\}_2]$ (**22**) bildet. Die Reduktion von Nickelocen mit Lithiumnaphthalid in der Gegenwart von $Dipp_2NHSi$ (**1**) führt zur Bildung des NHSi-verbrückten, diamagentischen Ni(I)-Dimers $[(\eta^5\text{-}C_5H_5)Ni(\mu\text{-}Dipp_2NHSi)]_2$ (**23**). Ähnlich hierzu reagiert der dimere Halb-Sandwichkomplex $\{[(\eta^5\text{-}C_5H_5)Fe(CO)_2]_2\}$ mit $Dipp_2NHSi$ (**1**) zum Silylen-verbrückten dinuklearen Eisenkomplex $[\{(\eta^5\text{-}C_5H_5)Fe(CO)\}_2(\mu\text{-}CO)(\mu\text{-}Dipp_2NHSi)]$ (**24**).

Weiterhin wurde die Insertion von $Dipp_2NHSi$ (**1**) in Metall–Halogen-Bindungen anhand einer Reihe von Mangankomplexen der Form $[Mn(CO)_5(X)]$ (X = Cl, Br, I) untersucht (Schema 23, oben). Die Reaktion von zwei Äquivalenten des Silylens **1** mit dem Iodokomplex $[Mn(CO)_5(I)]$ führt unter Abspaltung zweier Carbonylliganden zur Bildung des Tricarbonylkomplexes $[Mn(CO)_3(Dipp_2NHSi)_2(I)]$ (**25**), in dem der Iodidligand symmetrisch zwischen den beiden Siliciumatomen der Silylenliganden in der $\{Mn(CO)_3\}$-Ebene liegt. Ähnlich hierzu wird der Bis-Silylenkomplex $[Mn(CO)_3(Dipp_2NHSi)_2(Br)]$ (**26**) durch Umsetzung von $[Mn(CO)_5(Br)]$ mit **1** erhalten, wobei eine Wechselwirkung des Bromidliganden mit einem Silylenliganden beobachtet wird. Durch die Wechselwirkung kommt es zu einer deutlichen Abwinkelung des Bromidliganden aus der $\{Mn(CO)_3\}$ Ebene, was sowohl durch DFT Rechnungen als

auch durch Einkristallstrukturanalyse bestätigt werden konnte. Die Reaktion von $Dipp_2NHSi$ **1** mit $[Mn(CO)_5(Cl)]$ bei Raumtemperatur resultiert in der Bildung zweier Reaktionsprodukte, dem Bis-Silylenkomplex $[Mn(CO)_3(Dipp_2NHSi)_2(Cl)]$ (**27***) und dem Insertionsprodukt $[Mn(CO)_4(Dipp_2NHSi)(Dipp_2NHSi\text{-}Cl)]$ (**27**). Durch die Erhöhung der Reaktionstemperatur (100 °C) und durch längere Reaktionszeiten (7 Tage) konnte bevorzugt der Silylen-Silyl-Komplex **27** dargestellt werden. Spektroskopischen Daten und kristallographischen Untersuchungen belegen die Insertion des Silylenliganden in die Mangan–Chlor-Bindung.

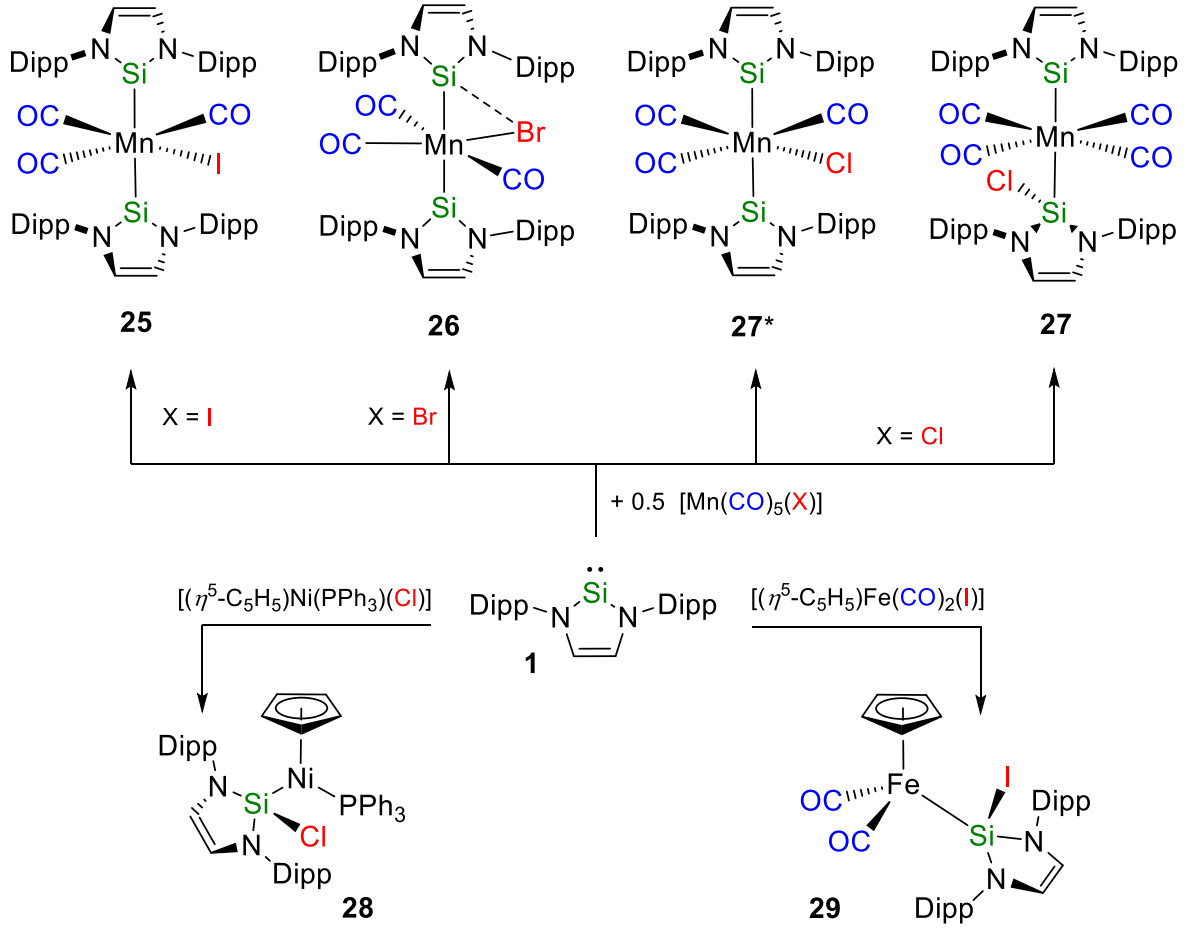

Schema 23. Umsetzung von $Dipp_2NHSi$ (**1**) mit $[Mn(CO)_5(X)]$ (X = Cl, Br, I) hin zu den Bis-Silylen-Komplexen $[Mn(CO)_3(Dipp_2NHSi)_2(I)]$ (**25**), $[Mn(CO)_3(Dipp_2NHSi)_2(Br)]$ (**26**) und $[Mn(CO)_3(Dipp_2NHSi)_2(Cl)]$ (**27***) und den Silyl-Komplexen $[Mn(CO)_4(Dipp_2NHSi)(Dipp_2NHSi\text{-}Cl)]$ (**27**), $[(\eta^5\text{-}C_5H_5)Ni(PPh_3)(Dipp_2NHSi\text{-}Cl)]$ (**28**) und $[(\eta^5\text{-}C_5H_5)Fe(CO)_2(Dipp_2NHSi\text{-}I)]$ (**29**).

Somit zeigen die Umsetzungen mit den Mangankomplexen [$Mn(CO)_5(X)$] einen Trend in Bezug auf die verschiedenen Halogenidoliganden auf: i) der große und gut polarisierbare Iodoligand bevorzugt eine symmetrische Wechselwirkung mit dem NHSi Siliciumatom. ii) Die Verwendung des kleineren, weniger polarisierbaren Bromidoliganden führt zu einer Verzerrung der Struktur, um die Silicium-Halogenid-Interaktion zu maximieren. iii) Für den kleinsten und am am wenigsten polarisierbaren Chloridoliganden mit der höchsten Si–X Affinität in dieser Reihe wird die vollständige Übertragung des Chloratoms auf das Siliciumatom des Silylenliganden unter Bildung des Komplexes ([$Mn(CO)_4$($Dipp_2$NHSi)($Dipp_2$NHSi-Cl)] (**27**) beobachtet. Somit ist die Aktivierung der Mangan–Halogenid-Bindung von [$Mn(CO)_5(X)$] (X = Cl, Br, I) mit **1** bei hohen Temperaturen für die Mn–Cl-Bindung aufgrund der Bildung einer starken Si–Cl-Bindung möglich, während die Mn–Br-Bindung in **26** verlängert, aber noch intakt ist und die Mn–I-Bindung in **25** vom Silylen **1** nahezu unbeeinflusst bleibt. Die vollständige Übertragung des Halogenidoliganden auf das Siliciumatom des Silylenliganden kann auch für den Halb-Sandwich-Komplex [(η^5-C_5H_5)Ni(PPh_3)(Cl)] beobachtet werden, wobei nicht wie erwartet die Substitution des Phosphanliganden, sondern die Insertion von $Dipp_2$NHSi (**1**) in die Ni–Cl-Bindung beobachtet wurde und so der Komplex [Ni(PPh_3)(η^5-C_5H_5)($Dipp_2$NHSi-Cl)] (**28**) (Schema 23, unten links) isoliert wird. Ähnlich hierzu führt die Reaktion von [(η^5-C_5H_5)Fe$(CO)_2$(I)] mit dem Silylen **1** ebenfalls zur Bildung des Insertionsproduktes [(η^5-C_5H_5)Fe$(CO)_2$($Dipp_2$NHSi-I)] (**29**) (Schema 23, unten rechts). In den Komplexen **28** und **29** wurde der Silylenligand durch formale Oxidation in einen Silylliganden überführt.

In dieser Arbeit wurde die Reaktivität von *N*-heterocyclischen Silylenen in Bezug auf eine Vielzahl von Beispielen aus der Hauptgruppenelement- und Übergangsmetallchemie untersucht und mit dem Reaktionsverhalten von *N*-heterocyclischen Carbenen verglichen. Es wurde festgestellt, dass i) sich die Grenzorbitalregion von NHSis erheblich von derjenigen von NHCs unterscheidet, was zu einem signifikant unterschiedlichen Reaktionsverhalten führt. ii) NHSis aktivieren leicht eine Vielzahl von Element–Halogenid-Bindungen und reagieren mit Aziden auf eine für NHCs unbekannte Weise. iii) NHSis neigen stark dazu als Brückenliganden zwischen zwei Metallzentren zu fungieren, während bislang keine derartigen NHC-

Komplexe bekannt sind, und iv) die Insertion des Silylens in Metall-Halogenid-Bindungen tritt aufgrund des starken halophilen Verhaltens des Silylens häufig auf, was für NHC-Halogenidokomplexe nicht beobachtet wird.

9 Appendix

9.1 Publications

9.1.1 Reprint Permission

The manuscript of the following publications:

N-Heterocyclic Silylenes as Ligands in Transition Metal Carbonyl Chemistry: Nature of their Bonding and Supposed Innocence
Mirjam J. Krahfuss, Jörn Nitsch, F. Matthias Bickelhaupt, Todd B. Marder, Udo Radius, *Chem. Eur. J.* **2020**, *26*, 11276 – 11292.
DOI: 10.1002/chem.202001062.

N-Heterocyclic Silylenes as Metal–Metal Bridges and Metal–Halide Activators in Transition Metal Complexes
Mirjam J. Krahfuss, Udo Radius, *Inorg. Chem*. **2020**, *59*, 10976 – 10985.
DOI: 10.1021/acs.inorgchem.0c01462

were used with permission from the American Chemical Society and from John Wiley and Sons according to the terms and conditions specified within the respective license agreement. The results of these publications are presented in Chapter 2.

9.1.2 List of Publications

Publications in peer-reviewed journals:

2020

N-Heterocyclic Silylenes as Ligands in Transition Metal Carbonyl Chemistry: Nature of their Bonding and Supposed Innocence
Mirjam J. Krahfuss, Jörn Nitsch, F. Matthias Bickelhaupt, Todd B. Marder, Udo Radius, *Chem. Eur. J.* **2020**, *26*, 11276 – 11292.

N-Heterocyclic Silylenes as Metal–Metal Bridges and Metal–Halide Activators in Transition Metal Complexes
Mirjam J. Krahfuss, Udo Radius, *Inorg. Chem*. **2020**, *59*, 10976 – 10985.

Large vs. Small NHC Ligands in Nickel(0) Complexes: The Coordination of Olefins, Ketones and Aldehydes at [Ni(NHC)$_2$]
Lukas Tendera, Thomas Schaub, Mirjam J. Krahfuss, Maximilian W. Kuntze-Fechner, Udo Radius, *Eur. J. Inorg. Chem*. **2020**, 3194 – 3207.

N-Heterocyclic Carbene and Cyclic (Alkyl)(amino)carbene Complexes of Titanium(IV) and Titanium(III)
Guenther Horrer, Mirjam J. Krahfuss, Katharina Lubitz, Ivo Krummenacher, Holger Braunschweig, Udo Radius, *Eur. J. Inorg. Chem*. **2020**, 281 – 291.

Nickel Tetracarbonyl as Starting Material for the Synthesis of NHC-stabilized Nickel(II) Allyl Complexes
Johannes H. J. Berthel, Mirjam J. Krahfuss, Udo Radius, *Z. Anorg. Allg. Chem*. **2020**, *646*, 692 – 704.

2019

Cyclic (Alkyl)(Amino) Carbene - Mehr als nur Liganden
Ursula S. D. Paul, Mirjam J. Krahfuss, Udo Radius, *Chem. unserer Zeit* **2019**, *53*, 212 – 223.

Intramolecular Ring-Expansion Reaction (RER) and Intermolecular Coordination of In Situ Generated Cyclic (Amino)(aryl)carbenes (cAArCs)
Jan Lorkowski, Mirjam J. Krahfuss, Maciej Kubicki, Udo Radius, Cezary Pietraszuk, *Chem. Eur. J*. **2019**, *25*, 11365 – 11374.

2018

Hydride Amide and Hydride Phenolate Complexes of NHC Coordinated Aluminum
Andreas Hock, Heidi Schneider, Mirjam J. Krahfuss, Udo Radius, *Z. Anorg. Allg. Chem*. **2018**, *644*, 1243 – 1251.

2016

To Rearrange or not to Rearrange: Reactivity of NHCs towards Chloro- and Hydrostannanes R_2SnCl_2 (R = Me, Ph) and Ph_3SnH
Heidi Schneider, Mirjam J. Krahfuss, Udo Radius, *Z. Anorg. Allg. Chem*. **2016**, *642*, 1282 – 1286.

9.2 Abbreviations

Substituents

Ad	adamantyl
Ar	aryl
Cy	cyclohexyl
Dipp	2,6-di*iso*propylphenyl
dcypb	bis(dicyclohexyl)-1,4-phosphinobutane
dippe	1,2-bis(di*iso*propylphosphino)ethane
Duryl	2,3,5,6-tetramethylphenyl
Et	ethyl
*i*Pr	*iso*propyl
*n*Pr	*n*-propyl
Me	methyl
Mes	mesityl
Neop	neopentyl
Ph	phenyl
Pyr	pyrido
*t*Bu	*tert*-butyl
Xyl	2,6-dimethylphenyl

Solvents and reagents

BAr^F	tris(pentafluorophenyl)borane
B_2pin_2	bis(pinacolato)diboron
C_6D_6	deuterated benzene

cod	1,5-cyclooctadiene
DABCO	1,4-diazabicyclo[2.2.2]octane
DCM	dichloromethane
DMAP	dimethylaminopyridin
Et_2O	diethyl ether
KO*t*Bu	potassium *tert*-butoxide
MeCN	acetonitrile
MeOH	methanol
nbd	nornornadiene
*n*BuLi	*n*butyllithium
OTf	trifluoromethanesulfonate
THF	tetrahydrofuran

_N_-heterocyclic carbenes and silylenes

Ad_2Im	1,3-Diadamanthylimidazol-2-ylidene
cAAC	cyclic (alkyl)(amino)carbene
cAASi	cyclic (alkyl)(amino)silylene
Cy_2Im	1,3-Dicyclohexylimidazolin-2-ylidene
$Dipp_2Im$	1,3-(2,6-Di*iso*propylphenyl)imidazolin-2-ylidene
$Dipp_2Im^{H2}$	1,3-(2,6-Di*iso*propylphenyl)imidazolidine-2-ylidene
$Dipp_2NHSi$	1,3-Bis(2,6-di*iso*propylphenyl)-1,3-diaza-2-silacyclopent-4-en-2-ylidene
H_2Im	1,3-Dihydroimidazolin-2-ylidene
iPr_2Im	1,3-Di*iso*propylimidazolin-2-ylidene
iPr_2Im^{Me}	1,3-Di*iso*propyl-4,5-dimethylimidazolin-2-ylidene
Me_2Im^{H2}	1,3,4,5-Tetramethylimidazolidin-2-ylidene

Me_2Im^{Me}	1,3,4,5-Tetramethylimidazolin-2-ylidene
Me_2NHSi	1,3-Dimethyl-1,3-diaza-2-silacyclopent-4-en-2-ylidene
Mes_2Im	1,3-Dimesitylimidazolin-2-ylidene
Np_2NHSi^{benz}	1,3-Dineopentylbenzimidazolin-2-ylidene
Ph_2Im	1,3,-Diphenylimidazolin-2-ylidene
nPr_2Im	1,3-Di-*n*propylimidazolin-2-ylidene
tBu_2Im	1,3-Di-*tert*-butylimidazolin-2-ylidene
tBu_2NHSi	1,3-Di-*tert*-butyl-1,3-diaza-2-silacyclopent-4-en-2-ylidene
tBu_2NHSi^{H2}	1,3-Di-*tert*-butyl-1,3-diaza-2-silacyclopentyl-2-ylidene

Analytical abbreviations

CSD	Cambridge Structural Database
d	doublet (in NMR spectroscopy); days
DFT	density functional theory
eq.	equivalent
h	hour
HMBC	heteronuclear multiple bond correlation
HMQC	heteronuclear multiple quantum correlation
m	multiplet (in NMR spectroscopy)
min	minute
NMR	nuclear magnetic resonance
q	quartet (in NMR spectroscopy)
rt	room temperature
s	singlet (in NMR spectroscopy)

sec	second
sept	septet (in NMR spectroscopy)
t	triplet (in NMR spectroscopy)

Other

FLP	frustrated Lewis pair
NHO	*N*-heterocyclic olefin

9.3 Symbols and non-SI units

Å	Ångström, 1 Å = 10^{-10} m
J	J-coupling constant in NMR spectroscopy, [Hz]
ppm	parts per million
Z	number of molecules per unit cell
δ	chemical shift in NMR spectroscopy, [ppm]
λ	wavelength
v	frequency, [s^{-1}]
wt%	weight percent

9.4 List of compounds

Chapter I: N-Heterocyclic Silylenes in Main Group Element Chemistry: Reactivity of the Lone Pair

1 $Dipp_2NHSi$

2 $Dipp_2NHSi{\cdot}AlI_3$

3 $Dipp_2NHSi{\cdot}Al(C_6F_5)_3$

4 $Dipp_2NHSi{\cdot}B(C_6F_5)_3$

5 $Dipp_2NHSiBr_2$

6 $Dipp_2NHSiI_2$

7 $Dipp_2NHSiPh_2$

8 $Dipp_2NHSiCl_2$

9 $\{Me_3SnN(Dipp)CH\}_2$

10 $Dipp_2NHSi(I)(Me)$

11 $Dipp_2NHSi(Cl)$(benzyl)

12 $Dipp_2NHSi(Br)$(benzyl)

13 1-$Dipp_2NHSi$-2,5-bis(adamantyl)-tetrazoline

14 bis(trimethylsilyl)amido azido silane

14* 1,4-bis(2-6-di*iso*propylphenyl)-1,4-bis(trimethylsilyl)-1,4-diazabut-2-ene

15 cyclosilamine

Chapter II: N-heterocyclic Silylenes as Ligands in Transition Metal Chemistry: Nature of Their Bonding and Supposed Innocence

16 $[Cr(CO)_5(Dipp_2NHSi)]$

17 $[Mo(CO)_5(Dipp_2NHSi)]$

18 $[W(CO)_5(Dipp_2NHSi)]$

19 $[W(CO)_5(i\text{Pr}_2\text{Im})]$

20 $[W(CO)_5(i\text{Pr}_2\text{Im}^{Me})]$

21 $[W(CO)_5(\text{Me}_2\text{Im}^{Me})]$

22 $[\{Ni(CO)_2(\mu\text{-Dipp}_2\text{NHSi})\}_2]$

23 $[\{(\eta^5\text{-}C_5H_5)Ni(\mu\text{-Dipp}_2\text{NHSi})\}_2]$

24 $[\{(\eta^5\text{-}C_5H_5)Fe(CO)\}_2(\mu\text{-CO})(\mu\text{-Dipp}_2\text{NHSi})]$

25 $[Mn(CO)_3(\text{Dipp}_2\text{NHSi})_2(I)]$

26 $[Mn(CO)_3(\text{Dipp}_2\text{NHSi})_2(Br)]$

27 $[Mn(CO)_4(\text{Dipp}_2\text{NHSi})(\text{Dipp}_2\text{NHSi-Cl})]$

28 $[(\eta^5\text{-}C_5H_5)Ni(PPh_3)(\text{Dipp}_2\text{NHSi-Cl})]$

29 $[(\eta^5\text{-}C_5H_5)Fe(CO)_2(\text{Dipp}_2\text{NHSi-I})]$

10 References

[1] A. J. Arduengo, III, R. L. Harlow, M. Kline, *J. Am. Chem. Soc.* **1991**, *113*, 361-363.

[2] V. Lavallo, Y. Canac, C. Prasang, B. Donnadieu, G. Bertrand, *Angew. Chem. Int. Ed.* **2005**, *44*, 5705-5709; *Angew. Chem*. **2005**, *117*, 5851-5855.

[3] a) W. A. Herrmann, *Angew. Chem. Int. Ed.* **2002**, *41*, 1290-1309; b) S. Nolan, *N-Heterocyclic Carbenes in Synthesis*, Wiley-VCH **2006**; c) F. Glorius, *N-Heterocyclic Carbenes in Transition Metal Catalysis, Vol. 21*, Springer **2007**; d) F. E. Hahn, M. C. Jahnke, *Angew. Chem. Int. Ed.* **2008**, *47*, 3122-3172; *Angew. Chem*. **2008**, *120*, 3166-3216; e) P. de Fremont, N. Marion, S. P. Nolan, *Coord. Chem. Rev.* **2009**, *253*, 862-892; f) S. Diez-Gonzalez, N. Marion, S. P. Nolan, *Chem. Rev.* **2009**, *109*, 3612-3676; g) M. Poyatos, J. A. Mata, E. Peris, *Chem. Rev.* **2009**, *109*, 3677-3707; h) S. Díez-González, *N-Heterocyclic Carbenes: From Laboratory Curiosities to Efficient Synthetic Tools*, **2010**; i) T. Rovis, S. P. Nolan, *Synlett* **2013**, *24*, 1188-1189; j) C. S. J. Cazin, *Dalton Trans.* **2013**, *42*, 7254; k) S. P. Nolan, *N-Heterocyclic Carbenes: Effective Tools for Organometallic Synthesis*, **2014**; l) A. A. Danopoulos, T. Simler, P. Braunstein, *Chem. Rev.* **2019**, *119*, 3730-3961.

[4] a) M. Melaimi, M. Soleilhavoup, G. Bertrand, *Angew. Chem. Int. Ed.* **2010**, *49*, 8810-8849; *Angew. Chem.* **2010**, *122*, 8992-9032; b) M. Soleilhavoup, G. Bertrand, *Acc. Chem. Res.* **2015**, *48*, 256-266; c) S. Roy, K. C. Mondal, H. W. Roesky, *Acc. Chem. Res.* **2016**, *49*, 357-369; d) M. Melaimi, R. Jazzar, M. Soleilhavoup, G. Bertrand, *Angew. Chem. Int. Ed.* **2017**, *56*, 10046-10068; *Angew. Chem*. **2017**, *129*, 10180-10203; e) U. S. D. Paul, U. Radius, *Eur. J. Inorg. Chem.* **2017**, 3362-3375.

[5] a) H. Jacobsen, A. Correa, C. Costabile, L. Cavallo, *J. Organomet. Chem.* **2006**, *691*, 4350-4358; b) R. Tonner, G. Heydenrych, G. Frenking, *Chem. Asian J.* **2007**, *2*, 1555-1567; c) U. Radius, F. M. Bickelhaupt, *Organometallics* **2008**, *27*, 3410-3414; d) U. Radius, F. M. Bickelhaupt, *Coord. Chem. Rev.* **2009**, *253*, 678-686; e) H. Jacobsen, A. Correa, A. Poater, C. Costabile, L. Cavallo, *Coord. Chem. Rev.* **2009**, *253*, 687-703; f) J. C. Bernhammer, G. Frison, H. V. Huynh, *Chem. Eur. J.* **2013**, *19*, 12892-12905.

[6] a) M. Denk, R. Lennon, R. Hayashi, R. West, A. V. Belyakov, H. P. Verne, A. Haaland, M. Wagner, N. Metzler, *J. Am. Chem. Soc.* **1994**, *116*, 2691-2692; b) B. Gehrhus, M. F. Lappert, J. Heinicke, R. Boese, D. Blaser, *J. Chem. Soc., Chem. Commun.* **1995**, 1931-1932; c) R. West, M. Denk, *Pure Appl. Chem.* **1996**, *68*, 785-788; d) M. Kira, S. Ishida, T. Iwamoto, C. Kabuto, *J. Am. Chem. Soc.* **1999**, 9722 - 9723; e) L. Kong, J. Zhang, H. Song, C. Cui, *Dalton Trans.* **2009**, 5444-5446; f) P. Zark, A. Schaefer, A. Mitra, D. Haase, W. Saak, R. West, T. Mueller, *J. Organomet. Chem.* **2010**, *695*, 398-408; g) B. Blom, M. Stoelzel, M. Driess, *Chem. - Eur. J.* **2013**, *19*, 40-62; h) B. Blom, D. Gallego, M. Driess, *Inorg. Chem. Front.* **2014**, *1*, 134-148; i) T. Kosai, S. Ishida, T. Iwamoto, *Angew. Chem. Int. Ed.* **2016**, *55*, 15554-15558; *Angew*. *Chem*. **2016**, *128*, 15783-15787; j) S. Raoufmoghaddam, Y.-P. Zhou, Y. Wang, M. Driess, *J. Organomet. Chem.* **2017**, *829*, 2-10.

[7] a) A. Meltzer, S. Inoue, C. Praesang, M. Driess, *J. Am. Chem. Soc.* **2010**, *132*, 3038-3046; b) H. W. Roesky, *J. Organomet. Chem.* **2013**, *730*, 57-62; c) R. Tacke, T. Ribbeck, *Dalton Trans.* **2017**, *46*, 13628-13659.

[8] H. Davy, *Philos. Trans. Royal Soc.* **1808**, *98*, 333-370.

[9] M. E. Weeks, *Discovery of the Elements*, Journal of chemical education, 6th Ed., **1960**.

[10] J. E. Huheey, E. A. Keiter, R. L. Keiter, *Anorganische Chemie - Prinzipien von Struktur und Reaktivität, Vol. 5*, De Gruyter, Berlin / Boston, **2014**.

[11] a) A. Ladenburg, *Ber. Dtsch. Chem. Ges.* **1908**, *41*, 966; b) A. Stock, *J. Chem. Soc., Abstr.* **1917**, *112*, 204; c) E. A. Hauser, *J. Phys. Colloid Chem.* **1948**, *52*, 1165-1174; d) F. Feher, G. Kuhlborsch, H. Luhleich, *Z. Anorg. Allg. Chem.* **1960**, *303*, 283-293; e) R. Mueller, *Wiss. Z. Tech. Univ. Dresden* **1963**, *12*, 1633-1642; f) H. Bock, *Fascinating silicon-chemistry - retrospection and perspectives*, Wiley-VCH Verlag GmbH, **2000**, 37-58; g) S. J. Clarson, *Silicon* **2014**, *6*, 209-210.

[12] R. Schwarz, G. Pietsch, *Z. Anorg. Allg. Chem.* **1937**, *232*, 249-256.

[13] T. J. Drahnak, J. Michl, R. West, *J. Am. Chem. Soc.* **1979**, *101*, 5427-5428.

[14] a) O. M. Nefedov, M. N. Manakov, *Angew. Chem. Int. Ed. Engl.* **1966**, *5*, 1021-1038; b) W. H. Atwell, D. R. Weyenberg, *Angew. Chem. Int. Ed. Engl.* **1969**, *8*, 469-477.

[15] P. Jutzi, D. Kanne, C. Kruger, *Angew. Chem. Int. Ed. Engl.* **1986**, *25*, 164.

[16] H. H. Karsch, U. Keller, S. Gamper, G. Mueller, *Angew. Chem. Int. Ed. Engl.* **1990**, *29*, 295-296; *Angew*. *Chem*. **1990**, *102*, 297-298.

[17] M. Denk, R. Lennon, R. Hayashi, R. West, A. V. Belyakov, H. P. Verne, A. Haaland, M. Wagner, N. Metzler, *J. Am. Chem. Soc.* **1994**, *116*, 2691-2692.

[18] a) C.-W. So, H. W. Roesky, J. Magull, R. B. Oswald, *Angew. Chem. Int. Ed.* **2006**, *45*, 3948-3950; *Angew. Chem.* **2006**, *118*, 4052-4054; b) W. Wang, S. Inoue, S. Yao, M. Driess, *J. Am. Chem. Soc.* **2010**, *132*, 15890-15892; c) K. Junold, J. A. Baus, C. Burschka, R. Tacke, *Angew. Chem. Int. Ed.* **2012**, *51*, 7020-7023; *Angew. Chem.* **2012**, *124*, 7126-7129; d) M. Stoelzel, C. Praesang, B. Blom, M. Driess, *Aust. J. Chem.* **2013**, *66*, 1163-1170; e) B. Blom, S. Enthaler, S. Inoue, E. Irran, M. Driess, *J. Am. Chem. Soc.* **2013**, *135*, 6703-6713; f) R. Tacke, C. Kobelt, J. A. Baus, R. Bertermann, C. Burschka, *Dalton Trans.* **2015**, *44*, 14959-14974; g) S. Khoo, J. Cao, M.-C. Yang, Y.-L. Shan, M.-D. Su, C.-W. So, *Chem. Eur. J.* **2018**, *24*, 14329-14334.

[19] M. Denk, J. C. Green, N. Metzler, M. Wagner, *J. Chem. Soc., Dalton Trans.* **1994**, 2405-2410.

[20] a) W. Li, N. J. Hill, A. C. Tomasik, G. Bikzhanova, R. West, *Organometallics* **2006**, *25*, 3802-3805; b) A. C. Tomasik, A. Mitra, R. West, *Organometallics* **2009**, *28*, 378-381.

[21] J. Heinicke, A. Oprea, M. K. Kindermann, T. Karpati, L. Nyulaszi, T. Veszpremi, *Chem. Eur. J.* **1998**, *4*, 541-545.

[22] M. Driess, S. Yao, M. Brym, C. Van Wuellen, D. Lentz, *J. Am. Chem. Soc.* **2006**, *128*, 9628-9629.

[23] M. Kira, S. Ishida, T. Iwamoto, C. Kabuto, *J. Am. Chem. Soc.* **1999**, *121*, 9722-9723.

[24] a) S. Ishida, T. Iwamoto, C. Kabuto, M. Kira, *Chem. Lett.* **2001**, 1102-1103; b) T. Iwamoto, N. Ohnishi, Z. Gui, S. Ishida, H. Isobe, S. Maeda, K. Ohno, M. Kira, *New J. Chem.* **2010**, *34*, 1637-1645; c) C. Watanabe, Y. Inagawa, T. Iwamoto, M. Kira, *Dalton Trans.* **2010**, *39*, 9414-9420; d) Y. Inagawa, S. Ishida, T. Iwamoto, *Chem. Lett.* **2014**, *43*, 1665-1667.

[25] a) S. Wuertemberger-Pietsch, U. Radius, T. B. Marder, *Dalton Trans.* **2016**, *45*, 5880-5895; b) G. D. Frey, J. D. Masuda, B. Donnadieu, G. Bertrand, *Angew. Chem. Int. Ed.* **2010**, *49*, 9444-9447; *Angew. Chem.* **2010**, *122*, 9634-9637.

[26] T. Wang, D. W. Stephan, *Chem. Eur. J.* **2014**, *20*, 3036-3039.

[27] U. S. D. Paul, U. Radius, *Chem. Eur. J.* **2017**, *23*, 3993-4009.

[28] D. Schmidt, J. H. J. Berthel, S. Pietsch, U. Radius, *Angew. Chem. Int. Ed.* **2012**, *51*, 8881-8885; *Angew. Chem.* **2012**, *124*, 9011-9015.

[29] a) H. Schneider, M. J. Krahfuss, U. Radius, *Z. Anorg. Allg. Chem.* **2016**, *642*, 1282-1286; b) M. Arrowsmith, M. S. Hill, G. Kociok-Koehn, D. J. MacDougall, M. F. Mahon, *Angew. Chem, Int. Ed.* **2012**, *51*, 2098-2100; *Angew. Chem*. **2012**, *124*, 2140-2142.

[30] M. Haaf, A. Schmiedl, T. A. Schmedake, D. R. Powell, A. J. Millevolte, M. Denk, R. West, *J. Am. Chem. Soc.* **1998**, *120*, 12714-12719.

[31] M. K. Denk, J. M. Rodezno, S. Gupta, A. J. Lough, *J. Organomet. Chem.* **2001**, *617-618*, 242-253.

[32] B. Gehrhus, P. B. Hitchcock, *J. Organomet. Chem.* **2004**, *689*, 1350-1354.

[33] M. Kira, S. Ishida, T. Iwamoto, C. Kabuto, *J. Am. Chem. Soc.* **2002**, *124*, 3830-3831.

[34] U. Radius, J. Nitsch, M. J. Krahfuß, F. M. Bickelhaupt, T. B. Marder, *Chem. Eur. J.* **2020**, *26*, 11276-11292.

[35] a) S. Kronig, E. Theuergarten, D. Holschumacher, T. Bannenberg, C. G. Daniliuc, P. G. Jones, M. Tamm, *Inorg. Chem.* **2011**, *50*, 7344-7359; b) D. Holschumacher, T. Bannenberg, C. G. Hrib, P. G. Jones, M. Tamm, *Angew. Chem. Int. Ed.* **2008**, *47*, 7428-7432; *Angew. Chem*. **2008**, *120*, 7538-7542; c) A. Winkler, M. Freytag, P. G. Jones, M. Tamm, *J. Organomet. Chem.* **2015**, *775*, 164-168; d) G. C. Welch, R. R. San Juan, J. D. Masuda, D. W. Stephan, *Science* **2006**, *314*, 1124-1126.

[36] B. Birkmann, T. Voss, S. J. Geier, M. Ullrich, G. Kehr, G. Erker, D. W. Stephan, *Organometallics* **2010**, *29*, 5310-5319.

[37] a) J. S. J. McCahill, G. C. Welch, D. W. Stephan, *Angew. Chem. Int. Ed.* **2007**, *46*, 4968-4971; *Angew. Chem.* **2007**, *119*, 5056-5059; b) A. Stirling, A. Hamza, T. A. Rokob, I. Papai, *Chem. Commun.* **2008**, 3148-3150; c) M. A. Dureen, D.

W. Stephan, *J. Am. Chem. Soc.* **2009**, *131*, 8396-8397; d) T. Voss, C. Chen, G. Kehr, E. Nauha, G. Erker, D. W. Stephan, *Chem. Eur. J.* **2010**, *16*, 3005-3008.

[38] C. M. Moemming, E. Otten, G. Kehr, R. Froehlich, S. Grimme, D. W. Stephan, G. Erker, *Angew. Chem. Int. Ed.* **2009**, *48*, 6643-6646; *Angew. Chem.* **2009**, *121*, 6770-6773.

[39] S. Porcel, G. Bouhadir, N. Saffon, L. Maron, D. Bourissou, *Angew. Chem. Int. Ed.* **2010**, *49*, 6186-6189; *Angew. Chem.* **2010**, *122*, 6322-6325.

[40] G. Schnee, O. Nieto Faza, D. Specklin, B. Jacques, L. Karmazin, R. Welter, C. Silva Lopez, S. Dagorne, *Chem. Eur. J.* **2015**, *21*, 17959-17972.

[41] N. Metzler, M. Denk, *Chem. Commun.* **1996**, 2657-2658.

[42] A. Jana, R. Azhakar, S. P. Sarish, P. P. Samuel, H. W. Roesky, C. Schulzke, D. Koley, *Eur. J. Inorg. Chem.* **2011**, 5006-5013.

[43] H. Li, F. Hung-Low, C. Krempner, *Organometallics* **2012**, *31*, 7117-7124.

[44] P. Roesch, R. Mueller, A. Dallmann, G. Scholz, M. Kaupp, T. Braun, B. Braun-Cula, P. Wittwer, *Chem. Eur. J.* **2019**, *25*, 4678-4682.

[45] H. H. Karsch, P. A. Schlueter, F. Bienlein, M. Herker, E. Witt, A. Sladek, M. Heckel, *Z. Anorg. Allg. Chem.* **1998**, *624*, 295-309.

[46] For example, the bonding enthalpies for Me_3Si-Cl is 472 kJ/mol, for Me_3Sn-Cl 425 kJ/mol and for Ph_3Sn-$SnPh_3$ 189 kJ/mol, see: Y.-R. Luo, *Comprehensive Handbook of Chemical Bond Energies*, CRC Press, Boca Raton, **2007**.

[47] a) M. Saito, Y. Okamoto, M. Yoshioka, *Appl. Organomet. Chem.* **2005**, *19*, 894-897; b) T. Imori, V. Lu, H. Cai, T. D. Tilley, *J. Am. Chem. Soc.* **1995**, *117*, 9931-9940.

[48] A. F. Holleman, N. Wiberg, *Lehrbuch der Anorganischen Chemie, Vol. 102*, de Gruyter, Berlin, Deutschland, **2008**.

[49] M. K. Denk, K. Hatano, A. J. Lough, *Eur. J. Inorg. Chem.* **1998**, 1067-1070.

[50] A. Gackstatter, H. Braunschweig, T. Kupfer, C. Voigt, N. Arnold, *Chem. Eur. J.* **2016**, *22*, 16415-16419.

[51] a) N. Kuhn, J. Fahl, R. Boese, G. Henkel, *Z. Naturforsch., B: Chem. Sci.* **1998**, *53*, 881-886; b) E. Mallah, N. Kuhn, C. Maichle-Moessmer, M. Steimann, M. Strobele, K.-P. Zeller, *Z. Naturforsch., B: J. Chem. Sci.* **2009**, *64*, 1176-1182; c) S. Styra, M. Melaimi, C. E. Moore, A. L. Rheingold, T. Augenstein, F. Breher, G. Bertrand, *Chem. Eur. J.* **2015**, *21*, 8441-8446; d) Y. Kim, E. Lee, *Chem.*

Commun. **2016**, *52*, 10922-10925; e) J. Emerson-King, S. A. Hauser, A. B. Chaplin, *Org. Biomol. Chem.* **2017**, *15*, 787-789; f) Z. R. Turner, *Chem. Eur. J.* **2016**, *22*, 11461-11468.

[52] a) M. Ohashi, H. Saijo, M. Shibata, S. Ogoshi, *Eur. J. Org. Chem.* **2013**, 443-447; b) M. C. Leclerc, S. I. Gorelsky, B. M. Gabidullin, I. Korobkov, R. T. Baker, *Chem. Eur. J.* **2016**, *22*, 8063-8067; c) A. J. Arduengo, III, J. C. Calabrese, H. V. R. Dias, F. Davidson, J. R. Goerlich, A. Jockisch, M. Kline, W. J. Marshall, J. W. Runyon, *Phosphorus, Sulfur, Silicon Relat. Elem.* **2016**, *191*, 527-534.

[53] a) A. J. Arduengo, III, J. C. Calabrese, F. Davidson, H. V. R. Dias, J. R. Goerlich, R. Krafczyk, W. J. Marshall, M. Tamm, R. Schmutzler, *Helv. Chim. Acta* **1999**, *82*, 2348-2364; b) A. J. Arduengo, III, F. Davidson, H. V. R. Dias, J. R. Goerlich, D. Khasnis, W. J. Marshall, T. K. Prakasha, *J. Am. Chem. Soc.* **1997**, *119*, 12742-12749.

[54] a) S. Ishida, T. Iwamoto, C. Kabuto, M. Kira, *Silicon Chem.* **2003**, *2*, 137-140; b) D. F. Moser, T. Bosse, J. Olson, J. L. Moser, I. A. Guzei, R. West, *J. Am. Chem. Soc.* **2002**, *124*, 4186-4187; c) D. F. Moser, A. Naka, I. A. Guzei, T. Mueller, R. West, *J. Am. Chem. Soc.* **2005**, *127*, 14730-14738.

[55] a) B. Gehrhus, M. F. Lappert, *J. Organomet. Chem.* **2001**, *617-618*, 209-223; b) R. H. Walker, K. A. Miller, S. L. Scott, Z. T. Cygan, J. M. Bartolin, J. W. Kampf, M. M. Banaszak Holl, *Organometallics* **2009**, *28*, 2744-2755.

[56] A. Jana, P. P. Samuel, G. Tavcar, H. W. Roesky, C. Schulzke, *J. Am. Chem. Soc.* **2010**, *132*, 10164-10170.

[57] V. S. V. S. N. Swamy, N. Parvin, K. Vipin Raj, K. Vanka, S. S. Sen, *Chem. Commun.* **2017**, *53*, 9850-9853.

[58] N. Wiberg, G. Ziegleder, *Chem. Ber.* **1978**, *111*, 2123-2129.

[59] A. Frenzel, J. J. Buffy, D. R. Powell, T. Muller, R. West, *Chem. Ber./Recl.* **1997**, *130*, 1579-1583.

[60] a) G. A. Miller, S. W. Lee, W. C. Trogler, *Organometallics* **1989**, *8*, 738-744; b) H.-W. Lerner, M. Bolte, N. Wiberg, *J. Organomet. Chem.* **2002**, *649*, 246-251; c) H.-W. Lerne, N. Wiberg, K. Polborn, *Z. Naturforsch., B: Chem. Sci.* **2002**, *57*, 1199-1206.

[61] a) N. Wiberg, K. Schurz, G. Fischer, *Angew. Chem.* **1985**, *97*, 1058-1059; b) N. Wiberg, K. Schurz, G. Reber, G. Mueller, *J. Chem. Soc., Chem. Commun.* **1986**, 591-592.

[62] a) B. Gehrhus, P. B. Hitchcock, M. F. Lappert, *Z. Anorg. Allg. Chem.* **2001**, *627*, 1048-1054; b) N. J. Hill, D. F. Moser, I. A. Guzei, R. West, *Organometallics* **2005**, *24*, 3346-3349; c) L.-B. Kong, C.-M. Cui, *Organometallics* **2010**, *29*, 5738-5740; d) P. P. Samuel, R. Azhakar, R. S. Ghadwal, S. S. Sen, H. W. Roesky, M. Granitzka, J. Matussek, R. Herbst-Irmer, D. Stalke, *Inorg. Chem.* **2012**, *51*, 11049-11054; e) R. Azhakar, H. W. Roesky, J. J. Holstein, K. Proepper, B. Dittrich, *Organometallics* **2013**, *32*, 358-361; f) Y.-L. Shan, B.-X. Leong, Y. Li, R. Ganguly, C.-W. So, *Inorg. Chem.* **2017**, *56*, 1609-1615; g) K. Yuvaraj, C. Jones, *Dalton Trans.* **2019**, *48*, 11961-11965.

[63] D. M. Khramov, C. W. Bielawski, *Chem. Commun.* **2005**, 4958-4960.

[64] S. Haslinger, G. Laus, V. Kahlenberg, K. Wurst, T. Bechtold, S. Vergeiner, H. Schottenberger, *Crystals* **2016**, *6*, 40/1-40/12.

[65] J. Back, J. Park, Y. Kim, H. Kang, Y. Kim, M. J. Park, K. Kim, E. Lee, *J. Am. Chem. Soc.* **2017**, *139*, 15300-15303.

[66] a) H. Quast, L. Bieber, G. Meichsner, D. Regnat, *Chem. Ber.* **1988**, *121*, 1285-1290; b) K. Peters, E. M. Peters, D. Regnat, H. Quast, *Z. Kristallogr. - New Cryst. Struct.* **1998**, *213*, 705-706.

[67] M. Denk, R. K. Hayashi, R. West, *J. Am. Chem. Soc.* **1994**, *116*, 10813-10814.

[68] a) D. Michalik, A. Schulz, A. Villinger, *Inorg. Chem.* **2008**, *47*, 11798-11806; b) M. I. Arz, D. Hoffmann, G. Schnakenburg, A. C. Filippou, *Z. Anorg. Allg. Chem.* **2016**, *642*, 1287-1294; c) K. Bläsing, J. Bresien, R. Labbow, D. Michalik, A. Schulz, M. Thomas, A. Villinger, *Angew. Chem. Int. Ed.* **2019**, *58*, 6540-6544; *Angew. Chem*. **2019**, *131*, 6610-6615.

[69] a) L. Cavallo, A. Correa, C. Costabile, H. Jacobsen, *J. Organomet. Chem.* **2005**, *690*, 5407-5413; b) H. D. Velazquez, F. Verpoort, *Chem. Soc. Rev.* **2012**, *41*, 7032-7060; c) S. J. Hock, L.-A. Schaper, W. A. Herrmann, F. E. Kuehn, *Chem. Soc. Rev.* **2013**, *42*, 5073-5089; d) Z. Wang, L. Jiang, D. K. B. Mohamed, J. Zhao, T. S. A. Hor, *Coord. Chem. Rev.* **2015**, *293-294*, 292-326; e) A. J. Jordan, C. M. Wyss, J. Bacsa, J. P. Sadighi, *Organometallics* **2016**, *35*, 613-616; f) J.

Cheng, L. Wang, P. Wang, L. Deng, *Chem. Rev.* **2018**, *118*, 9930-9987; g) A. A. Danopoulos, T. Simler, P. Braunstein, *Chem. Rev.* **2019**, *119*, 3730-3961.

[70] a) F. K. Zinn, M. S. Viciu, S. P. Nolan, *Annu. Rep. Prog. Chem., Sect. B: Org. Chem.* **2004**, *100*, 231-249; b) T. Strassner, *Top. Organomet. Chem.* **2007**, *22*, 125-148; c) X. Bantreil, J. Broggi, S. P. Nolan, *Annu. Rep. Prog. Chem., Sect. B: Org. Chem.* **2009**, *105*, 232-263; d) D. Zhang, G. Zi, *Chem. Soc. Rev.* **2015**, *44*, 1898-1921; e) Q. Zhao, G. Meng, M. Szostak, S. P. Nolan, *Chem. Rev.* **2020**, *120*, 1981-2048.

[71] a) M. Denk, R. K. Hayashi, R. West, *J. Chem. Soc., Chem. Commun.* **1994**, 33-34; b) T. A. Schmedake, M. Haaf, B. J. Paradise, A. J. Millevolte, D. R. Powell, R. West, *J. Organomet. Chem.* **2001**, *636*, 17-25.

[72] S. H. A. Petri, D. Eikenberg, B. Neumann, H.-G. Stammler, P. Jutzi, *Organometallics* **1999**, *18*, 2615-2618.

[73] W. J. Evans, J. M. Perotti, J. W. Ziller, D. F. Moser, R. West, *Organometallics* **2003**, *22*, 1160-1163.

[74] I. A. Cade, A. F. Hill, A. Kaempfe, J. Wagler, *Organometallics* **2010**, *29*, 4012-4017.

[75] J. M. Dysard, T. D. Tilley, *Organometallics* **2000**, *19*, 4726-4732.

[76] D. Amoroso, M. Haaf, G. P. A. Yap, R. West, D. E. Fogg, *Organometallics* **2002**, *21*, 534-540.

[77] M. Schmidt, B. Blom, T. Szilvasi, R. Schomaecker, M. Driess, *Eur. J. Inorg. Chem.* **2017**, 1284-1291.

[78] E. Neumann, A. Pfaltz, *Organometallics* **2005**, *24*, 2008-2011.

[79] T. A. Schmedake, M. Haaf, B. J. Paradise, D. Powell, R. West, *Organometallics* **2000**, *19*, 3263-3265.

[80] M. Zhang, X. Liu, C. Shi, C. Ren, Y. Ding, H. W. Roesky, *Z. Anorg. Allg. Chem.* **2008**, *634*, 1755-1758.

[81] A. Fuerstner, H. Krause, C. W. Lehmann, *Chem. Commun.* **2001**, 2372-2373.

[82] W. A. Herrmann, P. Harter, C. W. K. Gstottmayr, F. Bielert, N. Seeboth, P. Sirsch, *J. Organomet. Chem.* **2002**, *649*, 141-146.

[83] R. Waterman, R. C. Handford, T. D. Tilley, *Organometallics* **2019**, *38*, 2053-2061.

[84] M. M. Hanninen, K. Pal, B. M. Day, T. Pugh, R. A. Layfield, *Dalton Trans.* **2016**, *45*, 11301-11305.

[85] M. M. Hanninen, A. Baldansuren, T. Pugh, *Dalton Trans.* **2017**, *46*, 9740-9744.

[86] B. Gehrhus, P. B. Hitchcock, M. F. Lappert, H. Maciejewski, *Organometallics* **1998**, *17*, 5599-5601.

[87] A. G. Avent, B. Gehrhus, P. B. Hitchcock, M. F. Lappert, H. Maciejewski, *J. Organomet. Chem.* **2003**, *686*, 321-331.

[88] H. Yoo, P. J. Carroll, D. H. Berry, *J. Am. Chem. Soc.* **2006**, *128*, 6038-6039.

[89] S. B. Clendenning, B. Gehrhus, P. B. Hitchcock, D. F. Moser, J. F. Nixon, R. West, *J. Chem. Soc., Dalton Trans.* **2002**, 484-490.

[90] X. Cai, B. Gehrhus, P. B. Hitchcock, M. F. Lappert, *Can. J. Chem.* **2000**, *78*, 1484-1490.

[91] a) T. Weskamp, V. P. W. Bohm, W. A. Herrmann, *J. Organomet. Chem.* **1999**, *585*, 348-352; b) T. Weskamp, V. P. W. Bohm, W. A. Herrmann, *J. Organomet. Chem.* **2000**, *600*, 12-22; c) G. D. Frey, J. Schuetz, E. Herdtweck, W. A. Herrmann, *Organometallics* **2005**, *24*, 4416-4426; d) L.-A. Schaper, S. J. Hock, W. A. Herrmann, F. E. Kuehn, *Angew. Chem. Int. Ed.* **2013**, *52*, 270-289; *Angew. Chem*. **2013**, *125*, 284-304.

[92] Y.-P. Zhou, M. Driess, *Angew. Chem. Int. Ed.* **2019**, *58*, 3715-3728; *Angew. Chem*. **2019**, *131*, 3753-3766.

[93] P. Luger, G. Ruban, *Acta Crystallogr., Sect. B* **1971**, *27*, 2276-2279.

[94] M. F. Lappert, D. J. Cardin, B. Cetinkaya, L. Manojlovic-Muir, K. W. Muir, *J. Chem. Soc. D.* **1971**, 400-401.

[95] M. J. Doyle, M. F. Lappert, G. M. McLaughlin, J. McMeeking, *J. Chem. Soc., Dalton Trans.* **1974**, 1494-1501.

[96] a) J. C. Garrison, R. S. Simons, C. A. Tessier, W. J. Youngs, *J. Organomet. Chem.* **2003**, *673*, 1-4; b) J. C. Garrison, R. S. Simons, W. G. Kofron, C. A. Tessier, W. J. Youngs, *Chem. Commun.* **2001**, 1780-1781; c) V. J. Catalano, M. A. Malwitz, *Inorg. Chem.* **2003**, *42*, 5483-5485; d) V. J. Catalano, M. A. Malwitz, A. O. Etogo, *Inorg. Chem.* **2004**, *43*, 5714-5724; e) J. C. Garrison, C. A. Tessier, W. J. Youngs, *J. Comput. Chem.* **2005**, *690*, 6008-6020; f) S. Gischig, A. Togni, *Organometallics* **2005**, *24*, 203-205; g) B. Liu, W. Chen, S. Jin, *Organometallics* **2007**, *26*, 3660-3667; h) S. Diez-Gonzalez, E. C.

Escudero-Adan, J. Benet-Buchholz, E. D. Stevens, A. M. Z. Slawin, S. P. Nolan, *Dalton Trans.* **2010**, *39*, 7595-7606; i) X. Han, L.-L. Koh, Z.-P. Liu, Z. Weng, T. S. A. Hor, *Organometallics* **2010**, *29*, 2403-2405; j) V. S. Thoi, C. J. Chang, *Chem. Commun.* **2011**, *47*, 6578-6580; k) V. J. Catalano, L. B. Munro, C. E. Strasser, A. F. Samin, *Inorg. Chem.* **2011**, *50*, 8465-8476; l) A. Mrutu, D. A. Dickie, K. I. Goldberg, R. A. Kemp, *Inorg. Chem.* **2011**, *50*, 2729-2731; m) C. Topf, C. Hirtenlehner, M. Zabel, M. List, M. Fleck, U. Monkowius, *Organometallics* **2011**, *30*, 2755-2764; n) X. Liu, W. Chen, *Organometallics* **2012**, *31*, 6614-6622; o) B. Liu, C. Chen, Y. Zhang, X. Liu, W. Chen, *Organometallics* **2013**, *32*, 5451-5460; p) R. Della Pergola, M. Bruschi, A. Sironi, V. Colombo, A. Sironi, *Organometallics* **2014**, *33*, 5610-5613; q) B. R. M. Lake, C. E. Willans, *Organometallics* **2014**, *33*, 2027-2038; r) B. Liu, X. Ma, F. Wu, W. Chen, *Dalton Trans.* **2015**, *44*, 1836-1844; s) A. Seyboldt, B. Wucher, S. Hohnstein, K. Eichele, F. Rominger, K. W. Törnroos, D. Kunz, *Organometallics* **2015**, *34*, 2717-2725; t) S. Gu, J. Du, J. Huang, H. Xia, L. Yang, W. Xu, C. Lu, *Beilstein J. Org. Chem.* **2016**, *12*, 863-873.

[97] a) A. Wacker, H. Pritzkow, W. Siebert, *Eur. J. Inorg. Chem.* **1998**, 843-849; b) S. A. Mungur, S. T. Liddle, C. Wilson, M. J. Sarsfield, P. L. Arnold, *Chem. Commun.* **2004**, 2738-2739.

[98] M. F. Lappert, P. L. Pye, *J. Chem. Soc., Dalton Trans.* **1977**, 2172-2180.

[99] a) C. H. Lee, D. S. Laitar, P. Mueller, J. P. Sadighi, *J . Am. Chem. Soc.* **2007**, *129*, 13802-13803; b) T. Hashimoto, R. Hoshino, T. Hatanaka, Y. Ohki, K. Tatsumi, *Organometallics* **2014**, *33*, 921-929; c) S. C. Meier, A. Holz, J. Kulenkampff, A. Schmidt, D. Kratzert, D. Himmel, D. Schmitz, E.-W. Scheidt, W. Scherer, C. Buelow, M. Timm, R. Lindblad, S. T. Akin, V. Zamudio-Bayer, B. von Issendorff, M. A. Duncan, J. T. Lau, I. Krossing, *Angew. Chem. Int. Ed.* **2018**, *57*, 9310-9314; *Angew. Chem*. **2018**, *130*, 9454-9458.

[100] L. Rubio-Perez, M. Iglesias, J. Munarriz, V. Polo, P. J. Sanz Miguel, J. J. Perez-Torrente, L. A. Oro, *Chem. Commun.* **2015**, *51*, 9860-9863.

[101] R. J. Witzke, T. D. Tilley, *Chem. Commun.* **2019**, *55*, 6559-6562.

[102] A. A. Danopoulos, D. Pugh, J. A. Wright, *Angew. Chem. Int. Ed.* **2008**, *47*, 9765-9767; *Angew. Chem*. **2008**, *120*, 9911-9913.

[103] A. Kaiho, H. Suzuki, *Angew. Chem. Int. Ed.* **2012**, *51*, 1408-1411; *Angew. Chem*. **2012**, *124*, 1437-1440.

[104] A. Gackstatter, H. Braunschweig, T. Kupfer, C. Voigt, N. Arnold, *Chem. Eur. J.* **2016**, 16415 - 16419.

[105] M. T. Whited, A. M. Deetz, J. W. Boerma, D. E. DeRosha, D. E. Janzen, *Organometallics* **2014**, *33*, 5070-5073.

[106] E. O. Fischer, A. Maasboel, *Angew. Chem. Int. Ed.* **1964**, *3*, 580-581.

[107] K. H. Dötz, H. Fischer, P. Hofmann, F. R. Kreissl, U. Schubert, K. Weiss, *Transition Metal Carbene Complexes*, Verlag Chemie, Weinheim, **1983**.

[108] a) R. R. Schrock, *Acc. Chem. Res.* **1979**, *12*, 98-104; b) W. A. Nugent, J. M. Mayer, *Metal-Ligand Multiple Bonds* Wiley, New York, **1988**.

[109] a) H. Nakatsuji, M. Hada, K. Kondo, *Chem. Phys. Lett.* **1992**, *196*, 404-409; b) A. Marquez, J. Fernandez Sanz, *J. Am. Chem. Soc.* **1992**, *114*, 10019-10024; c) A. Marquez, J. Fernandez Sanz, *J. Am. Chem. Soc.* **1992**, *114*, 2903-2909; d) H. Jacobsen, G. Schreckenbach, T. Ziegler, *J. Phys. Chem.* **1994**, *98*, 11406-11410; e) H. Jacobsen, T. Ziegler, *Organometallics* **1995**, *14*, 224-230; f) H. Jacobsen, T. Ziegler, *Inorg. Chem.* **1996**, *35*, 775-783; g) S. F. Vyboishchikov, G. Frenking, *Chem. - Eur. J.* **1998**, *4*, 1428-1438; h) W. W. Schoeller, D. Eisner, S. Grigoleit, A. B. Rozhenko, A. Alijah, *J. Am. Chem. Soc.* **2000**, *122*, 10115-10120; i) G. Frenking, K. Wichmann, N. Frohlich, C. Loschen, M. Lein, J. Frunzke, V. M. Rayon, *Coord. Chem. Rev.* **2003**, *238-239*, 55-82; j) M.-T. Lee, C.-H. Hu, *Organometallics* **2004**, *23*, 976-983; k) I. Fernandez, F. P. Cossio, A. Arrieta, B. Lecea, M. J. Mancheno, M. A. Sierra, *Organometallics* **2004**, *23*, 1065-1071; l) G. Frenking, M. Sola, S. F. Vyboishchikov, *J. Organomet. Chem.* **2005**, *690*, 6178-6204; m) T. A. N. Nguyen, G. Frenking, *Chem. Eur. J.* **2012**, *18*, 12733-12748.

[110] a) G. Frenking, N. Froehlich, *Chem. Rev.* **2000**, *100*, 717-774; b) U. Pidun, G. Frenking, *J. Organomet. Chem.* **1996**, *525*, 269-278; c) A. W. Ehlers, G. Frenking, E. J. Baerends, *Organometallics* **1997**, *16*, 4896-4902; d) A. W. Ehlers, S. Dapprich, S. F. Vyboishchikov, G. Frenking, *Organometallics* **1996**, *15*, 105-117; e) R. A. Fischer, M. M. Schulte, J. Weiss, L. Zsolnai, A. Jacobi, G. Huttner, G. Frenking, C. Boehme, S. F. Vyboishchikov, *J. Am. Chem. Soc.* **1998**, *120*, 1237-1248; f) S. Dapprich, G. Frenking, *Z. Anorg. Allg. Chem.* **1998**, *624*,

583-589; g) S. F. Vyboishchikov, G. Frenking, *Chem. Eur. J.* **1998**, *4*, 1439-1448; h) J. Uddin, C. Boehme, G. Frenking, *Organometallics* **2000**, *19*, 571-582; i) A. Kovacs, G. Frenking, *Organometallics* **2001**, *20*, 2510-2524; j) G. Frenking, K. Wichmann, N. Froehlich, J. Grobe, W. Golla, D. L. Van, B. Krebs, M. Laege, *Organometallics* **2002**, *21*, 2921-2930; k) C. Esterhuysen, G. Frenking, *Chem. Eur. J.* **2003**, *9*, 3518-3529; l) N. Takagi, T. Shimizu, G. Frenking, *Chem. Eur. J.* **2009**, *15*, 8593-8604; m) N. Takagi, G. Frenking, *Theor. Chem. Acc.* **2011**, *129*, 615-623.

[111] K. Fukui, H. Fujimoto, in *Frontier Orbitals and Reaction Paths, Vol. 7*, World Scientific Pub. Co. Inc., Singapore, **1997**.

[112] N. Kuhn, T. Kratz, R. Boese, D. Blaeser, *J. Organomet. Chem.* **1994**, *470*, C8-C11.

[113] Z. Wang, S. Li, W. J. Teo, Y. T. Poh, J. Zhao, T. S. A. Hor, *J. Organomet. Chem.* **2015**, *775*, 188-194.

[114] a) A. Poater, B. Cosenza, A. Correa, S. Giudice, F. Ragone, V. Scarano, L. Cavallo, *Eur. J. Inorg. Chem.* **2009**, *2009*, 1759-1766; b) L. Falivene, R. Credendino, A. Poater, A. Petta, L. Serra, R. Oliva, V. Scarano, L. Cavallo, *Organometallics* **2016**, *35*, 2286-2293.

[115] W. Buchner, W. A. Schenk, *Inorg. Chem.* **1984**, *23*, 132-137.

[116] K. Junold, J. A. Baus, C. Burschka, T. Vent-Schmidt, S. Riedel, R. Tacke, *Inorg. Chem.* **2013**, *52*, 11593-11599.

[117] R. S. Ghadwal, D. Rottschaefer, D. M. Andrada, G. Frenking, C. J. Schuermann, H.-G. Stammler, *Dalton Trans.* **2017**, *46*, 7791-7799.

[118] a) C. A. Tolman, *Chem. Rev.* **1977**, *77*, 313 - 348; b) R. Dorta, E. D. Stevens, N. M. Scott, C. Costabile, L. Cavallo, C. D. Hoff, S. P. Nolan, *J. Am. Chem. Soc.* **2005**, *127*, 2485-2495.

[119] U. S. D. Paul, M. J. Krahfuss, U. Radius, *Chem. Unserer Zeit* **2019**, *53*, 212-223.

[120] a) T. Schaub, U. Radius, *Chem. Eur. J.* **2005**, *11*, 5024-5030; b) T. Schaub, M. Backes, U. Radius, *Organometallics* **2006**, *25*, 4196-4206; c) J. H. J. Berthel, M. W. Kuntze-Fechner, U. Radius, *Eur. J. Inorg. Chem.* **2019**, *2019*, 2618-2623; d) W. A. Herrmann, L. J. Goossen, G. R. J. Artus, C. Koecher, *Organometallics* **1997**, *16*, 2472-2477; e) R. Dorta, E. D. Stevens, C. D. Hoff, S. P. Nolan, *J. Am.*

Chem. Soc. **2003**, *125*, 10490-10491; f) N. M. Scott, H. Clavier, P. Mahjoor, E. D. Stevens, S. P. Nolan, *Organometallics* **2008**, *27*, 3181-3186.

[121] a) L. F. Dahl, J. K. Ruff, R. P. White, Jr., *J. Am. Chem. Soc.* **1971**, *93*, 2159-2176; b) R. Diercks, L. Stamp, J. Kopf, H. Tom Dieck, *Angew. Chem. Int. Ed.* **1984**, *23*, 893-894; Angew. Chem. **1984**, *96*, 891-895; c) A. K. Maity, M. Zeller, C. Uyeda, *Organometallics* **2018**, *37*, 2437-2441.

[122] a) U. S. D. Paul, C. Sieck, M. Haehnel, K. Hammond, T. B. Marder, U. Radius, *Chem. Eur. J.* **2016**, *22*, 11005-11014; b) U. S. D. Paul, U. Radius, *Organometallics* **2017**, *36*, 1398-1407.

[123] D. J. Nelson, S. P. Nolan, *Chem. Soc. Rev.* **2013**, *42*, 6723-6753.

[124] a) M. Vogt, V. Pons, D. M. Heinekey, *Organometallics* **2005**, *24*, 1832-1836; b) Y. Ohki, T. Hatanaka, K. Tatsumi, *J. Am. Chem. Soc.* **2008**, *130*, 17174-17186; c) Q. Liang, D. Song, *Inorg. Chem.* **2017**, *56*, 11956-11970; d) F. Ulm, A. I. Poblador-Bahamonde, S. Choppin, S. Bellemin-Laponnaz, M. J. Chetcuti, T. Achard, V. Ritleng, *Dalton Trans.* **2018**, *47*, 17134-17145; e) F. P. Malan, E. Singleton, P. H. van Rooyen, J. Conradie, M. Landman, *New J. Chem.* **2018**, *42*, 19193-19204; f) C. S. Day, D. E. Fogg, *Organometallics* **2018**, *37*, 4551-4555; g) K. Lubitz, U. Radius, *Organometallics* **2019**, *38*, 2558-2572; h) S. E. Kutniewska, R. Kaminski, W. Buchowicz, K. N. Jarzembska, *Inorg. Chem.* **2019**, *58*, 16712-16721; i) R. N. Osorio-Yanez, A. Hepp, T. T. Y. Tan, F. E. Hahn, *Organometallics* **2020**, Ahead of Print.

[125] a) V. Ritleng, C. Barth, E. Brenner, S. Milosevic, M. J. Chetcuti, *Organometallics* **2008**, *27*, 4223-4228; b) A. Wlodarska, A. Koziol, M. Dranka, A. Gryff-Keller, P. Szczecinski, J. Jurkowski, A. Pietrzykowski, *Organometallics* **2015**, *34*, 577-581; c) A. Wlodarska, J. Golaszewska-Gajda, M. Dranka, A. Pietrzykowski, *Mol. Catal.* **2017**, *440*, 25-35.

[126] C. D. Abernethy, J. A. C. Clyburne, A. H. Cowley, R. A. Jones, *J. Am. Chem. Soc.* **1999**, *121*, 2329-2330.

[127] a) V. Ritleng, A. M. Oertel, M. J. Chetcuti, *Dalton Trans.* **2010**, *39*, 8153-8160; b) A. M. Oertel, V. Ritleng, L. Burr, M. J. Chetcuti, *Organometallics* **2011**, *30*, 6685-6691.

[128] a) S. Pelties, D. Herrmann, B. de Bruin, F. Hartl, R. Wolf, *Chem. Commun.* **2014**, *50*, 7014-7016; b) S. Pelties, A. W. Ehlers, R. Wolf, *Chem. Commun.* **2016**, *52*, 6601-6604; c) S. Pelties, R. Wolf, *Organometallics* **2016**, *35*, 2722-2727.

[129] R. Diercks, L. Stamp, J. Kopf, H. Tom Dieck, *Angew. Chem. Int. Ed.* **1984**, *23*, 893-894; Angew. Chem. **1984**, *96*, 891-895.

[130] S.-M. Peng, V. L. Goedken, *J. Am. Chem. Soc.* **1976**, *98*, 8500-8510.

[131] U. Denninger, J. J. Schneider, G. Wilke, R. Goddard, C. Krueger, *Inorg. Chim. Acta* **1993**, *213*, 129-140.

[132] a) F. A. Cotton, B. A. Frenz, *Inorg. Chem.* **1974**, *13*, 253-256; b) C. P. Casey, P. J. Fagan, V. W. Day, *J. Am. Chem. Soc.* **1982**, *104*, 7360-7361; c) H. Sun, S. Xu, X. Zhou, H. Wang, R. Wang, X. Yao, *J. Organomet. Chem.* **1993**, *444*, C41-C43; d) N. Xiao, B. Wang, J. Yin, Q. Xu, N. Tsumori, J. Sun, J. Chen, *Organometallics* **2004**, *23*, 257-268; e) Z.-H. Ma, M.-X. Zhao, F. Li, H. Wang, X.-Z. Zheng, J. Lin, *Transition Met. Chem.* **2010**, *35*, 387-391; f) B. Zhu, T. Wang, Y. Li, R. Sun, S. Wu, B. Wang, *J. Organomet. Chem.* **2016**, *813*, 61-70.

[133] Y. Kawano, H. Tobita, M. Shimoi, H. Ogino, *J. Am. Chem. Soc.* **1994**, *116*, 8575-8581.

[134] T. A. Martin, C. E. Ellul, M. F. Mahon, M. E. Warren, D. Allan, M. K. Whittlesey, *Organometallics* **2011**, *30*, 2200-2211.

[135] R. Fraser, C. G. C. E. van Sittert, P. H. van Rooyen, M. Landman, *J. Organomet. Chem.* **2017**, *835*, 60-69.

[136] D. C. R. Hockless, I. R. Whittall, M. G. Humphrey, *Acta Crystallogr., Sect. C: Cryst. Struct. Commun.* **1996**, *C52*, 535-537.

[137] D. Serra, M. C. Correia, L. McElwee-White, *Organometallics* **2011**, *30*, 5568-5577.

[138] a) L. Mercs, G. Labat, A. Neels, A. Ehlers, M. Albrecht, *Organometallics* **2006**, *25*, 5648-5656; b) M. D. Bala, M. I. Ikhile, *J. Mol. Catal. A: Chem.* **2014**, *385*, 98-105; c) D. Bezier, F. Jiang, T. Roisnel, J.-B. Sortais, C. Darcel, *Eur. J. Inorg. Chem.* **2012**, *2012*, 1333-1337.

[139] C. L. L. Chai, W. L. F. Armaregon, *Purification of Laboratory Chemicals, Vol. 6*, Butterworth Heinemann, Oxford, England, **2008**.

[140] Y. Soltani, L. C. Wilkins, R. L. Melen, *Angew. Chem. Int. Ed.* **2017**, *56*, 11995-11999; *Angew. Chem.* **2017**, *129*, 12157-12161.

[141] J. Chen, E. Y. X. Chen, *Dalton Trans.* **2016**, *45*, 6105-6110.

[142] M. G. Finn, *Pentacarbonylchloromanganes*, e-EROS Encyclopedia of Reagens for Organic Synthesis, John Wiley & Sons, Ltd., **2001**, 1.

[143] Y. Kuninobu, Y. Nishina, T. Takeuchi, K. Takai, *Angew. Chem. Int. Ed.* **2007**, *46*, 6518-6520; *Angew. Chem.* **2007**, *119*, 6638-6640.

[144] B. Rong, W. Zhong, E. Gu, L. Long, L. Song, X. Liu, *Electrochim. Acta* **2018**, *283*, 27-35.

[145] X. Bantreil, S. P. Nolan, *Nat. Protoc.* **2011**, *6*, 69-77.

[146] G. M. Sheldrick, *Acta Crystallogr., Sect. A: Found. Adv.* **2015**, *71*, 3-8.

[147] a) R. Ahlrichs, M. Baer, M. Haeser, H. Horn, C. Koelmel, *Chem. Phys. Lett.* **1989**, *162*, 165-169; b) F. Furche, R. Ahlrichs, C. Haettig, W. Klopper, M. Sierka, F. Weigend, *Wiley Interdiscip. Rev.: Comput. Mol. Sci.* **2014**, *4*, 91-100.

[148] a) M. Haeser, R. Ahlrichs, *J. Comput. Chem.* **1989**, *10*, 104-111; b) O. Treutler, R. Ahlrichs, *J. Chem. Phys.* **1995**, *102*, 346-354; c) M. Sierka, A. Hogekamp, R. Ahlrichs, *J. Chem. Phys.* **2003**, *118*, 9136-9148.

[149] a) A. D. Becke, *Phys. Rev. A: Gen. Phys.* **1988**, *38*, 3098-3100; b) Perdew, *Phys. Rev. B Condens. Matter* **1986**, *33*, 8822-8824; c) Perdew, *Phys. Rev. B Condens. Matter* **1986**, *34*, 7406.

[150] a) A. Schaefer, C. Huber, R. Ahlrichs, *J. Chem. Phys.* **1994**, *100*, 5829-5835; b) K. Eichkorn, O. Treutler, H. Oehm, M. Haeser, R. Ahlrichs, *Chem. Phys. Lett.* **1995**, *242*, 652-660; c) K. Eichkorn, F. Weigend, O. Treutler, R. Ahlrichs, *Theor. Chem. Acc.* **1997**, *97*, 119-124; d) F. Weigend, R. Ahlrichs, *Phys. Chem. Chem. Phys.* **2005**, *7*, 3297-3305.

[151] a) S. H. Vosko, L. Wilk, M. Nusair, *Can. J. Phys.* **1980**, *58*, 1200-1211; b) A. D. Becke, *J. Chem. Phys.* **1986**, *84*, 4524; c) C. Lee, W. Yang, R. G. Parr, *Phys. Rev. B* **1988**, *37*, 785-789; d) A. D. Becke, *J. Chem. Phys.* **1993**, *98*, 5648-5652; e) P. J. Stephens, F. J. Devlin, C. F. Chabalowski, M. J. Frisch, *J. Phys. Chem.* **1994**, *98*, 11623-11627.

[152] P. Deglmann, K. May, F. Furche, R. Ahlrichs, *Chem. Phys. Lett.* **2004**, *384*, 103-107.

[153] a) C. Fonseca Guerra, J. G. Snijders, G. te Velde, E. J. Baerends, *Theor. Chem. Acc.* **1998**, *99*, 391-403; b) G. te Velde, F. M. Bickelhaupt, E. J. Baerends, C. Fonseca Guerra, S. J. A. van Gisbergen, J. G. Snijders, T. Ziegler, *J. Comput.*

Chem. **2001**, *22*, 931-967; c) E. J. Baerends, T. Ziegler, A. J. Atkins, J. Autschbach, O. Baseggio, D. Bashford, A. Bérces, F. M. Bickelhaupt, C. Bo, P. M. Boerrigter, L. Cavallo, C. Daul, D. P. Chong, D. V. Chulhai, L. Deng, R. M. Dickson, J. M. Dieterich, D. E. Ellis, M. van Faassen, L. Fan, T. H. Fischer, C. Fonseca Guerra, M. Franchini, A. Ghysels, A. Giammona, S. J. A. van Gisbergen, A. Goez, A. W. Götz, J. A. Groeneveld, O. V. Gritsenko, M. Grüning, S. Gusarov, F. E. Harris, P. van den Hoek, Z. Hu, C. R. Jacob, H. Jacobsen, L. Jensen, L. Joubert, J. W. Kaminski, G. van Kessel, C. König, F. Kootstra, A. Kovalenko, M. V. Krykunov, E. van Lenthe, D. A. McCormack, A. Michalak, M. Mitoraj, S. M. Morton, J. Neugebauer, V. P. Nicu, L. Noodleman, V. P. Osinga, S. Patchkovskii, M. Pavanello, C. A. Peeples, P. H. T. Philipsen, D. Post, C. C. Pye, H. Ramanantoanina, P. Ramos, W. Ravenek, J. I. Rodríguez, P. Ros, R. Rüger, P. R. T. Schipper, D. Schlüns, H. van Schoot, G. Schreckenbach, J. S. Seldenthuis, M. Seth, J. G. Snijders, M. Solà, M. Stener, M. Swart, D. Swerhone, V. Tognetti, G. te Velde, P. Vernooijs, L. Versluis, L. Visscher, O. Visser, F. Wang, T. A. Wesolowski, E. M. van Wezenbeek, G. Wiesenekker, S. K. Wolff, T. K. Woo, A. L. Yakovlev, ADF2016, SCM, Theoretical Chemistry, Vrije Universiteit, http://www.scm.com, Amsterdam, The Netherlands, **2016**.

[154] a) A. D. Becke, *J. Chem. Phys.* **1988**, *88*, 2547-2553; b) M. Franchini, P. H. T. Philipsen, L. Visscher, *J. Comput. Chem.* **2013**, *34*, 1819-1827.

[155] E. Van Lenthe, E. J. Baerends, *J. Comput. Chem.* **2003**, *24*, 1142-1156.

[156] J. C. Slater, *Quantum Theory of Molecules and Solids*, 4th Ed., McGraw-Hill, New York, **1974**.

[157] a) T. V. Russo, R. L. Martin, P. J. Hay, *J. Chem. Phys.* **1994**, *101*, 7729-7737; b) B. G. Johnson, P. M. W. Gill, J. A. Pople, *J. Chem. Phys.* **1993**, *98*, 5612-5626.

[158] a) E. v. Lenthe, E. J. Baerends, J. G. Snijders, *J. Chem. Phys.* **1993**, *99*, 4597-4610; b) E. van Lenthe, E. J. Baerends, J. G. Snijders, *J. Chem. Phys.* **1994**, *101*, 9783-9792; c) E. van Lenthe, J. G. Snijders, E. J. Baerends, *J. Chem. Phys.* **1996**, *105*, 6505-6516.

[159] S. Grimme, S. Ehrlich, L. Goerigk, *J. Comput. Chem.* **2011**, *32*, 1456-1465.

[160] a) A. Berces, R. M. Dickson, L. Y. Fan, H. Jacobsen, D. Swerhone, T. Ziegler, *Comput. Phys. Commun.* **1997**, *100*, 247-262; b) H. Jacobsen, A. Berces, D. P.

Swerhone, T. Ziegler, *Comput. Phys. Commun.* **1997**, *100*, 263-276; c) S. K. Wolff, *Int. J. Quantum Chem.* **2005**, *104*, 645-659.

[161] F. M. Bickelhaupt, N. J. R. van Eikema Hommes, C. Fonseca Guerra, E. J. Baerends, *Organometallics* **1996**, *15*, 2923-2931.

[162] a) T. Ziegler, A. Rauk, *Theor. Chim. Acta* **1977**, *46*, 1-10; b) F. M. Bickelhaupt, E. J. Baerends, *Rev. Comput. Chem.* **2000**, *15*, 1-86; c) M. Cho, N. Sylvetsky, S. Eshafi, G. Santra, I. Efremenko, J. M. L. Martin, M. Cho, S. Eshafi, *ChemPhysChem* **2020**, *21*, 688-696.

11 Danksagung

An erster Stelle gilt mein Dank Udo, der mir mit der Zusage zur Masterarbeit eine riesige Freude gemacht und eine Chance in seinem Arbeitskreis und im Anschluss die Möglichkeit zur Doktorarbeit gegeben hat. Vielen Dank für dein Vertrauen und deine unermüdliche Unterstützung und Geduld bei jeder Art Probleme und dafür, dass du einen kühlen Kopf bewahrt hast, auch wenn ich mal zu sehr Feuer und Flamme war – die Zeit ist wie im Flug vergangen!

Was mit den Stockkollegen begann und mit der Gang weiterging, war eine großartige Zeit, die ohne jeden einzelnen von euch nicht hätte stattfinden können! Vielen Dank an alle „Alten“ (Rumpel, Ulli, Sabrina, Heidi, Toni, Matti, Shorty, Michel, Landmann, Drisch und Philipp), die mich, so herzlich es eben bei ständigem Geschrei möglich ist, aufgenommen haben, an alle „Jungen“ (Katha, Max, Tatjana, Laura, Lukas, Gü, Andi, Michi, Steffen, Christian, Luis und Martin) und den AK Finze (Raphael, Jarno, Ludwig, Nils und Jan), die mich unterstützt und mir geholfen haben, selbst den Weg zu den „Alten“ zu gehen (Ideen sammeln, Korrekturlesen, Formulierungen ausdenken, sich mit mir freuen und leiden eingeschlossen). Die Ausflüge nach Regensburg und Hirschegg mitsamt Vortragsmarathons, den Höhenmetern zur Kanzelwand und dem Gewaltmarsch auf den Hohen Ifen waren unvergesslich. Danke für alles, was ich von und mit euch lernen konnte, für alle ChemCups, Feiern (mit und ohne guten Grund) und jedes Feierabendbier auf dem Weg! Meinen Praktikanten Lukas, Julian, Felix und Lena und meinem Azubi Lukas danke ich für die Unterstützung im Labor, das Vertrauen und die gemeinsame Zeit, in der wir hoffentlich gemeinsam Spaß an Chemie hatten.

Auch den stillen (und weniger stillen) Helfern aus der NMR-Abteilung (Rüdiger Bertermann, Marie-Luise Schäfer und Laura Wolz), dem Anführer der X-Minions Krzysztof (Gru) Radacki, der CHN-Abteilung (Sabine Timmroth und Lieselotte Michels), den Glasbläsern Berti und Berni, dem Technischen Betrieb sowie der Zentralwerkstatt, den fleißigen Bienen Conny, Birgit und Alfred Schertzer ein großes Dankeschön!

Danke, danke, danke meinen Schwestern und Brüdern im Geiste! Die vielen äußerst vergnüglichen Stunden mit euch waren manchmal das einzige, was mich davor

bewahrt hat endgültig verrückt zu werden oder die Sache an den Nagel zu hängen, wenn einfach so gar nichts rund lief. Ihr habt mich auf den Boden der Tatsachen zurückgeholt, mit mir geschimpft, gejammert und am wichtigsten – ihr wart immer da. Isi, Agnes, Maja, Jan und Gü – ich bin heilfroh, dass ihr mit am Start wart und freue mich auf alles, was noch auf uns zukommt!

Mit Sicherheit wäre das alles ohne meine Familien (ja, ich habe das Glück mehrere zu haben) nicht möglich gewesen – ihr wart unentbehrlich und habt mich in den letzten 10 Jahren (ups….) getragen, wann immer es nötig war. Danke Mama, Papa, Michi, Benni, Fabs, Flo, meinen Omas und Opas, Chris (mit Familie), Tantchen Myriel, dem Rinderwahn und allen, die ich Teil meiner Familie nennen darf!

Ein Toast auf jeden von euch – ihr wart die beste Reisebegleitung, die ich mir wünschen konnte!

Danke !

12 Eidesstattliche Erklärung

Hiermit erkläre ich an Eides statt, dass ich die Dissertation mit dem Titel

***N*-Heterocyclic Silylenes as ambiphilic Reagents in Main Group Chemistry and as Ligands in Transition Metal Chemistry**

selbständig angefertigt, übernommene Inhalte eindeutig gekennzeichnet und die Regeln der Universität Würzburg über gute wissenschaftliche Praxis eingehalten habe.

Ich erkläre außerdem, dass ich die Gelegenheit zum Promotionsvorhaben nicht kommerziell vermittelt bekommen und insbesondere nicht eine Person oder Organisation eingeschaltet habe, die gegen Entgelt Betreuerinnen bzw. Betreuer für die Anfertigung von Dissertationen sucht.

Ich habe früher außer den mit dem Promotionsgesuch urkundlich vorgelegten Graden keine weiteren akademischen Grade erworben oder zu erwerben versucht.

Die eingereichte und oben genannte Dissertation habe ich weder vollständig noch teilweise schon einmal einer anderen Fakultät mit dem Ziel einen akademischen Grad zu erwerben vorgelegt.

Würzburg, den 01.10.2020

_____

Originalunterschrift

(Vor- und Zuname)